5-20-2020

Synthesis, Characterization, and Investigation of Metal Ion Quenching in Fluorescent Carbon Dot Surrogates for Particulate Matter Black Carbon and Evaluation of Cellular Health Effects Due to the Surrogate Materials

Christopher Lee Sumner Jr
Louisiana State University and Agricultural and Mechanical College

SYNTHESIS, CHARACTERIZATION, AND INVESTIGATION OF METAL ION QUENCHING IN FLUORESCENT CARBON DOT SURROGATES FOR PARTICULATE MATTER BLACK CARBON AND EVALUATION OF CELLULAR HEALTH EFFECTS DUE TO THE SURROGATE MATERIALS

A Dissertation

Submitted to the Graduate Faculty of the
Louisiana State University and
Agricultural and Mechanical College
in partial fulfillment of the
requirements for the degree of
Doctor of Philosophy

in

The Department of Chemistry

by
Christopher Lee Sumner, Jr.
B.S., Shorter University, 2012
August 2020

This dissertation is dedicated to

My beautiful, supportive, and brilliant wife, Caitlin

My parents and siblings (Chris, Sheila, Catherine, and Chandler),

and

All my other friends and family

ACKNOWLEDGEMENTS

I would first like to thank my advisor, Prof. Robin McCarley for all the guidance and advice given during the 5 years I have spent at LSU. Without your guidance and encouragement, nothing I have accomplished would have been possible. You have taught me to think like a true scientist and become a complete chemist. I would also like to thank the McCarley group for all their support and help. I would particularly like to thank Dr. Zhenhua Shen, Dr. Ansonia Badgett, and Dr. Huy Nguyen for teaching and training me in the lab and setting an example for how to make my way through the chemistry program at LSU. Thank you also to Shaniqua Hayes, Peter Piers, and Amanda Owen for all your assistance with life at LSU and completion of my dissertation. The McGroup has been a family to me at LSU, and I would not have made it through without the support of my LSU Chemistry family.

I would like to thank Prof. Kermit Murray and Prof. Louis Haber for agreeing to serve on my committee and be a part of my time here at LSU. Prof. William Moe also deserves thanks for agreeing to be my Dean's Representative and serving on my committee. LSU Chemistry is a family; I have always felt welcome asking for help and guidance from all the faculty and staff, and I will miss the family that I have built here in Baton Rouge.

Within the LSU family, the scientists in the Shared Instrument Facility (SIF) have been crucial in the research I have produced. The assistance of Dr. Clayton Loehn and Dr. David Burk in getting trained on the instruments in the early stages of my research was a blessing, and they made the process incredibly easy. Dr. Ying Xiao was essential in collecting the low-resolution TEM images used in my cellular studies, and she was always ready and willing to take samples from me and help me run them. Dr. Dongmei Cao taught me more about instrumentation than anyone else at

LSU, guiding me on learning to use high-resolution TEM and XPS. Each of the scientists and staff at LSU are amazing people and have never hesitated to offer help when needed.

Last, but not least, I would like to thank my family. My parents, Chris and Sheila Sumner never wavered in their support and assistance in life. They pushed me to be better than I ever thought I could and picked me up continuously along the way. In addition to my parents, my other parents (in-laws), Dan and Rebekah Burnside, have always let me know I have a second home with them and a second support system should I ever need it. My siblings, Catherine and Chandler, were always the best of friends and supporters of me in my time at LSU. Though we don't always talk, whenever we do, they are there for me in support and laughs. Lastly, nothing in my life would be possible without my wife, Caitlin Sumner. She has been my rock when I am losing my mind, my encouragement when I am weighed by doubts, and my sounding board for when I need help figuring something out. Though she does not enjoy the sciences, she never hesitates to listen to me ramble on when I need it. The love and support from my family has carried me through my time here at LSU.

TABLE OF CONTENTS

LIST OF TABLES

LIST OF FIGURES

LIST OF SCHEMES

ABBREVIATIONS

AED	Aerodynamic equivalent diameter
ATR	Attenuated total reflectance
BC	Black Carbon
BEBM	Bronchial epithelial cell growth basal medium
COPD	Chronic obstructive pulmonary disease
CRP	C-reactive protein
DLS	Dynamic light scattering
DMEM	Dulbecco's modification of Eagle's medium
DTGS	Deuterated triglycine sulfide
EC	Elemental carbon
ECACC	European Collection of Authenticated Cell Cultures
EDTA	Ethylene diamine tetraacetic acid
EPA	Environmental Protection Agency
EPR	Electron paramagnetic resonance spectroscopy
FCDs	Fluorescent carbon dots
FTIR	Fourier-transform infrared spectroscopy
GSH	Glutathione
GSSG	Glutathione disulfide
HR-TEM	High-resolution transmission electron microscopy
ICD	Implanted cardioverter defibrillator

IR	Infrared spectroscopy
LR-TEM	Low-resolution transmission electron microscopy
LSU	Louisiana State University
MPA	Metaphosphoric acid
NADH	Nicotinamide adenine dinucleotide
NADPH	Nicotinamide adenine dinucleotide phosphate
NEXAFS	Near-edge X-ray absorption fine structure spectroscopy
PAL	Polymer Analysis Lab
PBS	Phosphate buffered saline
PEG	Polyethylene glycol
PES	Phenazine ethosulfate
PFA	Paraformaldehyde
PM	Particulate matter
QD	Quantum Dot
RIPA	Radioimmunoprecipitation assay
ROS	Reactive oxygen species
SAED	Selected area electron diffraction
SDS	Sodium dodecyl sulfate
SDT	Sodium dithionite
SIF	Shared Instrument Facility
SSA	5-sulfosalicylic acid

TEAM	Triethanolamine
UV-Vis	Ultraviolet-visible absorbance spectroscopy
WHO	World Health Organization
XPS	X-ray photoelectron spectroscopy
XRD	X-Ray diffraction spectroscopy

ABSTRACT

Black carbon (BC) is an environmental pollutant of particular concern to many international organizations for both its health effects and environmental effects. Fluorescent carbon dots (FCDs) were chosen to be used as a surrogate to evaluate BC individually. Characterization of the FCDs occurred with the use of dynamic light scattering (DLS), low-resolution transmission electron microscopy (LR-TEM), high-resolution transmission electron microscopy (HR-TEM), infrared spectroscopy (IR), X-ray photoelectron spectroscopy (XPS), and electron-paramagnetic spectroscopy (EPR). Evaluation of the optical properties were studied using fluorescence spectroscopy. The photostability, chemical stability, and physical stability was tested as well. The FCDs produced in this research ranged in size from 10-50 nm, exhibiting a graphene oxide structure with suggestions of hydroxide functional groups on the surface and semiquinone-type radicals. Fluorescence quenching was also tested. Metal ions were tested for their ability to quench the fluorescence of the FCDs, followed by a testing of fluorescence recovery by a reducing agent. Ferric ions were the optimal quencher, quenching 100% of the fluorescence. Only limited fluorescence recovery was possible. Characterization of the FCDs before and after fluorescence quenching allowed for proposal of a quenching mechanism. The proposed mechanism, involving the stabilization of a semiquinone radical by the ferric ions is the first of its kind reported in literature to this point. Cellular studies regarding the health effects of the FCDs, and therefore BC, was performed on lung epithelial cells (BEAS-2B). Uptake was evaluated by confocal fluorescence imaging and LR-TEM. Cytotoxicity was evaluated by trypan blue assay, MTT assay, and MTS assay and revealed cytotoxic effects when FCDs are exposed to cells for long time periods (8 hours) and high concentrations (8 mg/mL). The metal ion quencher increases the overall toxicity of the FCDs. Through an evaluation of the GSH:GSSG ratio, no cellular oxidative stress

was witnessed at short time periods, though further study is warranted. The cell studies of FCDs in this dissertation are more comprehensive regarding time period and FCD concentration than any found in literature.

CHAPTER 1
INTRODUCTION

1.1 Research Goals and Aims

The World Health Organization (WHO) estimates that particulate matter (PM) air pollution contributes to approximately 800,000 premature deaths each year as of 2011, ranking it the 13th leading cause of mortality worldwide.[1-3] PM is an incredibly heterogeneous material, consisting of extremely small particles and liquid droplets made up of acids, organic chemicals, metals, and soil or dust particles.[4] The extreme variability within PM makes it difficult to assign effects to PM as a whole or to individual causal agents within the PM. While this holds true, there are specific classes of materials within PM causing concern and interest, particularly $PM_{2.5}$, which is PM with a physical diameter less than 2.5 μm. $PM_{2.5}$ is known to travel faster within and deeper into the respiratory tract than larger PM species, causing greater health concerns. A particular $PM_{2.5}$ species of great interest to the Environmental Protection Agency (EPA) and the WHO is black carbon (BC). BC is partially combusted carbonaceous material composed of a variety of materials having a broad set of characteristics.[6] While extensive techniques and methodologies exist to analyze the composition of $PM_{2.5}$ as a whole, concerns are arising about the individual components and their effects. In fact, it is becoming more obvious that mass and diameter of the PM alone might not be able to explain the difference in health effects caused by $PM_{2.5}$. It is more likely the health effects could be due to the wide range of elements and chemical functionalities present, resulting in increased complexity in terms of composition and concentration.[7, 8] Methodologies to analyze individual components within $PM_{2.5}$ samples are difficult to create due to an inability to isolate individual components from within $PM_{2.5}$ collected from environmental analysis stations. To overcome this limitation in real-world conditions, surrogates for analysis of PM components can

be created to simulate the individual components and provide insight into their specific health effects.

The McCarley Group, through affiliation with the Louisiana State University (LSU) Superfund Research Program, has spent considerable time researching individual environmental health causative agents by recreating surrogates for them in a laboratory setting to analyze them as singular components rather than as a mosaic of thousands of components.[9] Development of a surrogate for BC would provide the ability to analyze the health effects, both in terms of mortality of cells, as well as cellular environment, and to determine both short- and long-term effects. If this surrogate is able to be actively monitored, it allows researchers to measure many different cellular interactions, including uptake mechanism (if the particles are taken up by the cells), localization within the cell, cell environmental effects, and short- and long-term cell viability. All of these factors are necessary considerations, as many of the health effects and diseases attributed to $PM_{2.5}$ and its component materials are associated with long-term extended exposure diseases, such as cardiovascular disease in the form of increased size and rate of atherosclerotic plaque formation, increased oxidative stress, cardiac arrhythmias, increased thrombus formation, and increased inflammation and oxidative stress in the heart.[10-12] Complementary to cardiovascular disease, PM2.5 can also affect the respiratory system through increased respiratory inflammation and exhaled nitric oxide (a known measure of airway inflammation), which can lead to exacerbation or development of respiratory diseases such as asthma and chronic obstructive pulmonary disease (COPD).[13-15]

Fluorescent monitoring of cellular interactions is a common and well understood technique, as it offers many tunable features, such as excitation and emission wavelength, intensity, fluorescence lifetime, and emission anisotropy. It also easily offers micrometer-scale

resolution and can offer nanometer-scale resolution and sensitivity down to the single-molecule level by using super-resolution confocal techniques. Selecting an imaging modality best suited for answering the question at hand, namely learning how pollutants, in the form of surrogates, interact with living cells, is vital when designing a system for cellular analysis of a specific pollutant through a surrogate. In the case of BC, the fluorescent material needs to mimic BC while also allowing for efficient analysis using fluorescent microscopy techniques. Fluorescent carbon dots (FCDs) fit the necessary characteristics, existing as carbonaceous materials similar to BC, with elemental components comparable to those commonly found in environmentally produced BC, thereby allowing for a high degree of control over the fluorescence mechanism through passivation or particle modification. Beyond those characteristics, it is a commonly known feature of FCDs that their fluorescence can be turned off and on via various, ill-defined paths, whose mechanisms are yet to be elucidated at the molecular level.[16-18] Understanding and thus being able to gain control over the off-on mechanism would allow for sophisticated cellular analyses of the transport and cellular impact of BC as a PM material, in the form of their surrogates. For example, by using the known quenching of FCD fluorescence with metal ions,[19-21] one could take advantage of the possibility of a fluorescence turn-on process resulting from FCD entrance into cells and their reduction by electron-donating species, such as glutathione (GSH), reduced nicotinamide adenine dinucleotide (NADH), or reduced nicotinamide adenine dinucleotide phosphate (NADPH).

The overall goal of my dissertation project is to design an analytical system to probe the cellular environmental effects of BC, a form of $PM_{2.5}$, through use of an FCD "turn-on" biosensor, as seen in Scheme 1.1. To attain this goal, specific research aims are: design a synthetic approach to create a fluorescent moieties that mimic BC, namely FCDs, followed by modification of said FCDs with metal ions such as Cu, Ni, and Fe to turn off the fluorescence. Once accomplished, a

"turn-on" mechanism will be established through reduction of the metal ions complexed with the FCDs upon cellular uptake by intracellular reducing agents such as GSH, NADH, or NADPH, allowing for analysis of uptake and localization within the cell with minimal background signal and high signal-to-noise ratio. While some of these specific aims could not be achieved, namely the "turn-on" mechanism, an understanding of the fluorescence "turn-off" mechanism was developed through extensive research experiments, which offer insight into the fluorescence mechanism itself.

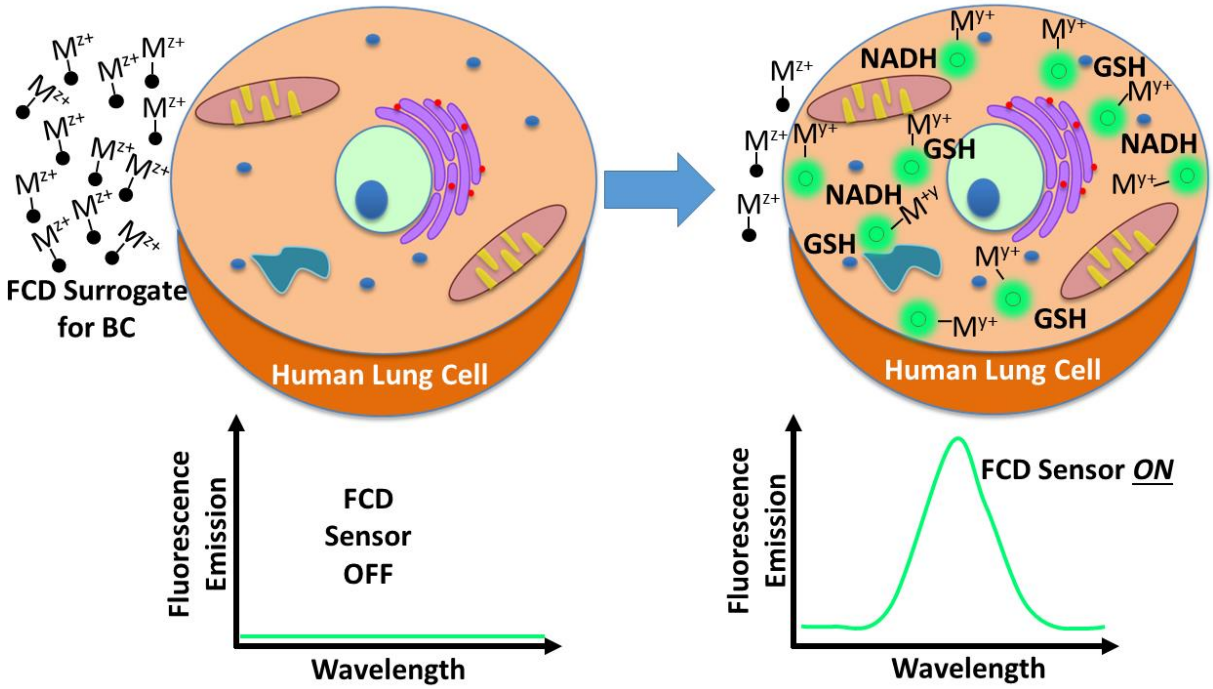

Scheme 1.1. Fluorescent carbon dots (FCDs) exposed to metal ions (represented by the **black** dots bound to M^{z+}) of various identities show a complete quenching of fluorescence, as seen in the representative fluorescence spectrum on the left side. Upon entrance of the turned-off FCDs into the cell, the charge on the metal ion is changed by the reducing agents within (GSH and NADH), showing a complete recovery of fluorescence in the FCDs (represented by the **green** dots bound to M^{y+}), seen in the representative fluorescence spectrum on the right.

1.2 Particulate Matter (PM) as an Environmental Pollutant

Particulate matter (PM), as an environmental pollutant, has been an issue connected to human health going far back in our history, as described below. Notable cases include a case in the Meuse Valley in Belgium in 1930, where several thousand people suffered acute pulmonary failure and 60 individuals died due to sulfur dioxide gas coupled with PM from factory emissions. Similarly, in London in 1952, sulfur dioxide gas and smoke PM caused over 3000 deaths in a three-week period. [22, 23] In these examples of large cases, the direct effects of high levels of PM can be readily observed on a large scale. PM presence in the atmosphere, and therefore long-term exposure, is most severe in urban centers. Unfortunately, the large populations in those urban centers can make evaluation of health effects due to PM difficult to identify amidst the large amount of health issues from other sources found in those large populations. PM was expressed to be a serious public concern in 1970 when the United States of America passed the *Clean Air Act*, which labels PM as a pollutant and places limits on its emission into the environment.[24] Health studies have since become more common in connecting PM and health effects, the latter primarily including cardiovascular[25-27] and respiratory[28-30] health effects. Systematic inflammation of the cardiovascular system is mediated by cytokines IL-6, TNF-α, and C-reactive protein (CRP) that regulate inflammation. Development of acute myocardial infarction has been shown to be linked to witnessed increases in IL-6 and CRP. Rucker et alia described elevations in both IL-6 and TNF-α in patients exposed to PM_{10} 2 days subsequent.[31] Other studies have shown increases in CRP upon exposure to both PM_{10} and $PM_{2.5}$, once again pointing to a higher likelihood of cardiovascular inflammation and myocardial infarction.[32-34] In addition to inflammatory effects seen in the cardiovascular system, decreases in overall respiratory function have been witnessed upon patient exposure to increased amounts of PM. Horak et alia showed a relationship between increased

organic fractions in PM and decreased lung function parameters in what exposed to PM containing the various amounts of organic materials.[35] One study showed the very interesting observation of a linear relationship between increasing levels of PM in a given residential area and admissions of residents within the area to a hospital or clinic for respiratory illness.[36] Interestingly enough, an equal number of papers have performed similar experiments with contradictory results, finding limited or no correlation between PM exposure and increased inflammatory response.[37-40] It is believed this apparent discrepancy results from differences in composition, variable exposure to anti-inflammatory medications, and differences in obtaining PM exposure data. What makes PM dangerous? Is it the size of the PM, the composition of the PM, the length of exposure, a combination or none of the above? These questions must be answered to fully determine countermeasures for PM exposure or motivation for preventing its production from anthropogenic sources.

One significant factor in the danger of PM is the size of the PM itself. It has long been known that the size of the particle in PM, better defined as the aerodynamic equivalent diameter (AED), determines much about its overall ability to contribute to health impacts. Traditionally, the AED allows for the classification of particles based on where the particles deposit in the human respiratory tract: PM_{10} (particles less than or equal to 10 μm in size), $PM_{2.5}$ (particles less than or equal to 2.5 μm in size), and $PM_{0.1}$ (particles less than or equal to 0.1 μm in size). In analyzing PM_{10}, it is difficult to attribute health effects to individual classes within PM_{10} due to the large amount of small particles that dominate the PM as compared to the smaller amount of large particles. Though the mass of PM significantly decreases with particle diameter, the number of particles in the ultrafine region (less than 100 nm in diameter) increases dramatically, as seen in Scheme 1.2. PM_{10}, due to its large size, tends to settle in the upper respiratory tract, allowing for

the human body to easily filter and subsequently dislodge it from the nose and upper airway, making PM_{10} slightly less dangerous than $PM_{2.5}$ and $PM_{0.1}$ in terms of respiratory impacts. The two smaller forms of PM, $PM_{2.5}$ and $PM_{0.1}$, are defined as fine and ultrafine, and they tend to accumulate much lower in the respiratory tract, particularly around the alveoli in the lungs, thereby

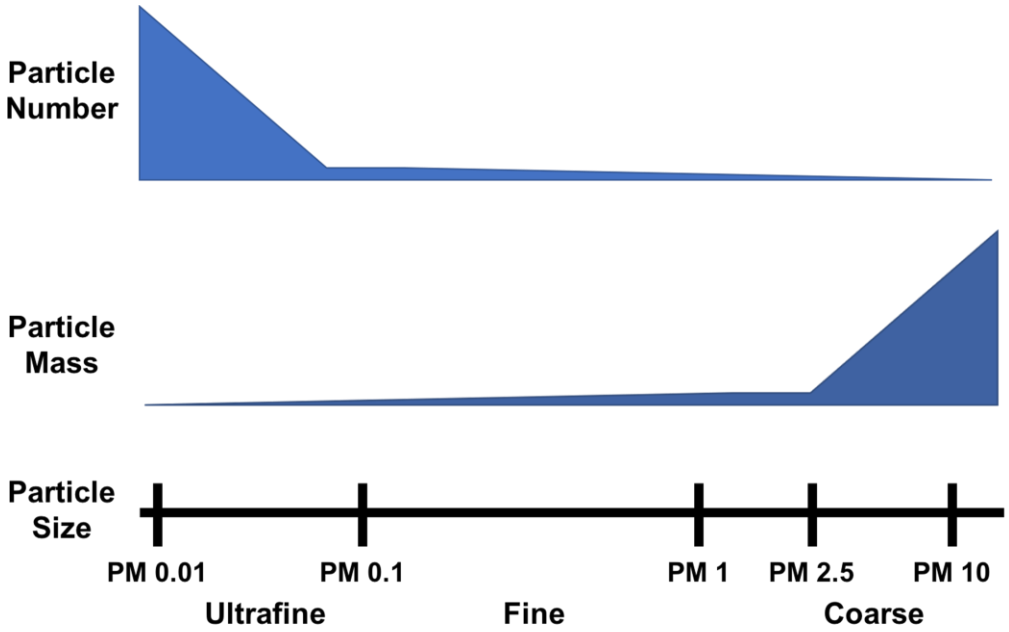

Scheme 1.2 Hypothetical breakdown of PM shows that though the total mass decreases exponentially due to ultrafine and fine particles, the number of those particles increases proportionally.

inhibiting oxygen exchange and leading to negative respiratory effects.[41] In fact, the fine and ultrafine PM classes have been shown to have the ability to translocate to organs other than the lungs, including the liver, brain, and central nervous system if the exposure is sufficiently severe and long term.[42]

1.3 Black Carbon

One class of $PM_{2.5}$ of great concern is black carbon (BC). Black carbon is an interesting component of PM to research, considering it is hailed as one of the key atmospheric particulate components driving climate change, air quality, and health effects. At the same time, there is no

clear definition or agreement on terminology defining its specific properties, definitions, measurement methods, or related uncertainties.[43] In a terminology review, Petzold et alia made an attempt to unify the terminology regarding BC with respect to its properties and measurement techniques. After an examination of the literature before and after the review was published, it seems Petzold's unification of terminology showed limited success. Their final definition for BC requires quite a few qualifiers:

> Black carbon (BC) is formally defined as an ideally light-absorbing substance composed of carbon. The formation process is excluded from this definition because of a variety of potential processes. While BC is mostly formed in incomplete combustion of carbonaceous matter, it can also be a product of pyrolysis of carbonaceous matter, i.e., the change of the chemical structure of carbonaceous compounds from the loss of hydrogen and/or oxygen atoms at temperatures above approximately 250 °C, of dehydration of sugar, or of heating of wood under and oxygen-free atmosphere…[43]

This definition, while establishing some key characteristics of BC, also emphasizes that BC is composed of an incredibly large number of categories of carbonaceous material, which is also abundant in environmental PM. The primary factors that can be used to describe BC are microstructure, morphology, thermal stability, solubility, and light absorption. Each of these factors can be used to define BC and establish its characteristics.[43]

The microstructure of BC is primarily graphitic carbon, consisting of layered graphene-like structures that contain a large amount of sp^2-hybridized carbon, though oxygen integrated into the structure can give a graphene oxide functionality while maintaining the sp^2-hybridization rather than diamond sp^3-hybridization, Scheme 1.3. This definition is vague, with generalized terms such as "graphite-like" and "large amount of sp^2 carbon" used, but it is the best definition that can be formed from the contributions of multiple research groups studying carbonaceous materials in the air.[43]

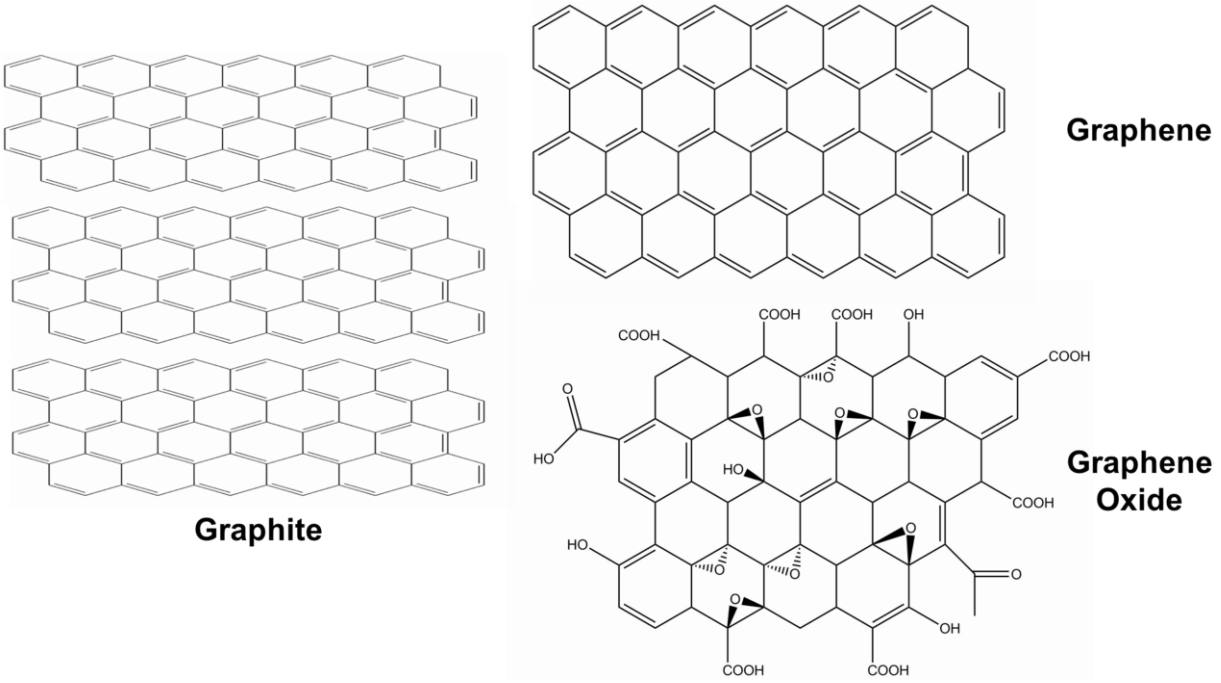

Scheme 1.3 Graphene is a carbonaceous structure made up of primarily sp2 carbon, with sp3 carbon spaced throughout. Layers of graphene form graphite. Graphene oxide is oxidized graphene, exhibiting oxygen functionalities throughout the structure, such as oxygen, hydroxyl groups, and carboxylic acids.

The most common method currently used to analyze the microstructure and morphology of carbonaceous materials from the atmosphere is Raman spectroscopy. Sze et alia analyzed the Raman spectra of different carbonaceous materials, such as briquetting graphite, synthetic graphite, powder graphite, crystalline graphite, glassy carbon, and activated carbon to determine characteristic Raman spectral energies (shifts) for each of these carbonaceous materials.[44] The shifts of greatest import to the research were those assigned to bulk crystalline graphite and graphite layers near the surface of the crystals. To evaluate the methods in a real world setting, carbonaceous materials were collected from diesel exhaust fumes and other environmental samples in urban settings. The carbonaceous materials collected had different properties and Raman shifts, but the shifts assigned to bulk graphite and graphite layers near the edge of the crystal were found

throughout the collected materials, implying a high level of graphite crystals present in the particulate matter. The differences were believed to be caused by variation in particle size, functional groups within and on the surface of the particles, and particle morphology.[44] Ivleva et alia took it a step further, establishing a 5-spectra Raman band matching process to establish the different amounts of BC and elemental carbon (EC) in atmospheric PM.[45] EC exists as essentially pure carbon, rather than being chemically combined with hydrogen and/or oxygen, in amorphous or crystalline structures.[46] Many more groups support these findings based on Raman spectral analysis.[47, 48] The significant characteristic imparted to BC based on its crystalline structure is low chemical reactivity in the atmosphere, leading to its slow removal by chemical processes. This property of BC and its closely related fellow carbonaceous material, carbon black, is extensively known and used in many filtration and extraction processes.[49-51]

BC, being mostly sp^2-hybridized carbon, whether in the form of graphene or graphene oxide, tends to form in a way that yields a structure possessing sheets similar to graphene, but the small amount of sp^3-hybridized carbon present in the BC structure gives it a morphology that is slightly different than graphene itself. The sheets of BC are either arranged in layers of larger sheets, similar to graphene, or are aggregated in the form of spherical "onion" shapes, with layer upon layer forming a spherical shape, as seen in Scheme 1.4.[6]

These graphitic spheres have diameters that usually range from 10–50 nm, with surface areas that range from 10 $m^2\ g^{-1}$ to 100 $m^2\ g^{-1}$. Beyond aggregating possessing spherical clusters, it is also a common feature of BC to have morphological features composed of aggregates of many particles connected in a long chain, creating structures having dimensions into the micrometer range.[52] The morphology of BC structures has been studied extensively by high- and low-resolution transmission electron microscopy (HR-TEM and LR-TEM).[53, 54] Further analysis into

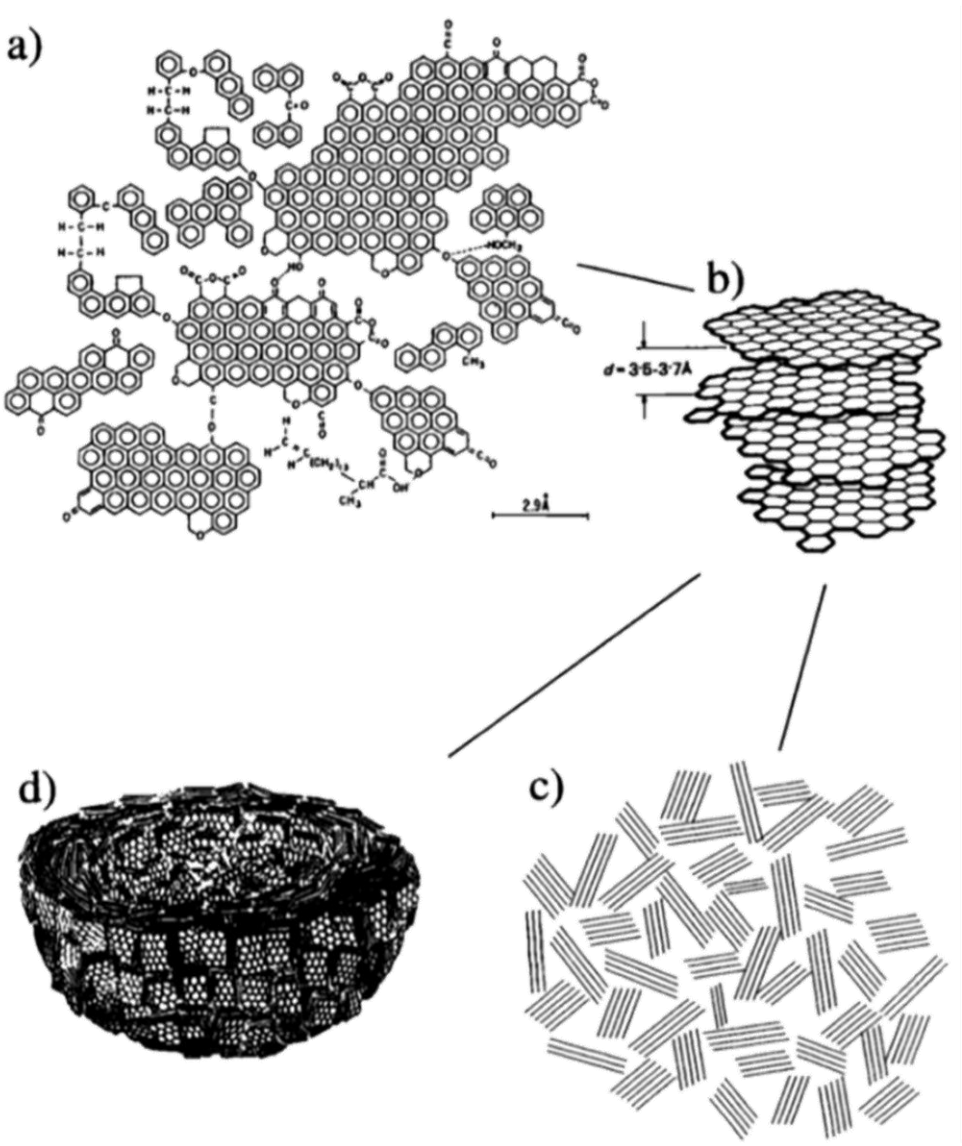

Scheme 1.4 Black carbon (BC) has, at its foundation, a graphitic-like structure made up of primarily sp^2 carbon with some sp^3 carbon throughout the structure as well, as seen in **a)** above. Unlike graphene, BC can also have other elements throughout its structure, giving it the ability to form sheets as seen in **b)**, but also to form "onion" type structures made up of overlapping sheets of BC as seen in **d)**.[6]

the morphology and structure, and also the elemental composition, is ongoing with near-edge X-ray absorption fine structure spectroscopy (NEXAFS). NEXAFS confirms the previously discussed morphology and also establishes the presence of structures and functionalities, such as aromatic hydrocarbons, quinones, carbonyl (C=O), carboxyl (COOH), and alcohol (C-OH) groups

throughout the structures, leading BC to possess the ability to readily sorb and carry other atomic or molecular groups when exposed to them in atmospheric conditions.[55]

The high temperature ranges that are a part of the processes that naturally produce BC impart a certain amount of thermal stability to the BC particles, allowing them to remain stable in the atmosphere at varying ranges of temperatures. BC is formed by an exothermic reaction of carbonaceous source material, which occurs between 280 °C and 500 °C. The most common sources of BC are wildfires or the burning of other biomass, which lead to transformation of as much as 90% of the original carbonaceous material into particulate matter in the form of BC, depending on burning conditions.[56-59] The burning of fossil fuels is a more common source of BC, with the amount and composition of the BC varying with the level of efficiency in the burning of fossil fuels. Coal, the largest fossil fuel source of BC, has seen optimization of burning processes in developed countries, leading to overall decreases in BC production. Therefore, the largest amounts of BC are produced from coal burning in developing countries that are not in a position to optimize burning efficiency.[60-62] Once BC has been created, its thermal stability is a well-known property, with no volatilization of the solid carbon nanoparticles in inert atmospheres at temperatures up to 3800 °C. Its gasification occurs only through oxidation at temperatures exceeding 340 °C.[63, 64] In a more real-life study, heating and subsequent measures of thermal stability show BC stability at temperatures ranging from 450 °C to >850 °C, depending on the composition of both the interior and exterior of the BC.[65] This variation in thermal stability is attributed to the stability of aromatic compounds against thermal oxidation, showing a trend of proportionality between degree of conjugation and stability. Additionally, and more importantly, there exists a positive correlation between the degree of molecular order and oxidative thermal stability, with an overall trend of higher crystallinity imparting thermal stability at higher

temperatures.[66-68] This high level of thermal stability gives BC a low reactivity in the atmosphere and allows for a much longer atmospheric residence time.

The solubility of BC in solvents is a vital part of what classifies a material as being denoted or classified as BC. While the origin of the solubility trends exhibited by these FCDs could not be determined by this scientist, the lack of solubility in water as well as organic solvents, such as ethanol and acetone, is a commonly recognized property of BC across literature.[69-72] While references confirming the insoluble nature of BC are numerous, it is worth acknowledging the variability in terminology and description when discussing BC again. As mentioned above, according to most literature, BC is insoluble in water, but many papers discuss dissolved black carbon and its existence in dissolved organic

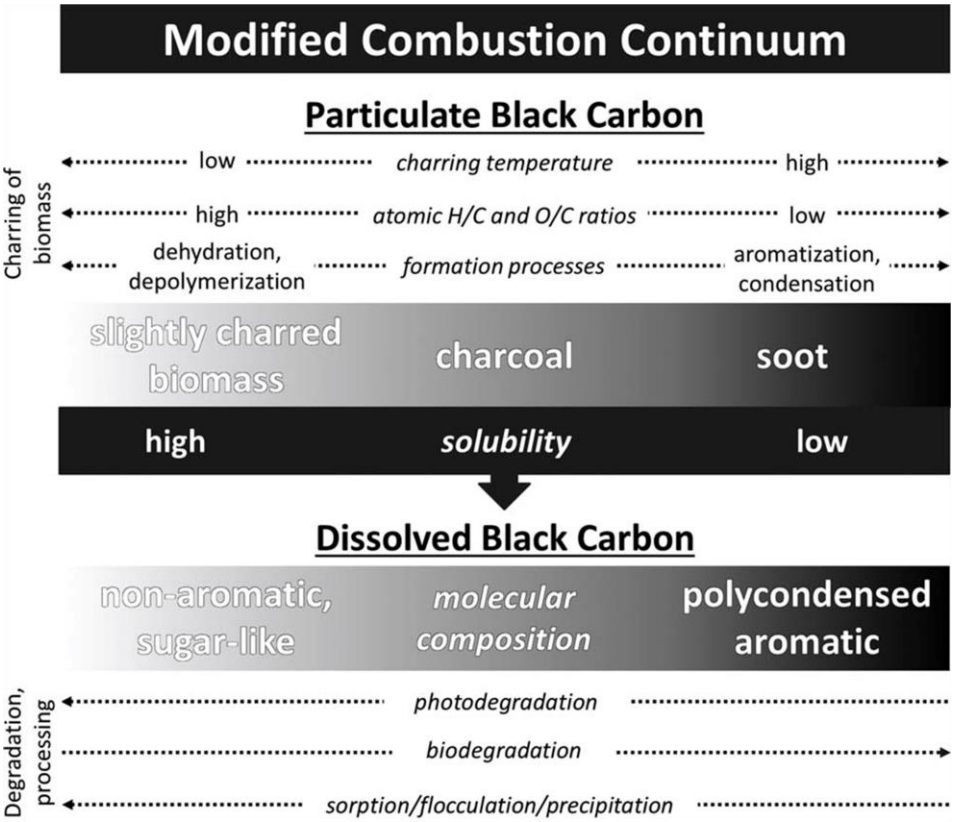

Scheme 1.5 Black carbon (BC), rather than existing as an insoluble environmental pollutant, exists on a spectrum of solubility; soot (highly charred and degraded carbonaceous material) maintains low solubility, but the slightly charred biomass is soluble.

matter.[73-77] Rather than thinking about BC as an insoluble substance, it seems wiser to consider a solubility continuum, as seen in Scheme 1.5.[78]

When carbonaceous material undergoes combustion, the differences in the charring temperature, atomic H/C and O/C ratios, and formation processes can all have an effect on the exact type of carbonaceous material produced, though all of it can be classified as BC. When the starting material is combusted at higher temperatures and thus more completely combusted and charred, the result is soot that possesses low solubility in water. On the other hand, if the combustion occurs at lower temperatures and is thus less thorough, the slightly charred biomass produced is soluble in aqueous solutions. High levels of conjugation due to large amounts of aromatic molecules produce less soluble atmospheric BC, while more soluble atmospheric BC is produced through interactions with ozone, generating extensive carboxylic acid groups across the surface of the individual BC particles.[69, 70] The general insolubility of BC gives it the property of atmospheric stability, being slow to leave the atmosphere and clouds through precipitation unless water-soluble groups are added to the surface of the BC, such as through interactions with ozone, as discussed previously.

The fifth and final, but arguably most significant property of BC is its light absorption. The name black carbon is a result of the ability of the PM to strongly absorb light in the visible and near-visible spectral ranges of the electromagnetic spectrum. BC is considered to have a mass absorption cross section of at least 5 m^2g^{-1} at a wavelength of 550 nm.[79, 80] This large absorption cross-section makes BC the strongest absorbing of any particulate matter of significant presence in the atmosphere. The strong light absorption properties of BC make it the ideal class of PM to use when developing spectroscopic methods to study airborne PM.[81] In fact, the first published use of an aethalometer to measure PM in the air was by Hansen et alia to measure BC due to its

nature as a consistently strong-absorbing airborne PM. In fact, the aethalometer was named after BC; its name is based on the Greek word, "αιθλουν," meaning, "to blacken with soot."[82] In the process of developing the aethalometer and its use in analyzing airborne PM, BC was studied to determine the impact of atmospheric conditions on its light absorption properties. The absorption properties were not believed to be particle size dependent, based on scattering principles, as well as the principles governing fractal clusters, and indeed that was proven; the absorption cross section remained unchanged relative to particle size.[83, 84] It was determined the most prominent variable affecting the absorption cross section and attenuation of the BC particles was the purity of the BC in regards to contaminants that absorb minimal light, but scatter extensively, termed transparent in this study. When in the presence of these highly scattering transparent constituents, light unabsorbed by the BC is continuously scattered back onto the BC until the light is absorbed, amplifying the witnessed absorption properties.[85] The ability of BC to absorb large amounts of light, particularly in the atmosphere, leads to the most significant impact BC has beyond health effects: its effect on global climate.[5]

As stated before, BC has the strongest light absorption per unit mass of any substance in the atmosphere in significant quantities. This ability to absorb large amounts of light, coupled with its long retention time in the atmosphere due to its low chemical reactivity and solubility, makes BC an important atmospheric component influencing global climate. These effects are far reaching, and are broken down very well by Bond et alia in Scheme 1.6.[5] The effects of BC on climate are very complex, with BC existing within clouds contributing to both cooling and warming effects, depending on the nucleation behavior within the cloud. Limited nucleation in the clouds leads to increased cloud lifetime, and if BC is within the liquid clouds in significant quantities, there is increased reflectivity, resulting in net cooling. BC can also decrease the lifetime

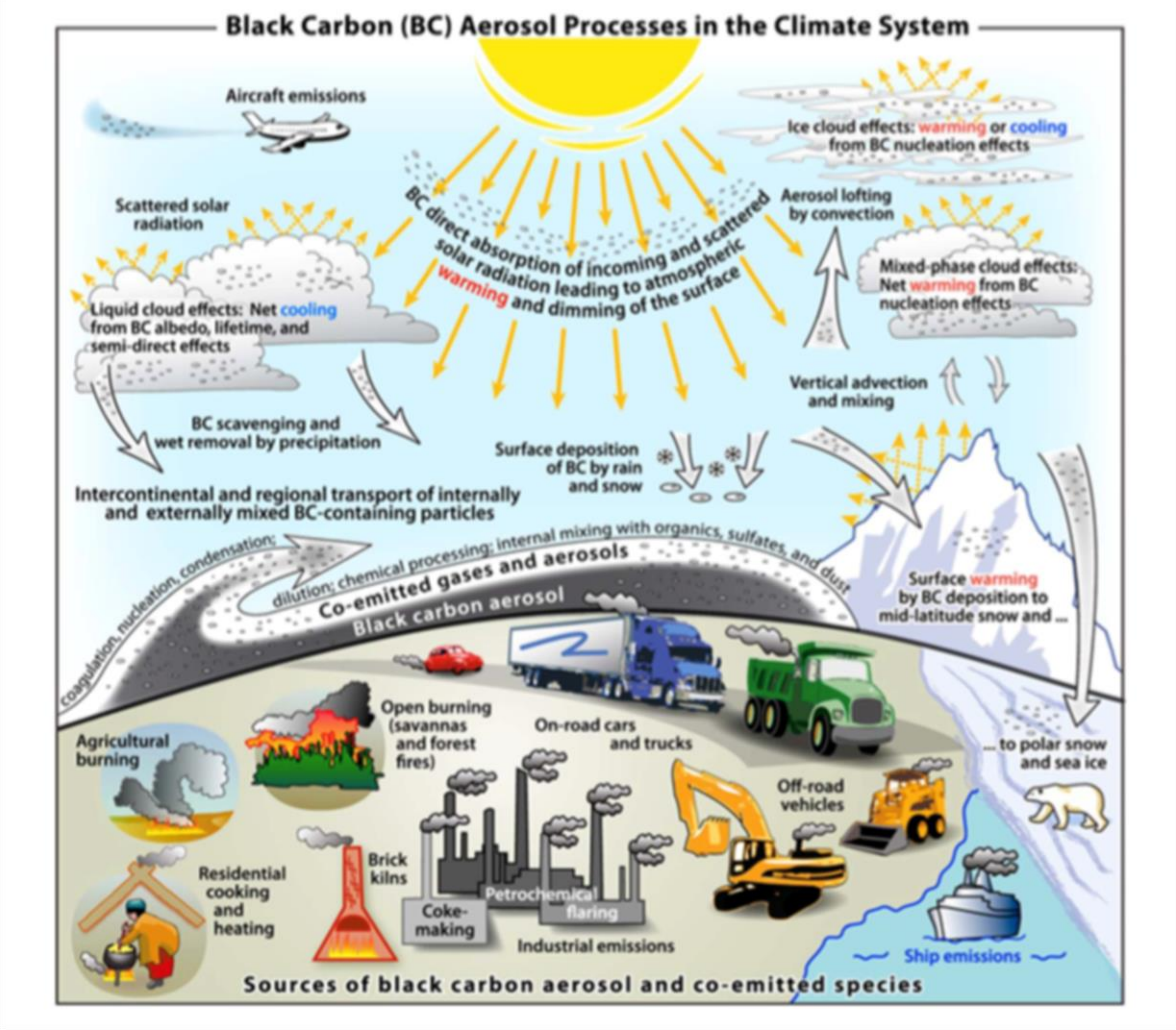

Scheme 1.6 Black carbon (BC) is emitted from many sources and has effects on global climate through atmospheric effects as well as surface effects due to deposition. [5]

of clouds if nucleation is extensive, causing cloudlessness and resulting in net warming.[86] The two main impacts of BC that are not variable take place in the atmosphere and on the surface, respectively. The atmospheric impact is a relatively simple process: with BC in the atmosphere absorbing large amounts of solar radiation, net warming of the atmosphere occurs. If the highly absorbing BC is centered above reflective surfaces, further atmospheric temperature increases occur. When solar radiation reflects from the surface back into the atmosphere containing BC, more radiation is absorbed, continuing the increase of the atmospheric temperature. Both of these

features can couple so as to increase global surface temperature, due to solar radiation not being able to escape back through the atmosphere, but these effects can also limit the amount of sunlight reaching Earth's surface. This lack of sunlight reaching the surface can result in large-scale alterations to the hydrological cycle through changes in latent heating, convection, and large-scale circulation patterns.[5] These combined effects of BC have been theorized to cause significant environmental impacts on large scale producers of BC and other organic pollutants, such as increased floods in south China and increased droughts in north China, India, and Afghanistan.[87]

Highly reflective surfaces, such as snow or ice decrease the global surface temperature, due to their low level of solar radiative absorption and high level of solar radiative reflection. When BC deposits on these naturally reflective surfaces, that relationship shifts from highly reflective to highly absorbing due to the large absorption coefficient of the BC, causing an increase in the surface temperature. This heating can cause increased melt rates, increased water levels, and other global climate changes.[88, 89] In 2005, the Goddard Institute for Space Studies' General Model-II Prime, coupled to a mixed-layer ocean model, predicted BC would be responsible for an increase in the annual surface air temperature by 0.20 K globally, with that number increasing to 0.37 K if sulfate aerosol levels in that year are added to the General Model-II Prime predictive software.[90] These well-established environmental and health effects of BC make it an important class of PM for study. To that end, Study of BC health effects and biological impacts of BC begins with a study of BC on a cellular level. Fluorescent methodologies offer an effective method to study many facets impacting cellular health: cellular uptake, localization, and cellular environment effects.

1.4 Fluorescence Spectroscopy and Quantum Dots

Fluorescent materials used for biological analysis are varied in both their mechanisms and excitation/emission wavelengths, providing a wide range of applications and experimental

workflows. Of particular interest to this research are fluorescence mechanisms for biological imaging. For fluorescent labels or trackers to be efficacious in biological studies, there are a range of characteristics that they must possess to varying degrees dependent upon the situation: convenient excitation with little background excitation, high molar absorption coefficient; sufficient quantum yield; solubility in relevant buffer, media, or bodily fluids; sufficient stability; known photophysics; and availability in sufficiently reproducible quantities. While there are always more considerations depending on the experiment, these are the primary characteristics of an effective biological fluorescent probe.[91]

Additionally, when selecting the most appropriate fluorescent probe to use as a BC surrogate, it is vital to ensure that it: (1) has synthesis conditions similar to those of BC production in order to ensure the fluorescent probe resembles BC in terms of chemical and physical microstructure and morphology, (2) possesses photo-, chemical, and thermal stability to ensure long-term cellular studies are possible, and (3) possesses no toxicity due to an induced fluorescence mechanism that is not found in naturally occurring atmospheric BC.

Arguably the most common fluorescent probe used to study biological materials are organic dyes. These probes can stain individual organelles and proteins, or even the entire cell. Recently, there has been a large push to develop fluorescent protein-based indicators, due to their ability to respond to a much greater variety of biological events and signals, be targeted to subcellular compartments, be introduced into a wider variety of tissues and intact organisms, and rarely cause photodynamic toxicity.[92] In fact, the McCarley group at LSU is known for its development of protein-activatable fluorescent probes, particularly for the targeting of hNQO1, a quinone oxidoreductase that makes use of NADPH to remove reactive oxygen species from the cell.[93, 94] As surrogates for BC, organic dyes meet requirement 3 with little to no innate toxicity

in most dyes, but requirements 1 and 2 are not met. Organic probes exist as small or large molecules rather than nanostructures like BC, meaning their microstructure and morphology are drastically different than BC. Additionally, organic dyes can suffer from poor photo- and thermal stability, limiting their ability to mimic combustion formed PM and perform long-term health fluorescent studies.[95-99]

Quantum dots (QDs) are another successful and thoroughly studied fluorescent probe that has generated much excitement in recent years, QDs are a type of nanostructure having dimensions <100 nm, which typically exhibit a distinct change in optical and electronic properties with systematic variation of particle size. A QD is zero-dimensional relative to the bulk, meaning no dimensions of individual nanoparticles are greater than nanoscale, and the limited number of electrons found within a QD results in discrete quantized energies in the density of states for non-aggregated zero-dimensional structures. [100, 101] Beyond this technical definition, a simpler description of QDs is that they are nanocrystal chromophores with size-dependent optical and physiochemical properties. The materials making up these QDs are very diverse, including semiconducting metals,[102, 103] carbon,[104] silicon nanoparticles,[105] or even self-luminescent organic nanoparticles.[106] The definition for QDs can be relatively broad, encompassing all of the previously mentioned structures, but in typical terminology QDs refer to metal or silicon fluorescent nanoparticles, as their fluorescence mechanisms are similar and well understood. Depending on the specific type of QDs one is discussing, the qualifications for a BC surrogate is met to varying degrees. Unfortunately, based on requirement 3, toxicity is a concern when considering QDs as surrogates. Many papers have reported QD toxicity, resulting in cell phenotype abnormalities or even cell death,[107-109] but interestingly enough, many papers have also reported no negative effects whatsoever.[110-112] This variability in health effects witnessed upon exposure

of cells to QDs has been proposed to be linked specifically to Cd ions within the QDs and the stability of those Cd ions.[108] While QDs hold great promise, any risk of cytotoxicity has to be considered a negative factor in their evaluation as a surrogate for BC.

Carbon-based QDs present an effective dual modality considering they have the efficiency and stability of QDs, while their carbon structure limits toxic effects from heavy metals such as Cd. Additionally, carbon-based QDs possess a structural and chemical composition similar to that of BC, a mixture of sp^2 and sp^3 carbon with primarily graphitic carbon structures. They also generally contain low elemental diversity, consisting primarily of carbon, hydrogen, oxygen, and trace nitrogen. This results in limited chemical moieties, including carboxylic acids, aromatics, quinones, and other carbon-/oxygen-based functional groups. The difficulty in using carbon-based QDs arises when considering their fluorescence mechanism. While the fluorescence mechanism and resulting properties of metal-based QDs are well understood and agreed upon, carbon-based QDs possess a fluorescence mechanism that is not uniformly agreed upon, with large variation in the suggested mechanism across varying synthesis methods and research groups. In fact, this discrepancy has led to many scientists referring to carbon-based QDs by a different name, fluorescent carbon dots (FCDs). Despite the discrepancy among scientists, an understanding of the fluorescence mechanism of QDs can allow for a subsequent understanding of the general fluorescence properties and uses of FCDs. While the mechanism of fluorescence in QDs is incredibly complicated, and has many exceptions and rules that govern it, a simplified explanation follows, disregarding exceptions and complex rules for the purposes of this research.

Fluorescence in QDs is produced by excitation of an electron by an outside energy source, in this case, a photon. When the electron absorbs the photon and is excited from the valence band to the conduction band, the space left behind by the electron as it moves out of the valence band

is referred to as an electron hole, which possesses a positive charge.[113] In QDs, due to their zero dimensional nature, when the electron and hole charge carriers are produced, both are trapped and have well-defined energy levels.[101] The Coulombic forces between the electron and hole cause the two charge carriers to exist in an electrically neutral quasiparticle known as an exciton. In QDs, excitons typically exist on the nanosecond scale, before the electron collapses back to its ground state, thereby filling the hole, which releases excess energy in the form of photons, producing fluorescence.[114]

The emissions produced from this process are referred to as intrinsic state emissions. What makes QDs special is the way that this fluorescence is governed by surface states, which are electronic quantum states resulting from unsatisfied bonds at the surface of the QDs that result during their synthesis. Considering QDs have extremely high surface-to-volume ratios with roughly 15% of the atoms in a 5-nm diameter QD existing on its surface, the surfaces of QDs possess an abundance of surface states if the synthesis method is not specifically tailored to minimize surface states.[115] The energies of these surface states tend to lie directly in the band-gap of the QDs, allowing them to trap both electrons and holes.[116] In general, the surface states reduce the quantum yield of the QDs by trapping the electrons and holes, effectively quenching formation of excitons and thus yielding radiative recombination.[117] This reduced radiative recombination effect can be seen more drastically in "blinking," whereupon QDs cycle from periods of fluorescence to quenched fluorescence and back. Rather than being due to surface states themselves, "blinking," is believed to be the result of ionization at the surface of the particles. Unlike surface states, which occur only in individual locations on the surface of the QDs, ionization occurs over the entire surface of the particles. The effect of the ionization is the same as the surface states, reducing the formation of excitons and subsequent radiative recombination,

though spread over the entire surface, decreasing the quantum yield by a much larger amount.[118, 119] This demonstrates the ability of a charged particle or surface to disrupt the recombination process of electron and hole, effectively quenching the fluorescence. It is worth noting that while surface states most often reduce the quantum yield, it is possible for them to increase the quantum yield through a process known as defect emission. This process occurs when a surface state has trapped enough electrons and holes that it has an excess amount of those species. If a surface state has trapped an abundance of holes, when an electron finds its way into the same surface trap, the electron has an abundance of holes it can form an exciton with, thereby producing fluorescence.[120] As stated above, this was only a cursory review of the fluorescence mechanisms of QDs, with many details and specific conventions not mentioned. Knowledge of the fluorescence mechanism of metallic QDs will help with the discussion of FCDs as a technique for fluorescence spectroscopy studies.

1.5 Fluorescent Carbon Dots

Fluorescent carbon dots (FCDs) are referred to by many names in literature, including FCDs, carbon nanodots, carbon quantum dots, and carbon nanoparticles. FCDs are nanocarbons, nanometer scale structures made of carbon with sizes generally below 10 nm, typically exhibiting particle size- and excitation-dependent photoluminescence. Some other common qualities of FCDs are excellent water solubility due to carboxylic acid surface groups, well-defined, nearly isotropic shapes, tunable surface functionalities, and a large variety of simple, fast, and inexpensive synthetic routes. The first FCDs were discovered accidentally during purification of single-walled carbon nanotubes.[121] In the process of purifying arc-synthesized single-walled carbon nanotubes through electrophoresis in agarose gel, two different impurities were discovered, one of which was a set of fluorescent water-soluble carbon nanoparticles. Studies of FCDs continued thereon with a

wide range of synthesis and purification methods being developed—one of the strengths of FCDs as a fluorescent tool.

Synthesis methods for FCDs fall within two categories: top-down and bottom-up. Top-down methods are those involving the cleaving or chemical breakdown of larger carbon materials into nanoparticles, while bottom-up methods involve the formation of nanoparticles from smaller molecular precursors. The most common top-down methods are arc discharge, laser ablation, electrochemical approaches, and plasma treatments. Arc discharge methods were the first FCD synthesis method used, being the method used when FCDs were discovered by Xu et alia.[121] Beyond the groundbreaking work of Xu, the most referenced arc-discharge methods for FCD production were published by Bottini et alia in a similar method as Xu: arc-discharge on single walled carbon nanotubes.[122] In both cases, the nanoparticles produced were hydrophobic with an oxidized outer layer, causing aggregation when dispersed in water. Unfortunately, the arc-discharge method produces a complex mixture of varying structural compositions, making extensive purification vital to collect only a limited amount of the desired FCDs. Due to the low yields and complex purification needed, arc-discharge methods are not typically used in modern FCD production. Laser ablation methods involve the laser irradiation of a carbon target. This method was first used by Sun et alia through the irradiation of a mixture of graphite powder and cement with a laser, followed by extensive modification.[104] The nanoscale particles obtained after laser ablation produced samples with no photoluminescence, necessitating modification by nitric acid refluxing and reaction with polyethylene glycol (PEG) to produce strongly photoluminescent FCDs. Other research groups have used similar methods involving laser ablation of a carbon source, with the carbon source ranging from carbon targets modified with PEG200 and mercaptosuccinic acid to graphite flakes modified with PEG1500N.[123, 124] While the laser ablation

method offers the ability to produce a wide range of nanostructures based on the regulated pulse width of the laser, the amount of carbonaceous starting material needed is very large, and the yields are low. The low yield is a product of extensive purification required to separate the larger, non-fluorescent materials from the smaller fluorescent materials, similar to the shortcomings of arc-discharge methods. Electrochemical methods involve the construction of an electrochemical cell with a carbon source, typically high purity graphite, as the anode and a counter electrode, made of materials such as platinum or titanium. A static potential is applied across the electrochemical cell to stimulate the exfoliation of the graphite. The exfoliation products are then washed to ensure a neutral pH, followed by purification through centrifugation.[125, 126] This method produces highly fluorescent FCDs that are easy to purify, are water soluble, and possess high thermal stability. Top-down methods typically require extensive purification and expensive and time-consuming setups, bottom-up methods typically offer simpler methods, while also requiring less purification.

The most common bottom-up methods are the pyrolytic, template, microwave-assisted, chemical oxidation, and reverse micelle methods. Pyrolytic methods involve the pyrolysis, or carbonization, of carbon precursors under high temperatures. Initially, this process was done under high alkali or acidic conditions in order to cleave and recombine the precursors into a carbon nanoparticle. One example of this involves the use of citric acid as a precursor, combined with octadecene and 1-hexadecylamine in a flask held at 300 °C for 3 hours. Upon reaction, purification of the products produced FCDs that are soluble in non-polar organic solvents and possess quantum yields reaching 53%.[127] Newer methods have been implemented that negate the need for any chemical assistance or modification to produce FCDs. Many groups have reported that by simply heating a carbon source, such as ascorbic acid, citric acid, sodium alginate, or watermelon peel, highly fluorescent FCDs can be produced with very little purification or washing required, with

the resulting materials possessing quantum yields ranging from 15–80.3%.[128-131] The template method for producing FCDs involves a two-step process: (1) synthesis of FCDs through calcination of a carbon source into a mesoporous template or silicon sphere, and (2) removal of the template or sphere to obtain the FCDs. For example, Zong et alia combined a complex group of salts and citric acid into a container of mesoporous silica spheres in a template structure, before eventually removing the silica spheres and then the template, resulting in FCDs.[132] There are also template methods involving a less rigid membrane, such as using a copolymer as a soft template built around a more rigid inner template of silica spheres. Creation of the soft template is followed by impregnation with organic carbon sources, such as trimethylbenzene, and the eventual removal of the template and passivation to produce the FCDs.[133, 134] It should also be noted that this method is a variation of the pyrolysis methodologies, as pyrolysis is required to produce the particles within the scaffold before removal of the scaffold itself. In fact, the pyrolysis requirement makes this method more difficult to use, due to the added steps of creation and then eventual removal of the template after heavy heating, though additional control of particle size and morphology is allowed with this methodology. Additionally, highly corrosive or alkali chemicals are involved in the etching process used to create the templates, making this method not only dangerous, but also expensive. The microwave-assisted method is also a variation of the pyrolysis process, involving the irradiation and rapid heating of a carbon source within a microwave to produce FCDs. A simple example is the process of placing folic acid dissolved in diethylene glycol in a 750 W microwave and heating for 40 sec. After removal from the microwave, the reddish-brown suspension was purified through dialysis, producing FCDs with a quantum yield of 18.9%.[135] Similar methods were attempted in different papers, with the main variation being the carbon source, power of the microwave, and heating time, all which resulting in FCDs with varied properties.[136-138] It is

interesting to note at this point that the slightest variation in the synthesis method produces a FCD with different fluorescence properties, such as single versus multiple emission peaks, excitation wavelength-independent versus dependent fluorescence, or sharp versus broad peak widths.

The chemical oxidation approach to FCD synthesis involves the treatment of carbon precursors with a strong oxidant. In one case, hair fiber was used as the carbon precursor which, upon treatment with sulfuric acid at 140 °C for 24 hours, produced FCDs that were highly tunable by varying the reaction temperature.[139] Interestingly enough, an oxidation method has been discovered that is automatic and self-producing. By mixing a carbon source, water, and P_2O_5, the reaction proceeds without heat or any other assistance, producing large, hollow FCDs up to 120 nm in diameter with excitation wavelength independent emission.[140, 141] The reverse micelle method is an interesting method involving the production of a reverse phase water-in-oil micelle, within which the carbon precursors aggregate to produce FCDs. In one case, a solution of glucose as the carbon precursor in water is emulsified in decane in the presence of dioctyl sodium sulfosuccinate, a surfactant, to produce water-in-oil micelles. Inside the micelles, as the solution evaporates due to heat, a supersaturation point is reached, upon which carbonization occurs and FCDs are produced. As the evaporation and stress on the system increases, the micelles themselves are weakened, eventually collapsing and releasing the FCDs.[142] Additionally, during the collapse of the micelles, surface passivation of the FCDs can naturally occur from the surfactant, such as the creation of alkyl-capped FCDs as mentioned in the method used by Linehan et alia.[143] Beyond the synthetic method used, surface passivation is an important consideration, due to its ability to further modify the FCDs, producing brighter fluorescence, increasing biocompatibility, and increasing long-term stability.[144] Surface passivation can also greatly affect the absorption and

therefore excitation wavelength of the FCDs, such as modification with 4,7,10-trioxa-1,13-tridecanediamine to push the absorption band into the 350 – 550 nm range for the FCDs.[145]

FCDs, as discussed previously, exhibit high absorbance values in the visible and ultraviolet region. The typical range of absorption for FCDs is a band from 250–300 nm, which corresponds to a π-π* transition peak.[146] Though the above absorption band applies to most FCDs, the wavelength of maximum absorbance can differ greatly based on synthesis method. For example, most laser passivation methods produce FCDs with maximum absorbance around 280 nm,[147] while electrochemically produced FCDs have energies of emission that are slightly blue shifted in comparison, with absorbance maxima occurring closer to 270 nm with narrow full width and half maximum peaks,[148] characteristics similar to that of microwave-produced FCDs.[149] While the absorption is vital for any photoluminescence effects witnessed from FCDs, the photoluminescent properties after the light has been absorbed are more chemically important when using FCDs as biosensors.[150] In addition to the individual synthetic method used to create the FCDs affecting the absorbance, differences in the photoluminescent properties are also witnessed based on synthesis method. For example, it was commonly understood that all FCDs exhibit emission wavelengths clearly dependent upon excitation wavelength—this was considered to be a property of all FCDs.[151] While this is true for most standard FCDs, recent reports indicate that FCDs can be produced so as to exhibit emissions whose wavelengths are independent of the wavelength of light used to excite the particles, establishing a gap in the fundamental knowledge thought to govern FCDs.[135, 152, 153]

The exact mechanism responsible for fluorescence in FCDs is not well understood, but some principles have been suggested in the literature. There are two main mechanisms suggested for the fluorescence in FCDs. The first is based on defect emission due to surface charge traps on

the FCDs, allowing unpaired electrons or holes to become trapped in a high density of other unpaired electrons or holes, which recombine to produce fluorescence, as explained above when discussing QDs. The second suggested mechanism is intrinsic state emissions, resulting from the pairing of electrons and holes to form excitons, producing fluorescence from the released energy as the exciton forms, outlined in more detail above when discussing QDs.[154] These theories have been supported through experimentation with FCDs exhibiting two emission peaks, one in the blue region (due to intrinsic state emissions) and one in the green region (due to defect state emissions). By modifying the surface of FCDs with reducing agent $NaBH_4$, the effective elimination of any surface traps was ensured, and a decrease in the green emission was correspondingly seen, while the blue remained unchanged, as one would expect if the green emission was in fact due to defect state emissions.[155] Beyond this study, very little has been confirmed experimentally regarding the fluorescence mechanism in FCDs. The prevailing theories only go so far as to say the fluorescence is related to energy traps, recombination of electron/hole pairs, quantum confinement effects, polyaromatic structures, edge effects, and oxygen-containing groups.[104, 156-158]

Another interesting feature of FCDs that allows for their ability to offer detection of individual analytes is fluorescence quenching or fluorescence recovery due to an analyte. The quenching mechanisms are varied and can consist of static quenching, dynamic quenching, energy transfer (including Forster resonance energy transfer, Dexter energy transfer, and surface energy transfer), photoinduced electron transfer, and the inner filter effect. A review of all of these quenching mechanisms is beyond the scope of this document. However, such a review is provided by Zu et alia; for the purposes of this research, I will focus on static quenching, particularly by metal ions.[159]

Static quenching occurs when a quencher interacts with the FCD to form a ground-state complex, immediately returning any excited electrons within the FCD structure to the ground state without emission when excited by light. Static quenching is also an ongoing process, not quenching fluorescence for an instant, but maintaining the quenching effects over time. In literature, FCDs have been shown to exhibit this static quenching when interacting with metal ions, particularly iron ions (Fe), copper ions (Cu), and mercury ions (Hg). The quenching mechanism is believed to be due to an electron transfer between the FCDs and the metal center upon binding and creation of a complex as discussed in the static quenching definition.[160]

Upon review of manuscripts discussing the production of FCDs for detection of metal ions through quenching, some interesting insights can be gained. In the quenching review by Zu et alia, different groups' research on the use of FCDs for the analysis of Fe^{3+}/Fe^{2+}, Hg^{2+}, and Cu^{2+} were all discussed, and are outlined as follows.[159] In FCDs produced by Iqbal et alia, they show similar quenching when exposed to Fe^{3+} and Fe^{2+}, with Fe^{3+} requiring a larger added amount to reach maximum quenching effects, but reaching an eventual lower fluorescence intensity endpoint when quenching reaches its maximum effect.[160] Fong et alia reported quenching of their FCDs by Fe^{3+} as well, but rather than seeing similar quenching effects due to Fe^{2+}, they expose the FCD/Fe^{3+} complex to a reducing agent, which produces a complete fluorescence recovery.[131] They theorize that by reducing the Fe^{3+} ions to Fe^{2+}, fluorescence is recovered, as Fe^{2+} does not produce quenching in the case of their FCDs. In the research of Gu et alia, their FCDs are quenched by Hg^{2+}, and when tested against other metal ions the presence of the metal ions does not lead to quenching, making their FCD sensor very selective for Hg^{2+}.[161] Interestingly enough, the Fe^{2+} tested by Gu et alia, showed no fluorescence quenching, but for reasons not stated, Gu et alia chose not to test Fe^{3+} in their publication. Wang et alia effectively quenched the fluorescence of their

FCDs using Cu^{2+}, even though Cu^{2+} showed no quenching effects in any of the previous metal ion quenching publications discussed.[162] It is important to establish that these discrepancies do not necessarily represent poorly performed experiments or false data, but rather can be due to differences in the individual synthetic or modification processes. While an understanding of how FCDs produced under every synthesis condition or modification process is the work of a lifetime, studies of FCDs produced through a particular synthesis mechanism with little to no subsequent modification can potentially give insights into the fluorescence and quenching mechanisms of FCDs produced by that particular synthesis mechanism.

Another area that is lacking information regarding FCDs are their cellular effects. FCDs are used throughout literature as biosensors, indeed, a review by Song et alia outlines many different uses of FCDs as biological sensors.[163] FCDs have been gaining much attention as effective biological sensors for many reasons, including their size-, surface chemistry-, and wavelength-dependent luminescence, high chemical stability, good biocompatibility, low toxicity, up-conversion emission, and resistance to photo bleaching. Of particular interest to this research project is the ability of the FCDs to perform as biosensors for individual analytes within cells due to the quenching effects observed upon interaction with metal ions. For example, Zhang et alia created nitrogen-doped FCDs that were exposed to cells, upon which Fe^{3+} in cells was detected by measuring the fluorescence quenching that occurred when the FCDs interacted with the metal ions.[164] In addition to detecting analytes through a turn-off mechanism as in Zhang et alia, FCDs can be used as turn-on probes as well. He et alia produced FCDs functionalized with MnO_2 sheets that effectively quench the fluorescence of the FCDs. Upon uptake into the cell and exposure to GSH, the MnO_2 is reduced to Mn^{2+}, resulting in recovery of fluorescence, making these MnO_2-functionalized FCDs effective turn-on biosensors for GSH.[165] While this research shows the

promising ability of FCDs to exhibit both fluorescence turn-off and turn-on in cellular environments, it also establishes the ability of FCDs to enter into the cell and be imaged using fluorescence microscopy techniques.

Unfortunately, though many studies have been performed using FCDs as biosensors, minimal studies have been done to examine the health effects resulting from the FCDs. One example of health effect evaluation is a paper published by Wang et alia who created FCDs and used an MTT cell viability assay to evaluate the effect of different concentrations of their particles in media (2 mg/mL and 7 mg/mL) in cells over a time period of hours. They state that they observed limited health effects, showing a 100% cell viability when exposed to 2 mg/mL particles and greater than 80% when exposed to 7 mg/mL particles.[136] These types of studies investigate the toxicity of FCDs on a cellular and tissue level, but they generally evaluate only cell toxicity, measuring cell death rather than evaluating the effect of FCDs on the cellular environment to determine detrimental effects beyond immediate cell death. Additionally, the studies are typically performed on time scales and concentrations not necessarily representative of all FCD biological usage. A more thorough evaluation is needed.

The comments above are not meant to discount any research performed by other scientists, but simply to establish how limited is our understanding of the fluorescence from and fluorescence quenching mechanisms for FCDs. The theories proposed governing the fluorescence of FCDs and how the synthesis, modification, or exposure to outside analytes affects that fluorescence are not easily elucidated, with the proposed theories changing depending on identity of the reporting research groups or simply different methodologies. Some similar trends are reported in literature, such as the quenching mechanisms and turn-off or turn-on fluorescence. This discrepancy between some observed processes being uniform and others being a case by case basis establishes the need

for more studies on the properties of FCDs, in particular focusing on one synthesis mechanism at a time, rather than trying to establish broad, all-encompassing theories for all FCDs, regardless of synthesis methods or modifications. Essner et alia state this well:

> Fluorescent carbon dots have attracted tremendous attention owing to their superlative optical properties which suggest opportunities for replacing conventional fluorescent materials in various application fields. Not surprisingly, the rapid pace of publication has been accompanied by a host of critical issues, errors, controversies, and misconceptions associated with these emergent materials, which present significant barriers to elucidating their true nature, substantially hindering the extensive exploitation of these nanomaterials. [153]

FCDs possess all the necessary requirements to be an effective fluorescent surrogate for BC, as outlined above. By utilizing a bottom-up pyrolytic synthesis method with a variety of carbon sources (sodium alginate, glucose, fructose, agarose, etc.), the pyrolytic synthesis method can be probed to gain an understanding of the underlying fluorescent mechanism. By attempting to use the FCDs as a turn-on sensor, the fluorescence can be quenched using metal ions and recovered using reducing agents to better understand the fluorescence quenching mechanism. With the FCD sensor designed and effectively produced, it yields itself to be used as a powerful tool to probe health effects of both BC and FCDs in lung cells. This information can go a long way to better understanding the impact of BC as a component of PM rather than the impact of PM as a whole. Additionally, the information gained regarding FCD fluorescence mechanisms and the health effects of FCDs is small in regard to the large field of FCDs, but is vital to establishing a foundation from which further research can be built.

1.6 References

1. Anderson, J.O., J.G. Thundiyil, and A. Stolbach, *Clearing the air: a review of the effects of particulate matter air pollution on human health.* J Med Toxicol, 2012. **8**(2): p. 166-75.

2. Agency, E.P. *Health and Environmental Effects of Particulate Matter (PM)*. Particulate Matter (PM) Pollution 2019 [cited 2019; Available from: https://www.epa.gov/pm-pollution/health-and-environmental-effects-particulate-matter-pm.

3. Organization, W.H., *World Health Report 2002*. 2002.

4. Environmental Protection Agency. *Particulate Matter (PM) Basics*. Particulate Matter (PM) Pollution 2019; Available from: https://www.epa.gov/pm-pollution/particulate-matter-pm-basics - PM.

5. Bond, T.C., et al., *Bounding the role of black carbon in the climate system: A scientific assessment.* Journal of Geophysical Research: Atmospheres, 2013. **118**(11): p. 5380-5552.

6. Schmidt, M.W.I. and A.G. Noack, *Black carbon in soils and sediments: Analysis, distribution, implications, and current challenges.* Global Biogeochemical Cycles, 2000. **14**(3): p. 777-793.

7. Zhou, J., et al., *Time-series analysis of mortality effects of fine particulate matter components in Detroit and Seattle.* Environ Health Perspect, 2011. **119**(4): p. 461-6.

8. Franklin, M., P. Koutrakis, and P. Schwartz, *The role of particle composition on the association between PM2.5 and mortality.* Epidemiology, 2008. **19**(5): p. 680-9.

9. Badgett, A., *Toward the Impact of Particulate Matter on Human Health: Evaluation of Fluorescent Environmentally Persistent Free Radical (EPFR) Surrogates*, in *Chemistry*. 2019, Louisiana State University.

10. Miller, F.J., et al., *Size Considerations for Establishing a Standard for Inhalable Particles.* Journal of the Air Pollution Control Association, 1979. **29**(6): p. 610-615.

11. Schwartz, J., D.W. Dockery, and L.M. Neas, *Is Daily Mortality Associated Specifically with Fine Particles?* J Air Waste Manag Assoc, 1996. **46**(10): p. 927-939.

12. Lord, K., et al., *Environmentally persistent free radicals decrease cardiac function before and after ischemia/reperfusion injury in vivo.* J Recept Signal Transduct Res, 2011. **31**(2): p. 157-67.

13. SALVI, S., et al., *Acute Inflammatory Responses in the Airways and Peripheral Blood After Short-Term Exposure to Diesel Exhaust in Healthy Human Volunteers.* American Journal of Respiratory and Critical Care Medicine, 1999. **159**(3): p. 702-709.

14. Gan, W.Q., et al., *Association between chronic obstructive pulmonary disease and systemic inflammation: a systematic review and a meta-analysis.* Thorax, 2004. **59**(7): p. 574-580.

15. Jones, S.L., et al., *Exhaled NO and assessment of anti-inflammatory effects of inhaled steroid: dose-response relationship.* European Respiratory Journal, 2002. **20**(3): p. 601-608.

16. Zhang, R. and W. Chen, *Nitrogen-doped carbon quantum dots: Facile synthesis and application as a "turn-off" fluorescent probe for detection of Hg2+ ions.* Biosensors and Bioelectronics, 2014. **55**: p. 83-90.

17. Yu, C., et al., *Carbon-dot-based ratiometric fluorescent sensor for detecting hydrogen sulfide in aqueous media and inside live cells.* Chemical Communications, 2013. **49**(4): p. 403-405.

18. Liu, Q., et al., *Distinguish cancer cells based on targeting turn-on fluorescence imaging by folate functionalized green emitting carbon dots.* Biosensors and Bioelectronics, 2015. **64**: p. 119-125.

19. Du, F., et al., *Carbon dots-based fluorescent probes for sensitive and selective detection of iodide.* Microchimica Acta, 2013. **180**(5): p. 453-460.

20. Das, P., et al., *A simplistic approach to green future with eco-friendly luminescent carbon dots and their application to fluorescent nano-sensor 'turn-off' probe for selective sensing of copper ions.* Materials Science and Engineering: C, 2017. **75**: p. 1456-1464.

21. Borse, V., et al., *N-doped multi-fluorescent carbon dots for 'turn off-on' silver-biothiol dual sensing and mammalian cell imaging application.* Sensors and Actuators B: Chemical, 2017. **248**: p. 481-492.

22. Nemery, B., P.H.M. Hoet, and A. Nemmar, *The Meuse Valley fog of 1930: an air pollution disaster.* The Lancet, 2001. **357**(9257): p. 704-708.

23. Bell, M.L. and D.L. Davis, *Reassessment of the lethal London fog of 1952: novel indicators of acute and chronic consequences of acute exposure to air pollution.* Environmental Health Perspectives, 2001. **109**(suppl 3): p. 389-394.

24. Rogers, P.G., *The Clean Air Act of 1970 Looking Back; Looking Ahead.* EPA Journal, 1990(1): p. 21-23.

25. Brook Robert, D., et al., *Particulate Matter Air Pollution and Cardiovascular Disease.* Circulation, 2010. **121**(21): p. 2331-2378.

26. Simkhovich, B.Z., M.T. Kleinman, and R.A. Kloner, *Air Pollution and Cardiovascular Injury.* Journal of the American College of Cardiology, 2008. **52**(9): p. 719.

27. Pope, C.A. and D.W. Dockery, *Health Effects of Fine Particulate Air Pollution: Lines that Connect.* Journal of the Air & Waste Management Association, 2006. **56**(6): p. 709-742.

28. Ristovski, Z.D., et al., *Respiratory health effects of diesel particulate matter.* Respirology, 2012. **17**(2): p. 201-212.

29. Peng, R.D., et al., *Coarse Particulate Matter Air Pollution and Hospital Admissions for Cardiovascular and Respiratory Diseases Among Medicare Patients.* JAMA, 2008. **299**(18): p. 2172-2179.

30. Jansen Karen, L., et al., *Associations between Health Effects and Particulate Matter and Black Carbon in Subjects with Respiratory Disease.* Environmental Health Perspectives, 2005. **113**(12): p. 1741-1746.

31. Rückerl, R., et al., *Air Pollution and Markers of Inflammation and Coagulation in Patients with Coronary Heart Disease.* American Journal of Respiratory and Critical Care Medicine, 2006. **173**(4): p. 432-441.

32. Hoffmann, B., et al., *Chronic Residential Exposure to Particulate Matter Air Pollution and Systemic Inflammatory Markers.* Environmental Health Perspectives, 2009. **117**(8): p. 1302-1308.

33. Chuang, K.-J., et al., *The Effect of Urban Air Pollution on Inflammation, Oxidative Stress, Coagulation, and Autonomic Dysfunction in Young Adults.* American Journal of Respiratory and Critical Care Medicine, 2007. **176**(4): p. 370-376.

34. Schicker, B., et al., *Particulate matter inhalation during hay storing activity induces systemic inflammation and platelet aggregation.* European Journal of Applied Physiology, 2009. **105**(5): p. 771-778.

35. Horak Jr, F., et al., *The chemical composition of particulate matter has a short term effect on the lung function of pre-school children.* Eur. Respri. J, 2001. **18**.

36. Neuberger, M., et al., *Acute effects of particulate matter on respiratory diseases, symptoms and functions:: epidemiological results of the Austrian Project on Health Effects of Particulate Matter (AUPHEP).* Atmospheric Environment, 2004. **38**(24): p. 3971-3981.

37. Sullivan, J.H., et al., *A community study of the effect of particulate matter on blood measures of inflammation and thrombosis in an elderly population.* Environmental Health, 2007. **6**(1): p. 3.

38. Steinvil, A., et al., *Short-term exposure to air pollution and inflammation-sensitive biomarkers.* Environmental Research, 2008. **106**(1): p. 51-61.

39. Forbes, L.J.L., et al., *Chronic Exposure to Outdoor Air Pollution and Markers of Systemic Inflammation.* Epidemiology, 2009. **20**(2): p. 245-253.

40. Diez Roux, A.V., et al., *Recent Exposure to Particulate Matter and C-reactive Protein Concentration in the Multi-Ethnic Study of Atherosclerosis.* American Journal of Epidemiology, 2006. **164**(5): p. 437-448.

41. Schwartz, J., F. Laden, and A. Zanobetti, *The concentration-response relation between PM(2.5) and daily deaths.* Environmental Health Perspectives, 2002. **110**(10): p. 1025-1029.

42. Oberdörster, G., et al., *Translocation of Inhaled Ultrafine Particles to the Brain.* Inhalation Toxicology, 2004. **16**(6-7): p. 437-445.

43. Petzold, A., et al., *Recommendations for reporting "black carbon" measurements.* Atmospheric Chemistry and Physics, 2013. **13**(16): p. 8365-8379.

44. Sze, S.K., et al., *Raman spectroscopic characterization of carbonaceous aerosols.* Atmospheric Environment, 2001. **35**(3): p. 561-568.

45. Ivleva, N.P., et al., *Raman Microspectroscopic Analysis of Size-Resolved Atmospheric Aerosol Particle Samples Collected with an ELPI: Soot, Humic-Like Substances, and Inorganic Compounds.* Aerosol Science and Technology, 2007. **41**(7): p. 655-671.

46. Buseck, P.R., et al., *Are black carbon and soot the same?* Atmospheric Chemistry and Physics Discussions, 2012. **12**(9): p. 24821-24846.

47. Sadezky, A., et al., *Raman microspectroscopy of soot and related carbonaceous materials: Spectral analysis and structural information.* Carbon, 2005. **43**(8): p. 1731-1742.

48. Mertes, S., B. Dippel, and A. Schwarzenböck, *Quantification of graphitic carbon in atmospheric aerosol particles by Raman spectroscopy and first application for the determination of mass absorption efficiencies.* Journal of Aerosol Science, 2004. **35**(3): p. 347-361.

49. Longfellow, C.A., A.R. Ravishankara, and D.R. Hanson, *Reactive and nonreactive uptake on hydrocarbon soot: HNO3, O3, and N2O5.* Journal of Geophysical Research: Atmospheres, 2000. **105**(D19): p. 24345-24350.

50. Goldman, A. and A. Bentur, *Properties of cementitious systems containing silica fume or nonreactive microfillers.* Advanced Cement Based Materials, 1994. **1**(5): p. 209-215.

51. Choi, H.-D., et al., *Removal characteristics of reactive black 5 using surfactant-modified activated carbon.* Desalination, 2008. **223**(1): p. 290-298.

52. van Poppel, L.H., et al., *Electron tomography of nanoparticle clusters: Implications for atmospheric lifetimes and radiative forcing of soot.* Geophysical Research Letters, 2005. **32**(24).

53. Tumolva, L., et al., *Morphological and Elemental Classification of Freshly Emitted Soot Particles and Atmospheric Ultrafine Particles using the TEM/EDS.* Aerosol Science and Technology, 2010. **44**(3): p. 202-215.

54. Murr, L.E. and K.F. Soto, *A TEM study of soot, carbon nanotubes, and related fullerene nanopolyhedra in common fuel-gas combustion sources.* Materials Characterization, 2005. **55**(1): p. 50-65.

55. Braun, A., et al., *Advantages of soft X-ray absorption over TEM-EELS for solid carbon studies—a comparative study on diesel soot with EELS and NEXAFS.* Carbon, 2005. **43**(1): p. 117-124.

56. Kuhlbusch, T.A.J., *Black Carbon and the Carbon Cycle.* Science, 1998. **280**(5371): p. 1903.

57. MacDonald, G.M., et al., *The reconstruction of boreal forest fire history from lake sediments: A comparison of charcoal, pollen, sedimentological, and geochemical indices.* Quaternary Science Reviews, 1991. **10**(1): p. 53-71.

58. Patterson, W.A., K.J. Edwards, and D.J. Maguire, *Microscopic charcoal as a fossil indicator of fire.* Quaternary Science Reviews, 1987. **6**(1): p. 3-23.

59. Reiner, T., et al., *Chemical characterization of pollution layers over the tropical Indian Ocean: Signatures of emissions from biomass and fossil fuel burning.* Journal of Geophysical Research: Atmospheres, 2001. **106**(D22): p. 28497-28510.

60. Novakov, T., et al., *Large historical changes of fossil-fuel black carbon aerosols.* Geophysical Research Letters, 2003. **30**(6).

61. *Construction of a 1° × 1° fossil fuel emission data set for carbonaceous aerosol and implementation and radiative impact in the ECHAM4 model.* Journal of Geophysical Research: Atmospheres, 1999. **104**(D18): p. 22137-22162.

62. Novakov, T., et al., *Origin of carbonaceous aerosols over the tropical Indian Ocean: Biomass burning or fossil fuels?* Geophysical Research Letters, 2000. **27**(24): p. 4061-4064.

63. Cachier, H., M.-P. Brémond, and P. Buat-Ménard, *Thermal Separation of Soot Carbon.* Aerosol Science and Technology, 1989. **10**(2): p. 358-364.

64. Jennings, S.G., et al., *Volatility of elemental carbon.* Geophysical Research Letters, 1994. **21**(16): p. 1719-1722.

65. Leifeld, J., *Thermal stability of black carbon characterised by oxidative differential scanning calorimetry.* Organic Geochemistry, 2007. **38**(1): p. 112-127.

66. Davis, K.A., et al., *Evolution of char chemistry, crystallinity, and ultrafine structure during pulverized-coal combustion.* Combustion and Flame, 1995. **100**(1): p. 31-40.

67. Feng, B., S.K. Bhatia, and J.C. Barry, *Structural ordering of coal char during heat treatment and its impact on reactivity.* Carbon, 2002. **40**(4): p. 481-496.

68. Cetin, E., R. Gupta, and B. Moghtaderi, *Effect of pyrolysis pressure and heating rate on radiata pine char structure and apparent gasification reactivity.* Fuel, 2005. **84**(10): p. 1328-1334.

69. Chughtai, A.R., et al., *Spectroscopic and Solubility Characteristics of Oxidized Soots.* Aerosol Science and Technology, 1991. **15**(2): p. 112-126.

70. Smith, D.M. and A.R. Chughtai, *The surface structure and reactivity of black carbon.* Colloids and Surfaces A: Physicochemical and Engineering Aspects, 1995. **105**(1): p. 47-77.

71. Diarra, M., et al., *Importance of Carbon Solubility and Wetting Properties of Nickel Nanoparticles for Single Wall Nanotube Growth.* Physical Review Letters, 2012. **109**(18): p. 185501.

72. Kleineidam, S., C. Schüth, and P. Grathwohl, *Solubility-Normalized Combined Adsorption-Partitioning Sorption Isotherms for Organic Pollutants.* Environmental Science & Technology, 2002. **36**(21): p. 4689-4697.

73. Jaffé, R., et al., *Global Charcoal Mobilization from Soils via Dissolution and Riverine Transport to the Oceans.* Science, 2013. **340**(6130): p. 345.

74. Santín, C., et al., *Towards a global assessment of pyrogenic carbon from vegetation fires.* Global Change Biology, 2016. **22**(1): p. 76-91.

75. Kramer, R.W., E.B. Kujawinski, and P.G. Hatcher, *Identification of Black Carbon Derived Structures in a Volcanic Ash Soil Humic Acid by Fourier Transform Ion Cyclotron Resonance Mass Spectrometry.* Environmental Science & Technology, 2004. **38**(12): p. 3387-3395.

76. Hockaday, W.C., et al., *Direct molecular evidence for the degradation and mobility of black carbon in soils from ultrahigh-resolution mass spectral analysis of dissolved organic matter from a fire-impacted forest soil.* Organic Geochemistry, 2006. **37**(4): p. 501-510.

77. Kim, S., et al., *Hydrogen-deficient molecules in natural riverine water samples—evidence for the existence of black carbon in DOM.* Marine Chemistry, 2004. **92**(1): p. 225-234.

78. Wagner, S., R. Jaffé, and A. Stubbins, *Dissolved black carbon in aquatic ecosystems.* Limnology and Oceanography Letters, 2018. **3**(3): p. 168-185.

79. Sheridan, P.J., et al., *The Reno Aerosol Optics Study: An Evaluation of Aerosol Absorption Measurement Methods.* Aerosol Science and Technology, 2005. **39**(1): p. 1-16.

80. Moosmüller, H., R.K. Chakrabarty, and W.P. Arnott, *Aerosol light absorption and its measurement: A review.* Journal of Quantitative Spectroscopy and Radiative Transfer, 2009. **110**(11): p. 844-878.

81. Arnott, W.P., et al., *Photoacoustic and filter-based ambient aerosol light absorption measurements: Instrument comparisons and the role of relative humidity.* Journal of Geophysical Research: Atmospheres, 2003. **108**(D1): p. AAC 15-1-AAC 15-11.

82. Hansen, A.D.A., H. Rosen, and T. Novakov, *The aethalometer — An instrument for the real-time measurement of optical absorption by aerosol particles.* Science of The Total Environment, 1984. **36**: p. 191-196.

83. Colbeck, I., E.J. Hardman, and R.M. Harrison, *Optical and dynamical properties of fractal clusters of carbonaceous smoke.* Journal of Aerosol Science, 1989. **20**(7): p. 765-774.

84. Rosen, H., et al., *Graphitic Carbon in Urban Environments and the Arctic*, in *Particulate Carbon: Atmospheric Life Cycle*, G.T. Wolff and R.L. Klimisch, Editors. 1982, Springer US: Boston, MA. p. 273-294.

85. Petzold, A., C. Kopp, and R. Niessner, *The dependence of the specific attenuation cross-section on black carbon mass fraction and particle size.* Atmospheric Environment, 1997. **31**(5): p. 661-672.

86. Ramanathan, V. and G. Carmichael, *Global and regional climate changes due to black carbon.* Nature Geoscience, 2008. **1**: p. 221.

87. Menon, S., et al., *Climate Effects of Black Carbon Aerosols in China and India.* Science, 2002. **297**(5590): p. 2250-2253.

88. Flanner, M.G., et al., *Present-day climate forcing and response from black carbon in snow.* Journal of Geophysical Research: Atmospheres, 2007. **112**(D11).

89. McConnell, J.R., et al., *20th-Century Industrial Black Carbon Emissions Altered Arctic Climate Forcing.* Science, 2007. **317**(5843): p. 1381.

90. Chung, S.H. and J.H. Seinfeld, *Climate response of direct radiative forcing of anthropogenic black carbon.* Journal of Geophysical Research: Atmospheres, 2005. **110**(D11).

91. Resch-Genger, U., et al., *Quantum dots versus organic dyes as fluorescent labels.* Nat Methods, 2008. **5**(9): p. 763-75.

92. Zhang, J., et al., *Creating new fluorescent probes for cell biology.* Nature Reviews Molecular Cell Biology, 2002. **3**(12): p. 906-918.

93. Shen, Z., et al., *A Near-Infrared, Wavelength-Shiftable, Turn-on Fluorescent Probe for the Detection and Imaging of Cancer Tumor Cells.* ACS Chemical Biology, 2017. **12**(4): p. 1121-1132.

94. Best, Q.A., et al., *Efficacious fluorescence turn-on probe for high-contrast imaging of human cells overexpressing quinone reductase activity.* Chemical Communications, 2017. **53**(4): p. 783-786.

95. Soper, S.A. and Q.L. Mattingly, *Steady-State and Picosecond Laser Fluorescence Studies of Nonradiative Pathways in Tricarbocyanine Dyes: Implications to the Design of Near-IR Fluorochromes with High Fluorescence Efficiencies.* Journal of the American Chemical Society, 1994. **116**(9): p. 3744-3752.

96. Mason, J.N., et al., *Novel fluorescence-based approaches for the study of biogenic amine transporter localization, activity, and regulation.* Journal of Neuroscience Methods, 2005. **143**(1): p. 3-25.

97. Panchuk-Voloshina, N., et al., *Alexa Dyes, a Series of New Fluorescent Dyes that Yield Exceptionally Bright, Photostable Conjugates.* Journal of Histochemistry & Cytochemistry, 1999. **47**(9): p. 1179-1188.

98. Berlier, J.E., et al., *Quantitative Comparison of Long-wavelength Alexa Fluor Dyes to Cy Dyes: Fluorescence of the Dyes and Their Bioconjugates.* Journal of Histochemistry & Cytochemistry, 2003. **51**(12): p. 1699-1712.

99. Eggeling, C., A. Volkmer, and C.A.M. Seidel, *Molecular Photobleaching Kinetics of Rhodamine 6G by One- and Two-Photon Induced Confocal Fluorescence Microscopy.* ChemPhysChem, 2005. **6**(5): p. 791-804.

100. Alivisatos, A.P., *Perspectives on the Physical Chemistry of Semiconductor Nanocrystals.* The Journal of Physical Chemistry, 1996. **100**(31): p. 13226-13239.

101. Bera, D., et al., *Quantum Dots and Their Multimodal Applications: A Review.* Materials, 2010. **3**(4): p. 2260-2345.

102. Weller, H., *Quantum size colloids: From size-dependent properties of discrete particles to self-organized superstructures.* Current Opinion in Colloid & Interface Science, 1998. **3**(2): p. 194-199.

103. Alivisatos, A.P., *Semiconductor Clusters, Nanocrystals, and Quantum Dots.* Science, 1996. **271**(5251): p. 933.

104. Sun, Y.-P., et al., *Quantum-Sized Carbon Dots for Bright and Colorful Photoluminescence.* Journal of the American Chemical Society, 2006. **128**(24): p. 7756-7757.

105. Warner, J.H., et al., *Water-Soluble Photoluminescent Silicon Quantum Dots.* Angewandte Chemie International Edition, 2005. **44**(29): p. 4550-4554.

106. Fu, H.-B. and J.-N. Yao, *Size Effects on the Optical Properties of Organic Nanoparticles.* Journal of the American Chemical Society, 2001. **123**(7): p. 1434-1439.

107. Parak, W.J., T. Pellegrino, and C. Plank, *Labelling of cells with quantum dots.* Nanotechnology, 2005. **16**(2): p. R9-R25.

108. Derfus, A.M., W.C.W. Chan, and S.N. Bhatia, *Probing the Cytotoxicity of Semiconductor Quantum Dots.* Nano Letters, 2004. **4**(1): p. 11-18.

109. Kirchner, C., et al., *Cytotoxicity of Colloidal CdSe and CdSe/ZnS Nanoparticles.* Nano Letters, 2005. **5**(2): p. 331-338.

110. Chen, F. and D. Gerion, *Fluorescent CdSe/ZnS Nanocrystal−Peptide Conjugates for Long-term, Nontoxic Imaging and Nuclear Targeting in Living Cells.* Nano Letters, 2004. **4**(10): p. 1827-1832.

111. Jaiswal, J.K., et al., *Long-term multiple color imaging of live cells using quantum dot bioconjugates.* Nature Biotechnology, 2003. **21**(1): p. 47-51.

112. Selvan, S.T., T.T. Tan, and J.Y. Ying, *Robust, Non-Cytotoxic, Silica-Coated CdSe Quantum Dots with Efficient Photoluminescence.* Advanced Materials, 2005. **17**(13): p. 1620-1625.

113. Couto, O.D.D., et al., *Charge control in InP/(Ga,In)P single quantum dots embedded in Schottky diodes.* Physical Review B, 2011. **84**(12): p. 125301.

114. Prikhotjko, A., *Absorption spectra of crystals at low temperatures.* J. Phys. USSR, 1944. **8**: p. 257.

115. Wang, Y. and N. Herron, *Nanometer-sized semiconductor clusters: materials synthesis, quantum size effects, and photophysical properties.* The Journal of Physical Chemistry, 1991. **95**(2): p. 525-532.

116. Kuçur, E., et al., *Determination of Defect States in Semiconductor Nanocrystals by Cyclic Voltammetry.* The Journal of Physical Chemistry B, 2005. **109**(43): p. 20355-20360.

117. Bang, J., H. Yang, and P.H. Holloway, *Enhanced and stable green emission of ZnO nanoparticles by surface segregation of Mg.* Nanotechnology, 2006. **17**(4): p. 973-978.

118. Efros, A.L. and M. Rosen, *Random Telegraph Signal in the Photoluminescence Intensity of a Single Quantum Dot.* Physical Review Letters, 1997. **78**(6): p. 1110-1113.

119. Stefani, F.D., et al., *Quantification of photoinduced and spontaneous quantum-dot luminescence blinking.* Physical Review B, 2005. **72**(12): p. 125304.

120. Issac, A., C. von Borczyskowski, and F. Cichos, *Correlation between photoluminescence intermittency of CdSe quantum dots and self-trapped states in dielectric media.* Physical Review B, 2005. **71**(16): p. 161302.

121. Xu, X., et al., *Electrophoretic Analysis and Purification of Fluorescent Single-Walled Carbon Nanotube Fragments.* Journal of the American Chemical Society, 2004. **126**(40): p. 12736-12737.

122. Bottini, M., et al., *Isolation and Characterization of Fluorescent Nanoparticles from Pristine and Oxidized Electric Arc-Produced Single-Walled Carbon Nanotubes.* The Journal of Physical Chemistry B, 2006. **110**(2): p. 831-836.

123. Gonçalves, H. and J.C.G. Esteves da Silva, *Fluorescent Carbon Dots Capped with PEG200 and Mercaptosuccinic Acid.* Journal of Fluorescence, 2010. **20**(5): p. 1023-1028.

124. Hu, S., et al., *Laser synthesis and size tailor of carbon quantum dots.* Journal of Nanoparticle Research, 2011. **13**(12): p. 7247-7252.

125. Lu, J., et al., *One-Pot Synthesis of Fluorescent Carbon Nanoribbons, Nanoparticles, and Graphene by the Exfoliation of Graphite in Ionic Liquids.* ACS Nano, 2009. **3**(8): p. 2367-2375.

126. Yao, S., Y. Hu, and G. Li, *A one-step sonoelectrochemical preparation method of pure blue fluorescent carbon nanoparticles under a high intensity electric field.* Carbon, 2014. **66**: p. 77-83.

127. Wang, F., et al., *One-Step Synthesis of Highly Luminescent Carbon Dots in Noncoordinating Solvents.* Chemistry of Materials, 2010. **22**(16): p. 4528-4530.

128. Zhou, J., et al., *Facile synthesis of fluorescent carbon dots using watermelon peel as a carbon source.* Materials Letters, 2012. **66**(1): p. 222-224.

129. Zhang, B., C.-y. Liu, and Y. Liu, *A Novel One-Step Approach to Synthesize Fluorescent Carbon Nanoparticles.* European Journal of Inorganic Chemistry, 2010. **2010**(28): p. 4411-4414.

130. Zhuo, Y., et al., *One-step synthesis of high quantum-yield and excitation-independent emission carbon dots for cell imaging.* Materials Letters, 2015. **139**: p. 197-200.

131. Fong, J.F.Y., S.F. Chin, and S.M. Ng, *A unique "turn-on" fluorescence signalling strategy for highly specific detection of ascorbic acid using carbon dots as sensing probe.* Biosensors and Bioelectronics, 2016. **85**: p. 844-852.

132. Zong, J., et al., *Synthesis of photoluminescent carbogenic dots using mesoporous silica spheres as nanoreactors.* Chemical Communications, 2011. **47**(2): p. 764-766.

133. Yang, Y., et al., *Bottom-up fabrication of photoluminescent carbon dots with uniform morphology via a soft–hard template approach.* Chemical Communications, 2013. **49**(43): p. 4920-4922.

134. Lai, C.-W., et al., *Facile synthesis of highly emissive carbon dots from pyrolysis of glycerol; gram scale production of carbon dots/mSiO2 for cell imaging and drug release.* Journal of Materials Chemistry, 2012. **22**(29): p. 14403-14409.

135. Guan, W., et al., *Microwave-assisted polyol synthesis of carbon nitride dots from folic acid for cell imaging.* International journal of nanomedicine, 2014. **9**: p. 5071-5078.

136. Wang, W., et al., *Water-soluble and phosphorus-containing carbon dots with strong green fluorescence for cell labeling.* Journal of Materials Chemistry B, 2014. **2**(1): p. 46-48.

137. Wang, Q., et al., *Microwave–hydrothermal synthesis of fluorescent carbon dots from graphite oxide.* Carbon, 2011. **49**(9): p. 3134-3140.

138. Zhai, X., et al., *Highly luminescent carbon nanodots by microwave-assisted pyrolysis.* Chemical Communications, 2012. **48**(64): p. 7955-7957.

139. Sun, D., et al., *Hair fiber as a precursor for synthesizing of sulfur- and nitrogen-co-doped carbon dots with tunable luminescence properties.* Carbon, 2013. **64**: p. 424-434.

140. Zuo, P., et al., *Single-step preparation of fluorescent carbon nanoparticles, and their application as a fluorometric probe for quercetin.* Microchimica Acta, 2014. **181**(11): p. 1309-1316.

141. Fang, Y., et al., *Easy Synthesis and Imaging Applications of Cross-Linked Green Fluorescent Hollow Carbon Nanoparticles.* ACS Nano, 2012. **6**(1): p. 400-409.

142. Kwon, W. and S.-W. Rhee, *Facile synthesis of graphitic carbon quantum dots with size tunability and uniformity using reverse micelles.* Chemical Communications, 2012. **48**(43): p. 5256-5258.

143. Linehan, K. and H. Doyle, *Efficient one-pot synthesis of highly monodisperse carbon quantum dots.* RSC Advances, 2014. **4**(1): p. 18-21.

144. Wolfbeis, O.S., *An overview of nanoparticles commonly used in fluorescent bioimaging.* Chemical Society reviews, 2015. **44**(14): p. 4743-4768.

145. Peng, H. and J. Travas-Sejdic, *Simple Aqueous Solution Route to Luminescent Carbogenic Dots from Carbohydrates.* Chemistry of Materials, 2009. **21**(23): p. 5563-5565.

146. Roy, P., et al., *Photoluminescent carbon nanodots: synthesis, physicochemical properties and analytical applications.* Materials Today, 2015. **18**(8): p. 447-458.

147. Hu, S.-L., et al., *One-step synthesis of fluorescent carbon nanoparticles by laser irradiation.* Journal of Materials Chemistry, 2009. **19**(4): p. 484-488.

148. Zhou, J., et al., *An Electrochemical Avenue to Blue Luminescent Nanocrystals from Multiwalled Carbon Nanotubes (MWCNTs).* Journal of the American Chemical Society, 2007. **129**(4): p. 744-745.

149. Zhu, H., et al., *Microwave synthesis of fluorescent carbon nanoparticles with electrochemiluminescence properties.* Chemical Communications, 2009(34): p. 5118-5120.

150. Li, H., et al., *Carbon nanodots: synthesis, properties and applications.* Journal of Materials Chemistry, 2012. **22**(46): p. 24230-24253.

151. Baker, S.N. and G.A. Baker, *Luminescent carbon nanodots: emergent nanolights.* Angew Chem Int Ed Engl, 2010. **49**(38): p. 6726-44.

152. Wang, D., et al., *Facile and Scalable Preparation of Fluorescent Carbon Dots for Multifunctional Applications.* Engineering, 2017. **3**(3): p. 402-408.

153. Essner, J.B., et al., *Artifacts and Errors Associated with the Ubiquitous Presence of Fluorescent Impurities in Carbon Nanodots.* Chemistry of Materials, 2018. **30**(6): p. 1878-1887.

154. Zhu, S., et al., *Surface Chemistry Routes to Modulate the Photoluminescence of Graphene Quantum Dots: From Fluorescence Mechanism to Up-Conversion Bioimaging Applications.* Advanced Functional Materials, 2012. **22**(22): p. 4732-4740.

155. Liu, F., et al., *Facile Synthetic Method for Pristine Graphene Quantum Dots and Graphene Oxide Quantum Dots: Origin of Blue and Green Luminescence.* Advanced Materials, 2013. **25**(27): p. 3657-3662.

156. Eda, G., et al., *Blue Photoluminescence from Chemically Derived Graphene Oxide.* Advanced Materials, 2010. **22**(4): p. 505-509.

157. Pan, D., et al., *Hydrothermal Route for Cutting Graphene Sheets into Blue-Luminescent Graphene Quantum Dots.* Advanced Materials, 2010. **22**(6): p. 734-738.

158. Tetsuka, H., et al., *Optically Tunable Amino-Functionalized Graphene Quantum Dots.* Advanced Materials, 2012. **24**(39): p. 5333-5338.

159. Zu, F., et al., *The quenching of the fluorescence of carbon dots: A review on mechanisms and applications.* Microchimica Acta, 2017. **184**(7): p. 1899-1914.

160. Iqbal, A., et al., *Carbon dots prepared by solid state method via citric acid and 1,10-phenanthroline for selective and sensing detection of Fe2+ and Fe3+*. Sensors and Actuators B: Chemical, 2016. **237**: p. 408-415.

161. Gu, D., et al., *Green synthesis of nitrogen-doped carbon dots from lotus root for Hg(II) ions detection and cell imaging.* Applied Surface Science, 2016. **390**: p. 38-42.

162. Wang, L., et al., *Carbon dots based turn-on fluorescent probes for the sensitive determination of glyphosate in environmental water samples.* RSC Advances, 2016. **6**(89): p. 85820-85828.

163. Song, Y., S. Zhu, and B. Yang, *Bioimaging based on fluorescent carbon dots.* RSC Advances, 2014. **4**(52): p. 27184-27200.

164. Zhang, H., et al., *Solid-Phase Synthesis of Highly Fluorescent Nitrogen-Doped Carbon Dots for Sensitive and Selective Probing Ferric Ions in Living Cells.* Analytical Chemistry, 2014. **86**(19): p. 9846-9852.

165. He, D., et al., *A sensitive turn-on fluorescent probe for intracellular imaging of glutathione using single-layer MnO2 nanosheet-quenched fluorescent carbon quantum dots.* Chem Commun (Camb), 2015. **51**(79): p. 14764-7.

CHAPTER 2
INSTRUMENTATION AND METHODS

2.1 Fluorescence Spectroscopy

Fluorescence spectroscopic measurements of the fluorescent carbon dots (FCDs) and standards were made on a Perkin-Elmer FL8500, using both a single-cell holder and Peltier single-cell temperature controller. The light source was a 150-W continuous source xenon arc lamp. For standard excitation/emission measurements, quenching studies, and turn-on studies, a working PMT voltage of 550 V was used in the single-cell holder with slit widths of 5 nm and 20 nm for excitation and emission, respectively. A scan speed of 240 nm/min was used with a scan accumulation number of 3 to reduce background noise. The detector was set to the medium photomultiplier voltage setting (550 V) with a PMT of x8. For quantum yield studies, a working voltage of 550 V was used with the single-cell holder, using slit widths of 2.5 nm and 2.5 nm for excitation and emission, respectively.[1] A scan speed of 240 nm/min was used with an scan accumulation number of 3 to reduce background noise. The detector was set to the medium photomultiplier voltage setting (550 V) with a PMT of x8. The cuvette used was quartz with a pathlength of 10 mm. After collection, the data was processed, and figures created using Origin Lab version 8.5.1.

2.2 UV-Visible Absorption Spectroscopy (UV-Vis)

Ultraviolet-visible absorption spectra were obtained on a Cary 50-Bio UV-Visible Spectrophotometer (UV-Vis). The UV-Vis was operated using Cary-WinUV software. When using the Cary-WinUV Scan, it was operated in dual-beam absorbance mode on a slow speed scan rate. The wavelength range varied depending on the sample or standard being measured. The Cary-WinUV Simple Reads program used an integration time of 1 sec, with the wavelength of the light being measured changing relative to the sample and experiment. For all measurements, a quartz

cuvette with a pathlength of 10 mm was used. After collection, the data was processed, and figures created using Origin Lab Version 8.5.1 (MicroCal).

2.3 Infrared Spectroscopy (IR)

For measurements of the FCDs to examine for chemical functional group presence, infrared spectroscopy (IR) was performed on a Bruker Alpha Fourier transform infrared (FTIR) spectrometer, with a room temperature deuterated triglycine sulfide (DTGS) detector, mid-IR source (4000 to 400 cm^{-1}), and a KBr beamsplitter. A Bruker Pt-diamond ATR cell sampling accessory was used for the analysis. The settings used for experiments are as follows: spectral range, 4000–400 cm^{-1}; resolution, 4 cm^{-1}; sample scan time, 16 scans; background scan time, 16 scans; and scan speed, 10 kHz. Samples for analysis were dried under a nitrogen flow to produce a powder. Background spectra were collected with the stainless steel plunger engaged on the diamond window after cleaning the window with acetone and allowing it to dry to ensure a clean background scan. Particles powder was placed on the diamond window of the ATR cell and compressed using the stainless steel plunger assembly of the sampling module before acquiring spectra.

2.4 Dynamic Light Scattering (DLS) and Zeta Potential (ζ)

For dynamic light scattering (DLS) and zeta potential (ζ) experiments to determine size of the FCDs and potential aggregation effects, a Malvern Zetasizer Nano ZS (ZS3500) equipped with a 532 nm green laser was used in the LSU Polymer Analysis Lab (PAL). FCD powders before and after centrifugation for DLS analysis were dissolved in water or buffers and were placed in Sarstedt polystyrene cuvettes with a pathlength of 10 mm. Solutions for measurements of ζ were placed in Zetasizer Nano Series disposable folded capillary cells (DTS1070) produced by Malvern for analysis. Standard conditions were used to operate the Zetasizer.[2]

2.5 X-Ray Photoelectron Spectroscopy (XPS)

Surface analysis of FCDs to determine elemental composition and surface functionalities were performed using X-ray photoelectron spectroscopy (XPS). A Scienta Omicron ESCA 2SR X-ray Photospectrometer was used for the measurements. A monochromatic aluminum X-ray source operated at a 15 kV accelerating voltage with a 500-mm Rowland circle was used with a power of 190 W under higher vacuum (approximately 2.04^{-7} mbar) and 300 W power under lower vacuum (approximately 2.04^{-9} mbar). Samples were prepared through grinding and then compression into a flat pellet on indium foil using a razor blade. Conditions for survey scans are as follows: 150 eV pass energy, 1200.0–0.0 eV scanning range, 100 ms dwell time, and step size of 1 eV. Individual interest area scans were taken for the following elements under the following conditions: Carbon: 150 eV pass energy, 298.0–278.0 eV scanning range, 1000 ms dwell time, and step size of 0.050 eV; Oxygen: 150 eV pass energy, 542.0–522.0 eV scanning range, 1000 ms dwell time, and step size of 0.050 eV; Nitrogen: 150 eV pass energy, 412.0–392.0 eV scanning range, 2000 ms dwell time, and step size of 0.050 eV; Sodium: 150 eV pass energy, 1082.0–1067.0 eV scanning range, 1000 ms dwell time, and step size of 0.050 eV. The spectra were calibrated to the C1s peak at 285.0 eV. Standards for comparison included graphite, graphene oxide, and carbon black.[3-5] Analysis and processing of all data was performed using CasaXPS software, with spectral graphs produced using Origin Lab version 8.5.1 (Microcal).

2.6 Electron Paramagnetic Resonance (EPR)

To gain information about both the radicals generated on the surface of the FCDs, as well as the oxidation state of the metal ions involved in the turn-off mechanism, electron paramagnetic resonance (EPR) spectroscopy was performed on a Bruker EMX EPR spectrometer. The EPR was operated with a microwave frequency of 9.95 GHz, an attenuation of 60 dB, and a microwave

power of 2.00 mW. FCD analysis settings were based on the work of Sealy et alia, including 100 kHz field modulation and microwave power of 0.5-1.0 mW.[6] Solutions for measurement were placed into Wilmad-LabGlass X-Band Capillary EPR tubes for aqueous samples purchased from Thomas Scientific (1187C71) and inserted into a 4-mm EPR tube before being placed into the EPR resonator for analysis. The sample was measured in absorption mode before taking the first derivative to obtain the g-factor spectrum.

2.7 Low-Resolution Transmission Electron Microscopy (LR-TEM)

Low-resolution TEM was performed on a JEOL JEM-1400 low-resolution transmission electron microscope in the Shared Instrument Facility (SIF) at LSU. The LR-TEM was operated at 120 keV accelerating voltage. Samples were prepared by dissolving FCDs in 18 M$\Omega \bullet$ cm water, followed by pipetting 10 μL of the solution onto Formvar 100 mesh carbon-coated copper grids from Electron Microscopy Sciences (FCF 100-Cu). Grids were allowed to dry in air overnight to remove the water from the surface of the grid, leaving behind the FCDs. Additional preparation steps involved using the Leica EM ACE600 for glow discharge surface modification to allow for minimal particle aggregation and faster drying before deposition of the FCD solution onto the grid. The standard settings used were 12 mA current, 3.2 x 10^{-6} mbar air pressure, 20-s exposure time, and 0 nm sample height.

2.8 High-Resolution Transmission Electron Microscopy (HR-TEM)

High-resolution TEM was performed on a JEOL JEM-2010 high-resolution transmission electron microscope in the SIF at LSU. The HR-TEM was operated at 200 keV accelerating voltage. Samples were prepared by dissolving FCDs in 18 M$\Omega \bullet$ cm water, followed by pipetting 10 μL of the solution onto Formvar 100 mesh carbon-coated copper grids from Electron Microscopy Sciences (FCF 100-Cu). Grids were allowed to dry in air overnight to remove the

water from the surface of the grid, leaving behind the FCDs. Additional preparation steps involved using the Leica EM ACE600 for glow discharge surface modification to allow for minimal particle aggregation and faster drying before deposition of the FCD solution onto the grid. The standard settings used were 12 mA current, 3.2 x 10^{-6} mbar air pressure, 20-s exposure time, and 0 nm sample height.

2.9 References

1. Mehta, V. N.; Jha, S.; Kailasa, S. K., One-pot green synthesis of carbon dots by using Saccharum officinarum juice for fluorescent imaging of bacteria (Escherichia coli) and yeast (Saccharomyces cerevisiae) cells. *Materials Science and Engineering: C* **2014,** *38*, 20-27.

2. Salinas-Castillo, A.; Ariza-Avidad, M.; Pritz, C.; Camprubí-Robles, M.; Fernández, B.; Ruedas-Rama, M. J.; Megia-Fernández, A.; Lapresta-Fernández, A.; Santoyo-Gonzalez, F.; Schrott-Fischer, A., Carbon dots for copper detection with down and upconversion fluorescent properties as excitation sources. *Chemical Communications* **2013,** *49* (11), 1103-1105.

3. Krishnamoorthy, K.; Veerapandian, M.; Yun, K.; Kim, S. J., The chemical and structural analysis of graphene oxide with different degrees of oxidation. *Carbon* **2013,** *53*, 38-49.

4. Blyth, R. I. R.; Buqa, H.; Netzer, F. P.; Ramsey, M. G.; Besenhard, J. O.; Golob, P.; Winter, M., XPS studies of graphite electrode materials for lithium ion batteries. *Applied Surface Science* **2000,** *167* (1), 99-106.

5. Shao, Y.; Yin, G.; Zhang, J.; Gao, Y., Comparative investigation of the resistance to electrochemical oxidation of carbon black and carbon nanotubes in aqueous sulfuric acid solution. *Electrochimica Acta* **2006,** *51* (26), 5853-5857.

6. Felix, C. C.; Sealy, R. C., o-Benzosemiquinone and its metal chelates. electron spin resonance investigation of radicals from the photolysis of catechol in the presence of complexing metal ions. *Journal of the American Chemical Society* **1982,** *104* (6), 1555-1560.

CHAPTER 3
SYNTHESIS AND CHARACTERIZATION OF FLUORESCENT CARBON DOTS

3.1 Introduction

Fluorescent carbon dots (FCDs) lend themselves well to multiple biological applications and wide-ranging studies of health effects, both at the whole-body and cellular levels. Additionally, the high quantum yields, tunable fluorescence, chemical simplicity, and range of synthesis pathways make them extremely versatile and applicable to study carbonaceous pollutants. Black carbon (BC) is one component of a class of particulate matter (PM) known as $PM_{2.5}$. It is a pollutant in dire need of study and evaluation, particularly on a cellular level. FCDs hold great potential as a valuable tool for gathering select information needed about BC and its health effects. PM is typically considered as a mosaic, studying PM gathered from the environment with its thousands of constituent materials.[1, 2] While this can be used to help measure the effects of environmental pollution on populations and to better understand the environmental impacts of individual materials, they must be isolated and studied.[3] Difficulties in isolation of individual components of PM abound, including issues pertaining to separating biological, organic, and inorganic components.[4-6] The issue is not only separating the components, but also collecting enough of the components during the separation process and using the individual components for testing. Designing surrogates that are chemically and structurally similar is a much simpler and efficacious method to analyze individual PM components.

Though FCDs can be synthesized through a multitude of pathways, certain methods offer the best chance to produce FCDs that mimic BC, particularly bottom-up methods. Top-down methods tend to require passivation and modification, making them less likely to resemble

naturally occurring BC.[7-9] Considering bottom-up methods, pyrolysis or thermal approaches offer the most viable route to produce FCDs similar enough to BC to be used as surrogates.

When selecting the most appropriate thermal method for synthesis of FCDs, it is important to consider the needs of the envisioned applications and how to modify existing approaches. Some approaches involve the use of a carbon source, which while producing carbon nanoparticles, the latter are not necessarily fluorescent without oxidation of the surface of the particles.[10-12] The simpler the pyrolysis process for synthesis, the more effective the comparison between the FCDs and BC, considering BC is produced through simple combustion processes. The other benefit of using a bottom-up, thermal method is that the starting materials are all carbonaceous materials that could likely be the source of naturally occurring combustion-produced BC. To that end, investigated here are thermal routes for making FCDs that will serve as an effective analysis tool for evaluating BC fate and its effects in cells.

3.2 Experimental Section

3.2.1 Materials

Sodium alginate was purchased from Ward's Science (Rochester, NY). Agarose (protein electrophoresis grade), sucrose, glucose, sodium phosphate monobasic anhydrous, and sodium phosphate dibasic anhydrous were purchased from Fisher Scientific (Hampton, NH). Graphene oxide was purchased from Tokyo Chemical Industries (Tokyo, Japan). Sephadex G-25 was purchased from Sigma-Aldrich (St. Louis, MO). Water from a Barnstead Nanopure Diamond Water System (18 M$\Omega \bullet$ cm) was used for all experiments. Qualitative filter paper 415 (25 μm pore size) and 413 (5 μm pore size) were purchased from VWR International (Radnor, PA). The quartz combustion boat was purchased from Technical Glass Products, Inc. (Painesville, OH).

TEM grids were Formvar carbon-coated square mesh Cu, 100 Mesh, purchased from Electron Microscopy Sciences (Hatfield, PA).

3.2.2 Synthesis

The carbon source was weighed (0.1-5 g) and placed into a quartz boat. The quartz boat was pushed into a glass combustion tube created in the LSU glass blowing facility. The glass tube was placed in a Lindberg/Blue M tube furnace and connected to tanks of gas (oxygen or compressed air). The glass combustion tube was then closed and sealed using an o-ring and glass cap that were connected to an air flow line leading into an exhaust vent. The furnace was then activated, and the temperature was set and allowed to ramp to the desired temperature before the time measurement was initiated. After the allotted pyrolysis time was reached, the furnace was turned off and allowed to cool down for approximately 20 minutes. The furnace lid was then lifted, and the glass combustion tube, quartz combustion boat, and carbon product were allowed to cool for an additional 20-30 minutes. The quartz boat was extracted, and the carbon was rinsed out of the boat using nanopure water into a beaker. The water/carbon solution was mixed to ensure the maximum amount possible is dissolved before the solution was filtered by being poured through VWR 415 filter paper. The resulting filtrate was then poured through VWR 413 filter paper. The collected filtrate was poured into a 50-mL plastic centrifuge tube and forced to dry under a constant flow of nitrogen gas to remove the water and dry the particles. Further purification through ultracentrifugation is outlined in section 3.3.2.3.

3.3 Results and Discussion

3.3.1 Synthesis Conditions

The synthesis performed in this research is a bottom-up thermal pyrolysis method using sodium alginate, after the model of Fong et alia.[13] In that work they reported the use of sodium

alginate as a carbon source, followed by pyrolysis of the alginate under a flow of gas at temperatures ranging from 150-300 °C. The optimal FCD synthesis temperature reported by the investigators was 250 °C, with the pyrolysis atmosphere not identified by the researchers. Following the general trend of Fong's research, the FCDs in this research were first created by combusting 0.5 g of sodium alginate under compressed air at 250 °C for 2.5 hours. A black powder that dissolved selectively in water to produce a dark colored liquid was produced. The particles, once dissolved, possessed fluorescent properties, though the fluorescence signal was reported to be weaker than desired. To optimize the synthesis, multiple conditions were tested and tabulated in Table 3.1. Temperatures were tested ranging from 150 °C to 400 °C at times ranging from 30 minutes to 3 hours. Following a protocol similar to that proposed by Fong et alia, pyrolysis at 250 °C for 2.5 hours produced fluorescent particles. Other time periods were tested at 250 °C before other temperatures were tested. A reaction time of 1 hour was sufficient to produce FCDs with strong fluorescence, so a 1 hour time period was tested at other temperatures first. After evaluating the yield and fluorescence signal generated at the different temperatures for 1 hour pyrolysis time, different time scales were tested. At a temperature of 300 °C, results appeared similar to those from 250 °C, so the full range of time periods was tested at that temperature. The other test temperatures, 150 °C, 200 °C, 350 °C, and 400 °C, did not produce FCDs in similar yields or fluorescence intensity, therefore only limited time scale studies were performed at those temperatures. Regarding the fluorescence intensity, to avoid extensive quantum yield or concentration optimization studies, small amounts of the FCDs were dissolved in water (0.5 mg/mL). The fluorescence was measured under the same conditions, and all spectra were

Table 3.1 Report of the effect of synthesis conditions on produced FCDs. Multiple temperatures and times were tested to evaluate percent yields and fluorescence intensity of the produced FCDs. All tests were performed with the same mass of sodium alginate, with fluorescence measured under the same conditions and settings. Percent yields are followed by standard deviation.

Temperature	Time	Yield	Fluorescence
150 °C	1 hr	65 ± 3 %	Weak
	2 hr	63 ± 5 %	Weak
	3 hr	62 ± 2 %	Weak
200 °C	1 hr	63 ± 8 %	Weak
	2 hr	62 ± 3 %	Medium
	3 hr	65 ± 5 %	Weak
250 °C	30 min	78 ± 1 %	Strong
	1 hr	77 ± 3 %	Strong
	1.5 hr	79 ± 7 %	Strong
	2 hr	73 ± 2 %	Strong
	2.5 hr	73 ± 3 %	Strong
	3 hr	66 ± 4 %	Weak
300 °C	30 min	67 ± 3 %	Strong
	1 hr	67 ± 2 %	Strong
	1.5 hr	65 ± 3 %	Strong
	2 hr	68 ± 5 %	Medium
	2.5 hr	63 ± 8 %	Medium
	3 hr	62 ± 9 %	Weak
350 °C	1 hour	60 ± 3 %	Weak
	2 hour	61 ± 6 %	Weak
	3 hour	65 ± 2 %	Weak
400 °C	1 hour	52 ± 4 %	Weak
	2 hour	51 ± 8 %	Weak
	3 hour	47 ± 11 %	Weak

compared and grouped into three fluorescence groups (strong, medium, and weak) based on the intensity of the signal. While not quantitative or completely comprehensive, this method was deemed sufficient to evaluate the effect of pyrolysis temperature and time on the fluorescence of the produced FCDs. Percent yields were evaluated by weighing the sodium alginate before it was placed in the furnace and dividing the final mass of produced FCDs by the original mass of the sodium alginate. The final mass of the FCDs was collected by weighing the plastic 50 mL centrifuge tube before pouring the filtered FCD solution into the tube and allowing all the water to evaporate off under a constant flow of nitrogen gas. Following the complete drying of the FCDs, the centrifuge tube and FCDs were weighed to obtain the mass of the FCDs before using that value to calculate the percent yield. All percent yields were measured 5 times for each analysis point, and the standard deviation is reported in Table 3.1, rounded to the nearest whole number.

The evaluation of pyrolysis temperatures shows that temperatures in the middle of the chosen range, i.e., 250 °C and 300 °C, are the most effective at producing FCDs possessing strong fluorescence in high yields. Temperatures on the lower and upper end of the range produce FCDs in significantly smaller quantities with lower witnessed fluorescence intensity. This can be explained by combustion processes that naturally occur in the atmosphere and, therefore, is to be expected. At temperatures greater than 300 °C, extensive charring of carbonaceous materials occurs. Charring is the incomplete combustion of the carbonaceous starting material, producing carbon materials that are insoluble in water and do not possess the highly organized structure of the materials that result from organic carbon or the carbon produced in the vapor phase from the carbon source as it is pyrolyzed.[14-16] At lower temperatures, the same problem occurs, but in a reverse process. Rather than a higher level of charring, there is less of the vapor phase organic carbon produced, resulting in less production of the highly organized carbonaceous materials. Both

processes result in lower production of the highly ordered carbon required to produce fluorescence, so a pyrolysis temperature of 250 °C was determined to be the optimal pyrolysis temperature for synthesis. Regarding the pyrolysis times, it is believed to have less impact than the temperature, with the time only determining how long it takes for the complete amount of pyrolysis to occur. At longer times, more extensive charring occurs, as with higher temperatures. Once a temperature threshold has been determined where extensive charring does not occur, reaction time was tested by decreasing the reaction time to 30 min. This reaction time produced FCDs with no diminished fluorescence, in yields comparable to the maximum measured. Due to this, a time of 30 minutes and a temperature of 250 °C were determined to be the optimal synthesis conditions. Evaluation of the gas under which the heating process occurred yielded more complex results.

The choice of gas under which synthesis occurred impacted the appearance of the dried FCDs significantly, as can be seen in Table 3.2. All gases were allowed enter the glass tube and flow across the sodium alginate at a pressure of 30 psi. By flowing compressed air over the sodium alginate as it was heated, a black powder that dissolved in water to produce a dark-colored solution

Table 3.2 The effect of gas under which synthesis occurred on FCDs. The effect on the particles can be seen visually, including a different colored solution produced when the FCDs are dissolved in water.

Gas	Particle Color	Example
Compressed Air	Black	
Oxygen	Tan	

was formed. If instead oxygen gas was allowed to flow across the sodium alginate, a tan-colored powder that dissolved in water to produce a clear and colorless solution was formed. Adjusting the pressure of the gas flow resulted in changes as well. When the oxygen flow entering the glass tube was reduced below 30 psi, the black particles formed again. This could suggest that the low flow rate allowed ambient air to enter the system, resulting in the black particles. In testing the optical and physical properties of the FCDs, as outlined below, both particles exhibited no differences. A further evaluation is presented in the characterization section of this chapter, but for the purpose of this discussion of optimal synthesis method, purely logistical concerns will be addressed here.

When measuring fluorescence of a solution-phase sample, the color and transparency of the sample are crucial factors to consider. Clear, colorless solutions absorb minimal amounts of the incident light from the excitation source as the sample is irradiated, in addition to exhibiting elastic Rayleigh scattering in the wavelength region used in these experiments.[17] These factors couple to mean that the fluorescent material will be allowed to absorb the maximum amount of light, with the maximum amount of fluorescent light therefore being measured. When solutions are darker in color and not transparent, much of the incident light is absorbed by the solution itself, limiting the amount light available to be absorbed by the fluorescent materials. Inner-filter effect in the dark solution can also reduce the produced fluorescence signal, both through absorbance of the incident light as well as absorbance of produced fluorescence.[18] Additionally, any fluorescence produced in a clear, colorless solution can scatter minimally, but will not be absorbed, allowing the light to be measured and observed. In darker solutions, the fluorescence produced can be absorbed by the solution itself, limiting the fluorescence measured. These considerations can combine to produce materials that appear less fluorescent, regardless of whether the actual fluorescence produced is less. Figure 3.1 exhibits this principle in evaluating the FCDs produced

under compressed air or oxygen. The maximum amount of fluorescence for the black materials resulting from production in air resulted at a concentration of 0.06 mg/mL in water, while the maximum amount of fluorescence obtained for the tan particles synthesized under oxygen was obtained at a concentration of 10 mg/mL. At concentrations higher than 0.06 mg/mL, the black particles produce a darker colored liquid that showed a decrease in the fluorescence signal, assumed to be due to the absorption of the light by the darker colored solution. The fluorescence intensity of the particles synthesized under oxygen increases as the concentration increases, until a maximum is reached at 10 mg/mL, where the solution begins to darken in color as more FCDs are added. While many fewer particles at a much lower concentration are required for the particles synthesized under air to produce fluorescence in significant quantities, the larger amount of fluorescence obtained from oxygen-produced FCDs makes them a more viable fluorescent probe

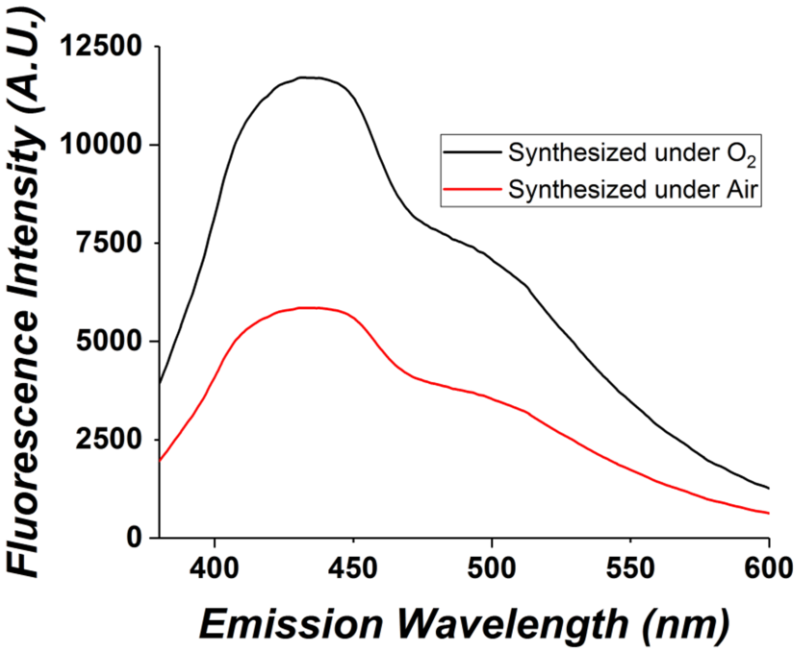

Figure 3.1 Fluorescence maxima exhibited by FCDs produced under oxygen and compressed air. The concentration was adjusted for both particles to obtain the maximum fluorescence, which is exhibited above. The particles produced under air are 0.06 mg/mL in water, while the particles produced under oxygen are 10 mg/mL in water.

for biological studies and therefore a more viable surrogate for BC. Although both the black and tan FCDs were evaluated for their properties, for future testing, the tan FCDs produced under oxygen were used. With pyrolysis temperature, time, and gas optimized, other carbon-based starting materials were tested.

As outlined previously, any carbon-based substance can be used as a starting material for the pyrolysis method of producing FCDs. While more complex materials made up of multiple types of carbon or carbon-based materials can require extensive purification or modification, simpler carbon-based starting materials containing few elements beyond carbon can offer FCDs that require less purification and no modification. Based on these factors, sugars were chosen as carbon sources for study. Agarose, sucrose, and glucose were all tested as a carbon source, using the optimized conditions of 250 °C pyrolysis temperature and 30 minutes for heating time under a 30 psi flow of oxygen gas entering the glass tube. While all three starting materials produced FCDs with structural and fluorescent properties similar to those produced from sodium alginate, their use resulted in some problems. All three new starting materials produced FCDs that, when dried, rather than forming a fine powder like that of the sodium alginate, formed a hard solid that was very difficult to break up and extract from the centrifuge tube in which they were dried. This production of hard, difficult to extract particles makes them difficult to use in any testing that involves solid phase samples. When using solid phase analysis techniques, such as X-ray diffraction, X-ray photoelectron spectroscopy, and infrared spectroscopy, more finely ground particles will allow for more effective testing. By having solid particles that resist being ground into fine powder, effective analysis using those techniques becomes difficult. For solution-phase analysis techniques, it is vital to control the amount of solid particles dissolved to ensure overconcentration effects, such as saturated detectors or inner-filter effects, and under concentration effects, mainly consisting of

lack of detection of the sample, do not occur. The color produced was similar to that of FCDs made from sodium alginate, though slightly darker in color, meaning the color of the solutions of dissolved FCDs fell somewhere in between the coloring of the sodium alginate FCDs produced under compressed air and oxygen, respectively. All of these factors combine to show the efficacy of the synthesis conditions to produce viable FCDs from a variety of carbon sources; however, all results support the use of sodium alginate as the carbon source for the FCDs to be examined in this research.

The mass of starting material was also tested, beginning with a mass of 0.5 g sodium alginate and decreasing the starting mass to as low as 0.1 g and as high as 5 g. It was found that decreasing the starting mass below 0.5 g had no effect on the percent yield, but due to the smaller amount of produced FCDs, using any amount less than 0.5 g in the synthesis process was abandoned. Under the optimal synthesis conditions, when amounts greater than 0.5 g were used, there was a decrease in the percent yield. If the pyrolysis temperature was increased, no percent yield increase was observed, but if the heating time was increased, the percent yield increased for starting material masses of 1 g and 2 g. Masses greater than 2 g showed a lowering of the percent yield to approximately 50% with an increased requirement for filtration and purification processes, so amounts greater than 2 g were abandoned as well. For starting material masses of 1 g and 2 g, when heating times were increased to 2.5 hours, the percent yield was comparable to that of the optimal conditions for 0.5 g. The overall time for production and isolation was found to be longer for the protocols that used an increased amount of starting material and produced larger yields of FCDs. Due to these factors, it was judged that though the overall amount of FCDs produced by 0.5 g starting material was less than that of 1 g or 2 g of starting material, the high throughput afforded by the decreased heating time and drying time would allow for an increase in the overall

production of FCDs. In conclusion, unless otherwise stated, FCDs used in this research were produced through pyrolysis 0.5 g of sodium alginate at a temperature of 250 °C for 30 minutes under a 30 psi flow of oxygen gas entering the glass tube.

3.3.2 Characterization

3.3.2.1 Optical Properties

Arguably the most important properties to characterize regarding the FCDs synthesized in this research are the optical properties. To be an effective cellular probe, the FCDs should absorb light and subsequently fluoresce. Studies to determine the fluorescence properties of the FCDs were carried out on a PerkinElmer FL8500 fluorimeter. The excitation wavelength (λ_{ex}) maximum that correlates to the region of maximum absorbance was measured, along with the emission wavelength (λ_{em}) maximum, as noted in Figure 3.2.

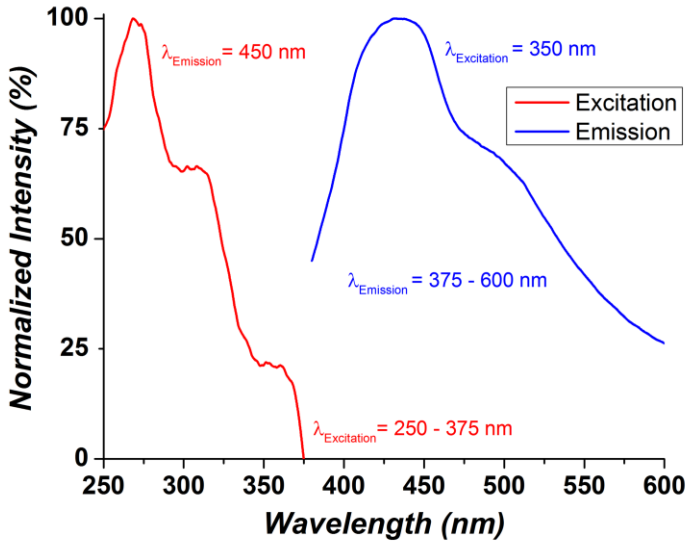

Figure 3.2 Excitation and emission scans of ultracentrifuge purified FCDs. The fluorescence signal was normalized to the maximum signal generated by the excitation scan to make the spectra easy to compare and was plotted against wavelength to determine the maximum excitation and emission wavelengths.

In order for a material to be fluorescent, it must first absorb significant amounts of light, therefore an analysis of absorbance and excitation of the FCDs is a vital first measurement. In order to determine the maximum absorption range, a Cary 50-Bio UV-Visible Spectrophotometer (UV-Vis) was used to measure the absorbance of 2 mg/mL ultracentrifuge purified FCDs dissolved in water. The FCDs showed a high amount of absorption in the 250-350 nm energy range. This range is in the region for which water scatters large amounts of light, so while the absorbance could clearly be measured, it is difficult to determine how much is attributed to water and how much to the FCDs. Background subtraction was done, subtracting the water signal to show the absorbance due to the particles, but it was determined that once absorption was confirmed, the more detailed analysis should focus on a study of the excitation wavelength to determine the best wavelength to use for the fluorescence. To measure the λ_{ex}, the λ_{em} was held at 450 nm while the λ_{ex} was swept from 250-375 nm to evaluate the range of high absorbance measured in the UV-Vis spectrum. The results show a maximum λ_{ex} around 250 nm, with two shoulders at 300 nm and 350 nm. While the 250 nm wavelength produced the maximum amount of absorbance, the peak at 350 nm was chosen to be the wavelength that was used to excite the FCDs in all subsequent studies. The reason 350 nm was chosen over 250 nm was to limit autofluorescence in biological systems. It is well known that cytosolic proteins and enzymes fluoresce when exposed to incident light in the blue/UV range. [19, 20] While 350 nm does not completely avoid the range of induced autofluorescence, it was decided by this scientist that the less energetic is the excitation wavelength, the better. The sacrifice in fluorescence intensity was deemed an acceptable loss in an attempt to avoid extensive autofluorescence. The emission spectrum was collected by holding the λ_{ex} at 350 nm and scanning the λ_{em} from 375-600 nm. The spectrum has a clear peak around 450 nm and a shoulder around 500 nm. The 450 nm peak, being an intense and sharp emission

band, was chosen as the λ_{em} to be used moving forward. Unless otherwise stated, for the fluorescence studies, the λ_{ex} is 350 nm and the λ_{em} is 450 nm.

The fluorescence profile, including the spectral pattern and the maximum excitation and emission wavelengths, can give insight into the fluorescent species responsible for the optical properties witnessed in the FCDs. In later discussions in this chapter, the physical and chemical characterization through TEM, IR, XPS, and EPR suggests that the FCDs are graphene oxide nanoparticles with catechol, quinone, hydroquinone, and semiquinone radicals in various states on the surface, and the fluorescence data supports those conclusions. Extensive fluorescence analysis of humic materials, carbonaceous substances with quinone, phenol, catechol, and sugar moieties, can be found in the literature.[21] It was concluded that a specific type of humic material, fulvic acid, typically exhibits fluorescence with a λ_{ex} maximum of 325-375 nm and a λ_{em} maximum of 450 nm.[22] Ariese et alia also evaluated the fluorescence of the fulvic acid materials as compared to a quinone/hydroquinone model system.[23] Upon comparison with the quinone/hydroquinone model system, the fluorescence pattern was similar, particularly at lower temperatures, with a consistent λ_{em} maximum of 450 nm witnessed in both cases. When considering any contribution of the bulk particle to the fluorescence, graphene oxide typically exhibits fluorescence in the red to near-IR range of light, with maximum intensity between 500-800 nm.[24] With a maximum λ_{ex} maximum of 325 nm and a maximum λ_{em} maximum of 450 nm, the fluorescence produced by the FCDs matches that of the quinone/hydroquinone model system and the humic materials, furthering the confirmation of graphene oxide nanoparticles with catechol, quinone, hydroquinone, and semiquinone radicals in various states on the surface contributing to the fluorescence mechanism.

In order for the potential of the FCDs to be realized regarding their being effective biological fluorescent probes, an evaluation of the stability of the FCDs is required. First, to assess the chemical stability of the FCDs, ultracentrifuge purified FCDs were dissolved in phosphate buffers of various pH before the fluorescence spectrum was measured. Three different pH values were tested: 4.1, 7.4, and 10.3. The fluorescence signal was the exact same in all three buffers, as seen in Figure 3.3, showing that the surface functionalities, while believed to be responsible for the fluorescence in the literature outlined in Chapter 1, are not affected by the pH significantly enough to impact the fluorescence emission energy or intensity. This demonstrated the FCDs should be effective regardless of the pH of the solution, which is valuable for a biological probe, considering the different pH values that exist outside the cell, in the cytoplasm, and in various organelles.

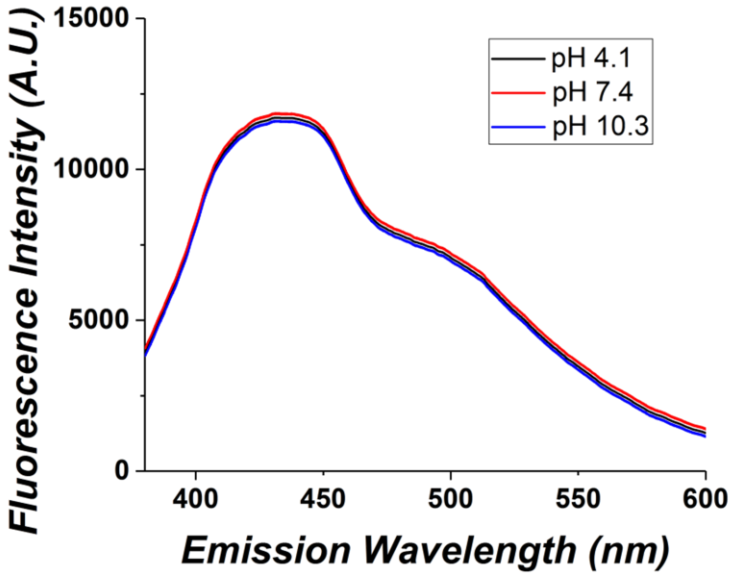

Figure 3.3 Evaluation of pH on fluorescence of FCDs. FCDs were dissolved in concentrations of 2 mg/mL in phosphate buffers of three different pH.

Examination of FCD photostability was performed, because probes for biological systems benefit from time-independent emission behavior. A 2 mg/mL solution of ultracentrifuge purified FCDs was continuously irradiated for a 12-hour period by the incident laser in the fluorimeter, with fluorescence being measured once every hour to evaluate any changes in the emission signal due to bleaching over time; however, no decrease in the fluorescence was observed, with the results seen in Figure 3.4 A. This experiment demonstrates that there is no significant impact of

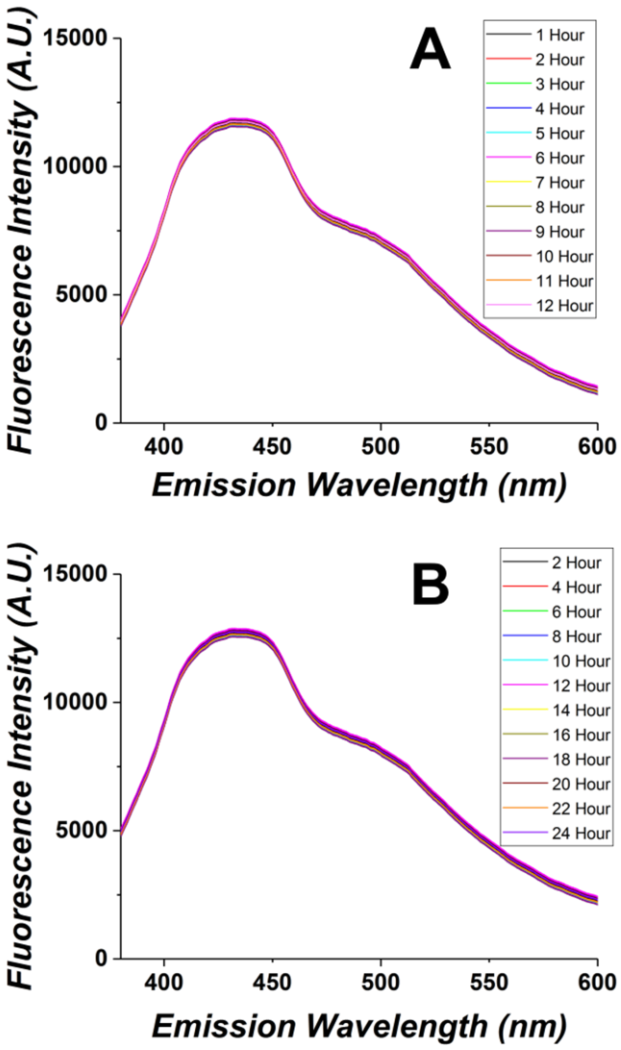

Figure 3.4 Evaluation of the photostability and solution phase stability of FCDs over time. 2mg/mL FCDs dissolved in pH 7.4 phosphate buffer A) Irradiated continuously over a 12-hour period with fluorescence measured every hour. B) FCD solution allowed to rest on the benchtop with fluorescence measured every hour for a 24-hour period.

continuous irradiation on the stability of the fluorescence emission intensity. In an attempt to evaluate the stability of the FCDs in solution over time, a solution of 2 mg/mL FCDs in phosphate buffer at a pH of 7.4 was created and analyzed via a fluorescence emission scan every morning for 24 days with no decrease in fluorescent signal, the results can be seen in Figure 3.4. During the time period, the solution remained sealed in a scintillation vial on the benchtop. To test the stability of the FCDs in the solid phase, the same sample of solid FCDs was used to make a fresh solution of 2 mg/mL ultracentrifuge purified FCDs every morning for the same 24-day period, with a fluorescence emission scan performed to evaluate potential changes in the fluorescence emission intensity and wavelength profile. Once again, no appreciable change occurred. These tests confirm the high level of stability seen in the FCDs made using the protocol I developed here, which includes chemical- and photo- stabilities.

One optical property of FCDs explored in Chapter 1 was the excitation wavelength-dependent emission wavelength. It is commonly seen in FCDs made by other routes that as the λ_{ex} is changed, the λ_{em} changes.[25] This property was explored in the FCDs created in this research; the data are presented in Figure 3.5. A solution of 2 mg/mL ultracentrifuge purified FCDs in pH 7.4 phosphate buffer was prepared as outlined above. The λ_{ex} was changed from 275 nm to 400 nm, with the fluorescence intensity measured from 300-700 nm with the exact λ_{em} range used varying based on the λ_{ex}. The first overall trend witnessed was a change in the fluorescence intensity, which is to be expected. As the λ_{ex} gets further from the optimal excitation wavelength determined previously, the fluorescence intensity will decrease. This trend holds true, with the fluorescence intensity reaching its maximum when excited at 300 nm. Furthermore, the important observation was found that there were no changes in fluorescence intensity at the various emission wavelengths nor were there any changes in peak emission energies. The shoulder at around 500

nm exhibits no significant change in position as the λ_{ex} is varied. The other, more substantial peak found at 450 nm upon excitation at 350 nm shifts slightly as the λ_{ex} changes. The emission peak is observed at 450 nm when the solution of FCDs is excited at 350 nm, but when an excitation wavelength where maximum absorption occurs (300 nm), the peak blue shifts, with the peak emission occurring at 400 nm. The energy of maximum intensity is a function of wavelength; when excited by higher energy light at 275, 300, and 325 nm, the peak is observed at 400 nm. When excited by lower energy light at 350, 375, and 400 nm, the peak is found closer to 450 nm. This observation is consistent with prior work with other types of FCDs, but differs from past observed FCD behavior in that the energy shifts found here do not exhibit a continuous change with systematic change in excitation energy. Typical FCDs show a shift in emission wavelength with every shift in excitation wavelength; the further blue-shifted the excitation is from the absorption maximum, the further blue-shifted is the emission. Similarly, the more red-shifted the excitation

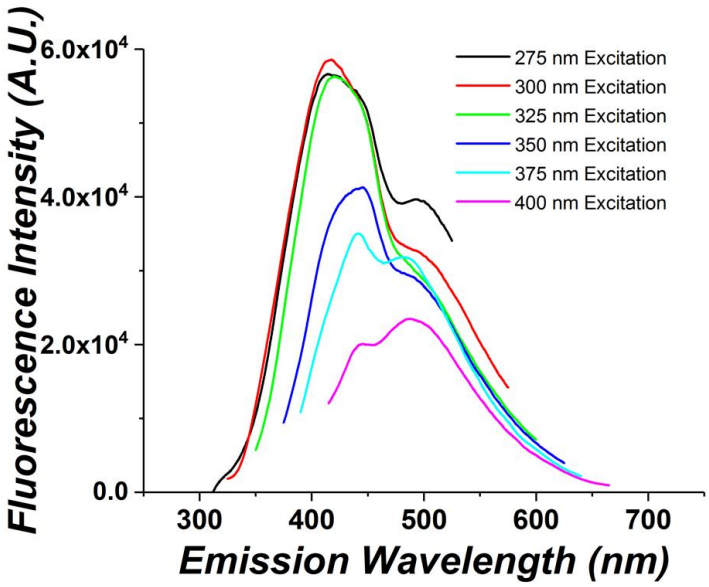

Figure 3.5 Effect of excitation wavelength on the emission spectra of ultracentrifuge purified FCDs. Changes in the fluorescence emission due to changing excitation wavelengths was probed through fluorescence emission scans of wavelengths ranging between 300-700 nm under varying excitation wavelengths.

is from the primary maximum absorption peak, the more red-shifted is the emission. The FCDs prepared here exhibit properties more akin to materials possessing quantized electronic states rather than a constantly shifting emission peak. This behavior is interesting, but not radically different than the FCDs that have come before.

3.3.2.2 Physical and Chemical Properties

Once the FCDs were confirmed to possess desired fluorescence properties, an evaluation of the structural properties was performed. The first evaluation of the FCDs in pH 4, 7.1, and 10.3 was by dynamic light scattering (DLS), in an attempt to determine the size of the particles in solution. Unfortunately, outcomes from the DLS were inconclusive for providing meaningful information about particle size in solution. Examination of DLS data using the associated instrument software led to reported particle sizes that range from 150 nm to >300 nm, which are sizes inconsistent with observations for FCDs prepared using pyrolysis methods in the literature, with said values being less than 50 nm. The large sizes obtained from DLS for the materials I have prepared are believed to be due to extensive aggregation of the FCD particles in the pH 4, 7.1, and 10.3 solution. Additionally, DLS provided some insight regarding aggregation, in the form of the zeta potential of the particles. Zeta potential is a measure of the electrostatic potential at the electrical double layer surrounding the nanoparticles in solution.[26] This potential gives insight into the particles' behavior in solution. Particles with zeta potentials between −10 mV and +10 mV are considered electrically neutral, with anything beyond those values pointing to particles being considered as charged. The charge of the nanoparticle correlates to its tendency to aggregate, with highly charged particles (± 40 mV) exhibiting a large amount of repulsive force between each other, thereby stabilizing the nanoparticles in solution and preventing their aggregation. On the other hand, when particles are closer to zero than −30 mV or +30 mV, aggregation is highly likely,

because the particles do not strongly repel each other.[27] The zeta potential of the FCDs was measured in phosphate buffers at pH, 4, 7.4, and 10.3 to determine if the charge is a product of the FCD surface or is relative to the solution in which they are dissolved. Under all conditions, the measured zeta potential was approximately −20 mV, indicating that the surface is negatively charged, but not sufficiently so as to prevent aggregation. Based on the zeta potentials measured under the solution conditions used here and in all biological studies, it seems likely the particles are aggregating due to insufficient electrostatic repulsion, which results from either low intrinsic surface charge of the FCDs or salt-induced screening of FCD surface charge. It should also be stated that when the black particles synthesized under air were tested using this method, the results were virtually identical, with DLS-derived sizes of greater than 150 nm and zeta potentials near −20 mV, regardless of the pH of the buffer containing the dissolved particles. These observations further demonstrate that the FCDs produced under different gas conditions have similar properties overall, other than their color.

To gain another measure of FCD size, as well as more information about the structure of the FCDs, low-resolution and high-resolution transmission electron microscopy (LR-TEM and HR-TEM) were pursued. Initially, TEM grids were prepared through typical methodologies, dissolving FCDs into water in amounts of 2 mg/mL before depositing 10 μL onto the surface of a TEM grid prior to drying overnight under ambient conditions. For initial studies of size, morphology, and chemical composition, FCDs that had not undergone ultracentrifuge purification were used. Ultracentrifuge purified FCDs were tested and are evaluated for size, morphology, and chemical composition in section 3.3.2.3. For initial analysis, LR-TEM was performed; representative images are presented in Figure 3.6. As seen in the images, the morphology of the FCDs is as expected, spherical and relatively regular. The sizes range from 20 to 50 nm. This

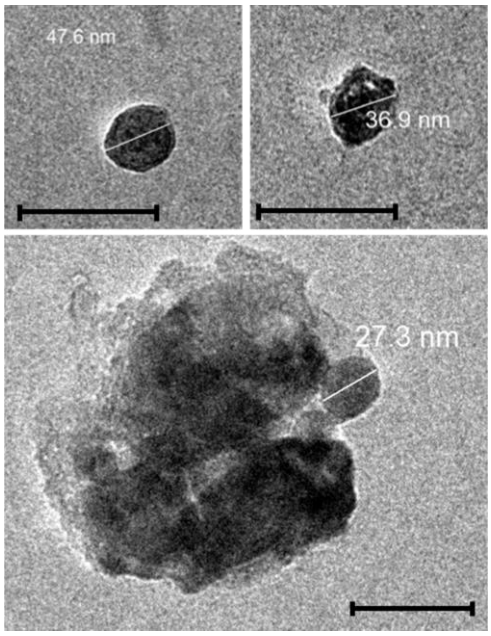

Figure 3.6 Low-resolution transmission electron microscopy (TEM) images of FCDs dissolved in water and allowed to dry on the TEM grid overnight. Black scale bar = 100 nm.

confirms the expected size of less than 50 nm, and also confirms the sizes being measured by the DLS experiment were not representative of the actual size of the individual FCDs. As seen in the bottom image of Figure 3.6, aggregation of FCDs is noted, in agreement with DLS results. However, in this case there was no salt present that would lead to electrostatic screening effects and thus particle aggregation, assuming that the zeta potential of the FCDs has a magnitude greater than 20 mV in pure water, which cannot be measured using the system available at LSU. As shown in the bottom image, the particles appear to have aggregated into a particle greater than 150 nm in size. A single FCD is readily noted in the aggregate, with a measured size that is similar to that of those that are isolated in the top images. Thus, it is possible that the observed aggregates in the bottom of Figure 3.6 led to the observation of larger-than-expected sizes by DLS. At the same time, it is also highly probable that the presence of salt would lead to aggregation of FCDS such as those in the top portion of Figure 3.6; however, attempts to perform TEM on such samples were

met with frustration, due to the abundance of salt crystals (not unexpected) that obscured images of the FCDs.

To get more information regarding the FCDs, HR-TEM was employed. HR-TEM, though more complex and time consuming, offers increased magnification and much higher resolution than LR-TEM, giving more information than LR-TEM can offer. The increased resolution and magnification allow for the evaluation of the lattice spacing of atoms that make up crystalline nanoparticles. Experiments aimed at measuring the lattice spacing of particles using oxygen and air for their formation were performed, and typical images are shown in Figure 3.7. The lattice spacing of the atoms in the nanoparticles was determined by physically measuring a region of the images containing lattices, counting the spaces, and then dividing the overall length by the number of lattice spaces. This value, once determined, allowed for an evaluation of the crystal structure in an effort to identify the material based on the unique lattice spacing for each type of known material. Routinely observed were nanoparticles, such as those in Figure 3.7 A and B, having crystal lattices. Particles prepared using either oxygen or air exhibit lattice spacings with a mean value of 0.28± 0.006 nm. This value is consistent with that for strained graphene oxide or graphene oxide with a slightly expanded lattice due to water or other repelling functionalities contained between faces of the crystal lattice.[28]

Identifying the FCDs as being made of graphene oxide is congruent with expected outcomes from the synthesis method, considering graphene oxide can be synthesized from thermal processes involving carbon starting materials in the presence of oxygen.[29] Finding individual particles to measure the lattice spacing was difficult in some regions of images, due to the large aggregation effects observed for the FCDs in solution phase, as can be seen in Figure 3.7 C. The crystal lattices of individual particles can be seen in the aggregate, showing the aggregates are

indeed made up of the FCDs, but the individual lattice for each particle within the aggregate is difficult to measure due to backscattering effects. These aggregation effects make other analysis methods difficult to perform as well. For example, a powerful capability of HR-TEM is selected-area electron diffraction (SAED), wherein is measured the electron diffraction pattern of a crystal so as to gain more in-depth information about the identifying crystal structure of the material. Unfortunately, due to the large level of aggregation noted for the FCDs, it was often impossible to obtain a clear diffraction pattern from an individual crystal. When multiple diffraction patterns from multiple crystals overlap, interference occurs, making a clear diffraction pattern impossible

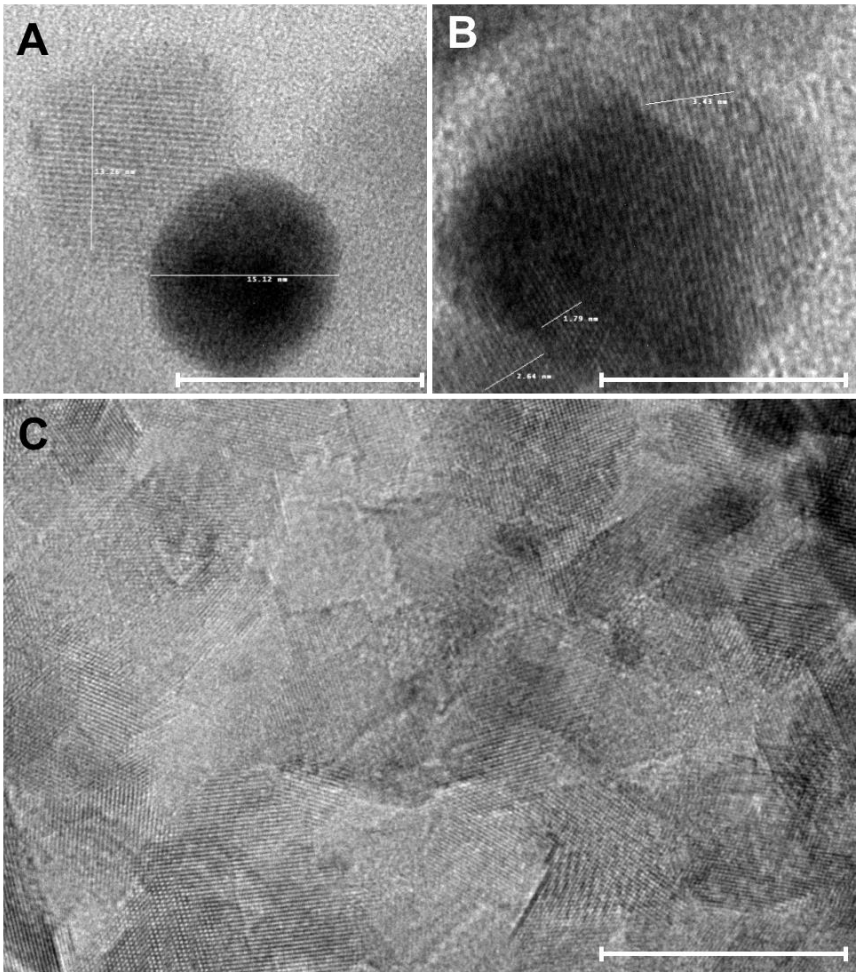

Figure 3.7 High-resolution transmission electron microscopy images of FCDs. A) FCDs produced under oxygen gas. B) FCDs produced under compressed air. C) Aggregate of FCDs produced under oxygen gas. Scale bar = 20 nm.

to obtain. To investigate the aggregation effects of the FCDs and in an attempt to alleviate some of the aggregation effects, glow-discharge protocols were tested as a preparation method for the TEM grids prior to sample deposition.

A Leica EM ACE600 was used to produce glow-discharge and charge the TEM grid before the FCD solution was dripped onto the grid to prepare it for analysis. Glow-discharge is a method of "wetting" the surface of the grid. In glow-discharge, the TEM grid is placed in a chamber under vacuum to remove most air before a current is run between the cathode and anode, ionizing the remaining gas molecules, producing negatively charged ions. These negative ions deposit on the surface of the grid, giving the grid a surface charge it did not possess before. This charged surface is now hydrophilic, allowing water deposited on the surface to spread over a wider surface area and evaporate faster due to decreased surface tension.[30] If the FCDs are aggregating in the solution deposited on the TEM grid over time as the water droplet evaporates, by decreasing the time required for the evaporation, the allowed aggregative effects should be decreased. The results of the study can be seen in Figure 3.8. In panel A of Figure 3.8 is an image of FCDs deposited onto TEM grids prepared without glow discharge, showing extensive FCD aggregation. However, in Figure 3.8 B are shown the results for TEM grids prepared through glow discharge,

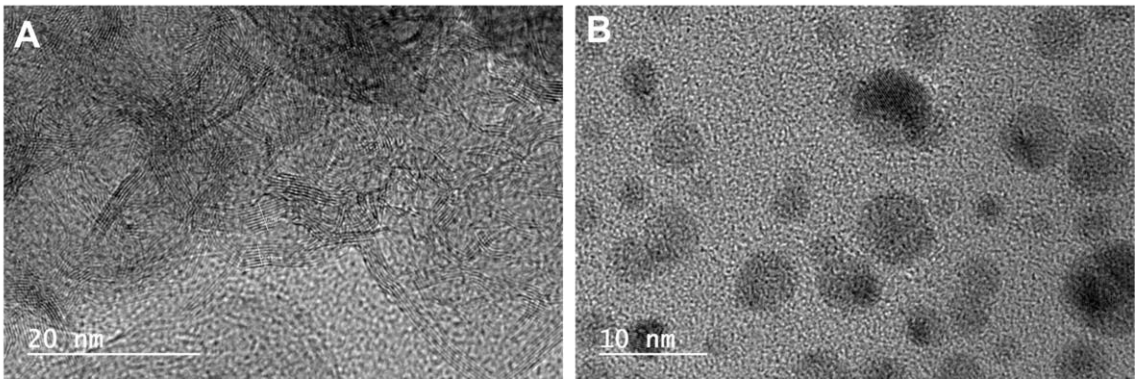

Figure 3.8 Testing of glow discharge to reduce aggregation using HR-TEM. A) FCD solution deposited on a grid with no preparation. B) FCD solution deposited on a grid that has undergone glow discharge.

demonstrating a lesser extent of FCD aggregation. As a result, glow discharge was used for all subsequent TEM experiments; however, the glow discharge, while allowing for less aggregation, could not completely eliminate the observed aggregation, therefore other methods were utilized in an effort to gain more information about the FCDs.

X-ray diffraction (XRD) was used to further assess the crystal structure of the FCDs, but similar to that found when trying to evaluate the diffraction pattern using HR-TEM, the results were inconclusive beyond identifying some of the elemental components of the FCDs. The XRD was indicative of multiple crystal structures that were carbon-based with oxygen, sodium, nitrogen, and possible other elements. The spectra gathered through XRD were too cluttered and complex to highlight any identifying peaks. Additionally, Raman spectroscopy was used to study carbonaceous materials to evaluate the bonding order of the carbon, allowing for the ability to determine the makeup of carbon-based materials.[31, 32] Unfortunately, due to the fluorescent nature of the FCDs, the Raman spectroscopy was inconclusive. It is a well-known shortfall of Raman spectroscopy that in samples that fluoresce, the fluorescent signal can mask the Raman peaks, preventing effective analysis of the sample. Most modern Raman spectrometers are equipped with the ability to correct for fluorescence, but unfortunately in this instance that proved to be impossible due to the significant overlap of the fluorescent peaks from the FCDs and the Raman scattering peaks, a result of the excitation light source having an energy that created substantial excitation of the fluorescent material in the FCDs.

From all of these structural studies, it was determined that the particles are roughly spherical with diameters less than 50 nm, and they possess a lattice spacing of 0.28 nm that is consistent with graphene oxide. To learn more about the structural makeup and begin to probe the

chemical makeup of the FCDs, infrared spectroscopy (IR), X-ray photoelectron spectroscopy (XPS), and electron paramagnetic resonance (EPR) spectroscopy were employed.

IR spectroscopy is a proven technique to evaluate the chemical composition of a wide range of organic materials. IR spectroscopy consists of irradiation of a sample by infrared radiation, which is swept over a range of wavelengths of IR light. The amount of IR light absorbed or transmitted through the sample at specific incident photon energies can aid in identification of the individual species present, considering different chemical functional groups will absorb IR light in different amounts and at different wavelengths. An IR spectrum of FCDs is shown in Figure 3.9. Many of the IR transitions whose peaks fall in the region less than 1500 cm^{-1} are attributed to the carbonaceous materials making up the bulk of the particles. The depth of penetration of infrared light can vary from 1 to 5 mm, depending on the wavelength, meaning that when evaluating nanoparticles, a large amount of the signal can be attributed to the bulk composition of the FCDs, rather than analyzing the surface of the nanoparticles. In this case, which uses a reflection-absorption technique, the evanescent wave typically penetrates beyond the IR optics sampling

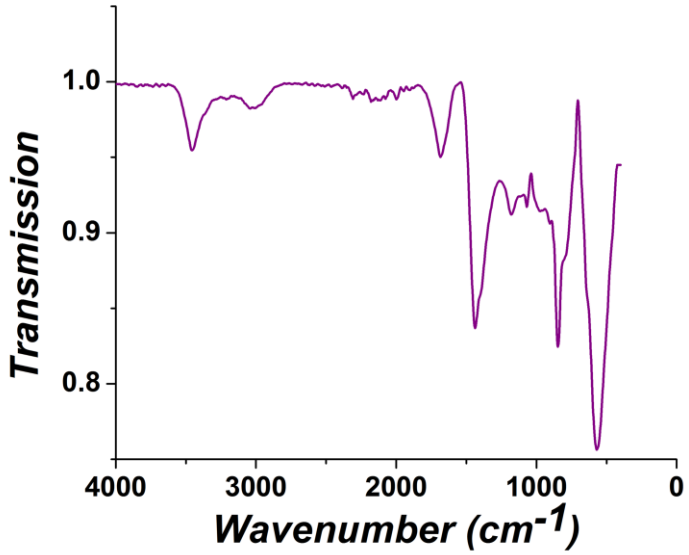

Figure 3.9 Infrared spectroscopy scan of FCDs in solid state as a dried powder.

crystal 0.5-2 micrometers, still leading to the spectra being representative of the bulk properties of the FCD powder. The peaks seen at 3500 and 1390 cm^{-1} represent the O-H transitions of hydroxyl or alcohol functionalities, specifically the O-H stretch and bend transitions, respectively. The peak at 1390 cm^{-1} could also have contributions from the C-O stretch witnessed in graphene oxide. Coupled with the peak near 740 cm^{-1} agreeing with the wavenumbers reported in the literature to correspond to C=O vibrations found in graphene oxide, the presence of graphene oxide seems highly likely.[33, 34] The peak at 1750 cm^{-1} is characteristic of a quinone carbonyl peak, particularly in the instance of quinone functionalities covalently attached to graphene surfaces, closely resembling the system that could be witnessed here.[35] The presence of the bands for the O-H and C=O functional groups demonstrate that the FCDs contain oxygen, and along with the lower energy carbon transitions, suggest that the purported (from TEM lattice data) graphene oxide component of the FCDs contains alcohol groups and quinone functionalities. These functionalities are commonly found on the surface of combustion-generated carbonaceous materials. However, due to the bulk-sampling characteristics of the IR method, it is impossible to state with certainty that these groups are on the exterior surface of the FCD particles. To further evaluate the chemical makeup of the FCDs in a highly surface-sensitive manner, X-ray photoelectron spectroscopy (XPS) was investigated.

XPS is a technique that uses X-rays to typically irradiate a solid sample, which causes electrons within the chemical structure to be released and ejected (photoelectrons) from the outermost surface of the sample. The amount of energy required to eject the electron, known as the binding energy, can be used to identify the atom from which it was ejected and its binding state, including hybridization and what elements to which it is proximal. XPS in this case was used in angle-resolved mode, meaning that the sample is rotated to adjust the angle at which the ejected

photoelectrons are measured. This allows for more sensitive surface analysis and less bulk analysis, with an effective depth of analysis being less than 1 nm at higher angles of photoelectron detection. Ejected photoelectrons are limited in their ability to escape the material for measurement due to scattering events and their low energy. By adjusting the angle of measurement of the ejected photoelectrons, photoelectrons ejected from the surface only of the material can be isolated.[36] When XPS is performed, a survey scan is first performed to evaluate all the elemental peaks present in the sample before focusing in on each individual peak to evaluate the elemental states contained within each peak (high-resolution mode).

A survey spectrum typical of the FCDs is provided in Figure 3.10, and in it is present several transitions associated with different elements. These include the carbon 1s peak at ~284 eV and the oxygen 1s peak at ~530 eV. While these two elemental peaks are the main interest here and high-resolution scans were performed in those two energy ranges for the two elements of interest, there are other elemental peaks present. The large peak at ~1070 eV is associated with the sodium 1s transition, which is attributed to leftover sodium from the sodium alginate starting material, which is not removed by the purification procedure. The binding energy of the sodium 1 s transition peak has a very small range of chemical shifts, making it difficult to determine the exact binding state of the sodium if the signal is low in intensity; other proximal elements must often be analyzed for any sodium component, with none witnessed in this instance.[37, 38] Conspicuously missing is a peak for the nitrogen 1s peak, typically found at ~400 eV, particularly when considering the survey scan for particles produced under air. One theory regarding the black color of FCDs when such FCDs were created under compressed air versus oxygen is that the black color is due to the presence of nitrogen in the FCD structure. This was a theory proposed by this scientist considering it is the element of greatest concentration present in the compressed air as

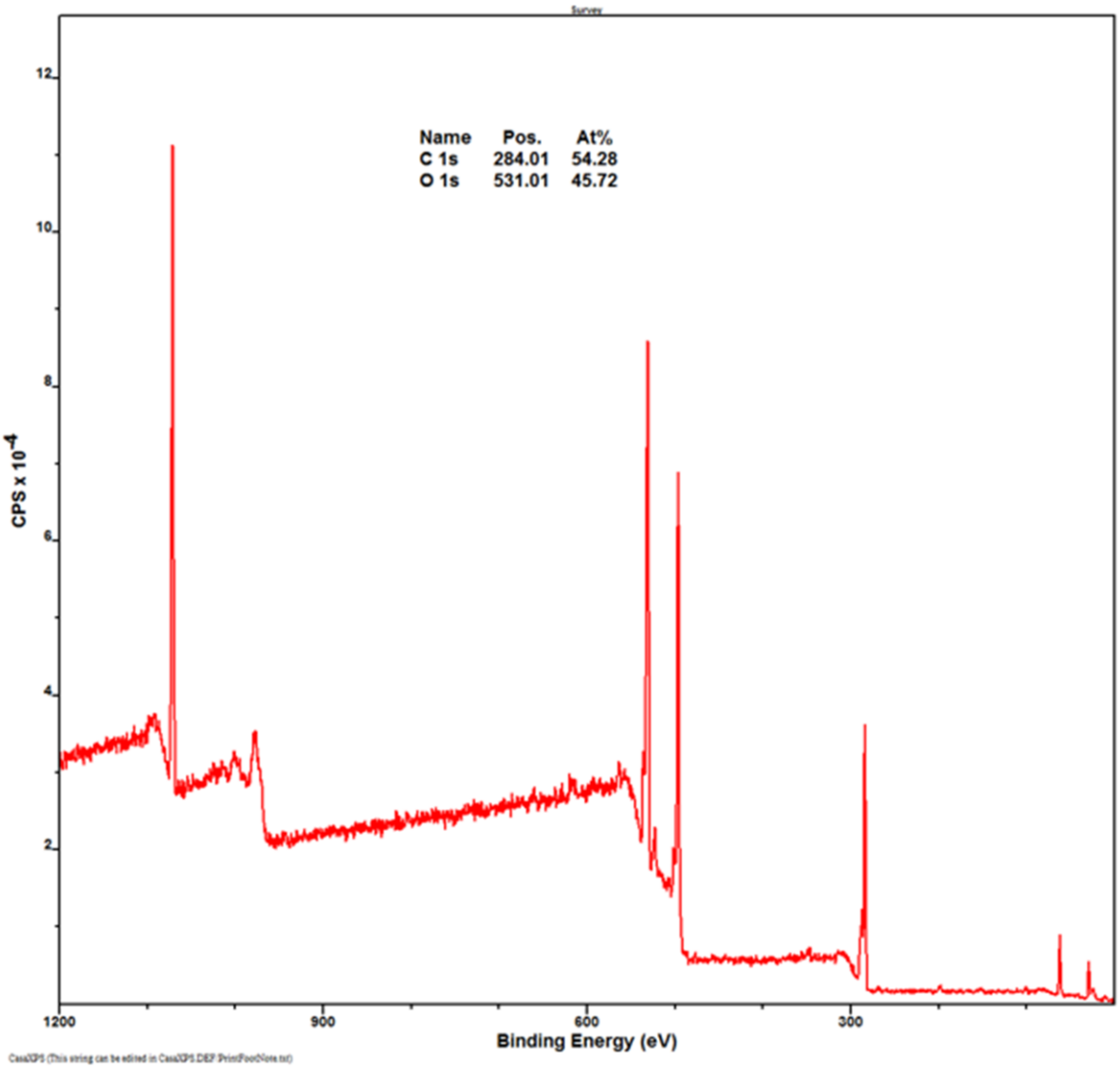

Figure 3.10 X-ray photoelectron spectroscopy (XPS) survey scan of solid state FCDs.

compared to the pure oxygen. However, there is no XPS evidence to support such a possibility. More important for purposes of evaluating the chemical properties of the FCDs is analysis of the carbon 1s and oxygen 1s regions, found in Figure 3.11. The spectra were fitted with CasaXPS software used for control of the spectrometer and analysis of the data collected. The fits were achieved using Gaussian-Lorentzian curve algorithms after performing a Shirley-type background subtraction.[39, 40] The fitting reveals curves that can be evaluated to determine the local bonding environment (chemical state) of the element associated with that peak, which is shown for the C

1s and O 1s regions, Figure 3.11. The carbon 1s spectrum reveals a large amount of C-C bonding, as to be expected from a carbonaceous nanomaterial. In addition to the C-C bonding, C-O and C=O bonding is also observed, which correlates with graphene oxide type material near the surface as well as possible oxygen-containing functional groups, such as those witnessed in graphene surfaces exposed to quinone functionalities.[35, 41] It is worth noting that if the XPS was measuring primarily the bulk graphene oxide of the particles, the peaks for the C-O (286 eV) and C=O (288 eV) would dominate the C 1s region. In the literature, when XPS is used to evaluate graphene

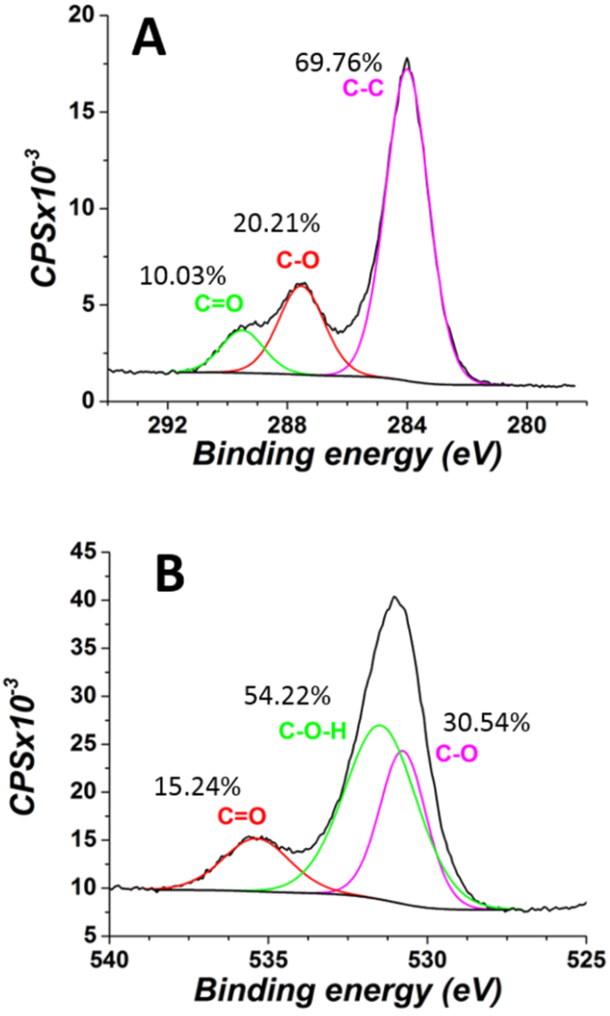

Figure 3.11 X-ray photoelectron spectroscopy focused scans of elemental regions. A) Carbon 1s scan. B) Oxygen 1s scan.

oxide, the C-O and C=O peaks make up over 60% of the total counts.[24, 42, 43] Considering the HR-TEM and IR data suggests graphene oxide makes up the bulk of the FCDs, the C-C dominating the counts in the C 1s spectra (69.76%), with C-O and C=O to a lesser extent (20.21% and 10.03%), denotes the measurement of the surface functionalities rather than bulk measurements. The oxygen 1s spectrum also provides information about the surface functionalities, confirming the presence of oxygen existing as C-O and C-O-H in nearly equal parts (30.54% and 54.22% respectively), with C-O-H slightly higher, and C=O contributing to the oxygen spectrum as well. In particular, the carbonyl peak seen in the oxygen 1s scan corresponds to that witnessed in quinone type functionalities on carbon surfaces.[44] In fact, the three peaks seen in the oxygen 1s scan and their percent compositions (C=O 15.24%, C-O 30.54%, and C-O-H 54.22%) and overall spectral pattern are similar to the XPS data generated from quinone containing carbonaceous materials, though the binding energy for each peak differs depending on the individual case.[44, 45] All three chemical bonding states in the C 1s and O 1s regions confirm the presence of surface alcohol and/or quinone functionalities that were suggested by the IR spectroscopy studies. To further evaluate chemical properties of the FCDs, EPR spectroscopy was performed to probe for the presence of radical species (unpaired electrons).

EPR spectroscopy experiments measure for the presence of unpaired electrons in materials by applying a magnetic field to the material and measuring the energy required to force an unpaired electron into an alternate spin state and allow it to relax back to its natural state when irradiated by microwave radiation.[46] As a result, EPR is able to identify paramagnetic versus diamagnetic inorganic materials. Importantly, when considering organic materials, it offers information regarding any radicals present. A 5,000-G field sweep range scan was first used to evaluate for the possible presence of a wide range of radical materials in the FCDs, Figure 3.12. In this EPR

experiment, the magnetic field is varied over a 5,000 G, while the applied energy in the form of microwaves was held constant at 9.95 GHz, measuring the amount of microwaves absorbed. As the applied magnetic field is varied it will eventually reach the value required to achieve resonance conditions wherein the difference in energy between the lower and higher electron spin states matches that of the incident microwave radiation. This can be seen through an increase in absorbance of the microwave radiation at a particular magnetic field strength. This specific amount of energy and magnetic field strength can be identified and applied to determine the identity of the electron that was excited. Although EPR spectra are collected as signal on the y-axis compared to magnetic field strength on the x-axis, typically the data is reported as the derivative of the absorption spectra relative to the magnetic field (dx/dB) for ease of analysis. Considering EPR experiments can also be performed with the magnetic field held constant under a changing microwave frequency, it is inconvenient to report the radical's identity through the energy or magnetic field used to cause the change in state, so the *g*-factor is most commonly used to identify the radicals. The *g*-factor is calculated from the Zeeman equation:

$$h\nu = g\mu_b B_0$$

where $h\nu$ is the applied energy, g is the *g*-factor, μ_b is a constant (Bohr magneton), and B_0 is the applied magnetic field.[47] By using the Zeeman equation, a *g*-factor can be assigned to an individual electron that should be the same regardless of whether the EPR experiment is performed with changing magnetic field or changing microwave energy. In this experiment, it was found that ultracentrifuge purified FCDs dissolved in water possess a transition near a *g*-factor of ~2.00. After the general region of the radical was identified, a 100-G scan was performed to generate more specific information regarding the identity of the radicals present. A response typical of the ultracentrifuge purified FCDs is presented in Figure 3.12. The *g*-factor measured by the 100-G

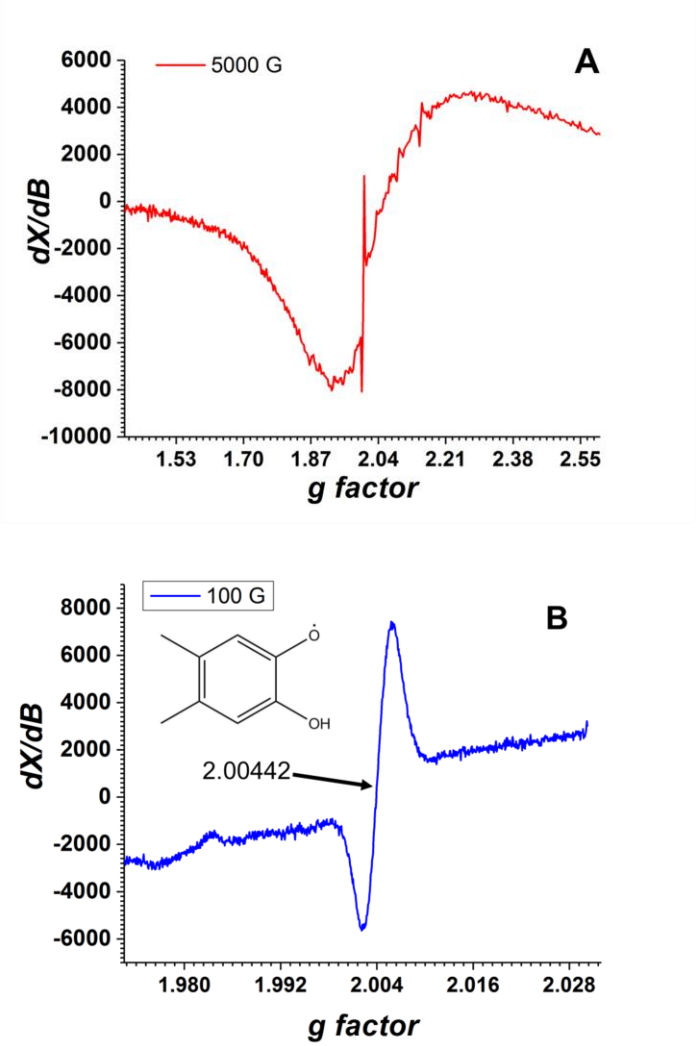

Figure 3.12 Electron paramagnetic resonance spectra of FCDs dissolved in water. A) 5000 G scan. B) 100 G scan with inset of an *o*-semiquinone-type radical.

scan reveals a *g*-value of 2.00442 ± 0.00001. This observed value of 2.00442 is consistent with that of *o*-semiquinone-type radicals, whose chemical structure can be seen in Figure 3.12.[48] The *o*-semiquinone-type radicals measured in this research can be a result of multiple starting phenolic materials, but these semiquinone type radicals yield themselves to being studied through ultrafine coupling EPR studies.[49, 50] The complexity of the ultrafine coupling studies required to examine the semiquinone-type radicals produced in this research is beyond the scope of this research, though future work could explore the formation of the semiquinone-type radicals more thoroughly.

The chemical experimentation done in the form of IR, XPS, and EPR all come together to suggest that chemically, the FCDs are graphitic carbon with oxygen throughout the structure and quinones and/or catechol functional groups on the surface. The presence of quinones is suggested in the IR (O-H transitions and carbonyl transitions) and XPS data (both carbon 1s and oxygen 1s scans), additionally the presence of O-H functionalities is confirmed. The EPR data reporting the likely presence of semiquinone-type radicals further confirms the presence of quinones and their hydrated form, catechols. While the IR, XPS, and EPR individually are not able to accurately confirm exactly what species is present, the three techniques create a likely picture of quinone and catechol groups on the surface that form semiquinone-type radicals.

3.3.2.3 Dependence of Fluorescence Emission Characteristics on Particle Size

An additional factor that most FCDs are reported to possess is a change in fluorescence properties with particle size. These changes can be represented as a decrease or increase in fluorescence or as a shift in the emission wavelength as the particle size changes.[51-53] An evaluation of the FCDs produced in this research was done to determine what effects, if any, particle size has on the fluorescence in the FCDs. To first evaluate the size dependence of the fluorescent properties, the FCDs needed to be separated into different-sized particles. A size-exclusion column was chosen to perform this separation. Sephadex G-25 is a sieving matrix commonly used for aqueous-phase separations, with it being routinely used to separate 100-5000 M.W. materials. The Sephadex G-25 was hydrated using 18 M$\Omega \bullet$ cm water and then poured into a plastic pipette containing cotton wool packed into the bottom of the pipette to prevent loss of the Sephadex. After the Sephadex was added to the column and water was passed through to pack the column, a sample of 10 mg/mL FCDs was dissolved in water and subsequently poured on top of the Sephadex. Samples were collected over time to accumulate (collect) differently sized particles.

Larger particles will elute early in the separation process, while smaller particles take a longer time to elute due to their interactions with the sieving matrix.

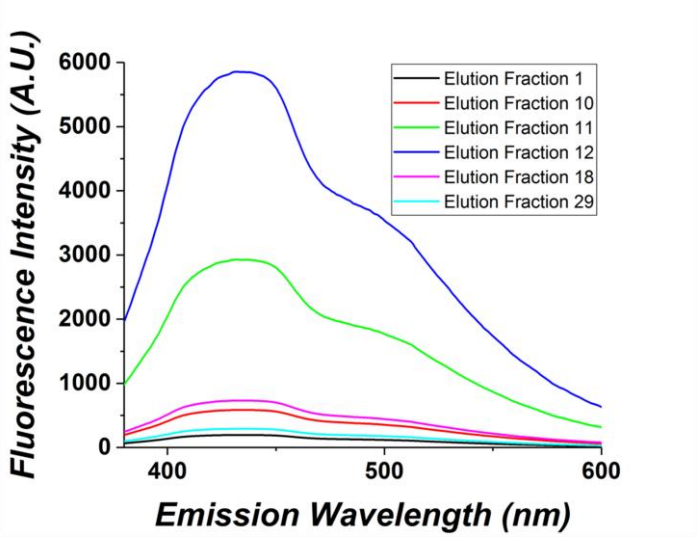

Figure 3.13 Fluorescence emission spectra of individual elution fractions collected over time from the size-exclusion column. Elution fractions are in order of collection, elution fraction 1 being the first collected, etc.

The fractions collected were each measured for their fluorescence properties in order to correlate the fluorescent properties with purported particle size, which is based on elution time. While 50 elution fractions were collected over the entire elution time of 20 min to ensure isolation of various possible particle sizes, a representative sampling of the results is shown in Figure 3.13. The most obvious result is that early collected samples exhibit no apparent fluorescence (Sample 1-Sample 9), but the later eluting fractions (assumed to possess smaller particles, Sample 10-Sample 20) exhibit fluorescence emission spectra that are virtually the same as those of the bulk/not separated materials but with an overall lower intensity at all energies. As the separation continued, the intensity of the characteristic emission spectrum decreased (Sample 21-Sample 50). Based on these observations and the assumption that the separation is efficient, it appears that there is no dependence of emission properties (overall spectral shape) on FCD particle size. If the separation is efficient, which it is assumed to be in this case based on the increase in fluorescence

and subsequent decrease, it can be concluded that largest particles (early elution fractions) and smallest particles (late elution fractions) exhibit less fluorescence. This is based on the fluorescent property of higher concentrations of fluorescent materials resulting in higher intensities of fluorescence. Considering the early and late elution fractions exhibit less fluorescence, but higher concentrations of large or small materials respectively, it can be concluded that the fluorescence of the FCDs is found in a specific size of FCD. Unfortunately, due to the limitations of sample mass that can be separated with this size-exclusion approach, the amount of FCDs in each fraction is very small, making their further analysis difficult at best. For example, in an attempt to evaluate particle size in the fraction exhibiting the highest fluorescence intensity, elution fraction 24, through use of LR-TEM, I was unable to identify sufficient particles to generate an effective size distribution. Additionally, the process of separating a sample in a size-exclusion column is very slow and takes a considerable amount of time. In order to obtain a sufficient amount of FCDs of different sizes to further evaluate the effects of particle size on the fluorescence of the FCDs, an ultracentrifuge purification method was used to purify the particles based on size.

Solutions of FCDs made by pyrolysis under oxygen gas at 20 mg/mL concentration were prepared in 7.4 pH phosphate buffer and then transferred to centrifuge tubes. The latter were then placed in an ultracentrifuge and centrifuged at 110,000 x *g* for 1.5 hr. It was noted that a black solid was present in the bottom of the tubes, with a dark yellow-colored solution remaining above the black solid. The supernatant solution was pipetted out of the centrifuge tube and its fluorescence spectrum was measured using λ_{ex} of 350 nm and λ_{em} of 450 nm. In addition, the black solid in the tubes was found to be readily re-suspended in water, yielding a tan colored transparent liquid. The fluorescence emission spectrum of the black solid that was re-suspended in water was also recorded. The supernatant produced a fluorescence spectrum identical to that of the FCDs,

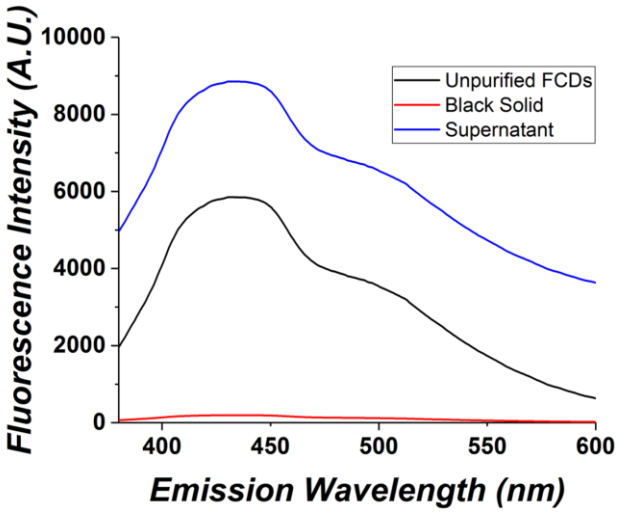

Figure 3.14 Fluorescence emission spectra of FCDs before and after ultracentrifuge purification. All samples are 2 mg/mL FCDs in pH 7.4 phosphate buffer. The black solid is the solid material that settled out during centrifugation while the supernatant was the liquid removed from the centrifuge tube after centrifugation and dried under nitrogen flow to produce a solid, allowing for weighing and dissolving in buffer.

though greater in intensity. At the same time, the black solid re-suspended in water did not give rise to any fluorescence signals (Figure 3.14). The increase in signal in the purified fluorescent FCDs was to be expected since the same mass of each sample was dissolved, but if the ultracentrifuge purified FCDs are made up of the smaller fluorescent particles and the larger non-fluorescent particles are removed, more fluorescent materials should be present in the supernatant.

In order to further evaluate the physical properties of the supernatant that is fluorescent and those of the isolated black solid that does not exhibit fluorescence, both materials were analyzed by HR-TEM. Both the supernatant and the black solid resuspended in water were deposited onto the TEM grid after glow discharge, as outlined above. The TEM images for both materials possess particles with distinct sizes, but have indistinguishable lattice spacing of approximately 0.28 nm, Figure 3.15. The particles in the fluorescent supernatant sample were 15 ± 7.4 nm in size, while the particles found in the non-fluorescent black solid sample were 30 ± 11.2 nm in size (300

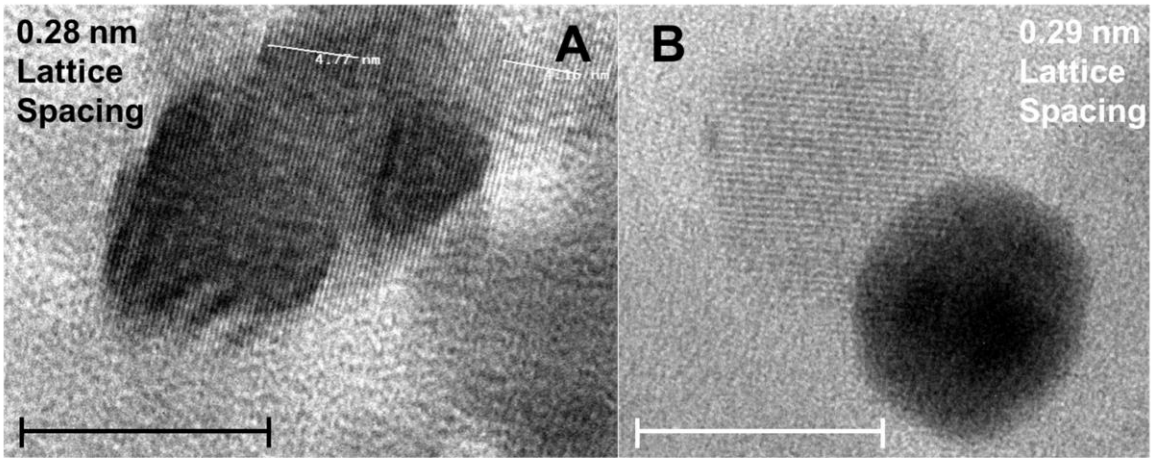

Figure 3.15 Comparison of particles remaining in solution and those that were isolated as a black solid during centrifugation: A. HR-TEM of fluorescent particles remaining in supernatant upon centrifugation (scale bar = 20 nm). B. HR-TEM of non-fluorescent black particles isolated by centrifugation (scale bar = 50 nm).

particles were counted and measured through HR-TEM to determine size and standard deviation). This seems to suggest that the only difference between the fluorescent particles and non-fluorescent particles is size, with smaller particles possessing fluorescence, while larger particles possess no fluorescence.

To further investigate possible differences in properties of the two isolated materials, IR spectroscopy and XPS was performed. The same procedures used for the TEM experiments were employed to isolate the two different solids. Interestingly, there is no appreciable difference noted in either analysis method, Figure 3.16. Experimentation by this scientist concludes that the only difference between the FCDs isolated from the supernatant and FCDs collected in the form of the black solid remaining after ultracentrifugation is the fluorescence and size of the FCDs.

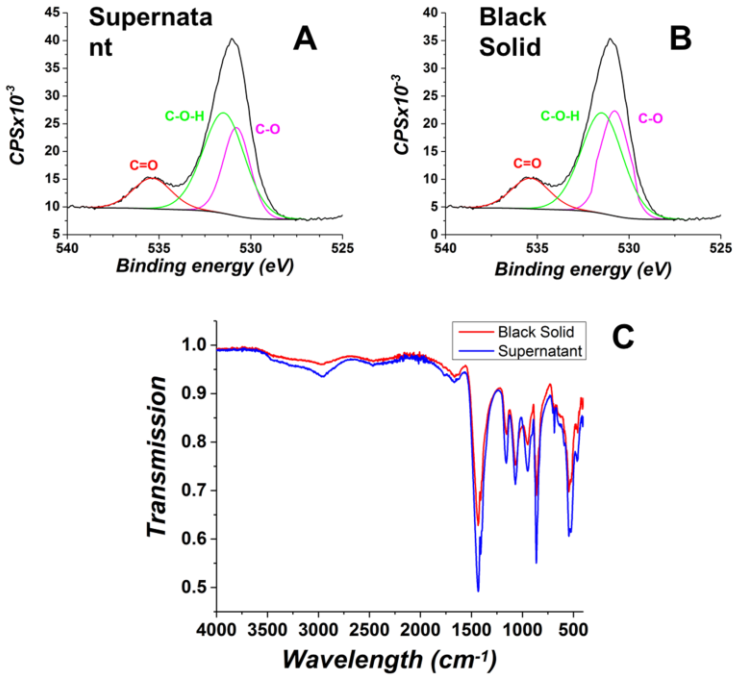

Figure 3.16 Comparison of infrared spectroscopy (IR) spectra and X-ray photoelectron spectroscopy spectra between the supernatant and black solid produced during ultracentrifuge purification. A. Oxygen 1s scan of FCDs gathered from drying of the supernatant under nitrogen gas. B. Oxygen 1s scan of the black solid gathered from the centrifuge tube after ultracentrifugation. C. IR spectra of the FCDs gathered from the supernatant and the black solid.

3.4 Conclusions

BC is an environmental pollutant of high importance to society today and requires extensive study in order to determine the health effects of BC. When attempting to study individual components of PM, isolating one individual component can be difficult and time consuming, particularly obtaining sufficient amounts of high enough purity for study. It was decided that rather than trying to isolate BC and study it as collected from environmental conditions, a surrogate would be designed to mimic BC, which would allow for in-depth investigations. FCDs were

chosen based on their similarities to the elemental, structural, and chemical properties of BC. In addition, FCDs possess fluorescent moieties to allow for ease of use in evaluation of cellular uptake and environmental effects.

A bottom-up pyrolysis approach was chosen to create FCDs similar to the methods that produce BC in the environment. By using a thermal pyrolysis process, the FCDs created should be similar to BC in the environment. A variety of carbon sources were tested and found to lead to successful creation of FCDs, but it was determined that sodium alginate led to production of FCDs in the highest yield. Furthermore, it was found that the highest yield of FCDs are achieved with a pyrolysis temperature of 250 °C and a reaction time of 30 minutes under a flow of 100% oxygen gas at 30 psi. The resulting FCDs are found to possess fluorescence properties that hold promise for their use as a probe in biological systems. Notably, the FCDs produced in this research show resistance to photobleaching, and their fluorescence is unaffected by their exposure to a large range of pH conditions. Additionally, their fluorescence is unaffected by storage in the ambient air and solution phase for times up to 24 days. Finally, the fluorescence properties are unaltered by storage of the solid the for 24 days, the longest time investigated.

Analyses of the structural properties of the FCDs using HR-TEM reveal a lattice spacing of 0.28 nm, consistent with a graphene oxide crystal structure. Chemical analysis using IR and XPS revealed oxygen-containing functional groups on the surface of the FCDs, with EPR revealing the presence of *o*-semiquinone type radicals. Combined outcomes from these studies, coupled with analysis of the fluorescence spectra, point to the presence of catechol, quinone, hydroquinone, and semiquinone radicals. Additionally, it was revealed through extensive studies that the FCDs designed and synthesized in this research possess a size-dependent fluorescence, with only FCDs less than 30 nm in size producing fluorescence. The fluorescence properties of

these FCDs indicate potential use as a BC surrogate so as to analyze the effects of BC on biological materials, particularly epithelial lung cells. However, the sensing capabilities of the FCDs needs to be studied; those endeavors are described in Chapter 4.

3.5 References

1. Gilmour, M.I., et al., Comparative Toxicity of Size-Fractionated Airborne Particulate Matter Obtained from Different Cities in the United States. Inhalation Toxicology, 2007. 19(sup1): p. 7-16.

2. Sacks, J.D., et al., Particulate Matter–Induced Health Effects: Who Is Susceptible? Environmental Health Perspectives, 2011. 119(4): p. 446-454.

3. Schwarze, P.E., et al., Particulate matter properties and health effects: consistency of epidemiological and toxicological studies. Human & Experimental Toxicology, 2006. 25(10): p. 559-579.

4. Womiloju, T.O., et al., Methods to determine the biological composition of particulate matter collected from outdoor air. Atmospheric Environment, 2003. 37(31): p. 4335-4344.

5. Sardar, S.B., P.M. Fine, and C. Sioutas, Seasonal and spatial variability of the size-resolved chemical composition of particulate matter (PM10) in the Los Angeles Basin. Journal of Geophysical Research: Atmospheres, 2005. 110(D7).

6. Murruni, L.G., et al., Concentrations and elemental composition of particulate matter in the Buenos Aires underground system. Atmospheric Environment, 2009. 43(30): p. 4577-4583.

7. Xu, X., et al., Electrophoretic Analysis and Purification of Fluorescent Single-Walled Carbon Nanotube Fragments. Journal of the American Chemical Society, 2004. 126(40): p. 12736-12737.

8. Sun, Y.-P., et al., Quantum-Sized Carbon Dots for Bright and Colorful Photoluminescence. Journal of the American Chemical Society, 2006. 128(24): p. 7756-7757.

9. Zhou, J., et al., An Electrochemical Avenue to Blue Luminescent Nanocrystals from Multiwalled Carbon Nanotubes (MWCNTs). Journal of the American Chemical Society, 2007. 129(4): p. 744-745.

10. Liu, H., T. Ye, and C. Mao, Fluorescent Carbon Nanoparticles Derived from Candle Soot. Angewandte Chemie International Edition, 2007. 46(34): p. 6473-6475.

11. Ray, S.C., et al., Fluorescent Carbon Nanoparticles: Synthesis, Characterization, and Bioimaging Application. The Journal of Physical Chemistry C, 2009. 113(43): p. 18546-18551.

12. Tian, L., et al., Nanosized Carbon Particles From Natural Gas Soot. Chemistry of Materials, 2009. 21(13): p. 2803-2809.

13. Fong, J.F.Y., S.F. Chin, and S.M. Ng, A unique "turn-on" fluorescence signalling strategy for highly specific detection of ascorbic acid using carbon dots as sensing probe. Biosensors and Bioelectronics, 2016. 85: p. 844-852.

14. Czimczik, C.I., et al., Effects of charring on mass, organic carbon, and stable carbon isotope composition of wood. Organic Geochemistry, 2002. 33(11): p. 1207-1223.

15. Cachier, H., M.-P. Bremond, and P. Buat-Ménard, Determination of atmospheric soot carbon with a simple thermal method. Tellus B: Chemical and Physical Meteorology, 1989. 41(3): p. 379-390.

16. Yang, H. and J.Z. Yu, Uncertainties in Charring Correction in the Analysis of Elemental and Organic Carbon in Atmospheric Particles by Thermal/Optical Methods. Environmental Science & Technology, 2002. 36(23): p. 5199-5204.

17. Melfi, S., J. Lawrence Jr, and M. McCormick, Observation of Raman scattering by water vapor in the atmosphere. Applied Physics Letters, 1969. 15(9): p. 295-297.

18. Fonin, A.V., et al., Fluorescence of dyes in solutions with high absorbance. Inner filter effect correction. PloS one, 2014. 9(7): p. e103878-e103878.

19. Aubin, J.E., Autofluorescence of viable cultured mammalian cells. Journal of Histochemistry & Cytochemistry, 1979. 27(1): p. 36-43.

20. Andersson, et al., Autofluorescence of living cells. Journal of Microscopy, 1998. 191(1): p. 1-7.

21. Stevenson, F.J., Humus chemistry: genesis, composition, reactions. 1994: John Wiley & Sons.

22. Bruccoleri, A., et al., Evaluation of primary photoproduct quantum yields in fulvic acid. Environmental Science & Technology, 1993. 27(5): p. 889-894.

23. Ariese, F., et al., Comparison of Laurentian Fulvic Acid luminescence with that of the hydroquinone/quinone model system: Evidence from low temperature fluorescence studies and EPR spectroscopy. Aquatic Sciences, 2004. 66(1): p. 86-94.

24. Shang, J., et al., The Origin of Fluorescence from Graphene Oxide. Scientific Reports, 2012. 2(1): p. 792.

25. Baker, S.N. and G.A. Baker, Luminescent carbon nanodots: emergent nanolights. Angew Chem Int Ed Engl, 2010. 49(38): p. 6726-44.

26. Clogston, J.D. and A.K. Patri, Zeta Potential Measurement, in Characterization of Nanoparticles Intended for Drug Delivery, S.E. McNeil, Editor. 2011, Humana Press: Totowa, NJ. p. 63-70.

27. Kumar, A. and C.K. Dixit, 3 - Methods for characterization of nanoparticles, in Advances in Nanomedicine for the Delivery of Therapeutic Nucleic Acids, S. Nimesh, R. Chandra, and N. Gupta, Editors. 2017, Woodhead Publishing. p. 43-58.

28. Panzarasa, G., et al., Convenient Preparation of Graphene Oxide from Expandable Graphite and Its Characterization by Positron Annihilation Lifetime Spectroscopy. C, 2019. 5(1).

29. Zhu, Y., et al., Graphene and Graphene Oxide: Synthesis, Properties, and Applications. Advanced Materials, 2010. 22(35): p. 3906-3924.

30. Aebi, U. and T.D. Pollard, A glow discharge unit to render electron microscope grids and other surfaces hydrophilic. Journal of Electron Microscopy Technique, 1987. 7(1): p. 29-33.

31. Dresselhaus, M.S., et al., Raman spectroscopy of carbon nanotubes. Physics Reports, 2005. 409(2): p. 47-99.

32. Schwan, J., et al., Raman spectroscopy on amorphous carbon films. Journal of Applied Physics, 1996. 80(1): p. 440-447.

33. Shahriary, L. and A.A. Athawale, Graphene oxide synthesized by using modified hummers approach. Int. J. Renew. Energy Environ. Eng, 2014. 2(01): p. 58-63.

34. Khanra, P., et al., Simultaneous bio-functionalization and reduction of graphene oxide by baker's yeast. Chemical Engineering Journal, 2012. 183: p. 526-533.

35. Ramesh, P. and S. Sampath, Electrochemical and spectroscopic characterization of quinone functionalized exfoliated graphite. Analyst, 2001. 126(11): p. 1872-1877.

36. Cumpson, P.J., Angle-resolved XPS and AES: Depth-resolution limits and a general comparison of properties of depth-profile reconstruction methods. Journal of Electron Spectroscopy and Related Phenomena, 1995. 73(1): p. 25-52.

37. Miura, Y., et al., X-ray photoelectron spectroscopy of sodium borosilicate glasses. Journal of non-crystalline solids, 2001. 290(1): p. 1-14.

38. Brisson, P.-Y., et al., X-ray photoelectron spectroscopy study of sodium reactions in carbon cathode blocks of aluminium oxide reduction cells. Carbon, 2006. 44(8): p. 1438-1447.

39. Sherwood, P.M., Data analysis in X-ray photoelectron spectroscopy. Practical surface analysis, 1983. 2: p. 555-586.

40. Jain, V., M.C. Biesinger, and M.R. Linford, The Gaussian-Lorentzian Sum, Product, and Convolution (Voigt) functions in the context of peak fitting X-ray photoelectron spectroscopy (XPS) narrow scans. Applied Surface Science, 2018. 447: p. 548-553.

41. Ramesh, P. and S. Sampath, Chemically functionalised exfoliated graphite: a new bulk modified, renewable surface electrode. Chemical Communications, 1999(21): p. 2221-2222.

42. Dreyer, D.R., et al., The chemistry of graphene oxide. Chemical society reviews, 2010. 39(1): p. 228-240.

43. Eda, G. and M. Chhowalla, Chemically derived graphene oxide: towards large-area thin-film electronics and optoelectronics. Advanced materials, 2010. 22(22): p. 2392-2415.

44. Maciá-Agulló, J.A., et al., Oxygen functional groups involved in the styrene production reaction detected by quasi in situ XPS. Catalysis Today, 2005. 102-103: p. 248-253.

45. Gardner, S.D., et al., Surface characterization of carbon fibers using angle-resolved XPS and ISS. Carbon, 1995. 33(5): p. 587-595.

46. Al'Tshuler, S.A. and B.M. Kozyrev, Electron paramagnetic resonance. 2013: Academic Press.

47. Karshenboim, S.G., Non-relativistic calculations of the g-factor of a bound electron. Physics Letters A, 2000. 266(4): p. 380-386.

48. Kalyanaraman, B., C.C. Felix, and R.C. Sealy, Semiquinone anion radicals of catechol(amine)s, catechol estrogens, and their metal ion complexes. Environmental Health Perspectives, 1985. 64: p. 185-198.

49. Adams, M., M. Blois Jr, and R.H. Sands, Paramagnetic resonance spectra of some semiquinone free radicals. The Journal of Chemical Physics, 1958. 28(5): p. 774-776.

50. Venkataraman, B. and G.K. Fraenkel, Proton Hyperfine Interactions in Paramagnetic Resonance of Semiquinones1. Journal of the American Chemical Society, 1955. 77(10): p. 2707-2713.

51. De, B. and N. Karak, A green and facile approach for the synthesis of water soluble fluorescent carbon dots from banana juice. RSC Advances, 2013. 3(22): p. 8286-8290.

52. Hu, C., et al., Chemically tailoring coal to fluorescent carbon dots with tuned size and their capacity for Cu (II) detection. Small, 2014. 10(23): p. 4926-4933.

53. Yang, Z.-C., et al., Intrinsically fluorescent carbon dots with tunable emission derived from hydrothermal treatment of glucose in the presence of monopotassium phosphate. Chemical communications, 2011. 47(42): p. 11615-11617.

CHAPTER 4
EXPLORATION OF FLUORESCENCE QUENCHING AND RECOVERY MECHANISM IN FLUORESCENT CARBON DOTS

4.1 Introduction

Fluorescent carbon dots (FCDs) have been used extensively as biological probes in a variety of modes, such as always-on, turn-on, or turn-off.[1-4] The potential benefits offered by a turn-on probe are numerous, with this mode providing an increased signal-to-noise ratio, high selectivity, and high sensitivity.[5-7] FCDs are a particularly logical choice to use when designing a turn-on fluorescent probe, due to the well-known ability of metal ions to quench fluorescence in FCDs; in fact, most FCDs used in turn-off mode are based on the loss of fluorescence when exposed to metal ions.[8-10] The exact quenching mechanism is not well understood, but this could be a result of the multitude of synthesis processes used to create FCDs, as well as the highly diverse properties of the multitude of metal ions exposed to the FCDs.[11, 12] Furthermore, there are several theories that have been presented to describe the mechanism associated with the fluorescence from fluorescent carbon dots made using the wide variety of synthetic conditions.

The two main types of quenching that have been observed in FCDs are static and dynamic quenching. In dynamic quenching, the quencher must diffuse to the fluorophore and interact with the latter during its excitation from the ground electronic energy state to the electronic energy excited state.[13] An important note to remember about dynamic quenching is that no permanent modification of the fluorophore occurs, although it may appear that modification has occurred because the quenching process is ongoing. In static quenching, a non-fluorescent complex forms as the quencher and fluorophore interact with each other while the fluorophore is in the ground state. The exact interactions that cause the lack of fluorescence in the formed complex are not known, but could be a result of excited-state reactions, molecular rearrangements, ground-state

complex formation, collisional quenching, energy/electron transfer, or destruction of the group associated with the emission process.[14]

Understanding the exact quenching mechanism is further complicated by the fact that the mechanism of quenching could be completely different depending on the methods used to synthesize the FCDs. It has been proposed that FCDs made with specific routes are believed to interact with the metal ion through an electron exchange process (photo induced electron transfer, Förster resonance electron transfer, Dexter electron transfer, etc.), which is denoted as being a static quenching mechanism; this has been observed in multiple types of FCDs upon their interacting with multiple types of metal ions, including those of iron, copper, and mercury.[15-17] Dynamic quenching mechanisms between FCDs and metal ions are much less common but have been reported in the literature, although the exact mechanisms have not been explored.[14, 18] The differences in characteristic behaviors for static and dynamic quenching allow for assignment of the class of quenching mechanism for a particular system, but an understanding of the detailed quenching process is not trivial to obtain. Manuscripts abound in the literature that report the quenching effects of metal ions on a particular FCD material, but very few focus on determining exactly how the quenching occurs. Most groups do not elucidate or provide a theory for the exact quenching mechanism.[2, 17] The typical modus operandi found in these studies is upon observation of fluorescence quenching with a given agent and assessment of its analytical capabilities, no further research into the underlying rationale for the quenching is carried out. In the rare paper where the quenching mechanism is probed, the research ceases upon establishment of a static or dynamic quenching mechanism.[2, 14, 18]

The recovery of fluorescence in FCDs by addition of another chemical species to a quenched system is also poorly understood, considering it hinges on the exact mechanism of

fluorescence quenching, particularly regarding static or dynamic quenching. One proposed method to recover the fluorescence is chemical reduction of the metal ion responsible for FCD fluorescence quenching by a reducing agent.[2, 19] The process of fluorescence recovery through reduction of the metal ion quencher implies an electron exchange is responsible for the quenching mechanism, considering the primary difference between a metal ion and its lower oxidation state variant are their standard reduction potentials. However, if the fluorescence quenching of FCDs by metal ions results in a chemical complex formed between the metal ions and surface functional groups on the FCDs, the only way to recover the fluorescence is to break apart the existing metal ion-surface group complex.[20, 21] It is the goal of this chapter to establish an understanding of the static quenching mechanism observed in the synthesized FCDs, as well as gaining knowledge about the recovery process, or lack thereof, to formulate a proposed fluorescence quenching mechanism.

4.2 Experimental

4.2.1 Materials

Ethylenediaminetetraacetic acid (EDTA) anhydrous (≥98.5%), iron(III) nitrate nonahydrate (99+%), iron(III) sulfate hydrate, iron(II) chloride tetrahydrate (98%), copper(II) nitrate, copper(II) sulfate anhydrous (≥99%), calcium chloride anhydrous (≥97%), tin(II) chloride dihydrate (≥99.995%), nickel(II) chloride anhydrous (99.99%), aluminum chloride anhydrous (99.99%), ruthenium(III) chloride hydrate (99.98%), sodium hydroxide, citric acid (≥99.5%), L-ascorbic acid, L-glutathione reduced (GSH) (>98.0%), sodium dithionite, ammonia, and 5-sulfosalicylic acid dehydrate (>99%) were purchased from Sigma-Aldrich (St. Louis, MO). Anhydrous sodium phosphate monobasic and anhydrous sodium phosphate dibasic were purchased from Fisher Scientific (Hampton, NH). Water from a Barnstead Nanopure Diamond Water System (18 M$\Omega \bullet$ cm) was used for all experiments.

4.2.2 Fluorescence Quenching

10 mg of FCDs were dissolved in 5 mL of pH 7.4 phosphate buffer to create a 2 mg/mL solution of FCDs. Each metal ion solution was prepared by dissolving solid metal salts in water to create a 0.076 M solution of each metal ion. A 0.076 M EDTA solution was made by dissolving 2.22 g EDTA in water with a pH adjusted to ~10 using 0.1 M sodium hydroxide. 5 mL of the metal ion solution was combined with 15 mL of the EDTA solution to produce 20 mL of solution with a metal ion concentration of 0.019 M and a final EDTA concentration of 0.057 M, thus providing a 1:3 metal ion to EDTA ratio. The fluorescence emission spectrum of 1.5 mL of the 2 mg/mL solution of FCDs was measured using a FL8500 fluorimeter to establish a maximum fluorescence baseline. 10 μL aliquots of a single metal ion species were added to the FCD solution followed by pipette mixing and subsequent fluorescence measurement (λ_{ex} = 350 nm and λ_{em} = 375-600 nm). The process was repeated, adding 10 μL aliquots, until a fluorescence quenching maximum is reached, and the signal decreased to a minimum. Five aliquots of 10 μL were added after the fluorescence signal reached its minimum to ensure maximum quenching. Different metal ions were carried out using the same experimental approach. Control experiments were also carried out using the same experimental approach, but in the absence of FCDS.

4.2.3 Fluorescence Recovery

Solutions of 0.019 M citric acid, ascorbic acid, and GSH were prepared by dissolving each solid reducing agent into pH 7.4 phosphate buffer. Solutions of FCDs and metal ions with completely quenched fluorescence were measured for their fluorescence to establish a quenched baseline. 10 μL aliquots of the reducing agent were added to the FCD/metal ion solution and pipette mixed before measuring the fluorescence. The process was repeated until a maximum recovered fluorescence signal was reached. Five additional aliquots of the reducing agent were

added and mixed before measuring the fluorescence to ensure no additional fluorescence recovery was witnessed. The experiment was repeated for each reducing agent.

4.2.4 5-sulfosalicylic acid Assay

A 10% (w/v) 5-sulfosalicylic acid (SSA) solution was created by dissolving solid SSA into water. A 25% (v/v) solution of ammonia was prepared in pH 7.4 phosphate buffer. A 2 mg/mL solution of FCDs was prepared in 3 mL of water, followed by the addition of 0.3 mL of the SSA solution. The solution fluorescence was measured to establish the fluorescence maximum. The absorbance of the solution was then measured at 500 nm on a Cary 50-Bio UV-Visible Spectrophotometer, before the solution was allowed to rest for 15 min followed by another absorbance measurement to ensure the reaction had sufficient time to complete itself. Then 0.3 mL of the 25% ammonia solution was added, and the absorbance was measured at 425 nm. After 15 min elapsed to ensure the reaction had time to reach completion the absorbance was measured again. It is important to note that each sample that was measured was a separately prepared sample, considering the assay could not be performed continuously. Due to the pH change required in the middle of the assay, it is impossible to perform the assay multiple times in one solution. The samples were all prepared from the same stock solutions at the same time in order to ensure consistency across the samples. The process was repeated for 4 different solutions as ferric ions ($FeNO_3$ dissolved in water) were added in 60 μL increments until a total amount of 240 μL ferric ions (0.0026 M) were added to the FCD solution. The process was then repeated on 4 more solutions as sodium dithionite (SDT) was added in 60 μL increments for a total added volume of 240 μL SDT (0.0026 M) to measure reduction of ferric ion.

4.3 Results and Discussion

4.3.1 Fluorescence Quenching

The quenching mechanism can be complex and varies depending on the synthesis method of the FCDs, therefore no specific quenching pathway is guaranteed among different FCDs. An initial probe of fluorescence quenching involves an investigation to determine if quenching does in fact occur. The first metal ion chosen to probe fluorescence quenching was ferric ion, that is iron(III), due to the large number of experiments performed in the literature establishing it as a quencher of FCD fluorescence.[3, 22-25] The ferric ions were produced by dissolving iron(III) nitrate in water. 10 μL (0.19 μmol) aliquots of the ferric ion solution were added to a 2 mg/mL solution of FCDs and mixed, followed by a measurement of the fluorescence signal. The solution was incubated in the laboratory ambient on the benchtop for 10 minutes before the fluorescence measurement was collected, so as to ensure sufficient time for establishing the conditions needed for the quenching process. After the addition of 70 μL (1.33 μmol) of the ferric ion solution, the fluorescence had reached approximately 50% of its original intensity; however, precipitate began to form in the cuvette. As more ferric ion solution was added, no additional fluorescence quenching occurred, and more precipitate formed. It was observed that once the FCDs were dissolved in the water, the pH became basic, changing from the initial value of 7.1 of the water to 10.2 when the FCDs were dissolved. Based on the basic pH, it was theorized that the precipitate being formed was insoluble ferric hydroxide. As more ferric ions were added, more precipitate forms, preventing the ferric ions from interacting with the FCDs and thus preventing additional quenching since the ions are not in the solution any longer. To solve this problem, a phosphate buffer of pH 7.3 was created and the ferric ion quenching experiment was repeated in the buffer rather than water. The

phosphate buffer was chosen based on its presence in the cellular environment and use as a buffer in a multitude of biological experiments.[26, 27]

The experiment with the buffered pH yielded slightly better results, with 100 μL of the ferric ion solution (0.019 M $Fe(NO_3)_3$ in phosphate buffer at pH 7.4) quenching approximately 75% of the fluorescence intensity. After the addition of aliquots beyond 100 μL (1.9 μmol), the same issue as before was witnessed: the production of an insoluble precipitate with no additional quenching. The pH was measured again to ensure the buffered pH remained at 7.3, and because the pH was confirmed to have remained the same, the hydroxide salt was no longer the problem. The suspected difficulty in this specific circumstance was the formation of the metal phosphate salt. To test if the metal phosphate salt was indeed the problem, a chelating ligand was chosen to attempt to keep the metal ion in solution and prevent the formation of any salt. EDTA was chosen for its high binding constant for a multitude of metal ions and its biocompatibility.[28, 29] To ensure

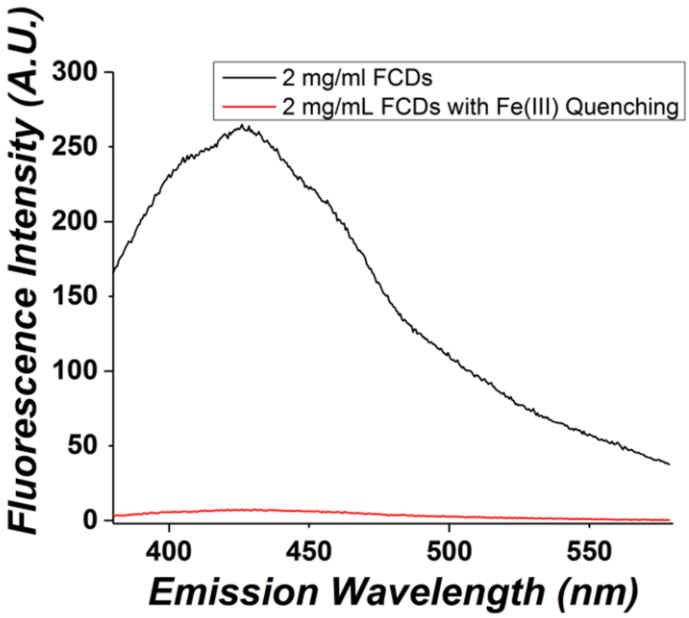

Figure 4.1 Fluorescence quenching of FCDs by ferric ions. The maximum fluorescence of a 2 mg/mL FCD standard is reported with the maximum quenching witnessed through the addition of 140 μL ferric nitrate ion solution for a final ferric ion concentration of 0.0016 M (performed in pH 7.4 phosphate buffer with EDTA).

every metal ion was bound by EDTA, the EDTA was added at a concentration 3 times higher than that of the metal ion.

The ferric ion quenching experiment was repeated once again, adding 10 μL aliquots until the addition of an aliquot made no change on the fluorescence signal. The experiment was successful this time due to the addition of the phosphate buffer in conjunction with EDTA. When 140 μL of the ferric ion solution were added (2.66 μmol), the fluorescence signal reached its maximum quenching with almost complete loss of fluorescence signal, seen in Figure 4.1. To ensure the nitrate in the salt had no impact on the quenching, in addition to confirming that it was the ferric ion that was responsible, the experiment was repeated with iron(III) sulfate as the salt source for the ferric ions. The experiment yielded nearly identical results as seen in Figure 4.2. This confirms the ferric ion is responsible for the quenching, with the anion of the salt not being involved in the process.

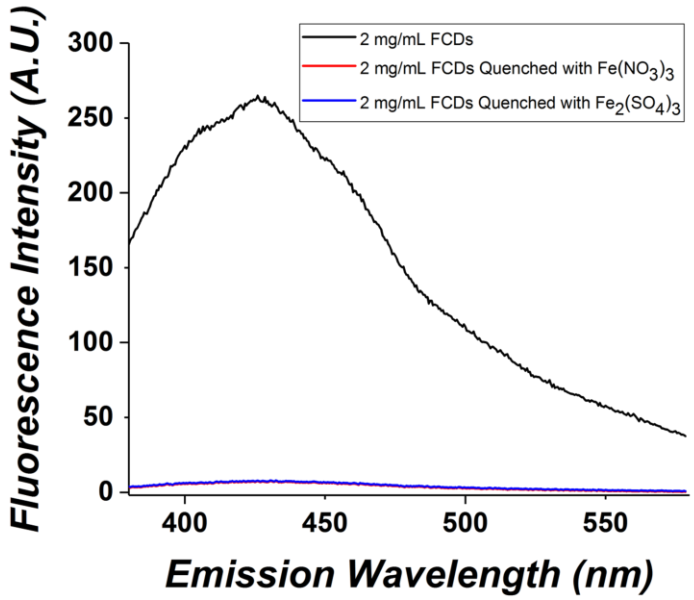

Figure 4.2 Comparison of the fluorescence quenching of FCDs by iron(III) nitrate and iron (III) sulfate. The final concentration of ferric ions is 0.0016 M in both experiments (performed in pH 7.4 phosphate buffer with EDTA).

Other metal ions were tested for their ability and efficacy in quenching the fluorescence of the FCDs: copper(II), tin(II), nickel(II), calcium(II), and aluminum(III). Aluminum and calcium both had no measurable effect on the fluorescence of the FCDs themselves due to the large amount of scattering observed when the fluorescence was attempted to be measured, most likely due to the presence of the hydroxides of these two metal ions. The effect of the other metal ions can be seen in Figure 4.3.

The tin(II) ion showed no fluorescence quenching, but red-shifted the fluorescence peak. Interestingly, the shift happened after the first aliquot of tin(II) was added, but after adding 6 more aliquots of the tin(II) solution, no additional change was witnessed. Use of nickel(II) and copper(II) both resulted in quenching similar to that seen by the ferric ion in that the spectral pattern of the FCDs does not change as more metal ion is added, only the intensity of the signal changes. Nickel(II) was only able to quench the fluorescence of the FCDs by approximately 50%. The

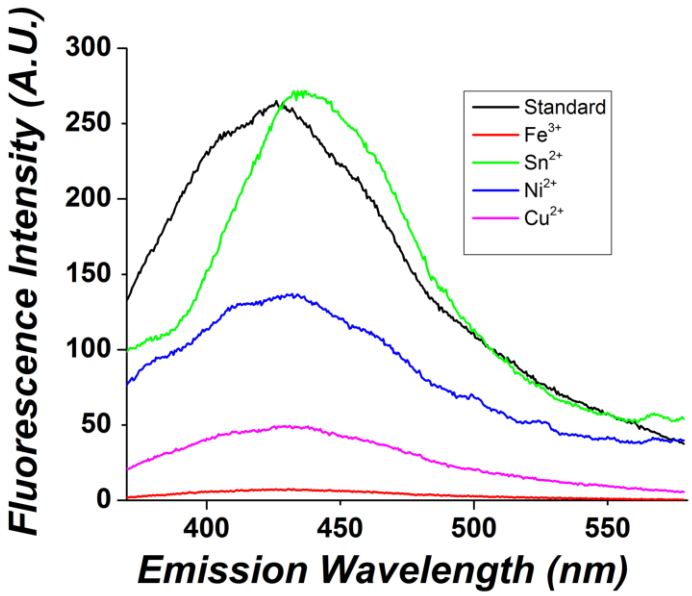

Figure 4.3 Fluorescence quenching of FCDs by metal ions. The maximum fluorescence signal of a 2 mg/mL FCD standard with the maximum achieved quenching of metal ions reported here with varying volumes of metal ions added to the FCD solution (performed in pH 7.4 phosphate buffer with EDTA).

amount of nickel required to quench the fluorescence to that point was 9 aliquots for a total volume of 90 μL of nickel(II) added (1.71 μmol). Copper(II) produced similar results, lowering the fluorescence maximum approximately 75% after the addition of 8 aliquots of copper(II) for a total volume of 80 μL of copper(II) added (1.52 μmol). Based on these results, the most effective quencher for the FCDs synthesized in this research was ferric ions in the form of iron(III) nitrate. Moving forward, iron (III) nitrate dissolved in phosphate buffer with EDTA in a 1:3 metal ion to EDTA ratio was the source of the quenching metal ion unless otherwise stated. If denoted that complete (100%) quenching occurred, 140 μL of the ferric ion solution was added per 1.5 mL of 2 mg/mL FCD solution (0.00162 M ferric ion). If denoted that 50% quenching occurred, 70 μL of the ferric ion solution was added to the 1.5 mL of 2mg/mL FCD solution (0.00085 M ferric ion). With quenching of the FCD fluorescence determined to occur, experimental studies aimed at determining the nature of the turn-on process were first initiated before starting an investigation of the overall quenching and eventual recovery process.

4.3.2 Fluorescence Recovery

As discussed in Chapter 1, the goal of the FCD biosensor proposed here is the effective quenching of the fluorescence of the FCD followed by the recovery of the fluorescence by reducing species found in mammalian cells. To test the initial fluorescence recovery, ascorbic acid (formal reduction potential, $E^{o'}$ = +0.051 V vs SHE) was used as the reducing agent, based on research published by Fong et alia.[2, 30, 31] Additional reducing agents were tested, including citric acid ($E^{o'}$ = + 1.1 V vs Ag/AgCl), GSH ($E^{o'}$ = -0.22 V vs SHE), and sodium dithionite ($E^{o'}$ = - 0.66 V vs SHE).[32-34] The results of the initial attempt at fluorescence recovery can be seen in Figure 4.4. The testing of AA as a potential agent to re-establish fluorescence signal in the iron-quenched FCDs led to meager increases in the fluorescence signal. The fluorescence recovery reported in

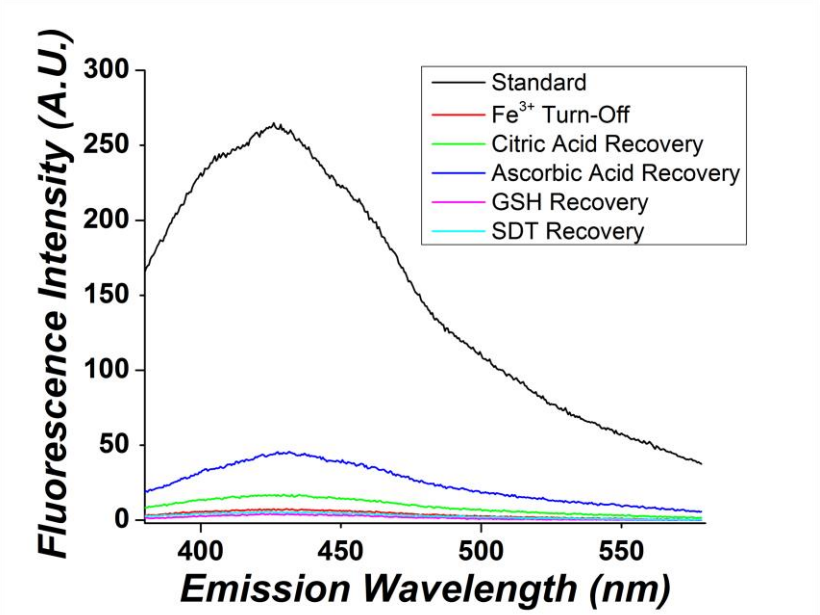

Figure 4.4 Fluorescence recovery after quenching by reducing agents. The maximum fluorescence signal of a 2 mg/mL FCD standard is reported with the maximum quenching obtained by exposure of the FCDs to ferric ions. Various reducing agents to attempt to recover fluorescence are reported (performed in pH 7.4 phosphate buffer with EDTA).

the research of Fong et alia was a complete recovery back to the original fluorescence before quenching by addition of iron(III). In this research, that was not the result, with ascorbic acid leading to recovery of at most 25% of the fluorescence signal for solutions having the same concentration of FCDs and no other added materials. 50 μL of ascorbic acid was added to the FCD/metal ion solution before maximum recovery was reached. Any additions beyond that amount produced no changes in the fluorescence signal. To test other reducing agents that are found readily in the cell, citric acid and GSH were tested. Citric acid was chosen because it is found in cells as it is formed in the mitochondrion after condensation of acetate with oxaloacetate.[35] Addition of citric acid did not result in any recovery of the fluorescence (Figure 4.4), so it was abandoned as a possible reducing agent for recovering the fluorescence of Fe(III)-quenched FCDs. GSH is a reducing agent found in cells in the range of 1-10 mM, and was one of

the reducing agents assumed to lead to observed recovery of fluorescence (turn-on) for FCDs upon their uptake into cells.[36] Unfortunately, addition of GSH did not result in significant changes in fluorescence; a fluorescence spectrum indistinguishable from that of the fully quenched FCDs was observed (Figure 4.4). To ensure reduction of the metal ion is occurring and the lack of fluorescence recovery is not a product of lack of reduction of the ion, sodium dithionite was tested as a reducing agent. Sodium dithionite is a strong reducing agent ($E^{o'}$ = - 0.66 V vs SHE) that has been used throughout literature to reduce a wide range of species, including iron(III).[37] If sodium dithionite cannot recover the fluorescence, then the recovery of the fluorescence is not based upon the reduction of the metal ion, and that proved to be true considering no fluorescence recovery was witnessed when sodium dithionite was added to the FCD/ferric ion solution. With a negative Gibb's free energy when considering the reduction of ferric ions by SDT, effective reduction should be occurring. More specific testing to ensure the reduction of the metal ion was performed using a 5-sulfosalicylic acid (SSA) assay and electron paramagnetic resonance (EPR).

When determining a method to measure the difference between the ferric (Fe^{3+}) and ferrous (Fe^{2+}) ions in solution, an assay method was chosen due to the ease of measurement in solution phase and the ease of measurement in a lab setting without complex equipment. When SSA interacts with iron ions in solution, a ferric-SSA complex is created that is red in color and absorbs at 500 nm. The SSA binds ferric ions selectively at low pH, forming the red ferric-SSA complex that absorbs at 500 nm, but at higher pH conditions, the SSA binds all iron ions regardless of charge state, forming a yellow total iron-SSA complex that absorbs at 425 nm.[38] To ensure complete reaction time, the absorbance was measured before allowing the solution to rest for 15 min before measuring again, but no difference in absorbance was witnessed in any samples after the 15 min had elapsed. In the experimental workflow, each fluorescence and absorbance

measurement in the assay were performed on a different sample due to the nature of the assay. To ensure consistency throughout, the solutions were prepared simultaneously from the same stock solutions. Additionally, to ensure no dilution effects occurred, as increased amounts of ferric ions or SDT were added, the amount of water was reduced by that much volume to ensure the final volume of each sample was identical. The results of the assay can be seen in Figure 4.5.

The results of the measurement of the iron oxidation state as they are added to a 2 mg/mL solution of FCDs to quench the fluorescence can be seen in Figure 4.5 A. The results are as expected, with the absorbance signal for the yellow total iron-SSA complex increasing as more ferric ions are added to the FCDs as the quenching of the FCD fluorescence progresses. One concern when quenching the FCDs with ferric ions was ensuring that the ferric ions were in fact existing as ferric ions when quenching the fluorescence of the FCDs, and this was confirmed considering the absorbance signal from the red ferric-SSA complex increased as more ferric ions were added. Assessment of the attempted recovery of fluorescence using SDT was the more vital experiment, and it offered confirmation that the SDT is in fact reducing the ferric ions in solution. As the amount of SDT added increased, the signal from the total iron-SSA complex remained constant, which is to be expected considering the concentration of total iron in solution should not have changed. More importantly, the absorbance signal from the red ferric-SSA complex decreased with increasing amounts of SDT. While the assay cannot confirm quantitatively how much of the ferric ion solution is reduced to ferrous ions, it does confirm that as more SDT is added, more ferric ions are reduced to ferrous ions. This confirms that the reduction does not recover the fluorescence as proposed in the literature.[2] To further gain information about possible changes in iron oxidation state, electron paramagnetic resonance (EPR) spectroscopy was used to evaluate the possibility of reduction of ferric ions to ferrous ions.

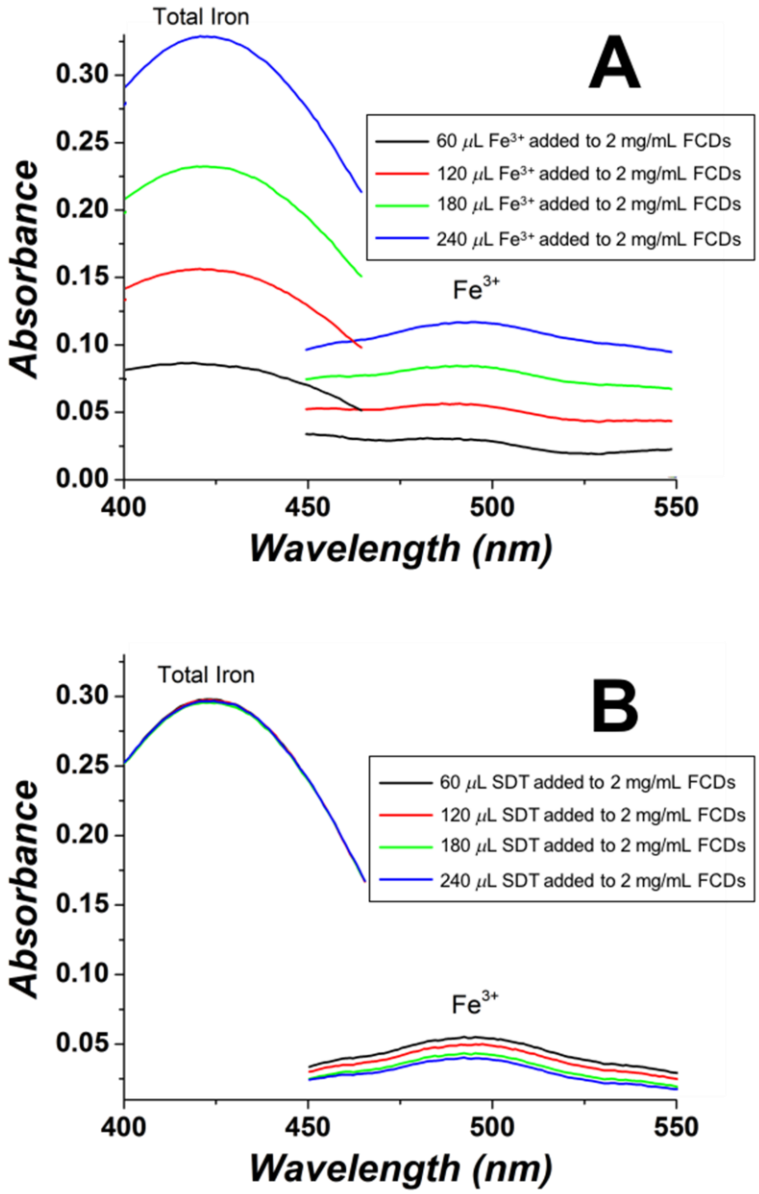

Figure 4.5 Results of the SSA assay experiment to measure the amount of ferric ions and ferrous ions present in a 2 mg/mL solution of FCDs dissolved in water during A) quenching with iron (III) nitrate (0.019 M) and B) attempted recovery of fluorescence by SDT (0.019 M).

EPR spectroscopy measures paramagnetic species with unpaired electrons, while diamagnetic species with paired electrons generate no EPR signal. Ferric ions possessing unpaired electrons generate an EPR signal, as seen in Figure 4.6. The signal for the iron(III) standard is in agreement with that in the literature, with the signal at low magnetic field (*g*-factor: 4.3 at 1600

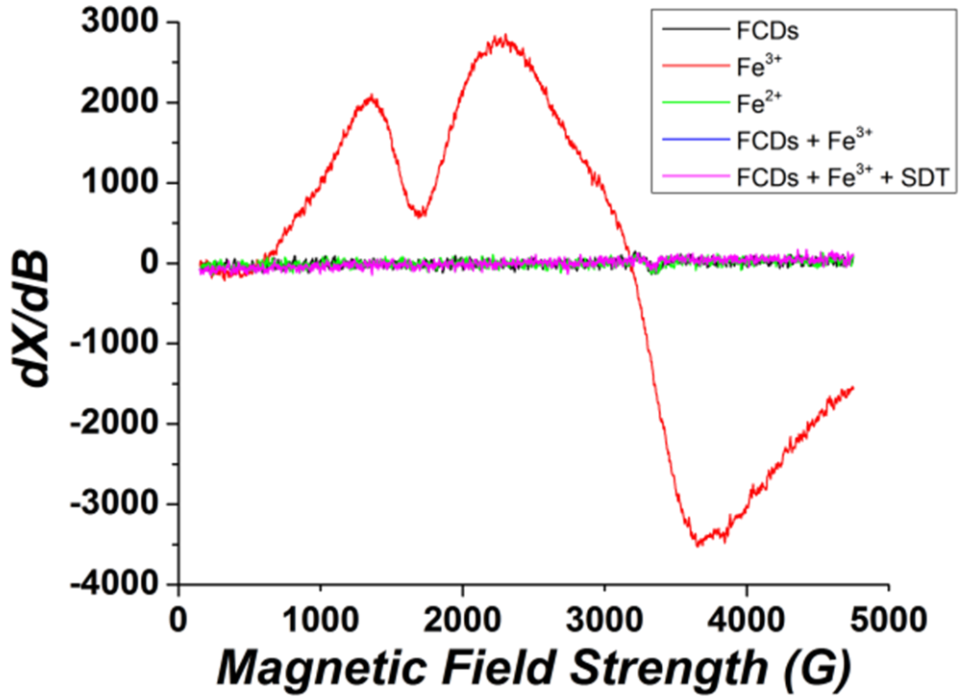

Figure 4.6 Electron paramagnetic resonance spectroscopy of 0.0016 M ferric and ferrous ions as standards, 2 mg/mL FCDs in water quenched by ferric ions (0.0016 M), and attempted recovery of fluorescence in FCDs quenched by ferric ions by SDT (0.0016 M) reduction (performed at low temperature, 4K).

G) being associated with framework iron and those at higher magnetic field (*g* factor: 2.3 at 3000 G and *g* factor: 2.0 at 3400 G) due to iron in interstitial oxide or hydroxide phases and iron in cation exchange sites, respectively.[39, 40] Ferrous ions possess paired electrons and should therefore exhibit no EPR signal, also seen in Figure 4.6. The FCDs did not exhibit any significant EPR signal that could be attributed to any ferric contaminant, but they do give rise to the EPR signal near 3600 G, giving the radical a *g*-factor of approximately 2.004, corresponding to semiquinone radicals, as discussed in Chapter 3. When the FCDs were exposed to ferric ions to quench their fluorescence, it was found that there is no signal present that can be attributed to the presence of ferric species. Additionally, when SDT was added in an attempt to reduce the ferric ions and recover the fluorescence, no signal was seen. Considering that the absorbance of the

ferric-SSA complex did not change over the 15 min elapsed while the FCD/ferric ion sample rested during the SSA assay, showing no reduction in the ferric ions, the loss of signal upon ferric ion exposure to FCDs was not initially expected. One possible explanation for the loss in the ferric ion EPR signal is the reduction of the ferric ions by the FCDs themselves, and while this is possible considering the fact that if there are indeed quinone, semiquinone, or catechol groups on the surface, they are capable of the reduction of the ferric ions, with potentials ranging from 0.91 V vs $Ag/AgNO_3$ for some catechols to -0.79 V vs $Ag/AgNO_3$ or 0.099 V vs NHE for quinones depending on the substitution.[41-43] If instead the ferric ions are complexing with quinone or catechol surface functionalities of the FCDs in a strong enough method to withdraw electron density from the ferric ion, without actual reduction, the EPR behavior exhibited could be similar to that of ferrous ions.[44-46] Unfortunately, due to this subtle difference in behavior, it makes an EPR experiment to determine reduction of ferric ions to ferrous ions difficult to apply. This does however provide evidence for the fluorescence quenching mechanism outlined in following sections. Due to the behavior of the ferric and ferrous ions established by both the SSA assay and EPR, it was decided that an evaluation of the quenching potential of ferrous ions could help determine what behavior is occurring in the quenching of these FCDs.

As mentioned previously, in literature, the recovery of fluorescence is tied to the conversion of ferric ions to ferrous ions. This implies an innate ability of ferric ions to quench while ferrous ions do not quench.[2] A study was performed to evaluate what iron species are able to quench the fluorescence of these FCDs and the results can be seen in Figure 4.7 A. When exposed to equal amounts of either ferric or ferrous ions, fluorescence quenching occurred. The maximum quenched fluorescence of the FCDs by ferric ions was near complete, with the fluorescence intensity decreased to near the baseline. However, maximum amount of fluorescence

quenching of the FCDs by ferrous ions was only approximately 25% of the initial fluorescence. Though the ferrous ions were not able to completely quench the fluorescence, a decrease to 25% of the original fluorescence is not trivial and makes the proposed turn-on FCD probe possibly

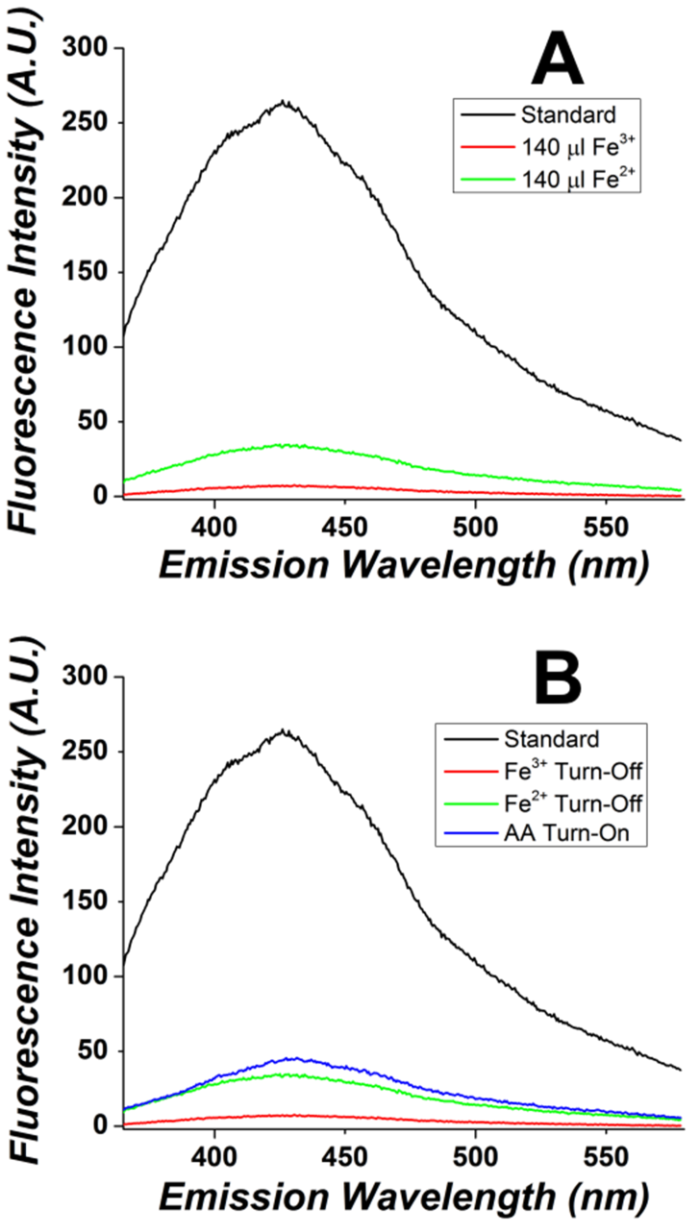

Figure 4.7 Comparison of quenching in a 2 mg/mL solution of FCDs by ferric and ferrous ions. Fluorescence emission scans of 2 mg/mL FCDs are labeled as standard to denote maximum fluorescence and scans of A) quenching abilities of ferric and ferrous ions and B) comparison of quenching by iron and recovery by ascorbic acid (performed in pH 7.4 phosphate buffer with EDTA).

ineffective. Additionally, as can be seen in Figure 4.7 B, the limited fluorescence recovery witnessed when quenched FCDs were exposed to ascorbic acid or other reducing agents seems to be a property of the conversion of ferric ions to ferrous ions. Rather than the complete recovery of fluorescence, as was predicted, the fluorescence signal is recovered to a slight extent due to the less effective quenching of the FCDs by the ferrous ions. Once a threshold of ferric to ferrous conversion is reached, the fluorescence recovery stops as the ferrous ions take over the quenching process. Determination of why certain metal ions quench as compared to other metal ions in the case of these FCDs is not a trivial matter to elucidate. To gain insight into this process, a metal ion was chosen for investigation that possesses properties similar to iron in most regards except reduction potential: ruthenium.

Iron and ruthenium, both existing as Group 8 elements on the periodic table, possess similar valence electron shells, giving them similar chemical properties and binding behavior. Ruthenium and iron both exist predominately in the +3 oxidation state, but possess very different reduction potentials, 0.249 V vs SHE for ruthenium(III) and 0.77 V vs SHE for the ferric ion.[47] A comparison of the behavior of ferric and ruthenium(III) ions should offer additional insight into the quenching mechanism. The results of ruthenium quenching experiments are seen in Figure 4.8. With the addition of 140 μL of 0.076 M ferric ions, the fluorescence quenching of 2 mg/mL FCDs is near complete, as can be seen in Figure 4.8. With the addition of 140 μL of 0.076 M ruthenium(III) ions, the fluorescence is quenched to an extent similar to that produced by ferric ions. This behavior further proves that the reduction potential of the metal ion is not the driving factor in the fluorescence quenching mechanism, considering metal ions with reduction potentials between those or more negative of iron(III) and ruthenium(III) (copper(II): 0.34 V vs SHE and nickel(II): -0.25 V vs SHE) show limited quenching as well, with no clear pattern connecting

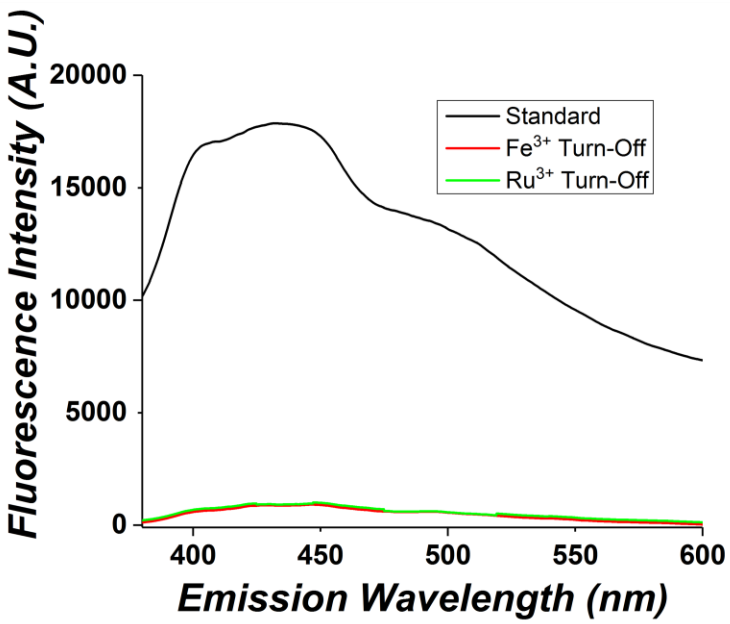

Figure 4.8 Fluorescence emission scan of 2 mg/mL to denote the maximum fluorescence signal as compared to maximum quenching achieved by ferric and ruthenium (III) ions (performed in 7.4 pH phosphate buffer with EDTA).

reduction potentials and quenching.[48, 49] While the recovery mechanism is more difficult to probe considering the fluorescence was not actually recovered by any reducing agent, significant information regarding the fluorescence quenching mechanism of the FCDs by ferric ions was obtained, producing the proposed mechanism outlined below.

4.3.3 Proposed Mechanism

Tests were first done in an attempt to determine whether the quenching mechanism observed in the case of FCDs and ferric ions is a dynamic or static quenching mechanism. As mentioned earlier in this chapter, the typical way to regard dynamic quenching is that a quencher interacts with the analyte during its existence in the excited state, preventing the energy release from a return to ground state. This prevention of energy release can be due to the inability of the fluorophore to return to the ground state through stabilization of an excited state.[50] It can also result from an alternate energy pathway being created to allow for the energy to be released through

a different pathway than fluorescence emission as the fluorophore moves from its excited state to ground state.[14] In a static quenching mechanism, a non-fluorescent complex forms. There are two common methods to identify a dynamic quenching mechanism: temperature controlled reactions and ligand bonding to prevent quenching. Both were explored in this research to evaluate a static versus dynamic quenching mechanism.

The temperature control measurements are based on the property of dynamic quenching mechanisms to rely on collisions between the quencher and the fluorophore. If the temperature during the experiment is increased, the molecules possess more kinetic energy and are therefore experiencing more collisions and therefore more fluorescence quenching.[18] In the case of FCDs synthesized in this research and their interactions with ferric ions, the quenching of the

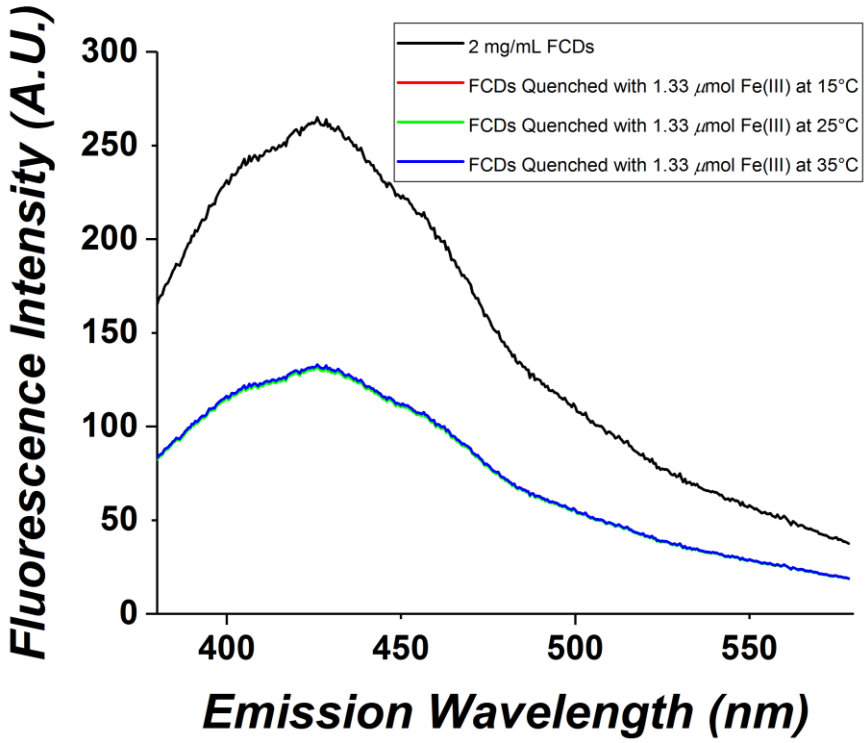

Figure 4.9 Evaluation of fluorescence quenching of 2 mg/mL FCDs by ferric ions at different temperatures. The fluorescence was quenched to ~50% by the ferric ions while being held at different temperatures (performed in pH 7.4 phosphate buffer with EDTA).

fluorescence was measured for the same system at different temperatures, as seen in Figure 4.9. A solution of 2 mg/mL FCDs was measured to establish a fluorescence baseline. Following this scan, the fluorescence was quenched to 50% maximum using ferric ions as outlined above. This experiment was performed through the exact same process at three temperatures (15 °C, 25 °C, and 35 °C). The volume of 0.0019 M ferric ions required to quench the fluorescence to 50% of maximum was compared across the three temperatures and was found to be the same. 70 μL of the 0.076 M ferric ion solution (1.33 μmol) reduced the fluorescence to approximately 50% in all three experiments. This seems to suggest a dynamic quenching mechanism is not occurring in this interaction between ferric ions and FCDs.

In the case of a static quenching mechanism, exposure of the metal ion quencher to a ligand prevents the formation of the non-fluorescent complex, effectively inhibiting any quenching behavior. This can be seen throughout literature as a way to identify a static quenching mechanism.[51] In the case of Wang et alia, their graphene quantum dots are quenched by Cu (II) ions, and to probe the quenching mechanism, they exposed their fluorophores quenched by the Cu (II) ions to EDTA.[52] They experienced a complete fluorescence recovery after the EDTA was introduced to the solution. This exhibited evidence that the EDTA-Cu(II) complex prevented the formation of the non-fluorescent FCD-Cu(II) complex. In the case of my FCDs quenched by ferric ions, EDTA is present in every quenching experiment that was performed with no quenching inhibition whatsoever. This could suggest a dynamic quenching mechanism rather than a static mechanism. At this point, one experiment suggests a dynamic quenching mechanism and one experiment suggests a static quenching mechanism. This scientist believes a static quenching mechanism is occurring and the experiment involving EDTA not inhibiting the fluorescence can

be explained by the proposed mechanism to follow, with said mechanism based on a stronger-than-EDTA coordination of iron species on the surface of the FCDs.

As concluded from the characterization experiments in Chapter 3, the FCDs exhibit what could be quinone and catechol groups on their surfaces. The quinone/catechol functionalities are believed to be the primary driving force behind the fluorescence quenching mechanism in this research. An examination of possible alterations to the nature of surface functionalities was investigated with XPS, as noted in Figure 4.10. The carbon 1s spectrum is changed both in binding energy and surface composition for the C=O and C-O transitions when comparing that for iron(III)-treated to the pristine FCDs. The binding energy of the C=O band in the ferric-exposed FCDs is found to be 1-2 eV lower than in the pristine FCDs, and its relative surface percentage is lower (10.03%-2.86%) Similarly, the C-O transition of the treated FCDs is found to be 1 eV lower

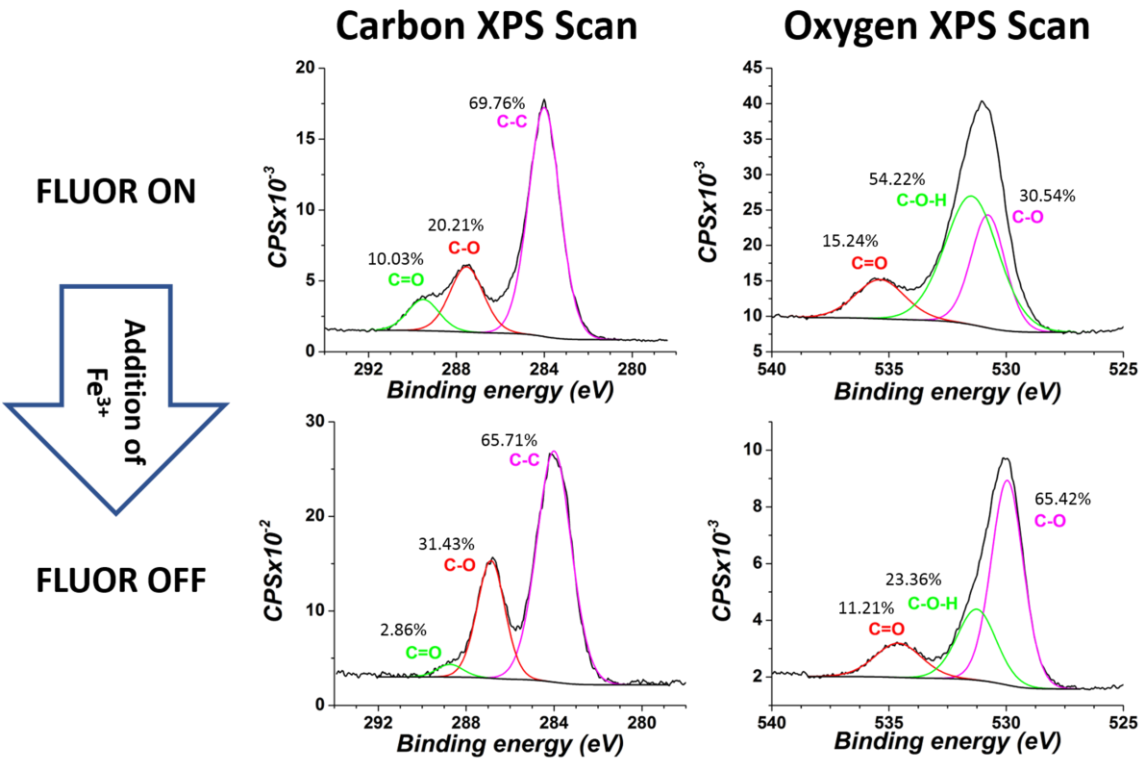

Figure 4.10 X-ray photoelectron spectroscopy in the carbon 1s and oxygen 1s regions for FCDs before (Fluor On) and after (Fluor Off) treatment with ferric nitrate solutions (quenching performed in pH 7.4 phosphate buffer with EDTA).

than in the untreated materials, with the relative surface amount increased from 20.21% to 31.43%. It is also noted that the C=O, C-O-H, and C-O transitions in the O 1s spectrum experiences changes upon ferric ion exposure. The shift in the C-O and C-O-H peaks can be explained by Scheme 4.1. It is a well-known property of catechol and quinone groups that they can form semiquinone radicals in the correct conditions.[41] Typically, the semiquinone radical has a very short lifetime due to its lack of stability and converts back to the catechol or quinone group quickly. In the case of the current experiment, it is believed that the metal ion can form a complex with the semiquinone radical to stabilize and increase the lifetime of that radical. This increase in the lifetime, and therefore quantity, of semiquinone radical in solution results in the quenching of the fluorescence. This increase in the semiquinone radical could be seen in the C-O peak increases in the oxygen 1s scan (30.54% to 65.42%) and the carbon 1s scan (20.21% to 31.43%). Further XPS study would need to be performed to fully understand the binding energy shifts and confirm the mechanism presented below, but there is additional evidence to support this scheme as well.

The formation of this complex would suggest a static quenching mechanism as stated above, however if that is the case, the EDTA should be able to chelate the metal ion and prevent quenching or recover the fluorescence. In this instance, the difference in expected behavior can be explained by an examination of formation constants. The formation constant (log K_f) of the EDTA-ferric ion complex is 25.1, which is typically high enough to allow EDTA to bind the ferric ion

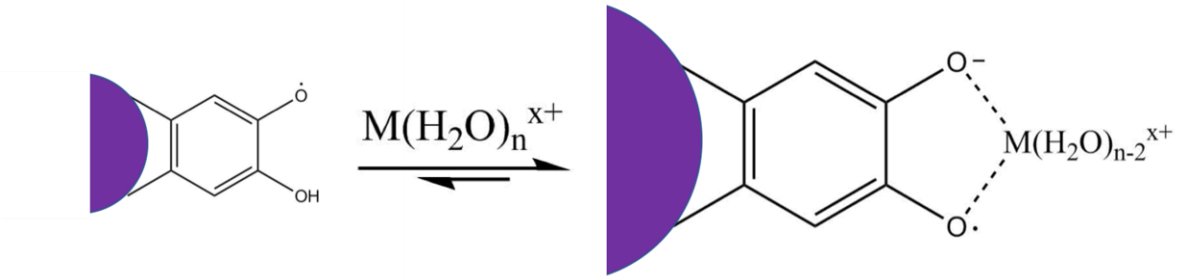

Scheme 4.1 Depiction of the stabilization of a semiquinone radical by a metal ion.

strongly enough to prevent its interaction with other species.[53] In this case, the binding constant for the semiquinone radical-ferric ion complex could be high enough to remove the ferric ion from the EDTA chelation and allow the formation of the non-fluorescent complex. The log K_f for the semiquinone radical-ferric ion complex has been reported as high as 49.[45] This could explain why EDTA would not be able to prevent the static quenching mechanism proposed in this research.

The strong binding constant for the semiquinone radical-ferric ion complex could also be witnessed in the data gathered from an analysis of the change in the lattice spacing of the crystal structure when fluorescence is quenched with ferric ions, Figure 4.11. It was stated in Chapter 3 that the lattice spacing of 0.28 nm measured in the FCDs was consistent with graphene oxide containing water within the crystal structure.[54] When quenched with the ferric ions, the lattice spacing shrinks, shifting to a 0.22 nm lattice spacing. This scientist believes this can be explained through intercalation of the ferric ions in between the graphene oxide layers. If the FCDs exist as layered graphene oxide, as discussed in Chapter 1 and 3, then the intercalation of the ferric ions in

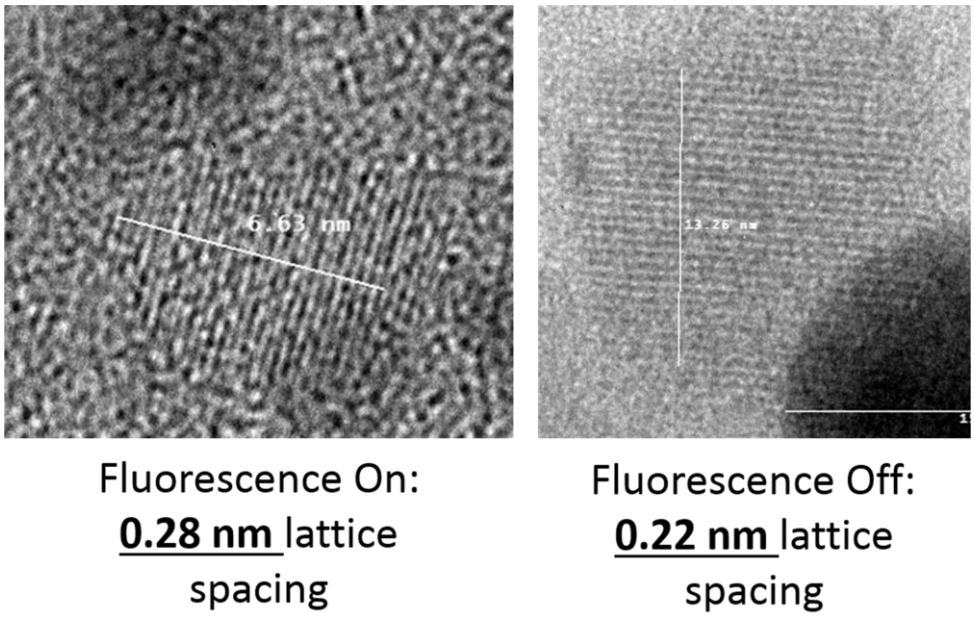

Figure 4.11 HR-TEM of FCDs before and after fluorescence quenching with ferric ions.

between those layers is real possibility as this type of intercalation is well reported in the literature.[55, 56] The catechols are known to bind the ferric ion in a bidentate method in multiple places to ideally produce an octahedral geometry.[57] This would allow for the formation of the semiquinone radical-ferric ion complex through interaction of the ferric ion with multiple semiquinone radicals form different layers of the graphene oxide within the structure of the FCDs. If this occurred, the lattice spacing would be expected to decrease as the water is displaced from the crystal structure and the layers are pulled closer together through the formation of the semiquinone radical-ferric ion complex. EPR was also used to evaluate this proposed mechanism.

As discussed in the characterization of the FCDs, radicals were measured in the FCDs with a *g*-factor corresponding to semiquinone type radicals. The presence of semiquinone radical production from quinone/catechol groups on the surface of the FCDs was shown through EPR, with the quinone/catechol groups further exhibited through IR and XPS measurements. To evaluate the stabilization of the semiquinone radicals, EPR experiments were run before and after fluorescence quenching to evaluate the radical signal around a *g*-factor of 2.00442. Preliminary results gathered by Dr. Kresmir Rupnik can be seen in Figure 4.12. While the results are preliminary, these experiments suggest an increase in the signal of radicals with a *g*-factor similar to those witnessed by semiquinone radicals in FCDs before quenching. The slight shift in *g*-factor is expected as the semiquinone radical is now complexing with the ferric ions and therefore has a different energy. More data would need to be collected to confirm these results, but they are promising evidence to support the proposed mechanism from Scheme 4.1.

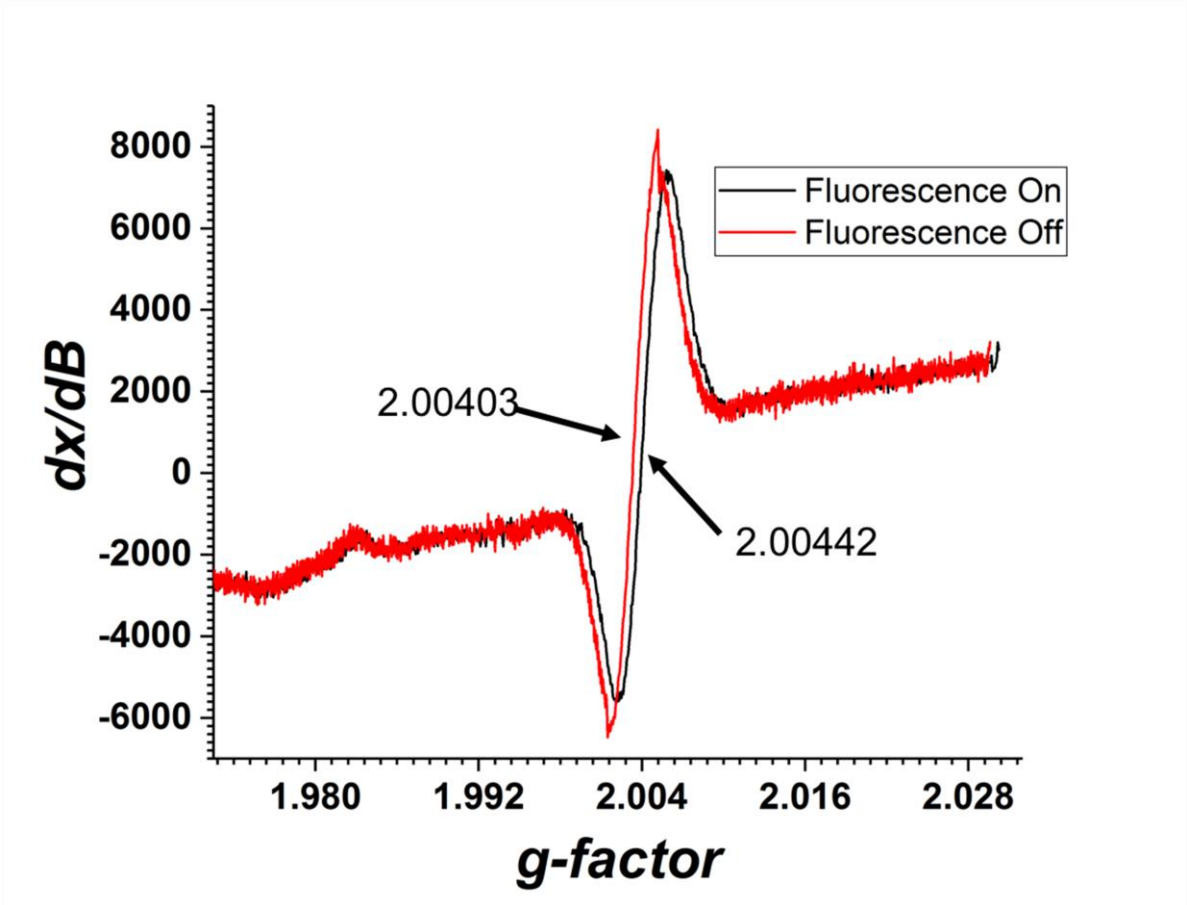

Figure 4.12 Electron paramagnetic resonance spectroscopy of 2 mg/mL FCDs in 7.4 pH phosphate buffer to measure semiquinone radical signal before and after fluorescence quenching with ferric ions.

4.4 Conclusions

Quenching mechanisms in FCDs typically fall into two broad categories: static and dynamic. Dynamic quenching involves the interaction of a quencher with the FCDs while in the excited state, preventing the emission of light as fluorescence. Static quenching mechanisms involve the formation of a non-fluorescent complex between the quencher and the FCD. Dynamic quenching mechanisms do not modify the FCD, while static quenching mechanisms do cause a modification in the FCD. Evaluation of which quenching mechanism occurs in FCDs is vital to

understand the quenching process. In the case of the quenching of FCDs synthesized in this research by ferric ions, it is believed that a static quenching mechanism is occurring.

The FCDs were evaluated to determine what metal ions quench the fluorescence and it was discovered that iron, copper, nickel, and ruthenium ions all quench the fluorescence of the FCDs synthesized in this research. The most effective quencher of these FCDs was ferric ions. A complete loss of fluorescence was produced when the FCDs were exposed to sufficient ferric ions. An evaluation of the fluorescence recovery via reducing agents to reduce the metal ion quencher was explored and found to be ineffective. The ineffective recovery of fluorescence is believed to be due to the fact that although the ferric ions in solution are indeed reduced to ferrous ions, the ferrous ions are also fluorescence quenchers. Since the fluorescence could not be recovered, evaluation of the FCDs and their quenching mechanism was explored.

The proposed static quenching mechanism of semiquinone stabilization is supported through multiple experiments. By adjusting the temperature at which the quenching occurred and seeing no changes in the fluorescence quenching, dynamic quenching was disproven. Analysis of the changes in the XPS spectrum before and after fluorescence quenching suggests the transition from primarily catechol groups to a large amount of semiquinone radicals produced from the catechol groups. EPR data suggests an increase in the number of semiquinone radicals after quenching has occurred. There is a suggested stabilization of the semiquinone radicals by the ferric ions, which is supported by the literature as these semiquinone radical-ferric ion complexes form very strong bonds that are well reported in the literature. This establishment of a possible path of quenching in FCDs by ferric ions is the first of its kind in the literature, indeed, it goes beyond most research into FCD quenching as it attempts to establish an actual mechanism rather than simply measuring the quenching. In conclusion, though more extensive research needs to be

performed to confirm the exact mechanism, a static quenching mechanism involving the formation and stabilization of a semiquinone radical is suggested and is the first of its kind seen in the literature.

4.5 References

1. Yang, Z.-C., et al., Intrinsically fluorescent carbon dots with tunable emission derived from hydrothermal treatment of glucose in the presence of monopotassium phosphate. Chemical communications, 2011. 47(42): p. 11615-11617.

2. Fong, J.F.Y., S.F. Chin, and S.M. Ng, A unique "turn-on" fluorescence signalling strategy for highly specific detection of ascorbic acid using carbon dots as sensing probe. Biosensors and Bioelectronics, 2016. 85: p. 844-852.

3. Han, C., et al., Highly fluorescent carbon dots as selective and sensitive "on-off-on" probes for iron(III) ion and apoferritin detection and imaging in living cells. Biosensors and Bioelectronics, 2016. 83: p. 229-236.

4. Borse, V., et al., N-doped multi-fluorescent carbon dots for 'turn off-on' silver-biothiol dual sensing and mammalian cell imaging application. Sensors and Actuators B: Chemical, 2017. 248: p. 481-492.

5. Cao, X., et al., A near-infrared fluorescent turn-on probe for fluorescence imaging of hydrogen sulfide in living cells based on thiolysis of dinitrophenyl ether. Chemical Communications, 2012. 48(85): p. 10529-10531.

6. Han, Q., et al., Turn-On Fluorescence Probe for Nitric Oxide Detection and Bioimaging in Live Cells and Zebrafish. ACS Sensors, 2019. 4(2): p. 309-316.

7. Zheng, M., et al., On–Off–On Fluorescent Carbon Dot Nanosensor for Recognition of Chromium(VI) and Ascorbic Acid Based on the Inner Filter Effect. ACS Applied Materials & Interfaces, 2013. 5(24): p. 13242-13247.

8. Guo, Y., et al., Fluorescent carbon nanoparticles for the fluorescent detection of metal ions. Biosensors and Bioelectronics, 2015. 63: p. 61-71.

9. Guo, Y., et al., Hydrothermal synthesis of highly fluorescent carbon nanoparticles from sodium citrate and their use for the detection of mercury ions. Carbon, 2013. 52: p. 583-589.

10. Liu, R., et al., Ultra-sensitive and selective Hg2+ detection based on fluorescent carbon dots. Materials Research Bulletin, 2013. 48(7): p. 2529-2534.

11. Qu, S., et al., A biocompatible fluorescent ink based on water-soluble luminescent carbon nanodots. Angewandte Chemie international edition, 2012. 51(49): p. 12215-12218.

12. Wang, F., et al., Down-and up-conversion luminescent carbon dot fluid: inkjet printing and gel glass fabrication. Nanoscale, 2014. 6(7): p. 3818-3823.

13. Lakowicz, J.R., Principles of fluorescence spectroscopy. 2013: Springer Science & Business Media.

14. Song, Y., et al., Investigation into the fluorescence quenching behaviors and applications of carbon dots. Nanoscale, 2014. 6(9): p. 4676-4682.

15. Iqbal, A., et al., Carbon dots prepared by solid state method via citric acid and 1,10-phenanthroline for selective and sensing detection of Fe2+ and Fe3+. Sensors and Actuators B: Chemical, 2016. 237: p. 408-415.

16. Gu, D., et al., Green synthesis of nitrogen-doped carbon dots from lotus root for Hg(II) ions detection and cell imaging. Applied Surface Science, 2016. 390: p. 38-42.

17. Wang, L., et al., Carbon dots based turn-on fluorescent probes for the sensitive determination of glyphosate in environmental water samples. RSC Advances, 2016. 6(89): p. 85820-85828.

18. Wang, F., et al., Fluorescence quenchometric method for determination of ferric ion using boron-doped carbon dots. Microchimica Acta, 2016. 183(1): p. 273-279.

19. Sun, X. and Y. Lei, Fluorescent carbon dots and their sensing applications. TrAC Trends in Analytical Chemistry, 2017. 89: p. 163-180.

20. Sachdev, A. and P. Gopinath, Green synthesis of multifunctional carbon dots from coriander leaves and their potential application as antioxidants, sensors and bioimaging agents. Analyst, 2015. 140(12): p. 4260-4269.

21. Hu, S., et al., Enhanced performance of Fe3+ detection via fluorescence resonance energy transfer between carbon quantum dots and Rhodamine B. RSC Advances, 2014. 4(77): p. 41069-41075.

22. Yan, F., et al., Fluorescent carbon dots for ratiometric detection of curcumin and ferric ion based on inner filter effect, cell imaging and PVDF membrane fouling research of iron flocculants in wastewater treatment. Sensors and Actuators B: Chemical, 2019. 287: p. 231-240.

23. Ye, Q., et al., Formation of N, S-codoped fluorescent carbon dots from biomass and their application for the selective detection of mercury and iron ion. Spectrochimica Acta Part A: Molecular and Biomolecular Spectroscopy, 2017. 173: p. 854-862.

24. Qu, K., et al., Carbon Dots Prepared by Hydrothermal Treatment of Dopamine as an Effective Fluorescent Sensing Platform for the Label-Free Detection of Iron(III) Ions and Dopamine. Chemistry – A European Journal, 2013. 19(22): p. 7243-7249.

25. Vikneswaran, R., S. Ramesh, and R. Yahya, Green synthesized carbon nanodots as a fluorescent probe for selective and sensitive detection of iron(III) ions. Materials Letters, 2014. 136: p. 179-182.

26. Gan, Z., et al., Enzymatic degradation of poly(ε-caprolactone) film in phosphate buffer solution containing lipases. Polymer Degradation and Stability, 1997. 56(2): p. 209-213.

27. Pikal-Cleland, K.A., et al., Protein Denaturation during Freezing and Thawing in Phosphate Buffer Systems: Monomeric and Tetrameric β-Galactosidase. Archives of Biochemistry and Biophysics, 2000. 384(2): p. 398-406.

28. Galler, K.M., et al., EDTA conditioning of dentine promotes adhesion, migration and differentiation of dental pulp stem cells. International Endodontic Journal, 2016. 49(6): p. 581-590.

29. Waters, R.S., et al., EDTA chelation effects on urinary losses of cadmium, calcium, chromium, cobalt, copper, lead, magnesium, and zinc. Biological Trace Element Research, 2001. 83(3): p. 207-221.

30. Borsook, H. and G. Keighley, Oxidation-Reduction Potential of Ascorbic Acid (Vitamin C). Proceedings of the National Academy of Sciences of the United States of America, 1933. 19(9): p. 875-878.

31. Ball, E.G., Studies on oxidation-reduction. 23. Ascorbic acid. Journal of Biological Chemistry, 1937. 118: p. 219-239.

32. Reipa, V., Direct spectroelectrochemical titration of glutathione. Bioelectrochemistry, 2004. 65(1): p. 47-49.

33. Colucci, J., et al., Electrochemical oxidation potential of photocatalyst reducing agents. Electrochimica Acta, 1999. 44(15): p. 2507-2514.

34. MAYHEW, S.G., The Redox Potential of Dithionite and SO−2 from Equilibrium Reactions with Flavodoxins, Methyl Viologen and Hydrogen plus Hydrogenase. European Journal of Biochemistry, 1978. 85(2): p. 535-547.

35. Poerwono, H., et al., Citric Acid, in Analytical Profiles of Drug Substances and Excipients, H.G. Brittain, Editor. 2001, Academic Press. p. 1-76.

36. Meister, A., Glutathione metabolism and its selective modification. Journal of Biological Chemistry, 1988. 263(33): p. 17205-8.

37. Dunitz, J., The structure of sodium dithionite and the nature of the dithionite ion. Acta Crystallographica, 1956. 9(7): p. 579-586.

38. Karamanev, D.G., L.N. Nikolov, and V. Mamatarkova, Rapid simultaneous quantitative determination of ferric and ferrous ions in drainage waters and similar solutions. Minerals Engineering, 2002. 15(5): p. 341-346.

39. Goldfarb, D., et al., Characterization of Iron in Zeolites by X-band and Q-Band ESR, Pulsed ESR, and UV-Visible Spectroscopies. Journal of the American Chemical Society, 1994. 116(14): p. 6344-6353.

40. McNicol, B. and G. Pott, Studies of the deammoniation and dehydroxylation processes in NH4 faujasite and NH4 mordenite zeolites. The use of the ESR of framework-substituted Fe3+ as a probe. Journal of Catalysis, 1972. 25(2): p. 223-229.

41. Huynh, M.T., et al., Quinone 1 e– and 2 e–/2 H+ Reduction Potentials: Identification and Analysis of Deviations from Systematic Scaling Relationships. Journal of the American Chemical Society, 2016. 138(49): p. 15903-15910.

42. Robole, Z.M., et al., Tuning the Electrochemical Redox Potentials of Catechol with Boronic Acid Derivatives. The Journal of Organic Chemistry, 2019. 84(4): p. 2346-2350.

43. Moulay, S. and R. Mehdaoui, Hydroquinone/catechol-bearing polyacrylic acid: redox polymer. Reactive and Functional Polymers, 2004. 61(2): p. 265-275.

44. Nugent, J.H.A., D.C. Doetschman, and D.J. Maclachlan, Characterization of the multiple EPR line shapes of iron-semiquinones in photosystem 2. Biochemistry, 1992. 31(11): p. 2935-2941.

45. Pierpont, C.G. and C.W. Lange, The chemistry of transition metal complexes containing catechol and semiquinone ligands. Progress in Inorganic Chemistry, 1994: p. 331-442.

46. Lynch, M.W., M. Valentine, and D.N. Hendrickson, Mixed-valence semiquinone-catecholate-iron complexes. Journal of the American Chemical Society, 1982. 104(25): p. 6982-6989.

47. 25 - Iron, Ruthenium and Osmium, in Chemistry of the Elements (Second Edition), N.N. Greenwood and A. Earnshaw, Editors. 1997, Butterworth-Heinemann: Oxford. p. 1070-1112.

48. Goss, D.J. and R.H. Petrucci, General Chemistry Principles & Modern Applications, Petrucci, Harwood, Herring, Madura: Study Guide. 2007: Pearson/Prentice Hall.

49. Ebbing, D.D. and M.S. Wrighton, General chemistry. 1990: Houghton Mifflin Boston etc.

50. Kyle, K.R. and P.C. Ford, Dynamic quenching of the metal-to-ligand charge-transfer excited state of Cu4I4(pyridine)4. Exciplex formation and self-quenching. Journal of the American Chemical Society, 1989. 111(13): p. 5005-5006.

51. Liu, J.-M., et al., Highly selective and sensitive detection of Cu2+ with lysine enhancing bovine serum albumin modified-carbon dots fluorescent probe. Analyst, 2012. 137(11): p. 2637-2642.

52. Wang, F., et al., Graphene quantum dots as a fluorescent sensing platform for highly efficient detection of copper(II) ions. Sensors and Actuators B: Chemical, 2014. 190: p. 516-522.

53. Broekaert, J.A., Daniel C. Harris: Quantitative chemical analysis. Analytical and bioanalytical chemistry, 2015. 407(30): p. 8943-8944.

54. Panzarasa, G., et al., Convenient Preparation of Graphene Oxide from Expandable Graphite and Its Characterization by Positron Annihilation Lifetime Spectroscopy. C, 2019. 5(1).

55. Zhao, W., et al., Intercalation of Few-Layer Graphite Flakes with FeCl3: Raman Determination of Fermi Level, Layer by Layer Decoupling, and Stability. Journal of the American Chemical Society, 2011. 133(15): p. 5941-5946.

56. Lian, W., et al., The transformation of acetylene black into onion-like hollow carbon nanoparticles at 1000°C using an iron catalyst. Carbon, 2008. 46(3): p. 525-530.

57. Yuen, A.K., et al., The interplay of catechol ligands with nanoparticulate iron oxides. Dalton Transactions, 2012. 41(9): p. 2545-2559.

CHAPTER 5
INTERACTIONS OF FLUORESCENT CARBON DOTS WITH BEAS-2B LUNG EPITHELIAL CELLS

5.1 Introduction

As mentioned in Chapter 1, black carbon (BC) is a recognized health concern by the World Health Organization (WHO) and the Environmental Protection Agency (EPA). Therefore, evaluation of the effect of BC on in vitro cellular behavior is vital to gain knowledge about understanding the role of BC in cellular death, stress, or modifications to cellular microenvironment in vivo.[1, 2] Particulate matter (PM), as a general class of materials, has associated with it many concerns regarding its effects on cells in the body.[3] The group of PM in which BC is included, $PM_{2.5}$, is of particular interest, due to the small size of the materials, which allows for deeper penetration into the respiratory system and high potential for cellular uptake.[4] The difficulty of studying PM is based on the sheer complexity of materials contained within a sample of naturally produced and collected PM. Thus, this complexity has led to scientists focusing on one component of PM, rather than the mosaic of compounds found within naturally occurring environmental PM. While the potentially symbiotic interactions of multiple species within PM could compound health effects and cause damage not witnessed with individual components, one must understand the cellular impacts of those individual components before developing causative relationships between the broad class of PM and observed health effects.

Studies of the health effects due to BC and PM abound in the literature, but most focus on specific illnesses or full body responses to PM exposure. One study evaluated the relationship between increased air pollution events and patients with an implanted cardioverter defibrillator (ICD) in order to analyze the effect of PM on arrhythmias. The study found that the ICD intervened to treat ventricular fibrillation or tachycardia at a 60% higher rate when patients were exposed to

PM concentrations as high as 22 μg/m^3.[5] Additional studies show that exposure to PM, in particular BC, has significant impacts on cardiac function, including increased risk of cardiac morbidity and decreased vascular reactivity.[6, 7] While these health effects are extremely concerning, they do not express the full picture of what BC is actually doing in the body.

Studies of the interactions between BC and individual cells could allow for insight into the mechanism causing these full body health effects. Some scientists agree with this assessment and have begun studies of this nature with individual PM components.[4, 8] These studies with PM components tend to focus specifically on the production of an individual protein to exhibit some cellular environment change, or focus on a particular type of cellular response. In the case of Ming et alia, due to their familiarity with lung inflammation, they studied the body's immune response to BC exposure by measuring changes in MAP4K4 levels. MAP4K4 is an enzyme involved in cell processes, such as inflammation, metabolic disorders, cancer, and heart disease.[9-11] The group sought to measure MAP4K4 levels and establish relationships with T-cell differentiation in inflamed lung tissue to determine how the BC affected inflammation.[12-14] The group reported a decrease in the MAP4K4 levels in T-cells, which caused decreased differentiation between healthy lung cells and inflamed lung cells, lowering the overall immune response and allowing for increased lung inflammation over time. Other groups focus rather on overall cell death due to presence of BC particles, such as work by Hussain et alia. This group's research focuses primarily on cellular apoptosis (death), rather than cell environment or overall cellular effects. The group found that apoptotic cell death was more prominent in cells exposed to BC, which was demonstrated by many observed effects, such as membrane blebbing, apoptotic body formation, DNA fragmentation, and caspase activation.[15] While these studies show awareness and concern regarding the health effects of BC, little information exists about uptake routes, if uptake occurs,

and the overall cellular environment effects. Surrogates created to mimic the structural and chemical effects of BC while also allowing for a fluorescent detection moiety are vital to measure not only particle uptake, but also to monitor said uptake, analyze localization, and then measure health effects relative to uptake or lack thereof.

Regarding cellular uptake of nano-scale materials, the cell membrane is the determining factor in not only uptake of foreign materials, but also the general function of the cell. While the plasma membrane of cells is known to regulate the uptake and release of nanoparticles, it is also responsible for maintaining the homeostasis of the cell.[16] Specifically, the uptake of nano-scale materials through the cell membrane depends on many factors, including size, shape, and surface charge of the materials.[17] The effect of the size of the particles on uptake through the cell membrane has been well studied and might be counterintuitive upon initial evaluation. One would assume that it would be easier for smaller particles to traverse the membrane, while larger materials are more effectively kept out. The overall conclusion from multiple research groups is that aggregation and increased sedimentation events in nanoparticles both lead to production of nanoparticle aggregates that result in increased cellular uptake.[18, 19] This conclusion is based on the realization that such larger assemblies of particles offer larger amounts of membrane receptor sites being occupied by the assembled materials, allowing for increased membrane infolding uptake processes, such as phagocytosis or pinocytosis. Conversely, if the particles are too large, the enfolding cannot occur as effectively, inhibiting the uptake. Studies have also shown that the ideal size for nanoparticle uptake is 50 nm, though the only sizes tested in this specific test were 14, 50, and 74 nm.[20] While this study is valuable to show the impact of size of nanoparticle on uptake into the cells, it is worth mentioning that the group attributed the effects they witnessed to interactions between proteins and surface sites on the gold nanoparticles they used.[20] These size

and aggregative factors suggest that experimental results could change significantly when altering the identity of the materials of the nanoparticles, including both the interior structure and the surface sites. The type of cell can have an impact as well, considering the possible existence of different proteins or enzymes found within or in the vicinity of different cells.

The effect of nanoparticle shape on cellular uptake has been found to be similar to that noted for nanoparticle size on cellular uptake, with the ease of membrane enfolding and subsequent increase in uptake resulting from increased particle-receptor interactions. For example, it is thought that spherical particles are easier to enfold, making their uptake more efficient than rod or other nanoparticle shapes.[20, 21] Additionally, the impact of surface charges due to innate charges of the nanoparticles or charged functional groups on the surface of the nanoparticles cannot be dismissed as an important factor in uptake into the cell. In general, it is reported that cationic surface-charged particles exhibit higher uptake in nonphagocytic cells and anionic surface-charged particles exhibit higher uptake in phagocytic cells.[22] Indeed, it appears that the surface charges and particle size are the most important factors influencing cellular uptake. Evaluation of effects of surface charges and sizes in organic nanoparticles, inorganic nanoparticles, and liposomes showed similar trends across all types of particles.[23]

Measurements to determine cellular health and cell death have been extensively studied and optimized in the literature, thereby offering many options for analysis. The most commonly used judge of cellular toxicity is that based on viability assays that measure overall cell death/survival, and include the MTT assay,[24-26] MTS assay,[27, 28] and trypan blue cell counting method.[29, 30] Both the MTT and MTS assays operate through similar methodologies, using a yellow tetrazole compound, which upon entering cells and interacting with active mitochondria are transformed (reduced) into a purple formazan product whose quantity can be measured using

optical absorption. Because it is well documented that mitochondrial activity is constant in living cells, a correlation can be drawn between the number of living cells and mitochondrial activity, if the latter can be measured.[27] The differences between the MTT and MTS assays are the solubility of the purple formazan compound formed and procedural steps in each method. In an MTT assay, the formazan product is insoluble, thus requiring a step to solubilize the formazan using a solubilization solution, such as those containing sodium dodecyl sulfate (SDS), before measuring the absorbance of the now dissolved purple formazan solution. The structure of the MTS molecule differs from that of the MTT, by the addition of a carboxylic acid group and a sulfonate on the phenyl rings of the molecule, as seen in Table 5.1. These additional functionalities allow the formazan molecule formed to be water soluble in the presence of electron coupling reagent

Table 5.1 Structures of tetrazole and formazan molecules associated with colorimetric MTT and MTS assays for assessing the mitochondrial activity of cells. The latter is determined by measurement of the purple formazan compound whose absorbance is measured at 490 nm.

	YELLOW COMPOUND (TETRAZOLE)	PURPLE COMPOUND (FORMAZAN)
MTT	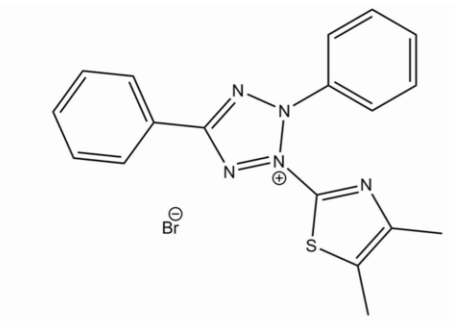	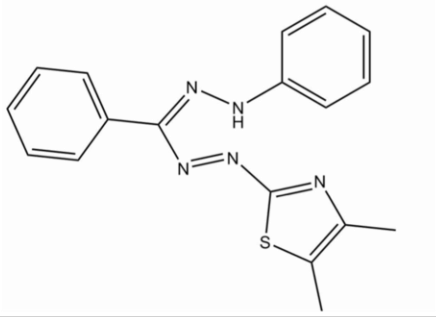
MTS	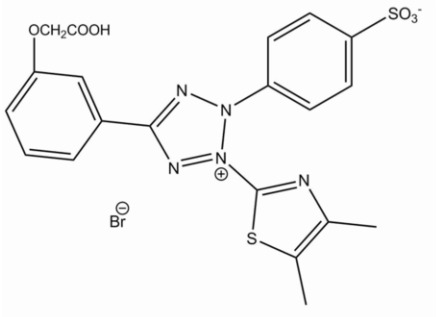	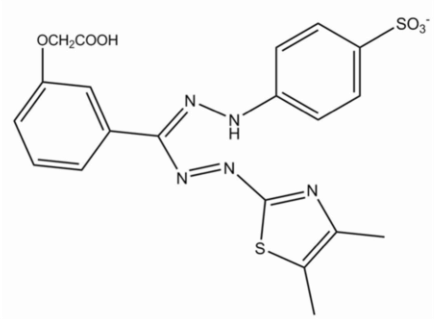

phenazine ethosulfate (PES).[31] The MTS assay is sometimes referred to as the one-step MTT assay, because the solubilization step is not necessary.

As opposed to the MTS and MTT assays, the trypan blue assay selectively dyes dead cells. Trypan blue is an azo dye that is not cell permeable, meaning if cells are alive (intact membranes), the trypan blue cannot enter cells. Conversely, if cells have died, their membranes are compromised and permeable, so the trypan blue enters cells and binds to intercellular proteins inside, and effectively stains the cells. A cell counting method is employed to count stained versus live cells to generate a percentage of live cells in a given cell sample. The trypan blue cell counting assay has an innate shortfall in that counting dead cells (blue colored) is easily done, and extremely reproducible and precise, while counting live cells (no color) is much more difficult and shows more variability. Live cells are more difficult to recognize and can be easily overlooked by both automated cell counters and scientists counting cells manually with a light microscope. This discrepancy can skew the percent of measured live cells; therefore, many scientists recommend the use of a two-dye method. In the two-dye method, a dye is used to label the live cells, such as neutral red, allowing for counting of easily visible red cells and easily visible blue cells due to trypan blue, preventing any overlook. Typically, due to the ease of use and relative accuracy, trypan blue is used in a one-dye method to obtain cell viability data. Beyond measuring whether cells live or die, further analysis can give information about the cellular environment, such as a measurement of the ratio between glutathione (GSH) and its oxidized form, glutathione disulfide (GSSG).

GSH is a tripeptide intracellular protein responsible for preventing cell damage by removing reactive oxygen species (ROS) from the cell. ROS, when present in cells in high concentrations, can cause oxidative stress. Oxidative stress can lead to many detrimental effects in

cells, such as enzyme deactivation and DNA damage.[32] Glutathione peroxidase aids in removal of excess ROS by catalyzing the reduction of ROS, such as lipid hydroperoxides to their corresponding alcohols and hydrogen peroxide to water, through the simultaneous oxidation of two units of GSH to form one unit of GSSG, as seen in Figure 5.1.[33] Glutathione reductase recycles GSSG back to its two units of GSH through the oxidation of NADPH to $NADP^+$, thus by analyzing the amount of GSSG present in a cell compared to GSH, insight about cellular health in regard to oxidative stress can be measured.[34] In healthy cells, greater than 90% of the GSH exists as its reduced form, GSH, with the remaining 10% or less as its oxidized form, GSSG. This correlates to a GSH:GSSG ratio of approximately 90:1 in live healthy cells. When cells begin to undergo oxidative stress, the GSH is converted to GSSG at an increased rate, as the glutathione peroxidase strives to remove the excess ROS from the cell. As oxidative stress increases, the ratio of GSH to GSSG decreases, with the result being a ratio of 10:1 or even 1:1. By measuring the ratio in cells as compared to a positive control (under heavy oxidative stress by the addition of H_2O_2), an evaluation of oxidative stress in cells can be obtained.

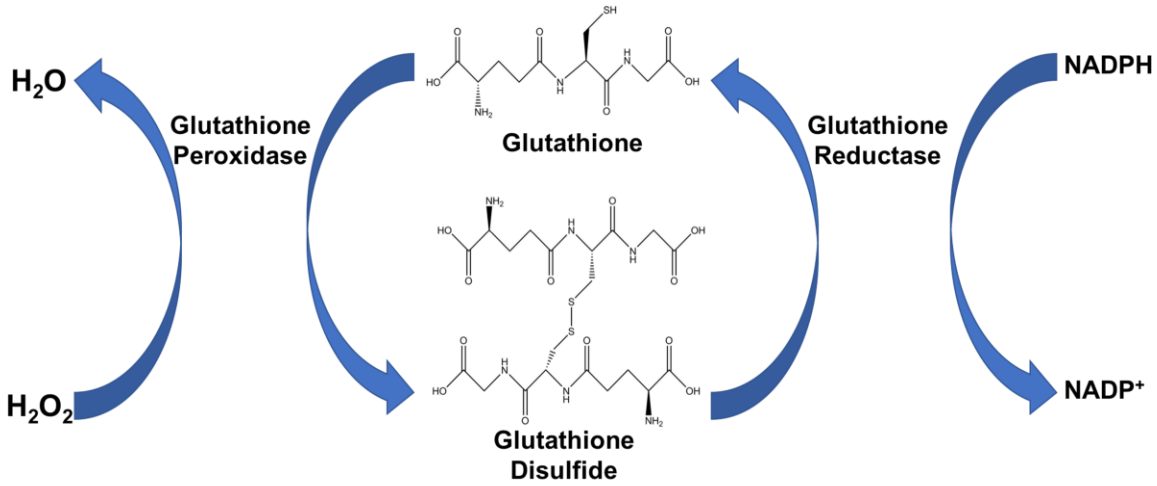

Figure 5.1 Schematic outlining the activity of the glutathione peroxidase to remove ROS from the cell, specifically H_2O_2 in this example, while oxidizing glutathione to glutathione disulfide, and the recovery of glutathione by the glutathione reductase.

An understanding of the health effects due to BC, but also caused by fluorescent carbon dots (FCDs) as a surrogate, can give foundational knowledge that is lacking in the literature to date. Extensive studies of cell viability using trypan blue assays, MTT assays, and MTS assays upon exposure to varied amounts of FCDs and other components at different time periods give information regarding overall toxicity of the materials. Additionally, by evaluating uptake and localization through confocal fluorescence imaging and transmission electron microscopy (TEM), information about whether BC and FCDs cause health effects from inside the cells or outside the cells can be evaluated. Studies regarding cellular environment can also provide valuable information about how the BC and FCDs impact the health of individual cells. All of this information is vital to truly understand this environmental pollutant (BC) and this class of evolving biological probes (FCDs).

5.2 Experimental Section

5.2.1 Materials

Bronchial epithelial cell growth basal medium (BEBM), supplements, and growth factors were purchased from Lonza Group AG (Basal, Switzerland). Normocin was purchased from Invivogen (San Diego, CA). Trypsin was purchased as phenol-red free 2.5% 10x from Thermo-Fischer (Gibco; Waltham, MA). The mounting media used was Prolong Diamond Antifade Mountant w/DAPI and was purchased from Thermo-Fischer (Invitrogen; Carlsbad, CA). Water from a Barnstead Nanopure Diamond Water System (18 M$\Omega \bullet$ cm) was used for all experiments. TEM grids were Formvar carbon-coated square mesh Cu, 100 Mesh, purchased from Electron Microscopy Sciences (Hatfield, PA).

5.2.2 BEAS-2B Culture

BEAS-2B human bronchial epithelial cells were purchased from the European Collection of Authenticated Cell Cultures (ECACC) through Millipore Sigma (England). BEAS-2B cells were originally derived from normal bronchial epithelium that was obtained by autopsy of a non-cancerous individual. In order to produce cells in quantities for distribution, they were infected with a replication-defective SV40/adenovirus 12 hybrid and cloned.[35] The cells were grown in Cellcoat TC flask, T75, 75 cm^2 flasks coated in Type 1 Collagen, purchased from Greiner Bio-One (Austria). Unless stated otherwise, BEBM complete media, purchased as BEGM-Bulletkit from Lonza, in addition to the antimicrobial agent Normacin was used for culturing. The complete media includes bovine pituitary extract, insulin, retinoic acid, transferrin, triiodothyronine, epinephrine, and human epidermal growth factor in amounts provided by Lonza. Normocin was added to a final concentration of 100 μg mL^{-1}. The flasks were incubated under 37 °C in a 5% CO_2/95% air humidified incubator.

5.2.3 Cellular Uptake Studies

5.2.3.1 Low-Resolution TEM Imaging

BEAS-2B cells were cultured in Type 1 Collagen-coated cell flasks under complete BEBM media in a humidified incubator at 37 °C in a 5% CO_2/95% air and allowed to reach 70% confluence. Upon reaching 70% confluence, the media was removed and 15 mL fresh media was added to the flask along with 2 mg/mL fluorescent carbon dots (FCDs) and the cells were incubated at 37 °C in a 5% CO_2/95% air humidified incubator for 3 h, or at 4 °C for 3 h for active transport inhibition studies. Upon completion of 3 h, the media with FCDs was removed, and 3 mL of trypsin (0.25%) was added to the flask. The flask with trypsin was incubated for 20 minutes under the same incubation conditions to allow for the cells to detach from the surface of the flask. After the

allotted time, a rubber policeman was used to scrape the bottom of the plate to aid in the removal of the cells before extracting the trypsin and cells and placing them into a 15 mL centrifuge tube. The cells were centrifuged at 900 rpm for 10 minutes to pellet the cells. The trypsin was removed from the pelleted cells and replaced with 3 mL of complete media. The pellet was then prepared for TEM imaging.

The media was removed and replaced with a fixative solution of 2% glutaraldehyde and 1% formaldehyde in 0.2 M phosphate buffer at a pH of 7.2. The cells were centrifuged under the fixative before the fixative was removed. The pellet was then embedded in 3% agarose and the fixative was added again before allowing the cells to sit overnight in the agarose and fixative at 4 °C. The following day, the cells were rinsed in a 0.1 M phosphate buffer at a pH of 7.2 five times over a period of 12 h. The cells were then post-fixed in a 2% osmium tetroxide solution (highly toxic, oxidizing agent, must be used in a fume hood) for 1 h in the dark before being rinsed three times by deuterated H_2O (> 99.9%). Following the rinse, the cells were *en bloc* stained using a solution of 1% uranyl acetate in the dark for 1 h. The sample was then rinsed with deuterated H_2O (> 99.9%) three more times. The cells were dehydrated in ethanol and propylene oxide (50% v/v) and subsequently rinsed with that solution three times. The cells were then exposed to propylene oxide (Peon-NMA resin series) for 48 h and embedded in Epon-NMA at 60 °C for 48 h. Ultra-thin sections for TEM were cut on a Dupont Sorvall MT-2 microtome. The TEM sections were mounted on carbon-coated copper grids and stained with Reynold's lead citrate. The grids with cell sections were imaged using a JEOL JEM-1400, as outlined in Chapter 2.

5.2.3.2 Fluorescent Confocal Imaging

A 6-well plate was used to prepare slides for confocal fluorescent imaging. Into each well was placed a glass coverslip (22 x 22 mm, no. 1-1/2 Corning). Before being placed into the wells,

the coverslips were cleaned by spraying with 70% ethanol and then exposing them to a flame from a Bunsen burner to evaporate the ethanol and water. Then 200,000 cells were pipetted into each well onto the glass coverslips, and each well was filled with 5 mL complete media. The 6-well plate with cells was placed in an incubator under 37 °C in a 5% CO_2/95% air humidified incubator for 24 h to allow cells to adhere to the coverslip. After 24 h, the media was removed and 5 mL of complete media with 2 mg/mL FCDs was added to the wells chosen to be dosed by the FCDs. At least one well was dosed with only complete media to serve as a negative control. Additional wells were dosed with various metal ions to quench the fluorescence of the FCDs as well as reducing agents to recover the fluorescence. The cells were exposed to the FCDs in their various forms for 3 h under 37 °C in a 5% CO_2/95% air-humidified incubator. After the 3 h, the media was removed and each well and coverslip was rinsed with phosphate-buffered saline (PBS) 3 times to remove excess FCDs or other materials. Then 1 mL of 4% paraformaldehyde (PFA) was added to each well to fix the cells. The 6-well plate with PFA was allowed to sit for 15 minutes in dark conditions at room temperature. The PFA was removed and each coverslip was removed from the well and placed cell side down onto a drop of Prolong Diamond Antifade Mountant on a glass slide. The glass slides with adhered coverslips were allowed to dry overnight before imaging. Slides were always imaged within 3 days of preparation using a Leica SP8 Confocal fluorescence microscope. Each set of images was collected using the same settings, with λ_{ex} at 405 nm and λ_{em} ranging from 430-500 nm. All image analyses were accomplished using Image J software.

5.2.4 Cell Viability Studies

5.2.4.1 Trypan Blue Cell Counting Assay

A trypan blue assay was used every time cells were trypsinzied to determine the number of cells per unit volume so that the proper number of cells could be used for experiments. Trypan blue used purely as a viability assay follows the same procedure, as outlined below.

The cells to be counted, suspended in trypsin after extraction from a flask or plate, were centrifuged at 900 rpm for 10 minutes to form a pellet. The trypsin was removed and replaced with complete media and the pellet and media were vortexed to suspend the cells into the media. 10 μL of the suspended cell solution was pipetted into a microcentrifuge tube, into which 10 μL of 4% (w/v) trypan blue (MP Biomedical) was added as well. The tube was vortexed to mix the cell suspension and trypan blue together before 10 μL was pipetted into each well of a Bio Rad cell counting slide and the slide was placed into a Bio Rad TC20 automated cell counter. The cell counter produces a number of total cells, live cells, and percent viable cells.

5.2.4.2 MTT Assay

Into each well of a 96-well plate containing 100 μL of complete media were pipetted 10,000 BEAS-2B cells. The 96 well-plate was incubated under 37 °C in a 5% CO_2/95% air-humidified incubator for 24 h to allow cells to adhere to the well. Wells were dosed with FCDs or other testing materials by pipetting 50 μL of the material dissolved in complete media into the well. For controls, 50 μL of complete media were pipetted into the well, devoid of any material. The 96-well plate with material was incubated in an incubator under the same conditions as above for varying time points (3 days, 2 days, 1 day, 8 h, 5 h, 3 h, 1 h, and 30 minutes). When the cells had been exposed to the materials for the designated amount of time, the solutions were removed from each well and replaced with 100 μL complete media and allowed to incubate for an additional

24 h. After 24 h, 10 μL of the MTT reagent was added to each well before being incubated under the same conditions as above for 3 h, or until a purple formazan precipitate was observed. 100 μL of SDS was added to dissolve the formazan crystals, and the 96-well plate was incubated for 2 additional h. Absorbance of each well of the 96-well plate was then measured at 570 nm using an Eppendorf AF2200 plate reader manufactured by Tecan.

5.2.4.3 MTS Assay

Into each well of a 96-well plate containing 100 μL of complete media were pipetted 5,000 BEAS-2B cells, excluding the positive control which contained no cells, representing complete cell death. 100 μL of complete media was added to each well before the 96-well plate was incubated under 37°C in a 5% CO_2/95% air humidified incubator for 24 h to allow cells to adhere to the well. Wells were then dosed with FCDs or other testing materials by pipetting 50 μL of the material dissolved in complete media into the well. For controls, 50 μL of complete media was pipetted into the well, devoid of any material. The 96-well plate with materials was incubated in an incubator under the same conditions as above for varying time points (3 days, 2 Days, 1 Day, 8 h, 5 h, 3 h, 1 h, and 30 minutes). After exposure for the varying time points, the media and materials were removed from each well and replaced with 100 μL of complete media. The CellTiter 96 AQ_{ueous} One Solution Reagent (Promega Corporation) was thawed and 10 μL of the solution was added to each well. The plate was incubated under 37 °C in a 5% CO_2/95% air-humidified incubator for 1.5 h until a purple formazan compound was observed in solution. Absorbance of each well was measured at 490 nm on an Eppendorf AF2200 plate reader manufactured by Tecan.

5.2.5 GSH:GSSG Assay

The GSH:GSSG ratio was determined using a glutathione assay kit purchased from Cayman Inc. (Item No. 703002). Into each well of a collagen coated 6-well plate in 5 mL of

Dulbecco's modification of Eagle's medium (DMEM) without sodium pyruvate with 4.5 g/L glucose, L-glutamine, 10% fetal bovine serum, and 10 IU/mL penicillin were plated 500,000 BEAS-2B cells. The 6-well plate with cells was incubated under 37 °C in a 5% CO_2/95% air-humidified incubator for 24 h. Wells of the 6-well plate were then incubated under 37 °C in a 5% CO_2/95% air-humidified incubator with FCDs and other materials for 3 h, or 500 μM H_2O_2 for 30 minutes as a positive control. After dosing, the cells were removed from each well using a rubber policeman to scrape the wells and remove the cells manually. The cell suspension was centrifuged at 900 rpm for 10 minutes to collect a pellet. The media was removed from the top of the pellet and the cells were lysed by the addition of 2 mL of cold radioimmunoprecipitation assay (RIPA) buffer to the pellet and allowed to sit for 20 minutes at 0 °C. The cells were then centrifuged at 10,000 x *g* for 15 minutes at 4 °C. The supernatant containing all the cellular material was removed and deproteination was achieved by adding 2 mL of metaphosphoric acid (MPA) reagent (5 g of MPA in 50 mL of water), followed by centrifugation at 5,000 x *g* for 10 minutes. The supernatant was then collected, and 50 μL of 4 M triethanolamine (TEAM) was added per mL of supernatant collected. Then 1 M 2-vinylpyridine dissolved in ethanol was added at a ratio of 10 μL per mL of sample. After that step, the samples were added to the 96-well plate by pipetting 50 μL of each sample into the appropriate wells. The assay cocktail was prepared by mixing 20 mL MES Buffer (11.25 mL), reconstituted cofactor mixture (0.45 mL), reconstituted enzyme mixture (2.1 mL), millipure water (2.3 mL), and reconstituted DTNB (0.45 mL). All chemicals were provided in the kit, whose composition can be found in the procedure provided with the kit. After preparation of the assay cocktail, 150 μL was added to each well of the 96-well plate. The 96-well plate was incubated for 25 minutes under the same conditions as above before absorbance was measured at 410 nm using an Eppendorf AF2200 plate reader manufactured by Tecan.

5.3 Results and Discussion

5.3.1 Cellular Uptake

As mentioned in the introduction of this chapter, cellular uptake of nanoparticles is a process that is governed by many characteristics of the nanoparticles themselves, but the method of uptake can vary even within the same type of particles. With this in mind, the designed surrogate must possess characteristics as similar as possible to that of BC. The FCDs created in this research are spherical, possess a negative surface charge, contain C, O, H, N, along with other trace elements, and are less than 2.5 μm in size. All of these factors combine to make this sensor/surrogate as similar to BC as possible. Any uptake experienced by the FCDs can therefore be considered comparable to that experienced by cells exposed to BC, both in uptake mechanism and relative amount of uptake. Determining whether uptake occurs is only the first step in analyzing the effects of a nanomaterial on cells. If the particles are confirmed to go into the cells, an investigation of what uptake mechanism is occurring begins. Many chemicals, such as water, carbon dioxide, and oxygen, are known to enter the cell based on a concentration gradient that requires no energy, making it a passive transport uptake mechanism. Many larger molecules and particles require an uptake method involving an energy-dependent process. This research strives to determine whether FCDs, and therefore BC, are taken up by cells and attempts to establish if the uptake is through an active or passive mechanism. The specific uptake mechanism (phagocytosis, pinocytosis, clathrin mediated endocytosis, etc.) can be theorized by this scientist but is beyond the scope of this research.

The possibility of cellular uptake of the FCDs was first investigated using fluorescence confocal microscopy. The inherent fluorescence of the FCDs allows them to be a perfect probe to measure whether they undergo cellular uptake as well as analyzing the location of the FCDs within

the cells. The cells were dosed with 10 mg FCDs/5 mL of complete media, while a negative control consisted of cells dosed with no FCDs, only 5 mL of complete media. Overlaid images of fluorescence and differential interference contrast are presented in Figure 5.2 and show that the cells exposed to FCDs have fluorescent objects present as apparent aggregates vs the negative control.

A visual evaluation of the fluorescence images suggests that the FCDs aggregate on the surface of the cells and undergo cellular uptake based on the fluorescence inside the cells. The apparent increase in fluorescence from the negative control image to the FCD-exposed cells seems to suggest fluorescence is being produced from FCDs. The small amount of background fluorescence in the negative control seen in the cell is due to autofluorescence from organelles and proteins within the cytoplasm excited by light in the 300-400 nm range.[36, 37] The nuclei can be clearly demarcated in the cells, thus, even though the emission wavelengths for the DAPI nuclear

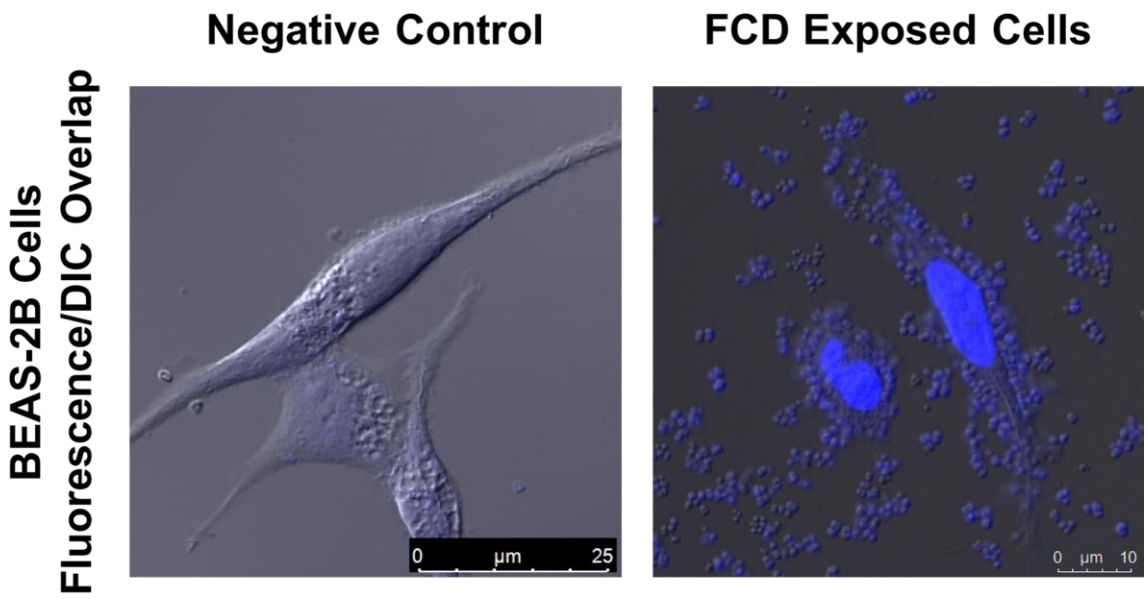

Figure 5.2 Fluorescence confocal images overlaid with differential interference contrast (DIC) images showing the presence of FCDs or lack thereof. The nuclei were stained with DAPI nuclear stain in the FCD-exposed cell images. λ_{ex} = 405 nm and λ_{em} = 430-500 nm)

stain and the FCDs overlap, the fluorescence due to the nucleus and FCDs can be clearly differentiated. The spherical shapes seen in solution around the cells and aggregating on the cells could be FCDs, as they are not seen in the negative control, but that cannot be absolutely confirmed by fluorescence confocal imaging. Additionally, though the overall fluorescence signal is increased from the negative control to the FCD-exposed cells, suggesting FCD presence in the cells, that cannot be absolutely confirmed either. Both of these concerns produced a need for an alternative method to confirm uptake into the cells.

Low-resolution TEM imaging (LR-TEM) can be used to visualize the cells and determine cellular uptake much less subjectively. BEAS-2B cells were dosed with FCDs for 3 h before the cells were prepared for imaging. The images seen in Figure 5.3 contain those for cells exposed to FCDs as well as negative control cells exposed to no FCDs (just a change in culture media). The TEM images above showing particles inside the cells are only a few of many showing clear images

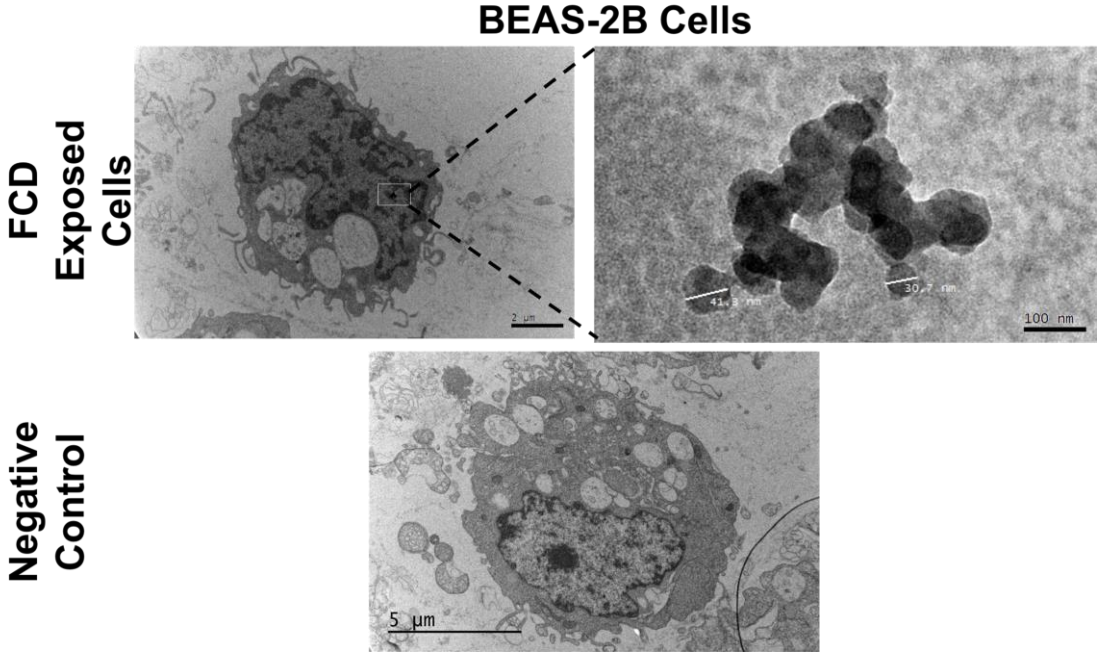

Figure 5.3 Low-resolution transmission electron microscopy images showing FCDs within the cell. Measurements of particles in upper right image show particles of size 41.3 nm and 30.7 nm. Negative control cells show no nanoparticles inside or outside of cells. (120 keV accelerating voltage)

of what appears to be FCDs inside the cells. The negative control images show no FCDs, or anything that looks similar to FCDs anywhere in the images. The combined evidence for increased fluorescence in cells when exposed to FCDs coupled with the clear visualization allowed by TEM showing nanoparticles inside of cells provides strong support for the internalization of FCDs by BEAS-2B cells.

In the LR-TEM images, FCDs were seen to be in the cells as individual particles; however, more often they existed as aggregates of multiple particles grouped together. In Figure 5.4, particles can be seen existing as aggregates, but can also be seen in what seems to be excretions from the cell and within vesicles inside the cell as individual particles. This makes determining the uptake mechanism particularly difficult, because if the particles are entering the cell as individual particles, of sizes less than 30 nm, the mechanism will be different than that of aggregates of

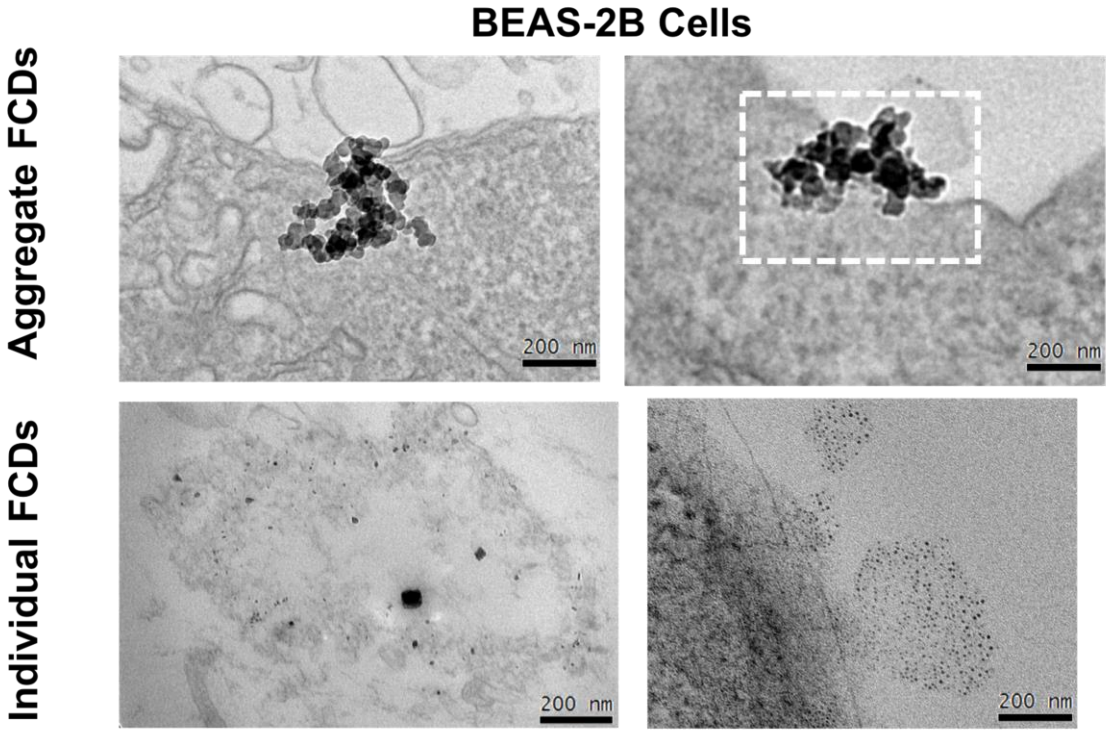

Figure 5.4 FCDs shown in low-resolution TEM images as both aggregates and individual particles inside the cell and when exiting and entering the cell. White dotted inset shows FCD/membrane interactions.

particles that has a cumulative size greater than 100 nm.[38, 39] Investigation of the uptake mechanism must begin with a differentiation of whether passive or active uptake mechanisms are responsible. The most common active transport mechanism witnessed in the uptake of nanomaterials is clathrin-mediated endocytosis; therefore, to measure if that process is occurring, one can inhibit that mode of active transport and evaluate if the FCDs still enter the cell.[40] Unfortunately, other modes of active transport can still occur, meaning to truly evaluate whether the transport is active or passive, one must inhibit all modes of one type of transport. By decreasing the temperature during incubation time to 4 °C, all active transport modes are inhibited, resulting in the conclusion that if particles still enter the cells, passive transport mechanisms dominate the uptake pathways for the FCDs. When cells were incubated with FCDs at low temperature (4 °C), there was no uptake witnessed among cells analyzed with LR-TEM. The media containing the FCDs was removed before the cells were removed from the flask and centrifuged down, causing difficulty in finding FCDs to image, however some FCDs were found and imaged outside of the cells, as seen in Figure 5.5.

In the images collected from the cells incubated at low temperature, very few had any FCDs in their interior. The cells incubated at higher temperature (37 °C) had FCDs throughout the cells, both as aggregates and individual particles. This experiment strongly suggests that the uptake of the FCDs into the cell is an active transport process, whether that be as individual particles or aggregates. The witnessed aggregates could be formed after uptake of the individual particles, as well as the individual particles seen resulting from a breakdown of aggregates after uptake, further complicating evaluation of the uptake process. The exact active transport path is also difficult to determine based on where the particles are found within the cell. Some nanoparticle clusters are found on top of the cellular membrane, appearing to pass directly through the membrane, as seen

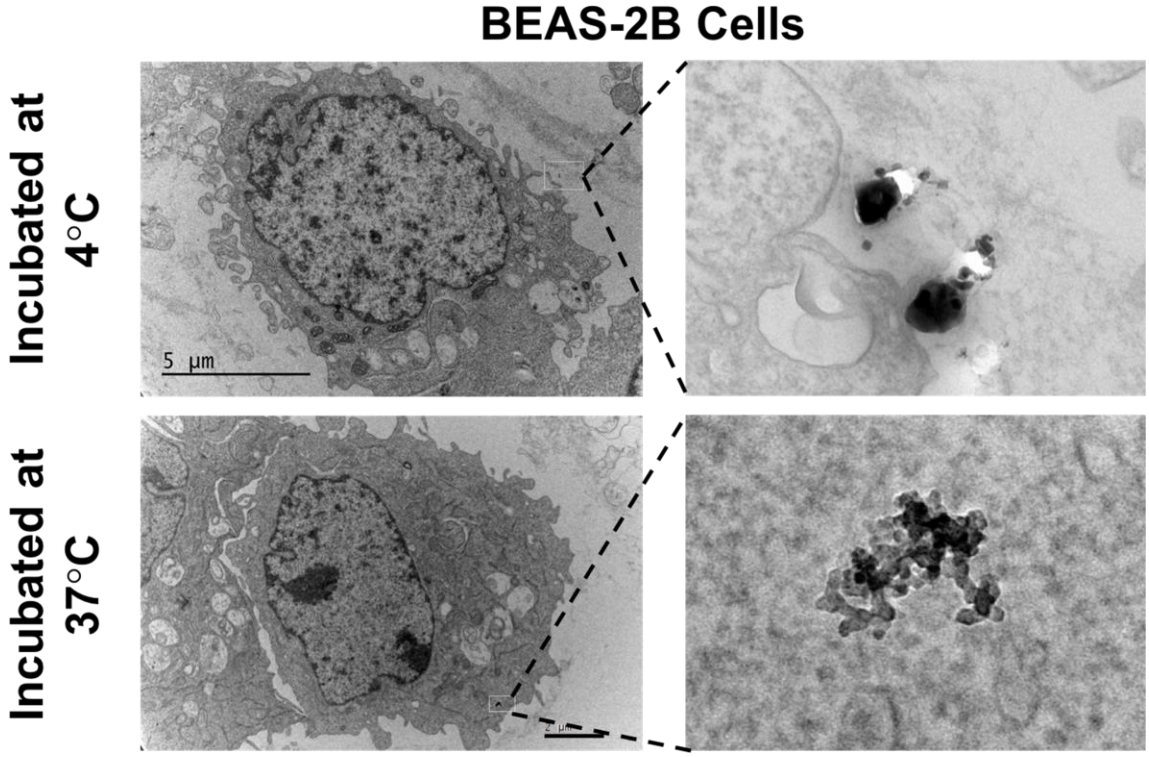

Figure 5.5 Evaluation of temperature on FCD uptake by cells. Low-Resolution TEM images of cells incubated with FCDs at low temperature (4 °C), thereby inhibiting active transport and cells incubated with FCDs at body temperature, allowing for both modes of cellular uptake.

in Figure 5.4 in the white dotted inset found in the top right image. Granted, due to the three-dimensional nature of the slice of cells, the nanoparticle cluster witnessed there could be due to an overlap of nanoparticles in the cytoplasm on a higher z-dimensional plane. Other nanoparticles appear to be entering or leaving vesicles, such as seen in the top left image of Figure 5.4, implying an endocytotic process for uptake of nanoparticles. An investigation of which active transport process is occurring would require selective inhibition of each active transport pathway followed by an evaluation of whether the FCDs entered the cells or not. However, evaluation of the individual pathway responsible for uptake of the FCDs is beyond the scope of this research. Once the uptake of the FCDs was confirmed, an evaluation of the health effects due to the FCDs was pursued.

5.3.2 Cell Viability Assays

5.3.2.1 Trypan Blue

The most common evaluation of health effects on cells is an assessment of cytotoxicity, namely, measuring cell death caused by a material. A trypan blue assay is a simple test to perform and gives a good baseline for evaluating cellular toxicity. Initial trypan blue studies can be seen in Figure 5.6. The percent cell viability collected was normalized to the cell viability from a negative control flask, exposed to no FCDs or other materials. This was done to obtain accurate data, considering even healthy cells in healthy conditions are rarely 100% viable. The trypan blue study shows that over a three-h period, FCD presence results in a minimal decrease in cell viability. While the decrease is significant, the percentage of live cells in the FCD-dosed flask is still within a reasonable range for a flask that has not been exposed to any outside material. Interestingly, by

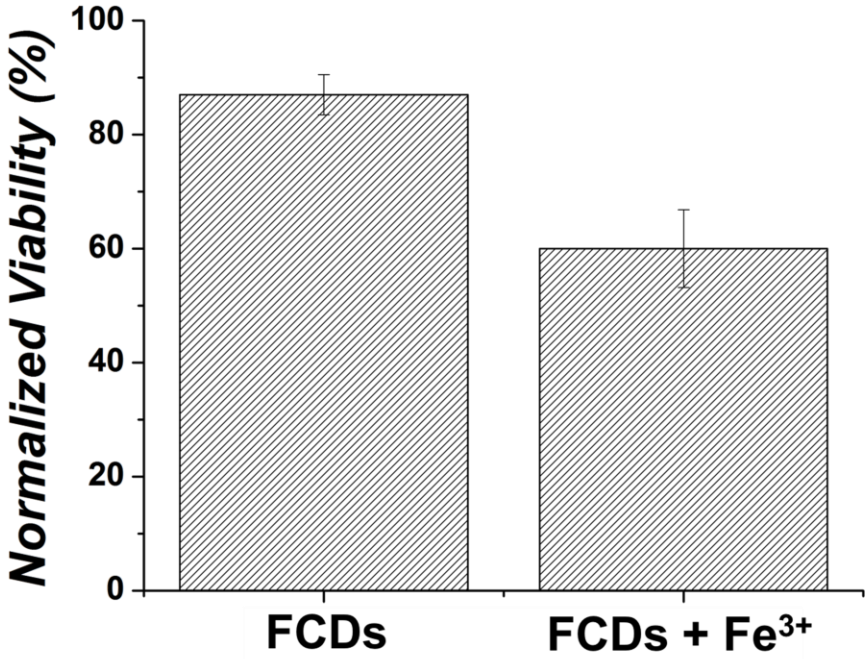

Figure 5.6 Percent cell viability normalized to a negative control flask with no exposure, showing the toxicity of both FCDs and FCDs turned off with Fe^{3+} after 3-h exposure. The viability was gathered through trypan blue assays.

adding the Fe^{3+} ions to quench the fluorescence, the toxicity of the FCDs increases. This is most likely due to the metal ions being taken up by the cells as they complex with the FCDs. The trypan blue assay gives a good starting point for evaluation of cytotoxicity, but MTT and MTS assays can give a more thorough evaluation and offer higher throughput to analyze more samples with different exposure times and concentrations.

5.3.2.2 MTT and MTS Assays

While the trypan blue assay to count viable cells is a very useful, and arguably the most popular assay to evaluate cell viability, MTT and MTS assays offer benefits trypan blue does not. Trypan blue assays are more effective if used with a larger number of cells, due to the fact that any error produced in counting dead cells and missing live cells due to their natural color, can be alleviated if larger numbers of cells are used. This means it is more effective if used with flasks of cells, rather than the smaller quantity of cells gathered from a 6-well plate or 96-well plate. This makes an assay involving a 96-well plate more useful for large experiments, testing a wide range of concentrations and dosing times. The MTT assay was used to test the cytotoxicity due to FCDs of concentrations of 0.5 mg/mL, 1 mg/mL, 2 mg/mL, 5 mg/mL, and 7 mg/mL at time periods of 1 h, 3 h, 5 h, 8 hr, 1 day, 2 day, and 3 day. Sadly, the step of the MTT assay where SDS is used to dissolve the formazan crystals was not effective. Upon attempting the assay a second time, the solubilizing of the formazan crystals was successful, but the incubation period to produce the formazan crystals was too long and therefore had so many formazan crystals formed that it was impossible to determine the impact of any of the tested parameters in an individual fashion. A method was sought that would work as effectively as the MTT assay but would not require a solubilizing step, so the MTS assay was chosen.

As outlined in the introduction, the MTS assay is the same as an MTT assay without the need for solubilizing the formazan; the MTS assay is sometimes referred to as a one-step MTT. FCD concentrations include 8 mg/mL, 5 mg/mL, 2 mg/mL, 1 mg/mL, and 0.5 mg/mL at exposure times of 3 days, 2 days, 1 day, 8 h, 5 h, and 1 h. Cells were also dosed with FCDs whose fluorescence was quenched with Fe^{3+} ions. The two samples chosen to test were FCDs whose fluorescence had been quenched by approximately 50% (70 μL of 0.176 M $Fe(NO_3)_3$ in phosphate buffer at pH 7.4) and FCDs whose fluorescence had been quenched 100% (140 μL of 0.176 M

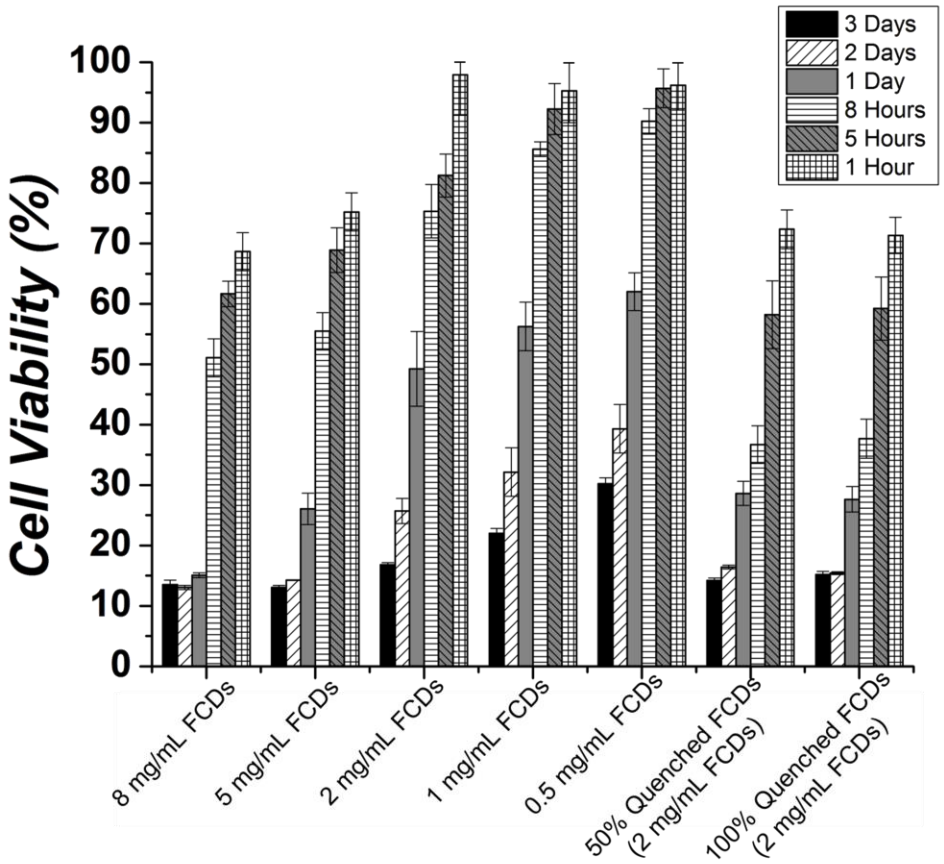

Figure 5.7 Cell viability based on the MTS assay. Data was normalized to a negative control wherein cells were not exposed to any material. Material identity and time points were tested in triplicate with error bars representing one standard deviation.

$Fe(NO_3)_3$ in phosphate buffer at pH 7.4). While the graph contains a large amount of data and can be hard to interpret, some conclusions and trends can be determined from the data in Figure 5.7.

The first and obvious trend is that cells exposed to FCDs of any concentration or fluorescent property exhibit cell death and lack of viability when exposed for time periods greater than 8 h. Even low concentrations of FCDs (0.5 mg/mL), amounts much smaller than used in the literature by most scientists, [41-43] showed a decrease in cell viability when exposed to cells for longer than 8 h. Additionally, there is a clear trend in increasing toxicity when cells are exposed to higher concentrations of FCDs, with the percent viability decreasing from approximately 60% when exposed to 0.5 mg/mL FCDs for 1 day to 15% when exposed to 8 mg/mL FCDs for 1 day. This data seems to suggest that if research is performed using FCDs on short time scales (< 8 h) or using low concentrations (2 mg/mL or less), the cytotoxicity due to FCDs will be minimal. Conversely, if high concentrations of particles are used or low concentrations for extended time periods, significant cytotoxicity can be contributed to the FCDs. Another interesting question raised by the initial MTS data was the role the iron ions played in the cytotoxicity.

An MTS assay was performed on samples with varying iron states to attempt to evaluate the effects of iron on the cytotoxicity, see Figure 5.8. As it appeared in the data from Figure 5.8, the toxicity of FCDs is increased by the addition of Fe^{3+} ions to quench the fluorescence. What is most interesting is that the toxicity of the Fe^{3+} ions themselves is significantly higher than when they are complexed with the FCDs. One theory of the fluorescence turn-off mechanism is an electron exchange between the FCDs and the Fe^{3+} ions, thereby converting the latter to Fe^{2+}. The decrease in cellular toxicity upon the addition of FCDs to the Fe^{3+} ions could suggest a decrease in toxicity due to conversion of the Fe^{3+} to Fe^{2+}. This is suggested to not be the case based on the fact that the cytotoxicity effects due to Fe^{3+} and Fe^{2+} are statistically the same. In a simpler process,

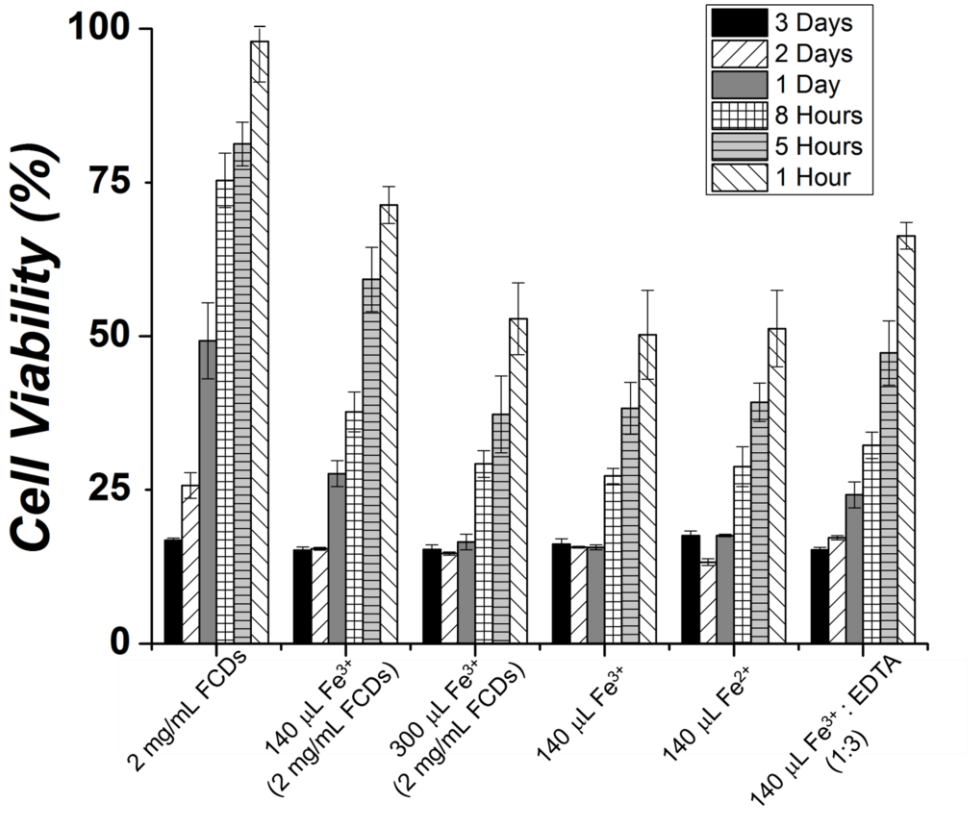

Figure 5.8 Cell viability based on MTS assay. The data was normalized to a negative control where cells were unaltered by material. Materials and time points were tested in triplicate with error bars reporting the standard deviation. Iron ion concentrations were all 0.176 M.

if catechol groups on the surface of the FCDs act as ligands for the Fe^{3+} ions, the Fe^{3+} could be rendered less toxic due to inability to bind or undergo electron exchange with components within the cells.[44, 45] To test this theory, Fe^{3+} ions were compared to Fe^{3+} ions bound to EDTA to determine if a decreased toxicity is provided by the presence of this ligand.

This hypothesis appears to be true, based on the fact that EDTA, when added to Fe^{3+} ions before exposing them to cells, significantly decreases the toxicity at time periods less than 2 days. This behavior of ligands decreasing the toxicity of metal ions is well reported, and the fact that the catechol/Fe^{3+} complex has a formation constant of 10^{49} as compared to 10^{25} in the Fe^{3+}/EDTA

complex, suggests the FCDs could prevent the toxicity of the Fe^{3+} ions more effectively than the EDTA.[46, 47] Once the uptake of FCDs into cells was confirmed, and cytotoxicity was studied, an evaluation of cell environment to determine a possible cause of the cytotoxicity was investigated through a measurement of ROS via a GSH:GGSG assay.

5.3.3 GSH:GSSG Assay

The GSH:GSSG assay reveals the general level of oxidative stress experienced by cells, with a large GSH:GSSG ratio representing cells not under oxidative stress, while a small ratio represents cells under oxidative stress. Tests evaluating various materials and their composition

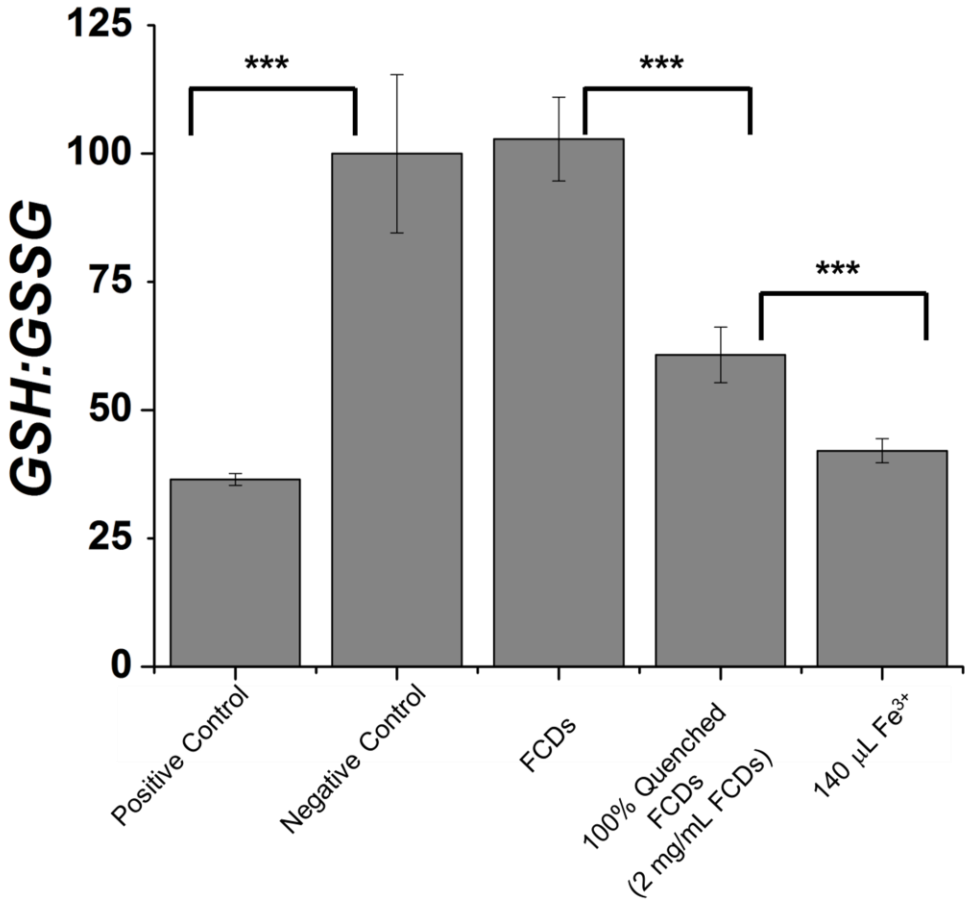

Figure 5.9 Ratio of GSH:GSSG in BEAS-2B cells after incubation with various a materials to represent oxidative stress of the cells. (***P<0.001)

and their exposure to BEAS-2B cells can be seen in Figure 5.9. The highest ratio represents the healthiest cells and is seen in the negative control and FCD dosed cells, with cells undergoing no oxidative stress outside of the limited amount occurring naturally. This suggests that though the FCDs possess a certain amount of cytotoxicity, as exhibited by the MTS assays, it appears to cause no oxidative stress beyond what is typical. The FCDs when dosed with Fe^{3+} to quench the fluorescence show an increase in the amount of oxidative stress, but similar to the cytotoxicity studies, show less oxidative stress than the Fe^{3+} ions alone. The trend of FCDs being less harmful than FCDs quenched with Fe^{3+} than Fe^{3+} alone follows in the GSH:GSSG assay as well. While the data here is valuable, it should be noted that this study was performed with an incubation time of 3 h for all tests. Considering the FCDs began to show large levels of cytotoxicity at time periods above 8 h suggests the oxidative stress could occur if dosed for a longer time period.

5.4 Conclusions

The results obtained from these experiments offer significant information concerning two classes of materials. The first class is FCDs. As discussed in the Chapter 1 and the introduction of Chapter 5, studies of FCDs, while numerous, have been limited in scope. Short time periods and low concentrations tend to be the typical cytotoxicity tests for FCDs reported in the literature referenced throughout this chapter. The research in this document shows that when considering longer time periods and higher concentrations, FCDs formed through bottom-up combustion processes are cytotoxic, reducing cell viability to as low as 10% when cells were dosed with 8 mg/mL FCDs for 3 days. In fact, the data seems to suggest that dosing times as short as 8 h at standard concentrations for biological analysis can reduce cell viability by as much as 20%. While various types of FCDs are a commonly used intracellular probe, the TEM data obtained and presented here suggests that the FCDs produced in this research enter through an active transport

mechanism, though the exact pathway is still up for determination. FCDs were also seen as individual particles and aggregates, suggesting individual particles can cluster to become aggregates and aggregates can divide into individual particles. In evaluating cellular environment of BEAS-2B cells exposed to various materials, it was also determined that the oxidative stress of cells does not increase in the short term when cells were exposed to 2 mg/mL FCDs.

Still pertaining to FCDs, interesting information was gathered regarding the effect of metal ions on the cytotoxicity and oxidative stress induced in cells by the FCDs. A common use of FCDs is to employ them as intracellular turn-on probes to detect reducing species, or as a turn-off probe to detect metal ions. If FCDs are used as a turn-on probe, where cells are exposed to FCDs quenched with a metal ion, cytotoxic effects will occur and oxidative stress will result, making results gained from research using those particular probes possibly misleading, depending on the aims of the research project. Alternately, when FCDs are quenched by their complexing metal ions, the toxic effects seem to decrease as compared to the metal ions themselves. This could lead to possible therapeutics or cellular environment stabilization agents. Additionally, the studies of cytotoxicity comparing cells exposed to Fe^{3+}, Fe^{2+}, FCDs quenched with Fe^{3+}, and Fe^{3+} with added EDTA seem to suggest that the Fe^{3+} ions are indeed being chelated by the FCDs, with the functionalities present acting as a ligand similar to EDTA. This outcome offers reasonable support for the catechol binding model proposed in Chapter 4.

The second class of materials this research offers insight into is black carbon (BC). The overall goal of this research is to evaluate health effects of BC by using FCDs as a surrogate for BC. The characterization of the FCDs suggests that they mimic BC in structure, both chemical and physical, meaning any health effects evaluated regarding the FCDs can easily be compared to those theoretically produced by BC. The cells in this research were exposed to FCD concentrations as

high as 8 mg/mL, which correlates to 0.008 $\mu g/m^3$; research shows exposure to BC could be in amounts as high as 6.4 $\mu g/m^3$ during transport and as low as 1.2 $\mu g/m^3$ while sleeping.[48] While these numbers are not representative of the amount of BC being exposed to individual cells in the human body, they provide a valuable baseline to evaluate exposure amounts. Considering the amounts of FCDs exposed to cells in this research are orders of magnitude less than the BC exposure discussed above and that concentrations I have studied are toxic for cells and can cause oxidative stress, it can be inferred BC can also cause cell death or other negative cellular effects. This coupled with long term compounding exposure suggests severe cellular health risks. While the health risks of BC are well reported, evaluation of individual cellular effects due to BC is scarce. The research regarding the cellular impact of BC exposure performed in this research provides a foundation for the evaluation and hopeful prevention or mitigation of full body health effects in the future.

5.5 References

1. Agency, E.P. *Health and Environmental Effects of Particulate Matter (PM)*. Particulate Matter (PM) Pollution 2019 [cited 2019; Available from: https://www.epa.gov/pm-pollution/health-and-environmental-effects-particulate-matter-pm.

2. Organization, W.H., *World Health Report 2002*. 2002.

3. Kim, K.-H., E. Kabir, and S. Kabir, *A review on the human health impact of airborne particulate matter.* Environment International, 2015. **74**: p. 136-143.

4. Rohr, A.C. and R.E. Wyzga, *Attributing health effects to individual particulate matter constituents.* Atmospheric Environment, 2012. **62**: p. 130-152.

5. Peters, A., et al., *Air Pollution and Incidence of Cardiac Arrhythmia.* Epidemiology, 2000. **11**(1): p. 11-17.

6. Gold, D.R., et al., *Air Pollution and ST-Segment Depression in Elderly Subjects.* Environmental Health Perspectives, 2005. **113**(7): p. 883-887.

7. O'Neill, M.S., et al., *Diabetes Enhances Vulnerability to Particulate Air Pollution–Associated Impairment in Vascular Reactivity and Endothelial Function.* Circulation, 2005. **111**(22): p. 2913-2920.

8. Schwarze, P.E., et al., *Particulate matter properties and health effects: consistency of epidemiological and toxicological studies.* Human & Experimental Toxicology, 2006. **25**(10): p. 559-579.

9. Aouadi, M., et al., *Orally delivered siRNA targeting macrophage Map4k4 suppresses systemic inflammation.* Nature, 2009. **458**(7242): p. 1180-1184.

10. Virbasius, J.V. and M.P. Czech, *Map4k4 Signaling Nodes in Metabolic and Cardiovascular Diseases.* Trends in Endocrinology & Metabolism, 2016. **27**(7): p. 484-492.

11. Gao, X., et al., *MAP4K4: an emerging therapeutic target in cancer.* Cell & Bioscience, 2016. **6**(1): p. 56.

12. Jin, M., et al., *MAP4K4 deficiency in CD4+ T cells aggravates lung damage induced by ozone-oxidized black carbon particles.* Environmental Toxicology and Pharmacology, 2016. **46**: p. 246-254.

13. Brook Robert, D., et al., *Particulate Matter Air Pollution and Cardiovascular Disease.* Circulation, 2010. **121**(21): p. 2331-2378.

14. Laden, F., et al., *Reduction in fine particulate air pollution and mortality: extended follow-up of the Harvard Six Cities study.* American journal of respiratory and critical care medicine, 2006. **173**(6): p. 667-672.

15. Hussain, S., et al., *Carbon black and titanium dioxide nanoparticles elicit distinct apoptotic pathways in bronchial epithelial cells.* Particle and Fibre Toxicology, 2010. **7**(1): p. 10.

16. Lodish, H., et al., *Molecular cell biology*. 2008: Macmillan.

17. Behzadi, S., et al., *Cellular uptake of nanoparticles: journey inside the cell.* Chemical Society Reviews, 2017. **46**(14): p. 4218-4244.

18. Chaudhuri, A., G. Battaglia, and R. Golestanian, *The effect of interactions on the cellular uptake of nanoparticles.* Physical biology, 2011. **8**(4): p. 046002.

19. Cho, E.C., Q. Zhang, and Y. Xia, *The effect of sedimentation and diffusion on cellular uptake of gold nanoparticles.* Nature nanotechnology, 2011. **6**(6): p. 385.

20. Chithrani, B.D., A.A. Ghazani, and W.C.W. Chan, *Determining the Size and Shape Dependence of Gold Nanoparticle Uptake into Mammalian Cells.* Nano Letters, 2006. **6**(4): p. 662-668.

21. Chithrani, B.D. and W.C. Chan, *Elucidating the mechanism of cellular uptake and removal of protein-coated gold nanoparticles of different sizes and shapes.* Nano letters, 2007. **7**(6): p. 1542-1550.

22. Fröhlich, E., *The role of surface charge in cellular uptake and cytotoxicity of medical nanoparticles.* International journal of nanomedicine, 2012. **7**: p. 5577-5591.

23. He, C., et al., *Effects of particle size and surface charge on cellular uptake and biodistribution of polymeric nanoparticles.* Biomaterials, 2010. **31**(13): p. 3657-3666.

24. O'Toole, S.A., et al., *The MTS assay as an indicator of chemosensitivity/resistance in malignant gynaecological tumours.* Cancer Detection and Prevention, 2003. **27**(1): p. 47-54.

25. Goodwin, C., et al., *Microculture tetrazolium assays: a comparison between two new tetrazolium salts, XTT and MTS.* Journal of immunological methods, 1995. **179**(1): p. 95-103.

26. KHABAR, K.S., et al., *MTS interferon assay: a simplified cellular dehydrogenase assay for interferon activity using a water-soluble tetrazolium salt.* Journal of interferon & cytokine research, 1996. **16**(1): p. 31-33.

27. van Meerloo, J., G.J.L. Kaspers, and J. Cloos, *Cell Sensitivity Assays: The MTT Assay*, in *Cancer Cell Culture: Methods and Protocols*, I.A. Cree, Editor. 2011, Humana Press: Totowa, NJ. p. 237-245.

28. Ciapetti, G., et al., *In vitro evaluation of cell/biomaterial interaction by MTT assay.* Biomaterials, 1993. **14**(5): p. 359-364.

29. Derenzis, F.A. and A. Schechtman, *Staining by Neutral Red and Trypan Blue in Sequence for Assaying Vital and Nonvital Cultured Cells.* Stain Technology, 1973. **48**(3): p. 135-136.

30. Strober, W., *Trypan Blue Exclusion Test of Cell Viability.* Current Protocols in Immunology, 1997. **21**(1): p. A.3B.1-A.3B.2.

31. Cory, A.H., et al., *Use of an Aqueous Soluble Tetrazolium/Formazan Assay for Cell Growth Assays in Culture.* Cancer Communications, 1991. **3**(7): p. 207-212.

32. Storz, G. and J.A. Imlayt, *Oxidative stress.* Current Opinion in Microbiology, 1999. **2**(2): p. 188-194.

33. Barlow-Walden, L., et al., *Melatonin stimulates brain glutathione peroxidase activity.* Neurochemistry international, 1995. **26**(5): p. 497-502.

34. Li, S., et al., *The Role of Cellular Glutathione Peroxidase Redox Regulation in the Suppression of Tumor Cell Growth by Manganese Superoxide Dismutase.* Cancer Research, 2000. **60**(14): p. 3927.

35. (ECACC), E.C.o.A.C.C. *General Cell Collection Detail*. [cited 2020; Available from: https://www.phe-culturecollections.org.uk/products/celllines/generalcell/detail.jsp?refId=95102433&collection=ecacc_gc.

36. Zipfel, W.R., et al., *Live tissue intrinsic emission microscopy using multiphoton-excited native fluorescence and second harmonic generation.* Proc Natl Acad Sci U S A, 2003. **100**(12): p. 7075-80.

37. Georgakoudi, I., et al., *NAD(P)H and collagen as in vivo quantitative fluorescent biomarkers of epithelial precancerous changes.* Cancer Res, 2002. **62**(3): p. 682-7.

38. Huang, J., et al., *Effects of nanoparticle size on cellular uptake and liver MRI with polyvinylpyrrolidone-coated iron oxide nanoparticles.* ACS nano, 2010. **4**(12): p. 7151-7160.

39. Lu, F., et al., *Size effect on cell uptake in well-suspended, uniform mesoporous silica nanoparticles.* Small, 2009. **5**(12): p. 1408-1413.

40. Margarucci, L., et al., *Chemical proteomics reveals bolinaquinone as a clathrin-mediated endocytosis inhibitor.* Mol Biosyst, 2011. **7**(2): p. 480-5.

41. Zheng, M., et al., *Self-targeting fluorescent carbon dots for diagnosis of brain cancer cells.* ACS nano, 2015. **9**(11): p. 11455-11461.

42. Han, B., et al., *Polyethyleneimine modified fluorescent carbon dots and their application in cell labeling.* Colloids and Surfaces B: Biointerfaces, 2012. **100**: p. 209-214.

43. Fong, J.F.Y., S.F. Chin, and S.M. Ng, *A unique "turn-on" fluorescence signalling strategy for highly specific detection of ascorbic acid using carbon dots as sensing probe.* Biosensors and Bioelectronics, 2016. **85**: p. 844-852.

44. Sorvari, J. and M. Sillanpää, *Influence of metal complex formation on heavy metal and free EDTA and DTPA acute toxicity determined by Daphnia magna.* Chemosphere, 1996. **33**(6): p. 1119-1127.

45. Sillanpää, M. and A. Oikari, *Assessing the impact of complexation by EDTA and DTPA on heavy metal toxicity using microtox bioassay.* Chemosphere, 1996. **32**(8): p. 1485-1497.

46. Pierpont, C.G. and C.W. Lange, *The chemistry of transition metal complexes containing catechol and semiquinone ligands.* Progress in Inorganic Chemistry, 1994: p. 331-442.

47. Martell, A., R. Smith, and R. Motekaitis, *NIST critical stability constants of metal complexes database.* US Department of Commerce, Gaithersburg, 1993.

48. Dons, E., et al., *Impact of time–activity patterns on personal exposure to black carbon.* Atmospheric Environment, 2011. **45**(21): p. 3594-3602.

CHAPTER 6
SUMMARY, CONCLUSIONS, AND FUTURE DIRECTIONS

6.1 Summary and Conclusions

The overall goal of the research presented herein was to evaluate the cellular health effects of an environmental particulate matter (PM) pollutant, black carbon (BC), through the design, synthesis, and study of fluorescent carbon dot (FCD) materials that are surrogates of BC. The WHO has ranked PM as the 13th leading cause of mortality worldwide in 2011.[1] Particularly concerning is PM, known as $PM_{2.5}$, which is PM that is less than 2.5 μm in size. $PM_{2.5}$ is incredibly complex, as it is made up of an intricate blend of materials, which makes the study of individual components vital to understanding the effects caused by $PM_{2.5}$.[2, 3] BC as a component of $PM_{2.5}$ was chosen as the focus of this research based on EPA reports and extensive research about the abundance of its negative health effects and its impact on the environment.[4-7] FCDs were chosen as a surrogate of BC based on its similarities to BC with regard to chemical properties and physical structure.[8-10] FCDs were synthesized that possess a turn-off mechanism of fluorescence quenching by metal ions. Fluorescence recovery was attempted by exposure of the FCD-metal ion materials in solution to a reducing agent, with the goal of designing a fluorescence probe that will turn-on when exposed to reducing agents within mammalian cells.

The initial synthesis procedure consisted of the combustion of sodium alginate in a furnace for 2.5 h at 250 °C. Synthesis conditions were optimized by testing multiple combustion times (30 min, 1 h, 1.5 h, 2 h, 2.5 h, and 3 hr, combustion temperatures (150 °C, 200 °C, 250 °C, 300 °C, 350 °C, and 400 °C), and gas under which combustion occurred (compressed air and oxygen gas). The optimal conditions were determined to be heating 0.5 g of sodium alginate at 250 °C for 30 min under a 30 psi flow of oxygen gas entering the combustion tube. The fluorescent properties of

the FCDs were characterized, and it was determined that an excitation energy (λ_{ex}) of 350 nm and emission energy (λ_{em}) of 450 nm would be used for all fluorescence studies. The chemical stability of the synthesized FCDs was assessed and determined through testing the fluorescence of the FCDs at various pH points (4.1, 7, and 10.3). Their optical stability was assessed and determined through constant irradiation of the FCDs for a 6-hour time period with no loss of fluorescence signal. Physical stability was also examined, and it was found that there was no loss in fluorescence signal from FCDs stored as a solid or when present in aqueous, buffered solutions over a 24-day period of exposure to the ambient. The FCDs also exhibit a λ_{ex} -dependent fluorescence emission intensity and wavelength. The intensity of emission increases or decreases as the λ_{ex} changes, but the main fluorescence emission peak also shifts from its position at 450 nm. Through evaluation of the FCDs using low-resolution transmission electron microscopy, high-resolution transmission electron microscopy, dynamic light scattering, infrared spectroscopy, and X-ray photoelectron spectroscopy, the FCDs were determined to be composed of graphene oxide; this conclusion is supported mainly by the observed crystal lattice spacing of 0.28 nm found in high-resolution electron microscopy studies, which corresponds to hydrated graphene oxide.[11] The FCDs were also determined to be approximately spherical in shape possessing dimensions of 20–100 nm. It was determined through a particle isolation method (ultracentrifugation) that the FCD particles are composed of two major size distributions, with one population of particle sizes (20–50 nm) being the cause of the fluorescence noted in the FCDs produced using the methods described here, which are similar to routes reported in the literature.[12-14] It was also determined that the functionalities on the surface of the FCDs are dominated by carboxylic acid and catechol groups, with the catechol groups forming hydroquinone radicals. The catechol groups and semiquinone radicals derived

from them are proposed by this scientist to be responsible for the fluorescence properties of the FCDs made here, with the fluorescence being quenched by various metal ions.

The ability of numerous metal ions to quench the fluorescence of the FCDs was tested, including Fe^{3+}, Ni^{2+}, Cu^{2+}, Sn^{2+}, Ca^{2+}, and Al^{3+}. It was determined that the ferric ion was the most effective quencher of the fluorescence in the FCDs, so it was used for all quenching experiments carried out from that point onward. In an effort to move toward use of the FCDs as turn-on sensors of biological reducing agents such as glutathione, fluorescence recovery of the FCDs through exposure to a reducing agent was attempted with multiple agents, including ascorbic acid, glutathione, citric acid, and sodium dithionite. In each case, fluorescence was not fully recovered to the value for pristine FCDs (no exposure to any metal ion), with only ascorbic acid showing any recovery. This attempted recovery of fluorescence was initially hypothesized to be feasible based on the ability of the reducing agent to reduce the oxidation state of the metal ion quencher, thereby affording "de-quenching" of fluorescence. To ensure that the quenching occurred, a 5-sulfosalicylic acid assay and electron paramagnetic resonance was performed to confirm the reduction of ferric ions to ferrous ions by the reducing agents studied above. Once the reduction was confirmed, experiments were done to investigate the possibility of ferrous ion-induced quenching of FCD fluorescence. In sum, the outcomes from the de-quenching/recovery studies indicate that it is unlikely that the initially proposed FCD-based probe system can function as a turn-on fluorescence sensor for cellular reducing agents. Based on the quenching and ineffective recovery of the fluorescence with relevant reducing agents, a proposed quenching mechanism was proposed. The quenching mechanism was tested, and it was determined to be static quenching that operates through the formation of an FCD-ferric ion complex that is not fluorescent. This complex

is suggested to result from reaction of the catechol groups on the surface of the FCDs and the ferric ions, which leads to iron coordinated to semiquinone radical species on the surface of the FCDs.

Though the FCDs produced in this research could not be used as turn-on fluorescence probes, they still proved to be an effective surrogate for measuring the cellular effects of BC on cells. Studies were done to determine if the FCDs are taken up by human lung cells, in an effort to tie the known health effects of BC to behavior of the BC surrogates made here. Confocal fluorescence microscopy and LR-TEM confirmed the uptake of the FCDs by the lung cells. Additional studies were done to determine the nature of FCD uptake, with the uptake process most likely being one that is an energy-requiring one (active process). Trypan blue, MTT, and MTS assays were all done to evaluate the cellular toxicity of the FCDs. Studies show that at short time periods (< 8 h) and low concentrations (< 2 mg/mL) the cellular toxicity effects are minimal, but at concentrations and times higher than those, cellular toxicity is significant and must be considered when evaluating experimental data from studies that use FCDs at levels/times above these values. The addition of metal ions to quench the fluorescence of the FCDs, a common practice in the literature, increases the cellular toxicity of the probe. A straightforward approach was taken to evaluate the effect of the FCDs on the oxidative stress of human lung cells through measurement of the glutathione:glutathione disulfide (GSH:GSSG) ratio. The results suggest that at short time periods (< 3 h), the FCDs do not increase the oxidative stress of the cells significantly. Similar to the results from the cellular toxicity studies, there is an increase in the oxidative stress in the cells after exposure to FCDs that have been quenched by metal ions.

FCDs and their applications are an extremely popular field of study, because of their potential capabilities as useful cellular fluorescent sensors and their apparent low cytotoxicity. Unfortunately, most of the research regarding FCDs is incomplete, with the focus being on

individual factors of importance to the authors of the numerous studies, such as synthesis of FCDs, evaluation of their optical properties, characterization of the FCDs, or cellular studies; a common thread in the literature of FCDs is the limited number of manuscripts with comprehensive evaluation of their properties and cellular impacts. This research was geared towards producing an unprecedented view of a given type of FCDs: synthesis conditions, optical properties, quenching properties, fluorescence recovery, and biological impact. Prior to this work the majority of the literature focused on the ability of researchers to easily make FCDs in a multitude of methods, with it being found that the properties of FCDs vary greatly depending on the synthetic conditions. Additionally, establishing fluorescence and fluorescence quenching mechanisms is not a trivial matter in the face of literature that yields FCDs with diverse properties, even when said studies purportedly use the same synthesis methodologies as each other or this scientist.[12, 15, 16] This is the first research providing evidence to support a semiquinone-iron ion quenching complex on the surface of FCDs treated with the well-known FCD fluorescence quenching agent. In addition to the quenching mechanism, to the knowledge of this scientist, the evaluation of the cellular effects of FCDs in this research is more comprehensive with regard to time of exposure and particle concentration than any found in the literature.

In addition to the evaluation of FCDs that was established by this research, the health effects of BC must also be considered. By demonstrating the uptake of FCDs by cells in a passive pathway, it is posited that BC of similar size and surface composition would also have a similar uptake route by human lung cells. The observation that FCDs enter cultured human lungs cells often used as a model for study of the impact of PM on human health point to the possibility that the environmental pollutant BC may remain in cells of the respiratory system for extended periods of time beyond reasons associated with its size. The fact that cells exposed to FCDs for time

periods longer than 8 hours show increased cell death suggests that cells exposed to BC of similar dimensions for similar times most likely exhibit increased cell death. The research also demonstrates that cultured human lung cells exposed to FCDs in amounts greater than 2 mg/mL show increased cell death, which corresponds to a concentration of 0.008 $\mu g/m^3$. Considering BC breathed in daily could be as high as 6.4 $\mu g/m^3$ during transport and as low as 1.2 $\mu g/m^3$ while sleeping, the possible cell toxicity effects could be substantial over long exposure periods.[17] This research provides interesting observations that provide pieces for a foundation that can be elaborated to firmly establish the pathways of BC as a cytotoxic pollutant, to understand the quenching mechanism of metal ions with pyrolytically produced FCDs, and identify the overall fluorescence mechanism of the FCDs.

6.2 Future Directions

The research outlined in this document provides new foundational seeds for studies that can be designed to more fully develop our understanding of many aspects of FCDs. The research here strove to provide a full picture of FCD behavior for a synthetically restricted class of FCDs. Therefore, further experimentation regarding individual parts of this research could provide more insight. While multiple starting materials were tested and proved successful for their use in producing FCDs, extensive studies of the properties of the FCDs should be taken up by a future scientist. The variability in properties reported for FCDs in the literature using very similar synthetic methodologies leads this scientist to find viable future research pathways wherein a comprehensive study of the differences imparted on the FCDs through variation in starting material and combustion conditions would be one significant direction for future activities. Additional studies should also be performed to further understand the fluorescence mechanism in these FCDs. Understanding the fluorescence mechanism and applying it to FCDs as an entire class of

fluorescent probes is not easily accomplished, due to the large variation in FCDs and their properties reported in the literature. To counteract that difficulty, the fluorescence mechanism must be explored in individual FCDs and applied to an understanding of FCDs as an entire class. In this research, the method of quenching was based on the stabilization of a semiquinone radical by iron ions, which implies the fluorescence quenching pathway is linked to the transition from semiquinone to catechol and vice versa. It is important to note that others have identified the presence of semiquinone radicals and various metal ions in atmospheric PM, with stabilization of semiquinone radicals by metal ion species in metal oxides being a hallmark of that work.[18-20] Thus, it is clear from that work and the outcomes here that there is a common thread with PM materials, and so study of routes to prevent or mitigate stabilized radical formation could be of significant importance in the study of BC. Future directions could include modification of the FCDs synthesized in this research to prevent or diminish radical formation/presence on the surface of the FCDs to determine if this approach impacts the cellular health effects of the BC surrogates and what roles radical presence/absence has on FCD emission characteristics.

The cellular studies performed in this research provide a very important foundation for the evaluation of FCDs as well as environmental particulate matter pollutants. An active transport uptake process was established to be occurring in cells taking up the FCDs, but the specific active transport process occurring should be probed by a future scientist. By inhibiting specific active transport processes and measuring uptake, the exact transport pathway can be probed and determined.[21, 22] Further understanding of the uptake process of these FCDs can yield information regarding the uptake of other forms of nanomaterials. There is some knowledge regarding the uptake of certain nanomaterials such as nanoplastics, quantum dots, or carbon nanotubes, but a similar picture is painted to that of FCDs, with a large amount of variability.[23-25] In addition to

the cellular uptake, evaluation of the cytotoxic and cellular stress effects of the FCDs needs to be more extensive. While the time periods and concentrations used to evaluate cellular toxicity in this research are more comprehensive than any other study known to date, more investigations of their effects are needed. Extensive studies of the cellular environment would aid in evaluation of FCDs as a cellular probe and knowledge of BC and its effects on cells. The oxidative stress effects of the FCDs were studied in a limited capacity in this research, but longer time periods and different concentrations should be studied moving forward.

As stated above, this research provides a breadth of foundational knowledge regarding the optical and physical properties of a well-defined type of FCD and the cellular effects of those FCDs, with the outcomes being important to the community studying BC and other environmental atmospheric pollutants. The diversity is great for directions of future investigations based on the research in this dissertation. Further research has the potential to provide more knowledge toward a true evaluation of FCDs as biological probes with that knowledge used to study in more depth the underlying effects of BC on human health.

6.3 References

1. Organization, W.H., *World Health Report 2002*. 2002.

2. Querol, X., et al., *Speciation and origin of PM10 and PM2.5 in selected European cities.* Atmospheric Environment, 2004. **38**(38): p. 6547-6555.

3. Turpin, B.J. and H.-J. Lim, *Species contributions to PM2. 5 mass concentrations: Revisiting common assumptions for estimating organic mass.* Aerosol Science & Technology, 2001. **35**(1): p. 602-610.

4. Environmental Protection Agency. *Particulate Matter (PM) Basics*. Particulate Matter (PM) Pollution 2019; Available from: https://www.epa.gov/pm-pollution/particulate-matter-pm-basics - PM.

5. Goldberg, E.D., *Black carbon in the environment: properties and distribution*. 1985: J. Wiley New York.

6. Kuhlbusch, T.A., *Black carbon and the carbon cycle.* Science, 1998. **280**(5371): p. 1903-1904.

7. Ramanathan, V. and G. Carmichael, *Global and regional climate changes due to black carbon.* Nature Geoscience, 2008. **1**: p. 221.

8. Smith, D.M. and A.R. Chughtai, *The surface structure and reactivity of black carbon.* Colloids and Surfaces A: Physicochemical and Engineering Aspects, 1995. **105**(1): p. 47-77.

9. Keiluweit, M., et al., *Dynamic molecular structure of plant biomass-derived black carbon (biochar).* Environmental science & technology, 2010. **44**(4): p. 1247-1253.

10. Song, Y., S. Zhu, and B. Yang, *Bioimaging based on fluorescent carbon dots.* RSC Advances, 2014. **4**(52): p. 27184-27200.

11. Panzarasa, G., et al., *Convenient Preparation of Graphene Oxide from Expandable Graphite and Its Characterization by Positron Annihilation Lifetime Spectroscopy.* C, 2019. **5**(1).

12. Fong, J.F.Y., S.F. Chin, and S.M. Ng, *A unique "turn-on" fluorescence signalling strategy for highly specific detection of ascorbic acid using carbon dots as sensing probe.* Biosensors and Bioelectronics, 2016. **85**: p. 844-852.

13. De, B. and N. Karak, *A green and facile approach for the synthesis of water soluble fluorescent carbon dots from banana juice.* RSC Advances, 2013. **3**(22): p. 8286-8290.

14. Hu, S.-L., et al., *One-step synthesis of fluorescent carbon nanoparticles by laser irradiation.* Journal of Materials Chemistry, 2009. **19**(4): p. 484-488.

15. Ma, X., et al., *Highly fluorescent carbon dots from peanut shells as potential probes for copper ion: The optimization and analysis of the synthetic process.* Materials Today Chemistry, 2017. **5**: p. 1-10.

16. Qin, J., L. Zhang, and R. Yang, *Solid pyrolysis synthesis of excitation-independent emission carbon dots and its application to isoniazid detection.* Journal of Nanoparticle Research, 2019. **21**(3): p. 59.

17. Dons, E., et al., *Impact of time–activity patterns on personal exposure to black carbon.* Atmospheric Environment, 2011. **45**(21): p. 3594-3602.

18. Pierpont, C.G. and C.W. Lange, *The chemistry of transition metal complexes containing catechol and semiquinone ligands.* Progress in Inorganic Chemistry, 1994: p. 331-442.

19. Kalyanaraman, B., C.C. Felix, and R.C. Sealy, *Semiquinone anion radicals of catechol(amine)s, catechol estrogens, and their metal ion complexes.* Environmental Health Perspectives, 1985. **64**: p. 185-198.

20. Squadrito, G.L., et al., *Quinoid redox cycling as a mechanism for sustained free radical generation by inhaled airborne particulate matter.* Free Radical Biology and Medicine, 2001. **31**(9): p. 1132-1138.

21. Gustafson, H.H., et al., *Nanoparticle uptake: The phagocyte problem.* Nano Today, 2015. **10**(4): p. 487-510.

22. Davda, J. and V. Labhasetwar, *Characterization of nanoparticle uptake by endothelial cells.* International Journal of Pharmaceutics, 2002. **233**(1): p. 51-59.

23. Kelf, T.A., et al., *Non-specific cellular uptake of surface-functionalized quantum dots.* Nanotechnology, 2010. **21**(28): p. 285105.

24. Gigault, J., et al., *Current opinion: What is a nanoplastic?* Environmental Pollution, 2018. **235**: p. 1030-1034.

25. Kostarelos, K., et al., *Cellular uptake of functionalized carbon nanotubes is independent of functional group and cell type.* Nature Nanotechnology, 2007. **2**(2): p. 108-113.

APPENDIX: PERMISSION AGREEMENT

JOHN WILEY AND SONS LICENSE
TERMS AND CONDITIONS
May 20, 2020

This Agreement between Louisiana State University -- Christopher Sumner ("You") and John Wiley and Sons ("John Wiley and Sons") consists of your license details and the terms and conditions provided by John Wiley and Sons and Copyright Clearance Center.

License Number	4813220421695
License date	Apr 20, 2020
Licensed Content Publisher	John Wiley and Sons
Licensed Content Publication	Global Biogeochemical Cycles
Licensed Content Title	Black carbon in soils and sediments: Analysis, distribution, implications, and current challenges
Licensed Content Author	Angela G. Noack, Michael W. I. Schmidt
Licensed Content Date	Sep 1, 2000
Licensed Content Volume	14
Licensed Content Issue	3
Licensed Content Pages	17
Type of use	Dissertation/Thesis
Requestor type	University/Academic
Format	Print and electronic
Portion	Figure/table
Number of figures/tables	1
Will you be translating?	No
Title	SYNTHESIS, CHARACTERIZATION, AND INVESTIGATION OF METAL ION QUENCHING IN

	FLUORESCENT CARBON DOT SURROGATES FOR PARTICULATE MATTER BLACK CARBON AND EVALUATION OF CELLULAR HEALTH EFFECTS DUE TO THE SURROGATE MATERIALS
Institution name	Louisiana State University
Expected presentation date	May 2020
Portions	Figure 2 on page 779
Requestor Location	Louisiana State University 2525 O'Neal Lane Apt 113 BATON ROUGE, LA 70816 United States Attn: Louisiana State University
Publisher Tax ID	EU826007151
Total	0.00 USD

Terms and Conditions

TERMS AND CONDITIONS

This copyrighted material is owned by or exclusively licensed to John Wiley & Sons, Inc. or one of its group companies (each a"Wiley Company") or handled on behalf of a society with which a Wiley Company has exclusive publishing rights in relation to a particular work (collectively "WILEY"). By clicking "accept" in connection with completing this licensing transaction, you agree that the following terms and conditions apply to this transaction (along with the billing and payment terms and conditions established by the Copyright Clearance Center Inc., ("CCC's Billing and Payment terms and conditions"), at the time that you opened your RightsLink account (these are available at any time at http://myaccount.copyright.com).

Terms and Conditions

- The materials you have requested permission to reproduce or reuse (the "Wiley Materials") are protected by copyright.
- You are hereby granted a personal, non-exclusive, non-sub licensable (on a stand-alone basis), non-transferable, worldwide, limited license to reproduce the Wiley Materials for the purpose specified in the licensing process. This license, **and any CONTENT (PDF or image file)**

purchased as part of your order, is for a one-time use only and limited to any maximum distribution number specified in the license. The first instance of republication or reuse granted by this license must be completed within two years of the date of the grant of this license (although copies prepared before the end date may be distributed thereafter). The Wiley Materials shall not be used in any other manner or for any other purpose, beyond what is granted in the license. Permission is granted subject to an appropriate acknowledgement given to the author, title of the material/book/journal and the publisher. You shall also duplicate the copyright notice that appears in the Wiley publication in your use of the Wiley Material. Permission is also granted on the understanding that nowhere in the text is a previously published source acknowledged for all or part of this Wiley Material. Any third party content is expressly excluded from this permission.

- With respect to the Wiley Materials, all rights are reserved. Except as expressly granted by the terms of the license, no part of the Wiley Materials may be copied, modified, adapted (except for minor reformatting required by the new Publication), translated, reproduced, transferred or distributed, in any form or by any means, and no derivative works may be made based on the Wiley Materials without the prior permission of the respective copyright owner.**For STM Signatory Publishers clearing permission under the terms of the STM Permissions Guidelines only, the terms of the license are extended to include subsequent editions and for editions in other languages, provided such editions are for the work as a whole in situ and does not involve the separate exploitation of the permitted figures or extracts,** You may not alter, remove or suppress in any manner any copyright, trademark or other notices displayed by the Wiley Materials. You may not license, rent, sell, loan, lease, pledge, offer as security, transfer or assign the Wiley Materials on a stand-alone basis, or any of the rights granted to you hereunder to any other person.

- The Wiley Materials and all of the intellectual property rights therein shall at all times remain the exclusive property of John Wiley & Sons Inc, the Wiley Companies, or their respective licensors, and your interest therein is only that of having possession of and the right to reproduce the Wiley Materials pursuant to Section 2 herein during the continuance of this Agreement. You agree that you own no right, title or interest in or to the Wiley Materials or any of the intellectual property rights therein. You shall have no rights hereunder other than the license as provided for above in Section 2. No right, license or interest to any trademark, trade name,

service mark or other branding ("Marks") of WILEY or its licensors is granted hereunder, and you agree that you shall not assert any such right, license or interest with respect thereto

- NEITHER WILEY NOR ITS LICENSORS MAKES ANY WARRANTY OR REPRESENTATION OF ANY KIND TO YOU OR ANY THIRD PARTY, EXPRESS, IMPLIED OR STATUTORY, WITH RESPECT TO THE MATERIALS OR THE ACCURACY OF ANY INFORMATION CONTAINED IN THE MATERIALS, INCLUDING, WITHOUT LIMITATION, ANY IMPLIED WARRANTY OF MERCHANTABILITY, ACCURACY, SATISFACTORY QUALITY, FITNESS FOR A PARTICULAR PURPOSE, USABILITY, INTEGRATION OR NON-INFRINGEMENT AND ALL SUCH WARRANTIES ARE HEREBY EXCLUDED BY WILEY AND ITS LICENSORS AND WAIVED BY YOU.

- WILEY shall have the right to terminate this Agreement immediately upon breach of this Agreement by you.

- You shall indemnify, defend and hold harmless WILEY, its Licensors and their respective directors, officers, agents and employees, from and against any actual or threatened claims, demands, causes of action or proceedings arising from any breach of this Agreement by you.

- IN NO EVENT SHALL WILEY OR ITS LICENSORS BE LIABLE TO YOU OR ANY OTHER PARTY OR ANY OTHER PERSON OR ENTITY FOR ANY SPECIAL, CONSEQUENTIAL, INCIDENTAL, INDIRECT, EXEMPLARY OR PUNITIVE DAMAGES, HOWEVER CAUSED, ARISING OUT OF OR IN CONNECTION WITH THE DOWNLOADING, PROVISIONING, VIEWING OR USE OF THE MATERIALS REGARDLESS OF THE FORM OF ACTION, WHETHER FOR BREACH OF CONTRACT, BREACH OF WARRANTY, TORT, NEGLIGENCE, INFRINGEMENT OR OTHERWISE (INCLUDING, WITHOUT LIMITATION, DAMAGES BASED ON LOSS OF PROFITS, DATA, FILES, USE, BUSINESS OPPORTUNITY OR CLAIMS OF THIRD PARTIES), AND WHETHER OR NOT THE PARTY HAS BEEN ADVISED OF THE POSSIBILITY OF SUCH DAMAGES. THIS LIMITATION SHALL APPLY NOTWITHSTANDING ANY FAILURE OF ESSENTIAL PURPOSE OF ANY LIMITED REMEDY PROVIDED HEREIN.

- Should any provision of this Agreement be held by a court of competent jurisdiction to be illegal, invalid, or unenforceable, that provision shall be deemed amended to achieve as nearly as possible the same economic effect as the original provision, and the legality, validity and enforceability of the remaining provisions of this Agreement shall not be affected or impaired thereby.

- The failure of either party to enforce any term or condition of this Agreement shall not constitute a waiver of either party's right to enforce each and every term and condition of this Agreement. No breach under this agreement shall be deemed waived or excused by either party unless such waiver or consent is in writing signed by the party granting such waiver or consent. The waiver by or consent of a party to a breach of any provision of this Agreement shall not operate or be construed as a waiver of or consent to any other or subsequent breach by such other party.

- This Agreement may not be assigned (including by operation of law or otherwise) by you without WILEY's prior written consent.

- Any fee required for this permission shall be non-refundable after thirty (30) days from receipt by the CCC.

- These terms and conditions together with CCC's Billing and Payment terms and conditions (which are incorporated herein) form the entire agreement between you and WILEY concerning this licensing transaction and (in the absence of fraud) supersedes all prior agreements and representations of the parties, oral or written. This Agreement may not be amended except in writing signed by both parties. This Agreement shall be binding upon and inure to the benefit of the parties' successors, legal representatives, and authorized assigns.

- In the event of any conflict between your obligations established by these terms and conditions and those established by CCC's Billing and Payment terms and conditions, these terms and conditions shall prevail.

- WILEY expressly reserves all rights not specifically granted in the combination of (i) the license details provided by you and accepted in the course of this licensing transaction, (ii) these terms and conditions and (iii) CCC's Billing and Payment terms and conditions.

- This Agreement will be void if the Type of Use, Format, Circulation, or Requestor Type was misrepresented during the licensing process.

- This Agreement shall be governed by and construed in accordance with the laws of the State of New York, USA, without regards to such state's conflict of law rules. Any legal action, suit or proceeding arising out of or relating to these Terms and Conditions or the breach thereof shall be instituted in a court of competent jurisdiction in New York County in the State of New York in the United States of America and each party hereby consents and submits to the personal jurisdiction of such court, waives any objection to venue in such court and consents to service of process by registered or certified mail, return receipt requested, at the last known address of such party.

WILEY OPEN ACCESS TERMS AND CONDITIONS

Wiley Publishes Open Access Articles in fully Open Access Journals and in Subscription journals offering Online Open. Although most of the fully Open Access journals publish open access articles under the terms of the Creative Commons Attribution (CC BY) License only, the subscription journals and a few of the Open Access Journals offer a choice of Creative Commons Licenses. The license type is clearly identified on the article.

The Creative Commons Attribution License

The Creative Commons Attribution License (CC-BY) allows users to copy, distribute and transmit an article, adapt the article and make commercial use of the article. The CC-BY license permits commercial and non-

Creative Commons Attribution Non-Commercial License

The Creative Commons Attribution Non-Commercial (CC-BY-NC)License permits use, distribution and reproduction in any medium, provided the original work is properly cited and is not used for commercial purposes.(see below)

Creative Commons Attribution-Non-Commercial-NoDerivs License

The Creative Commons Attribution Non-Commercial-NoDerivs License (CC-BY-NC-ND) permits use, distribution and reproduction in any medium, provided

REFERENCE LIST

25 - Iron, Ruthenium and Osmium, in Chemistry of the Elements (Second Edition), N.N. Greenwood and A. Earnshaw, Editors. 1997, Butterworth-Heinemann: Oxford. p. 1070-1112.

Adams, M., M. Blois Jr, and R.H. Sands, Paramagnetic resonance spectra of some semiquinone free radicals. The Journal of Chemical Physics, 1958. 28(5): p. 774-776.

Aebi, U. and T.D. Pollard, A glow discharge unit to render electron microscope grids and other surfaces hydrophilic. Journal of Electron Microscopy Technique, 1987. 7(1): p. 29-33.

Agency, E.P. Health and Environmental Effects of Particulate Matter (PM). Particulate Matter (PM) Pollution 2019 cited 2019; Available from: https://www.epa.gov/pm-pollution/health-and-environmental-effects-particulate-matter-pm.

Alivisatos, A.P., *Perspectives on the Physical Chemistry of Semiconductor Nanocrystals.* The Journal of Physical Chemistry, 1996. **100**(31): p. 13226-13239.

Alivisatos, A.P., *Semiconductor Clusters, Nanocrystals, and Quantum Dots.* Science, 1996. **271**(5251): p. 933.

Al'Tshuler, S.A. and B.M. Kozyrev, Electron paramagnetic resonance. 2013: Academic Press.

Anderson, J.O., J.G. Thundiyil, and A. Stolbach, *Clearing the air: a review of the effects of particulate matter air pollution on human health.* J Med Toxicol, 2012. **8**(2): p. 166-75.

Andersson, et al., Autofluorescence of living cells. Journal of Microscopy, 1998. 191(1): p. 1-7.

Aouadi, M., et al., *Orally delivered siRNA targeting macrophage Map4k4 suppresses systemic inflammation.* Nature, 2009. **458**(7242): p. 1180-1184.

Ariese, F., et al., Comparison of Laurentian Fulvic Acid luminescence with that of the hydroquinone/quinone model system: Evidence from low temperature fluorescence studies and EPR spectroscopy. Aquatic Sciences, 2004. 66(1): p. 86-94.

Arnott, W.P., et al., *Photoacoustic and filter-based ambient aerosol light absorption measurements: Instrument comparisons and the role of relative humidity.* Journal of Geophysical Research: Atmospheres, 2003. **108**(D1): p. AAC 15-1-AAC 15-11.

Aubin, J.E., Autofluorescence of viable cultured mammalian cells. Journal of Histochemistry & Cytochemistry, 1979. 27(1): p. 36-43.

Badgett, A., *Toward the Impact of Particulate Matter on Human Health: Evaluation of Fluorescent Environmentally Persistent Free Radical (EPFR) Surrogates*, in *Chemistry*. 2019, Louisiana State University.

Baker, S.N. and G.A. Baker, *Luminescent carbon nanodots: emergent nanolights.* Angew Chem Int Ed Engl, 2010. **49**(38): p. 6726-44.

Ball, E.G., Studies on oxidation-reduction. 23. Ascorbic acid. Journal of Biological Chemistry, 1937. 118: p. 219-239.

Bang, J., H. Yang, and P.H. Holloway, *Enhanced and stable green emission of ZnO nanoparticles by surface segregation of Mg.* Nanotechnology, 2006. **17**(4): p. 973-978.

Barlow-Walden, L., et al., *Melatonin stimulates brain glutathione peroxidase activity.* Neurochemistry international, 1995. **26**(5): p. 497-502.

Behzadi, S., et al., *Cellular uptake of nanoparticles: journey inside the cell.* Chemical Society Reviews, 2017. **46**(14): p. 4218-4244.

Bell, M.L. and D.L. Davis, *Reassessment of the lethal London fog of 1952: novel indicators of acute and chronic consequences of acute exposure to air pollution.* Environmental Health Perspectives, 2001. **109**(suppl 3): p. 389-394.

Bera, D., et al., *Quantum Dots and Their Multimodal Applications: A Review.* Materials, 2010. **3**(4): p. 2260-2345.

Berlier, J.E., et al., *Quantitative Comparison of Long-wavelength Alexa Fluor Dyes to Cy Dyes: Fluorescence of the Dyes and Their Bioconjugates.* Journal of Histochemistry & Cytochemistry, 2003. **51**(12): p. 1699-1712.

Best, Q.A., et al., *Efficacious fluorescence turn-on probe for high-contrast imaging of human cells overexpressing quinone reductase activity.* Chemical Communications, 2017. **53**(4): p. 783-786.

Blyth, R. I. R.; Buqa, H.; Netzer, F. P.; Ramsey, M. G.; Besenhard, J. O.; Golob, P.; Winter, M., XPS studies of graphite electrode materials for lithium ion batteries. *Applied Surface Science* **2000,** *167* (1), 99-106.

Bond, T.C., et al., *Bounding the role of black carbon in the climate system: A scientific assessment.* Journal of Geophysical Research: Atmospheres, 2013. **118**(11): p. 5380-5552.

Borse, V., et al., *N-doped multi-fluorescent carbon dots for 'turn off-on' silver-biothiol dual sensing and mammalian cell imaging application.* Sensors and Actuators B: Chemical, 2017. **248**: p. 481-492.

Borsook, H. and G. Keighley, Oxidation-Reduction Potential of Ascorbic Acid (Vitamin C). Proceedings of the National Academy of Sciences of the United States of America, 1933. 19(9): p. 875-878.

Bottini, M., et al., *Isolation and Characterization of Fluorescent Nanoparticles from Pristine and Oxidized Electric Arc-Produced Single-Walled Carbon Nanotubes.* The Journal of Physical Chemistry B, 2006. **110**(2): p. 831-836.

Braun, A., et al., *Advantages of soft X-ray absorption over TEM-EELS for solid carbon studies—a comparative study on diesel soot with EELS and NEXAFS.* Carbon, 2005. **43**(1): p. 117-124.

Brisson, P.-Y., et al., X-ray photoelectron spectroscopy study of sodium reactions in carbon cathode blocks of aluminium oxide reduction cells. Carbon, 2006. 44(8): p. 1438-1447.

Broekaert, J.A., Daniel C. Harris: Quantitative chemical analysis. Analytical and bioanalytical chemistry, 2015. 407(30): p. 8943-8944.

Brook Robert, D., et al., *Particulate Matter Air Pollution and Cardiovascular Disease.* Circulation, 2010. **121**(21): p. 2331-2378.

Bruccoleri, A., et al., Evaluation of primary photoproduct quantum yields in fulvic acid. Environmental Science & Technology, 1993. 27(5): p. 889-894.

Buseck, P.R., et al., *Are black carbon and soot the same?* Atmospheric Chemistry and Physics Discussions, 2012. **12**(9): p. 24821-24846.

Cachier, H., M.-P. Bremond, and P. Buat-Ménard, Determination of atmospheric soot carbon with a simple thermal method. Tellus B: Chemical and Physical Meteorology, 1989. 41(3): p. 379-390.

Cachier, H., M.-P. Brémond, and P. Buat-Ménard, *Thermal Separation of Soot Carbon.* Aerosol Science and Technology, 1989. **10**(2): p. 358-364.

Cao, X., et al., A near-infrared fluorescent turn-on probe for fluorescence imaging of hydrogen sulfide in living cells based on thiolysis of dinitrophenyl ether. Chemical Communications, 2012. 48(85): p. 10529-10531.

Cetin, E., R. Gupta, and B. Moghtaderi, *Effect of pyrolysis pressure and heating rate on radiata pine char structure and apparent gasification reactivity.* Fuel, 2005. **84**(10): p. 1328-1334.

Chaudhuri, A., G. Battaglia, and R. Golestanian, *The effect of interactions on the cellular uptake of nanoparticles.* Physical biology, 2011. **8**(4): p. 046002.

Chen, F. and D. Gerion, *Fluorescent CdSe/ZnS Nanocrystal−Peptide Conjugates for Long-term, Nontoxic Imaging and Nuclear Targeting in Living Cells.* Nano Letters, 2004. **4**(10): p. 1827-1832.

Chithrani, B.D. and W.C. Chan, *Elucidating the mechanism of cellular uptake and removal of protein-coated gold nanoparticles of different sizes and shapes.* Nano letters, 2007. **7**(6): p. 1542-1550.

Chithrani, B.D., A.A. Ghazani, and W.C.W. Chan, *Determining the Size and Shape Dependence of Gold Nanoparticle Uptake into Mammalian Cells.* Nano Letters, 2006. **6**(4): p. 662-668.

Cho, E.C., Q. Zhang, and Y. Xia, *The effect of sedimentation and diffusion on cellular uptake of gold nanoparticles.* Nature nanotechnology, 2011. **6**(6): p. 385.

Choi, H.-D., et al., *Removal characteristics of reactive black 5 using surfactant-modified activated carbon.* Desalination, 2008. **223**(1): p. 290-298.

Chuang, K.-J., et al., *The Effect of Urban Air Pollution on Inflammation, Oxidative Stress, Coagulation, and Autonomic Dysfunction in Young Adults.* American Journal of Respiratory and Critical Care Medicine, 2007. **176**(4): p. 370-376.

Chughtai, A.R., et al., *Spectroscopic and Solubility Characteristics of Oxidized Soots.* Aerosol Science and Technology, 1991. **15**(2): p. 112-126.

Chung, S.H. and J.H. Seinfeld, *Climate response of direct radiative forcing of anthropogenic black carbon.* Journal of Geophysical Research: Atmospheres, 2005. **110**(D11).

Ciapetti, G., et al., *In vitro evaluation of cell/biomaterial interaction by MTT assay.* Biomaterials, 1993. **14**(5): p. 359-364.

Clogston, J.D. and A.K. Patri, Zeta Potential Measurement, in Characterization of Nanoparticles Intended for Drug Delivery, S.E. McNeil, Editor. 2011, Humana Press: Totowa, NJ. p. 63-70.

Colbeck, I., E.J. Hardman, and R.M. Harrison, *Optical and dynamical properties of fractal clusters of carbonaceous smoke.* Journal of Aerosol Science, 1989. **20**(7): p. 765-774.

Colucci, J., et al., Electrochemical oxidation potential of photocatalyst reducing agents. Electrochimica Acta, 1999. 44(15): p. 2507-2514.

Construction of a 1° × 1° fossil fuel emission data set for carbonaceous aerosol and implementation and radiative impact in the ECHAM4 model. Journal of Geophysical Research: Atmospheres, 1999. **104**(D18): p. 22137-22162.

Cory, A.H., et al., *Use of an Aqueous Soluble Tetrazolium/Formazan Assay for Cell Growth Assays in Culture.* Cancer Communications, 1991. **3**(7): p. 207-212.

Couto, O.D.D., et al., *Charge control in InP/(Ga,In)P single quantum dots embedded in Schottky diodes.* Physical Review B, 2011. **84**(12): p. 125301.

Cumpson, P.J., Angle-resolved XPS and AES: Depth-resolution limits and a general comparison of properties of depth-profile reconstruction methods. Journal of Electron Spectroscopy and Related Phenomena, 1995. 73(1): p. 25-52.

Czimczik, C.I., et al., Effects of charring on mass, organic carbon, and stable carbon isotope composition of wood. Organic Geochemistry, 2002. 33(11): p. 1207-1223.

Das, P., et al., *A simplistic approach to green future with eco-friendly luminescent carbon dots and their application to fluorescent nano-sensor 'turn-off' probe for selective sensing of copper ions.* Materials Science and Engineering: C, 2017. **75**: p. 1456-1464.

Davda, J. and V. Labhasetwar, *Characterization of nanoparticle uptake by endothelial cells.* International Journal of Pharmaceutics, 2002. **233**(1): p. 51-59.

Davis, K.A., et al., *Evolution of char chemistry, crystallinity, and ultrafine structure during pulverized-coal combustion.* Combustion and Flame, 1995. **100**(1): p. 31-40.

De, B. and N. Karak, A green and facile approach for the synthesis of water soluble fluorescent carbon dots from banana juice. RSC Advances, 2013. 3(22): p. 8286-8290.

Derenzis, F.A. and A. Schechtman, *Staining by Neutral Red and Trypan Blue in Sequence for Assaying Vital and Nonvital Cultured Cells.* Stain Technology, 1973. **48**(3): p. 135-136.

Derfus, A.M., W.C.W. Chan, and S.N. Bhatia, *Probing the Cytotoxicity of Semiconductor Quantum Dots.* Nano Letters, 2004. **4**(1): p. 11-18.

Diarra, M., et al., *Importance of Carbon Solubility and Wetting Properties of Nickel Nanoparticles for Single Wall Nanotube Growth.* Physical Review Letters, 2012. **109**(18): p. 185501.

Diez Roux, A.V., et al., *Recent Exposure to Particulate Matter and C-reactive Protein Concentration in the Multi-Ethnic Study of Atherosclerosis.* American Journal of Epidemiology, 2006. **164**(5): p. 437-448.

Dons, E., et al., *Impact of time–activity patterns on personal exposure to black carbon.* Atmospheric Environment, 2011. **45**(21): p. 3594-3602.

Dresselhaus, M.S., et al., Raman spectroscopy of carbon nanotubes. Physics Reports, 2005. 409(2): p. 47-99.

Dreyer, D.R., et al., The chemistry of graphene oxide. Chemical society reviews, 2010. 39(1): p. 228-240.

Du, F., et al., *Carbon dots-based fluorescent probes for sensitive and selective detection of iodide.* Microchimica Acta, 2013. **180**(5): p. 453-460.

Dunitz, J., The structure of sodium dithionite and the nature of the dithionite ion. Acta Crystallographica, 1956. 9(7): p. 579-586.

(ECACC), E.C.o.A.C.C. General Cell Collection Detail. [cited 2020; Available from: https://www.phe-culturecollections.org.uk/products/celllines/generalcell/detail.jsp?refId=95102433&collection=ecacc_gc.

Ebbing, D.D. and M.S. Wrighton, General chemistry. 1990: Houghton Mifflin Boston etc.

Eda, G. and M. Chhowalla, Chemically derived graphene oxide: towards large-area thin-film electronics and optoelectronics. Advanced materials, 2010. 22(22): p. 2392-2415.

Eda, G., et al., *Blue Photoluminescence from Chemically Derived Graphene Oxide.* Advanced Materials, 2010. **22**(4): p. 505-509.

Efros, A.L. and M. Rosen, *Random Telegraph Signal in the Photoluminescence Intensity of a Single Quantum Dot.* Physical Review Letters, 1997. **78**(6): p. 1110-1113.

Eggeling, C., A. Volkmer, and C.A.M. Seidel, *Molecular Photobleaching Kinetics of Rhodamine 6G by One- and Two-Photon Induced Confocal Fluorescence Microscopy.* ChemPhysChem, 2005. **6**(5): p. 791-804.

Environmental Protection Agency. Particulate Matter (PM) Basics. Particulate Matter (PM) Pollution 2019; Available from: https://www.epa.gov/pm-pollution/particulate-matter-pm-basics - PM.

Essner, J.B., et al., *Artifacts and Errors Associated with the Ubiquitous Presence of Fluorescent Impurities in Carbon Nanodots.* Chemistry of Materials, 2018. **30**(6): p. 1878-1887.

Fang, Y., et al., *Easy Synthesis and Imaging Applications of Cross-Linked Green Fluorescent Hollow Carbon Nanoparticles.* ACS Nano, 2012. **6**(1): p. 400-409.

Felix, C. C.; Sealy, R. C., o-Benzosemiquinone and its metal chelates. electron spin resonance investigation of radicals from the photolysis of catechol in the presence of complexing metal ions. *Journal of the American Chemical Society* **1982**, *104* (6), 1555-1560.

Feng, B., S.K. Bhatia, and J.C. Barry, *Structural ordering of coal char during heat treatment and its impact on reactivity.* Carbon, 2002. **40**(4): p. 481-496.

Flanner, M.G., et al., *Present-day climate forcing and response from black carbon in snow.* Journal of Geophysical Research: Atmospheres, 2007. **112**(D11).

Fong, J.F.Y., S.F. Chin, and S.M. Ng, *A unique "turn-on" fluorescence signalling strategy for highly specific detection of ascorbic acid using carbon dots as sensing probe.* Biosensors and Bioelectronics, 2016. **85**: p. 844-852.

Fonin, A.V., et al., Fluorescence of dyes in solutions with high absorbance. Inner filter effect correction. PloS one, 2014. 9(7): p. e103878-e103878.

Forbes, L.J.L., et al., *Chronic Exposure to Outdoor Air Pollution and Markers of Systemic Inflammation.* Epidemiology, 2009. **20**(2): p. 245-253.

Franklin, M., P. Koutrakis, and P. Schwartz, *The role of particle composition on the association between PM2.5 and mortality.* Epidemiology, 2008. **19**(5): p. 680-9.

Fröhlich, E., *The role of surface charge in cellular uptake and cytotoxicity of medical nanoparticles.* International journal of nanomedicine, 2012. **7**: p. 5577-5591.

Fu, H.-B. and J.-N. Yao, *Size Effects on the Optical Properties of Organic Nanoparticles.* Journal of the American Chemical Society, 2001. **123**(7): p. 1434-1439.

Galler, K.M., et al., EDTA conditioning of dentine promotes adhesion, migration and differentiation of dental pulp stem cells. International Endodontic Journal, 2016. 49(6): p. 581-590.

Gan, W.Q., et al., *Association between chronic obstructive pulmonary disease and systemic inflammation: a systematic review and a meta-analysis.* Thorax, 2004. **59**(7): p. 574-580.

Gan, Z., et al., Enzymatic degradation of poly(ε-caprolactone) film in phosphate buffer solution containing lipases. Polymer Degradation and Stability, 1997. 56(2): p. 209-213.

Gao, X., et al., *MAP4K4: an emerging therapeutic target in cancer.* Cell & Bioscience, 2016. **6**(1): p. 56.

Gardner, S.D., et al., Surface characterization of carbon fibers using angle-resolved XPS and ISS. Carbon, 1995. 33(5): p. 587-595.

Georgakoudi, I., et al., *NAD(P)H and collagen as in vivo quantitative fluorescent biomarkers of epithelial precancerous changes.* Cancer Res, 2002. **62**(3): p. 682-7.

Gigault, J., et al., *Current opinion: What is a nanoplastic?* Environmental Pollution, 2018. **235**: p. 1030-1034.

Gilmour, M.I., et al., Comparative Toxicity of Size-Fractionated Airborne Particulate Matter Obtained from Different Cities in the United States. Inhalation Toxicology, 2007. 19(sup1): p. 7-16.

Gold, D.R., et al., *Air Pollution and ST-Segment Depression in Elderly Subjects.* Environmental Health Perspectives, 2005. **113**(7): p. 883-887.

Goldberg, E.D., *Black carbon in the environment: properties and distribution*. 1985: J. Wiley New York.

Goldfarb, D., et al., Characterization of Iron in Zeolites by X-band and Q-Band ESR, Pulsed ESR, and UV-Visible Spectroscopies. Journal of the American Chemical Society, 1994. 116(14): p. 6344-6353.

Goldman, A. and A. Bentur, *Properties of cementitious systems containing silica fume or nonreactive microfillers.* Advanced Cement Based Materials, 1994. **1**(5): p. 209-215.

Gonçalves, H. and J.C.G. Esteves da Silva, *Fluorescent Carbon Dots Capped with PEG200 and Mercaptosuccinic Acid.* Journal of Fluorescence, 2010. **20**(5): p. 1023-1028.

Goodwin, C., et al., *Microculture tetrazolium assays: a comparison between two new tetrazolium salts, XTT and MTS.* Journal of immunological methods, 1995. **179**(1): p. 95-103.

Goss, D.J. and R.H. Petrucci, General Chemistry Principles & Modern Applications, Petrucci, Harwood, Herring, Madura: Study Guide. 2007: Pearson/Prentice Hall.

Gu, D., et al., *Green synthesis of nitrogen-doped carbon dots from lotus root for Hg(II) ions detection and cell imaging.* Applied Surface Science, 2016. **390**: p. 38-42.

Guan, W., et al., *Microwave-assisted polyol synthesis of carbon nitride dots from folic acid for cell imaging.* International journal of nanomedicine, 2014. **9**: p. 5071-5078.

Guo, Y., et al., Fluorescent carbon nanoparticles for the fluorescent detection of metal ions. Biosensors and Bioelectronics, 2015. 63: p. 61-71.

Guo, Y., et al., Hydrothermal synthesis of highly fluorescent carbon nanoparticles from sodium citrate and their use for the detection of mercury ions. Carbon, 2013. 52: p. 583-589.

Gustafson, H.H., et al., *Nanoparticle uptake: The phagocyte problem.* Nano Today, 2015. **10**(4): p. 487-510.

Han, B., et al., *Polyethyleneimine modified fluorescent carbon dots and their application in cell labeling.* Colloids and Surfaces B: Biointerfaces, 2012. **100**: p. 209-214.

Han, C., et al., Highly fluorescent carbon dots as selective and sensitive “on-off-on” probes for iron(III) ion and apoferritin detection and imaging in living cells. Biosensors and Bioelectronics, 2016. 83: p. 229-236.

Han, Q., et al., Turn-On Fluorescence Probe for Nitric Oxide Detection and Bioimaging in Live Cells and Zebrafish. ACS Sensors, 2019. 4(2): p. 309-316.

Hansen, A.D.A., H. Rosen, and T. Novakov, *The aethalometer — An instrument for the real-time measurement of optical absorption by aerosol particles.* Science of The Total Environment, 1984. **36**: p. 191-196.

He, C., et al., *Effects of particle size and surface charge on cellular uptake and biodistribution of polymeric nanoparticles.* Biomaterials, 2010. **31**(13): p. 3657-3666.

He, D., et al., *A sensitive turn-on fluorescent probe for intracellular imaging of glutathione using single-layer MnO2 nanosheet-quenched fluorescent carbon quantum dots.* Chem Commun (Camb), 2015. **51**(79): p. 14764-7.

Hockaday, W.C., et al., *Direct molecular evidence for the degradation and mobility of black carbon in soils from ultrahigh-resolution mass spectral analysis of dissolved organic matter from a fire-impacted forest soil.* Organic Geochemistry, 2006. **37**(4): p. 501-510.

Hoffmann, B., et al., *Chronic Residential Exposure to Particulate Matter Air Pollution and Systemic Inflammatory Markers.* Environmental Health Perspectives, 2009. **117**(8): p. 1302-1308.

Horak Jr, F., et al., *The chemical composition of particulate matter has a short term effect on the lung function of pre-school children.* Eur. Respri. J, 2001. **18**.

Hu, C., et al., Chemically tailoring coal to fluorescent carbon dots with tuned size and their capacity for Cu (II) detection. Small, 2014. 10(23): p. 4926-4933.

Hu, S., et al., Enhanced performance of Fe3+ detection via fluorescence resonance energy transfer between carbon quantum dots and Rhodamine B. RSC Advances, 2014. 4(77): p. 41069-41075.

Hu, S., et al., *Laser synthesis and size tailor of carbon quantum dots.* Journal of Nanoparticle Research, 2011. **13**(12): p. 7247-7252.

Hu, S.-L., et al., *One-step synthesis of fluorescent carbon nanoparticles by laser irradiation.* Journal of Materials Chemistry, 2009. **19**(4): p. 484-488.

Huang, J., et al., *Effects of nanoparticle size on cellular uptake and liver MRI with polyvinylpyrrolidone-coated iron oxide nanoparticles.* ACS nano, 2010. **4**(12): p. 7151-7160.

Hussain, S., et al., *Carbon black and titanium dioxide nanoparticles elicit distinct apoptotic pathways in bronchial epithelial cells.* Particle and Fibre Toxicology, 2010. **7**(1): p. 10.

Huynh, M.T., et al., Quinone 1 e– and 2 e–/2 H+ Reduction Potentials: Identification and Analysis of Deviations from Systematic Scaling Relationships. Journal of the American Chemical Society, 2016. 138(49): p. 15903-15910.

Iqbal, A., et al., *Carbon dots prepared by solid state method via citric acid and 1,10-phenanthroline for selective and sensing detection of Fe2+ and Fe3+*. Sensors and Actuators B: Chemical, 2016. **237**: p. 408-415.

Issac, A., C. von Borczyskowski, and F. Cichos, *Correlation between photoluminescence intermittency of CdSe quantum dots and self-trapped states in dielectric media.* Physical Review B, 2005. **71**(16): p. 161302.

Ivleva, N.P., et al., *Raman Microspectroscopic Analysis of Size-Resolved Atmospheric Aerosol Particle Samples Collected with an ELPI: Soot, Humic-Like Substances, and Inorganic Compounds.* Aerosol Science and Technology, 2007. **41**(7): p. 655-671.

Jaffé, R., et al., *Global Charcoal Mobilization from Soils via Dissolution and Riverine Transport to the Oceans.* Science, 2013. **340**(6130): p. 345.

Jain, V., M.C. Biesinger, and M.R. Linford, The Gaussian-Lorentzian Sum, Product, and Convolution (Voigt) functions in the context of peak fitting X-ray photoelectron spectroscopy (XPS) narrow scans. Applied Surface Science, 2018. 447: p. 548-553.

Jaiswal, J.K., et al., *Long-term multiple color imaging of live cells using quantum dot bioconjugates.* Nature Biotechnology, 2003. **21**(1): p. 47-51.

Jansen Karen, L., et al., *Associations between Health Effects and Particulate Matter and Black Carbon in Subjects with Respiratory Disease.* Environmental Health Perspectives, 2005. **113**(12): p. 1741-1746.

Jennings, S.G., et al., *Volatility of elemental carbon.* Geophysical Research Letters, 1994. **21**(16): p. 1719-1722.

Jin, M., et al., *MAP4K4 deficiency in CD4+ T cells aggravates lung damage induced by ozone-oxidized black carbon particles.* Environmental Toxicology and Pharmacology, 2016. **46**: p. 246-254.

Jones, S.L., et al., *Exhaled NO and assessment of anti-inflammatory effects of inhaled steroid: dose-response relationship.* European Respiratory Journal, 2002. **20**(3): p. 601-608.

Kalyanaraman, B., C.C. Felix, and R.C. Sealy, Semiquinone anion radicals of catechol(amine)s, catechol estrogens, and their metal ion complexes. Environmental Health Perspectives, 1985. 64: p. 185-198.

Karamanev, D.G., L.N. Nikolov, and V. Mamatarkova, Rapid simultaneous quantitative determination of ferric and ferrous ions in drainage waters and similar solutions. Minerals Engineering, 2002. 15(5): p. 341-346.

Karshenboim, S.G., Non-relativistic calculations of the g-factor of a bound electron. Physics Letters A, 2000. 266(4): p. 380-386.

Keiluweit, M., et al., *Dynamic molecular structure of plant biomass-derived black carbon (biochar).* Environmental science & technology, 2010. **44**(4): p. 1247-1253.

Kelf, T.A., et al., *Non-specific cellular uptake of surface-functionalized quantum dots.* Nanotechnology, 2010. **21**(28): p. 285105.

KHABAR, K.S., et al., *MTS interferon assay: a simplified cellular dehydrogenase assay for interferon activity using a water-soluble tetrazolium salt.* Journal of interferon & cytokine research, 1996. **16**(1): p. 31-33.

Khanra, P., et al., Simultaneous bio-functionalization and reduction of graphene oxide by baker's yeast. Chemical Engineering Journal, 2012. 183: p. 526-533.

Kim, K.-H., E. Kabir, and S. Kabir, *A review on the human health impact of airborne particulate matter.* Environment International, 2015. **74**: p. 136-143.

Kim, S., et al., *Hydrogen-deficient molecules in natural riverine water samples—evidence for the existence of black carbon in DOM.* Marine Chemistry, 2004. **92**(1): p. 225-234.

Kirchner, C., et al., *Cytotoxicity of Colloidal CdSe and CdSe/ZnS Nanoparticles.* Nano Letters, 2005. **5**(2): p. 331-338.

Kleineidam, S., C. Schüth, and P. Grathwohl, *Solubility-Normalized Combined Adsorption-Partitioning Sorption Isotherms for Organic Pollutants.* Environmental Science & Technology, 2002. **36**(21): p. 4689-4697.

Kostarelos, K., et al., *Cellular uptake of functionalized carbon nanotubes is independent of functional group and cell type.* Nature Nanotechnology, 2007. **2**(2): p. 108-113.

Kramer, R.W., E.B. Kujawinski, and P.G. Hatcher, *Identification of Black Carbon Derived Structures in a Volcanic Ash Soil Humic Acid by Fourier Transform Ion Cyclotron Resonance Mass Spectrometry.* Environmental Science & Technology, 2004. **38**(12): p. 3387-3395.

Krishnamoorthy, K.; Veerapandian, M.; Yun, K.; Kim, S. J., The chemical and structural analysis of graphene oxide with different degrees of oxidation. *Carbon* **2013,** *53*, 38-49.

Kuçur, E., et al., *Determination of Defect States in Semiconductor Nanocrystals by Cyclic Voltammetry*. The Journal of Physical Chemistry B, 2005. **109**(43): p. 20355-20360.

Kuhlbusch, T.A., *Black carbon and the carbon cycle.* Science, 1998. **280**(5371): p. 1903-1904.

Kuhlbusch, T.A.J., *Black Carbon and the Carbon Cycle.* Science, 1998. **280**(5371): p. 1903.

Kumar, A. and C.K. Dixit, 3 - Methods for characterization of nanoparticles, in Advances in Nanomedicine for the Delivery of Therapeutic Nucleic Acids, S. Nimesh, R. Chandra, and N. Gupta, Editors. 2017, Woodhead Publishing. p. 43-58.

Kwon, W. and S.-W. Rhee, *Facile synthesis of graphitic carbon quantum dots with size tunability and uniformity using reverse micelles.* Chemical Communications, 2012. **48**(43): p. 5256-5258.

Kyle, K.R. and P.C. Ford, Dynamic quenching of the metal-to-ligand charge-transfer excited state of Cu4I4(pyridine)4. Exciplex formation and self-quenching. Journal of the American Chemical Society, 1989. 111(13): p. 5005-5006.

Laden, F., et al., *Reduction in fine particulate air pollution and mortality: extended follow-up of the Harvard Six Cities study.* American journal of respiratory and critical care medicine, 2006. **173**(6): p. 667-672.

Lai, C.-W., et al., *Facile synthesis of highly emissive carbon dots from pyrolysis of glycerol; gram scale production of carbon dots/mSiO2 for cell imaging and drug release.* Journal of Materials Chemistry, 2012. **22**(29): p. 14403-14409.

Lakowicz, J.R., Principles of fluorescence spectroscopy. 2013: Springer Science & Business Media.

Leifeld, J., *Thermal stability of black carbon characterised by oxidative differential scanning calorimetry.* Organic Geochemistry, 2007. **38**(1): p. 112-127.

Li, H., et al., *Carbon nanodots: synthesis, properties and applications.* Journal of Materials Chemistry, 2012. **22**(46): p. 24230-24253.

Li, S., et al., *The Role of Cellular Glutathione Peroxidase Redox Regulation in the Suppression of Tumor Cell Growth by Manganese Superoxide Dismutase.* Cancer Research, 2000. **60**(14): p. 3927.

Lian, W., et al., The transformation of acetylene black into onion-like hollow carbon nanoparticles at 1000°C using an iron catalyst. Carbon, 2008. 46(3): p. 525-530.

Linehan, K. and H. Doyle, *Efficient one-pot synthesis of highly monodisperse carbon quantum dots.* RSC Advances, 2014. **4**(1): p. 18-21.

Liu, F., et al., *Facile Synthetic Method for Pristine Graphene Quantum Dots and Graphene Oxide Quantum Dots: Origin of Blue and Green Luminescence.* Advanced Materials, 2013. **25**(27): p. 3657-3662.

Liu, H., T. Ye, and C. Mao, Fluorescent Carbon Nanoparticles Derived from Candle Soot. Angewandte Chemie International Edition, 2007. 46(34): p. 6473-6475.

Liu, J.-M., et al., Highly selective and sensitive detection of Cu2+ with lysine enhancing bovine serum albumin modified-carbon dots fluorescent probe. Analyst, 2012. 137(11): p. 2637-2642.

Liu, Q., et al., *Distinguish cancer cells based on targeting turn-on fluorescence imaging by folate functionalized green emitting carbon dots.* Biosensors and Bioelectronics, 2015. **64**: p. 119-125.

Liu, R., et al., Ultra-sensitive and selective Hg2+ detection based on fluorescent carbon dots. Materials Research Bulletin, 2013. 48(7): p. 2529-2534.

Lodish, H., et al., *Molecular cell biology*. 2008: Macmillan.

Longfellow, C.A., A.R. Ravishankara, and D.R. Hanson, *Reactive and nonreactive uptake on hydrocarbon soot: HNO3, O3, and N2O5.* Journal of Geophysical Research: Atmospheres, 2000. **105**(D19): p. 24345-24350.

Lord, K., et al., *Environmentally persistent free radicals decrease cardiac function before and after ischemia/reperfusion injury in vivo.* J Recept Signal Transduct Res, 2011. **31**(2): p. 157-67.

Lu, F., et al., *Size effect on cell uptake in well-suspended, uniform mesoporous silica nanoparticles.* Small, 2009. **5**(12): p. 1408-1413.

Lu, J., et al., *One-Pot Synthesis of Fluorescent Carbon Nanoribbons, Nanoparticles, and Graphene by the Exfoliation of Graphite in Ionic Liquids.* ACS Nano, 2009. **3**(8): p. 2367-2375.

Lynch, M.W., M. Valentine, and D.N. Hendrickson, Mixed-valence semiquinone-catecholate-iron complexes. Journal of the American Chemical Society, 1982. 104(25): p. 6982-6989.

Ma, X., et al., *Highly fluorescent carbon dots from peanut shells as potential probes for copper ion: The optimization and analysis of the synthetic process.* Materials Today Chemistry, 2017. **5**: p. 1-10.

MacDonald, G.M., et al., *The reconstruction of boreal forest fire history from lake sediments: A comparison of charcoal, pollen, sedimentological, and geochemical indices.* Quaternary Science Reviews, 1991. **10**(1): p. 53-71.

Maciá-Agulló, J.A., et al., Oxygen functional groups involved in the styrene production reaction detected by quasi in situ XPS. Catalysis Today, 2005. 102-103: p. 248-253.

Margarucci, L., et al., *Chemical proteomics reveals bolinaquinone as a clathrin-mediated endocytosis inhibitor.* Mol Biosyst, 2011. **7**(2): p. 480-5.

Martell, A., R. Smith, and R. Motekaitis, *NIST critical stability constants of metal complexes database.* US Department of Commerce, Gaithersburg, 1993.

Mason, J.N., et al., *Novel fluorescence-based approaches for the study of biogenic amine transporter localization, activity, and regulation.* Journal of Neuroscience Methods, 2005. **143**(1): p. 3-25.

MAYHEW, S.G., The Redox Potential of Dithionite and SO−2 from Equilibrium Reactions with Flavodoxins, Methyl Viologen and Hydrogen plus Hydrogenase. European Journal of Biochemistry, 1978. 85(2): p. 535-547.

McConnell, J.R., et al., *20th-Century Industrial Black Carbon Emissions Altered Arctic Climate Forcing.* Science, 2007. **317**(5843): p. 1381.

McNicol, B. and G. Pott, Studies of the deammoniation and dehydroxylation processes in NH4 faujasite and NH4 mordenite zeolites. The use of the ESR of framework-substituted Fe3+ as a probe. Journal of Catalysis, 1972. 25(2): p. 223-229.

Mehta, V. N.; Jha, S.; Kailasa, S. K., One-pot green synthesis of carbon dots by using Saccharum officinarum juice for fluorescent imaging of bacteria (Escherichia coli) and yeast (Saccharomyces cerevisiae) cells. *Materials Science and Engineering: C* **2014,** *38*, 20-27.

Meister, A., Glutathione metabolism and its selective modification. Journal of Biological Chemistry, 1988. 263(33): p. 17205-8.

Melfi, S., J. Lawrence Jr, and M. McCormick, Observation of Raman scattering by water vapor in the atmosphere. Applied Physics Letters, 1969. 15(9): p. 295-297.

Menon, S., et al., *Climate Effects of Black Carbon Aerosols in China and India.* Science, 2002. **297**(5590): p. 2250-2253.

Mertes, S., B. Dippel, and A. Schwarzenböck, *Quantification of graphitic carbon in atmospheric aerosol particles by Raman spectroscopy and first application for the determination of mass absorption efficiencies.* Journal of Aerosol Science, 2004. **35**(3): p. 347-361.

Miller, F.J., et al., *Size Considerations for Establishing a Standard for Inhalable Particles.* Journal of the Air Pollution Control Association, 1979. **29**(6): p. 610-615.

Miura, Y., et al., X-ray photoelectron spectroscopy of sodium borosilicate glasses. Journal of non-crystalline solids, 2001. 290(1): p. 1-14.

Moosmüller, H., R.K. Chakrabarty, and W.P. Arnott, *Aerosol light absorption and its measurement: A review.* Journal of Quantitative Spectroscopy and Radiative Transfer, 2009. **110**(11): p. 844-878.

Moulay, S. and R. Mehdaoui, Hydroquinone/catechol-bearing polyacrylic acid: redox polymer. Reactive and Functional Polymers, 2004. 61(2): p. 265-275.

Murr, L.E. and K.F. Soto, *A TEM study of soot, carbon nanotubes, and related fullerene nanopolyhedra in common fuel-gas combustion sources.* Materials Characterization, 2005. **55**(1): p. 50-65.

Murruni, L.G., et al., Concentrations and elemental composition of particulate matter in the Buenos Aires underground system. Atmospheric Environment, 2009. 43(30): p. 4577-4583.

Nemery, B., P.H.M. Hoet, and A. Nemmar, *The Meuse Valley fog of 1930: an air pollution disaster.* The Lancet, 2001. **357**(9257): p. 704-708.

Neuberger, M., et al., *Acute effects of particulate matter on respiratory diseases, symptoms and functions:: epidemiological results of the Austrian Project on Health Effects of Particulate Matter (AUPHEP).* Atmospheric Environment, 2004. **38**(24): p. 3971-3981.

Novakov, T., et al., *Large historical changes of fossil-fuel black carbon aerosols.* Geophysical Research Letters, 2003. **30**(6).

Novakov, T., et al., *Origin of carbonaceous aerosols over the tropical Indian Ocean: Biomass burning or fossil fuels?* Geophysical Research Letters, 2000. **27**(24): p. 4061-4064.

Nugent, J.H.A., D.C. Doetschman, and D.J. Maclachlan, Characterization of the multiple EPR line shapes of iron-semiquinones in photosystem 2. Biochemistry, 1992. 31(11): p. 2935-2941.

O'Neill, M.S., et al., *Diabetes Enhances Vulnerability to Particulate Air Pollution–Associated Impairment in Vascular Reactivity and Endothelial Function.* Circulation, 2005. **111**(22): p. 2913-2920.

O'Toole, S.A., et al., *The MTS assay as an indicator of chemosensitivity/resistance in malignant gynaecological tumours.* Cancer Detection and Prevention, 2003. **27**(1): p. 47-54.

Oberdörster, G., et al., *Translocation of Inhaled Ultrafine Particles to the Brain.* Inhalation Toxicology, 2004. **16**(6-7): p. 437-445.

Organization, W.H., *World Health Report 2002*. 2002.

Pan, D., et al., *Hydrothermal Route for Cutting Graphene Sheets into Blue-Luminescent Graphene Quantum Dots.* Advanced Materials, 2010. **22**(6): p. 734-738.

Panchuk-Voloshina, N., et al., *Alexa Dyes, a Series of New Fluorescent Dyes that Yield Exceptionally Bright, Photostable Conjugates.* Journal of Histochemistry & Cytochemistry, 1999. **47**(9): p. 1179-1188.

Panzarasa, G., et al., Convenient Preparation of Graphene Oxide from Expandable Graphite and Its Characterization by Positron Annihilation Lifetime Spectroscopy. C, 2019. 5(1).

Parak, W.J., T. Pellegrino, and C. Plank, *Labelling of cells with quantum dots.* Nanotechnology, 2005. **16**(2): p. R9-R25.

Patterson, W.A., K.J. Edwards, and D.J. Maguire, *Microscopic charcoal as a fossil indicator of fire.* Quaternary Science Reviews, 1987. **6**(1): p. 3-23.

Peng, H. and J. Travas-Sejdic, *Simple Aqueous Solution Route to Luminescent Carbogenic Dots from Carbohydrates.* Chemistry of Materials, 2009. **21**(23): p. 5563-5565.

Peng, R.D., et al., *Coarse Particulate Matter Air Pollution and Hospital Admissions for Cardiovascular and Respiratory Diseases Among Medicare Patients.* JAMA, 2008. **299**(18): p. 2172-2179.

Peters, A., et al., *Air Pollution and Incidence of Cardiac Arrhythmia.* Epidemiology, 2000. **11**(1): p. 11-17.

Petzold, A., C. Kopp, and R. Niessner, *The dependence of the specific attenuation cross-section on black carbon mass fraction and particle size.* Atmospheric Environment, 1997. **31**(5): p. 661-672.

Petzold, A., et al., *Recommendations for reporting "black carbon" measurements.* Atmospheric Chemistry and Physics, 2013. **13**(16): p. 8365-8379.

Pierpont, C.G. and C.W. Lange, The chemistry of transition metal complexes containing catechol and semiquinone ligands. Progress in Inorganic Chemistry, 1994: p. 331-442.

Pikal-Cleland, K.A., et al., Protein Denaturation during Freezing and Thawing in Phosphate Buffer Systems: Monomeric and Tetrameric β-Galactosidase. Archives of Biochemistry and Biophysics, 2000. 384(2): p. 398-406.

Poerwono, H., et al., Citric Acid, in Analytical Profiles of Drug Substances and Excipients, H.G. Brittain, Editor. 2001, Academic Press. p. 1-76.

Pope, C.A. and D.W. Dockery, *Health Effects of Fine Particulate Air Pollution: Lines that Connect.* Journal of the Air & Waste Management Association, 2006. **56**(6): p. 709-742.

Prikhotjko, A., *Absorption spectra of crystals at low temperatures.* J. Phys. USSR, 1944. **8**: p. 257.

Qin, J., L. Zhang, and R. Yang, *Solid pyrolysis synthesis of excitation-independent emission carbon dots and its application to isoniazid detection.* Journal of Nanoparticle Research, 2019. **21**(3): p. 59.

Qu, K., et al., Carbon Dots Prepared by Hydrothermal Treatment of Dopamine as an Effective Fluorescent Sensing Platform for the Label-Free Detection of Iron(III) Ions and Dopamine. Chemistry – A European Journal, 2013. 19(22): p. 7243-7249.

Qu, S., et al., A biocompatible fluorescent ink based on water-soluble luminescent carbon nanodots. Angewandte Chemie international edition, 2012. 51(49): p. 12215-12218.

Querol, X., et al., *Speciation and origin of PM10 and PM2.5 in selected European cities.* Atmospheric Environment, 2004. **38**(38): p. 6547-6555.

Ramanathan, V. and G. Carmichael, *Global and regional climate changes due to black carbon.* Nature Geoscience, 2008. **1**: p. 221.

Ramesh, P. and S. Sampath, Chemically functionalised exfoliated graphite: a new bulk modified, renewable surface electrode. Chemical Communications, 1999(21): p. 2221-2222.

Ramesh, P. and S. Sampath, Electrochemical and spectroscopic characterization of quinone functionalized exfoliated graphite. Analyst, 2001. 126(11): p. 1872-1877.

Ray, S.C., et al., Fluorescent Carbon Nanoparticles: Synthesis, Characterization, and Bioimaging Application. The Journal of Physical Chemistry C, 2009. 113(43): p. 18546-18551.

Reiner, T., et al., *Chemical characterization of pollution layers over the tropical Indian Ocean: Signatures of emissions from biomass and fossil fuel burning.* Journal of Geophysical Research: Atmospheres, 2001. **106**(D22): p. 28497-28510.

Reipa, V., Direct spectroelectrochemical titration of glutathione. Bioelectrochemistry, 2004. 65(1): p. 47-49.

Resch-Genger, U., et al., *Quantum dots versus organic dyes as fluorescent labels.* Nat Methods, 2008. **5**(9): p. 763-75.

Ristovski, Z.D., et al., *Respiratory health effects of diesel particulate matter.* Respirology, 2012. **17**(2): p. 201-212.

Robole, Z.M., et al., Tuning the Electrochemical Redox Potentials of Catechol with Boronic Acid Derivatives. The Journal of Organic Chemistry, 2019. 84(4): p. 2346-2350.

Rogers, P.G., *The Clean Air Act of 1970 Looking Back; Looking Ahead.* EPA Journal, 1990(1): p. 21-23.

Rohr, A.C. and R.E. Wyzga, *Attributing health effects to individual particulate matter constituents.* Atmospheric Environment, 2012. **62**: p. 130-152.

Rosen, H., et al., *Graphitic Carbon in Urban Environments and the Arctic*, in *Particulate Carbon: Atmospheric Life Cycle*, G.T. Wolff and R.L. Klimisch, Editors. 1982, Springer US: Boston, MA. p. 273-294.

Roy, P., et al., *Photoluminescent carbon nanodots: synthesis, physicochemical properties and analytical applications.* Materials Today, 2015. **18**(8): p. 447-458.

Rückerl, R., et al., *Air Pollution and Markers of Inflammation and Coagulation in Patients with Coronary Heart Disease.* American Journal of Respiratory and Critical Care Medicine, 2006. **173**(4): p. 432-441.

Sachdev, A. and P. Gopinath, Green synthesis of multifunctional carbon dots from coriander leaves and their potential application as antioxidants, sensors and bioimaging agents. Analyst, 2015. 140(12): p. 4260-4269.

Sacks, J.D., et al., Particulate Matter–Induced Health Effects: Who Is Susceptible? Environmental Health Perspectives, 2011. 119(4): p. 446-454.

Sadezky, A., et al., *Raman microspectroscopy of soot and related carbonaceous materials: Spectral analysis and structural information.* Carbon, 2005. **43**(8): p. 1731-1742.

Salinas-Castillo, A.; Ariza-Avidad, M.; Pritz, C.; Camprubí-Robles, M.; Fernández, B.; Ruedas-Rama, M. J.; Megia-Fernández, A.; Lapresta-Fernández, A.; Santoyo-Gonzalez, F.; Schrott-Fischer, A., Carbon dots for copper detection with down and upconversion fluorescent properties as excitation sources. *Chemical Communications* **2013,** *49* (11), 1103-1105.

SALVI, S., et al., *Acute Inflammatory Responses in the Airways and Peripheral Blood After Short-Term Exposure to Diesel Exhaust in Healthy Human Volunteers.* American Journal of Respiratory and Critical Care Medicine, 1999. **159**(3): p. 702-709.

Santín, C., et al., *Towards a global assessment of pyrogenic carbon from vegetation fires.* Global Change Biology, 2016. **22**(1): p. 76-91.

Sardar, S.B., P.M. Fine, and C. Sioutas, Seasonal and spatial variability of the size-resolved chemical composition of particulate matter (PM10) in the Los Angeles Basin. Journal of Geophysical Research: Atmospheres, 2005. 110(D7).

Schicker, B., et al., *Particulate matter inhalation during hay storing activity induces systemic inflammation and platelet aggregation.* European Journal of Applied Physiology, 2009. **105**(5): p. 771-778.

Schmidt, M.W.I. and A.G. Noack, *Black carbon in soils and sediments: Analysis, distribution, implications, and current challenges.* Global Biogeochemical Cycles, 2000. **14**(3): p. 777-793.

Schwan, J., et al., Raman spectroscopy on amorphous carbon films. Journal of Applied Physics, 1996. 80(1): p. 440-447.

Schwartz, J., D.W. Dockery, and L.M. Neas, *Is Daily Mortality Associated Specifically with Fine Particles?* J Air Waste Manag Assoc, 1996. **46**(10): p. 927-939.

Schwartz, J., F. Laden, and A. Zanobetti, *The concentration-response relation between PM(2.5) and daily deaths.* Environmental Health Perspectives, 2002. **110**(10): p. 1025-1029.

Schwarze, P.E., et al., Particulate matter properties and health effects: consistency of epidemiological and toxicological studies. Human & Experimental Toxicology, 2006. 25(10): p. 559-579.

Selvan, S.T., T.T. Tan, and J.Y. Ying, *Robust, Non-Cytotoxic, Silica-Coated CdSe Quantum Dots with Efficient Photoluminescence.* Advanced Materials, 2005. **17**(13): p. 1620-1625.

Shahriary, L. and A.A. Athawale, Graphene oxide synthesized by using modified hummers approach. Int. J. Renew. Energy Environ. Eng, 2014. 2(01): p. 58-63.

Shang, J., et al., The Origin of Fluorescence from Graphene Oxide. Scientific Reports, 2012. 2(1): p. 792.

Shao, Y.; Yin, G.; Zhang, J.; Gao, Y., Comparative investigation of the resistance to electrochemical oxidation of carbon black and carbon nanotubes in aqueous sulfuric acid solution. *Electrochimica Acta* **2006,** *51* (26), 5853-5857.

Shen, Z., et al., *A Near-Infrared, Wavelength-Shiftable, Turn-on Fluorescent Probe for the Detection and Imaging of Cancer Tumor Cells.* ACS Chemical Biology, 2017. **12**(4): p. 1121-1132.

Sheridan, P.J., et al., *The Reno Aerosol Optics Study: An Evaluation of Aerosol Absorption Measurement Methods.* Aerosol Science and Technology, 2005. **39**(1): p. 1-16.

Sherwood, P.M., Data analysis in X-ray photoelectron spectroscopy. Practical surface analysis, 1983. 2: p. 555-586.

Sillanpää, M. and A. Oikari, *Assessing the impact of complexation by EDTA and DTPA on heavy metal toxicity using microtox bioassay.* Chemosphere, 1996. **32**(8): p. 1485-1497.

Simkhovich, B.Z., M.T. Kleinman, and R.A. Kloner, *Air Pollution and Cardiovascular Injury.* Journal of the American College of Cardiology, 2008. **52**(9): p. 719.

Smith, D.M. and A.R. Chughtai, *The surface structure and reactivity of black carbon.* Colloids and Surfaces A: Physicochemical and Engineering Aspects, 1995. **105**(1): p. 47-77.

Song, Y., et al., Investigation into the fluorescence quenching behaviors and applications of carbon dots. Nanoscale, 2014. 6(9): p. 4676-4682.

Song, Y., S. Zhu, and B. Yang, *Bioimaging based on fluorescent carbon dots.* RSC Advances, 2014. **4**(52): p. 27184-27200.

Soper, S.A. and Q.L. Mattingly, *Steady-State and Picosecond Laser Fluorescence Studies of Nonradiative Pathways in Tricarbocyanine Dyes: Implications to the Design of Near-IR Fluorochromes with High Fluorescence Efficiencies.* Journal of the American Chemical Society, 1994. **116**(9): p. 3744-3752.

Sorvari, J. and M. Sillanpää, *Influence of metal complex formation on heavy metal and free EDTA and DTPA acute toxicity determined by Daphnia magna.* Chemosphere, 1996. **33**(6): p. 1119-1127.

Squadrito, G.L., et al., *Quinoid redox cycling as a mechanism for sustained free radical generation by inhaled airborne particulate matter.* Free Radical Biology and Medicine, 2001. **31**(9): p. 1132-1138.

Stefani, F.D., et al., *Quantification of photoinduced and spontaneous quantum-dot luminescence blinking.* Physical Review B, 2005. **72**(12): p. 125304.

Steinvil, A., et al., *Short-term exposure to air pollution and inflammation-sensitive biomarkers.* Environmental Research, 2008. **106**(1): p. 51-61.

Stevenson, F.J., Humus chemistry: genesis, composition, reactions. 1994: John Wiley & Sons.

Storz, G. and J.A. Imlayt, *Oxidative stress.* Current Opinion in Microbiology, 1999. **2**(2): p. 188-194.

Strober, W., *Trypan Blue Exclusion Test of Cell Viability.* Current Protocols in Immunology, 1997. **21**(1): p. A.3B.1-A.3B.2.

Sullivan, J.H., et al., *A community study of the effect of particulate matter on blood measures of inflammation and thrombosis in an elderly population.* Environmental Health, 2007. **6**(1): p. 3.

Sun, D., et al., *Hair fiber as a precursor for synthesizing of sulfur- and nitrogen-co-doped carbon dots with tunable luminescence properties.* Carbon, 2013. **64**: p. 424-434.

Sun, X. and Y. Lei, Fluorescent carbon dots and their sensing applications. TrAC Trends in Analytical Chemistry, 2017. 89: p. 163-180.

Sun, Y.-P., et al., *Quantum-Sized Carbon Dots for Bright and Colorful Photoluminescence.* Journal of the American Chemical Society, 2006. **128**(24): p. 7756-7757.

Sze, S.K., et al., *Raman spectroscopic characterization of carbonaceous aerosols.* Atmospheric Environment, 2001. **35**(3): p. 561-568.

Tetsuka, H., et al., *Optically Tunable Amino-Functionalized Graphene Quantum Dots.* Advanced Materials, 2012. **24**(39): p. 5333-5338.

Tian, L., et al., Nanosized Carbon Particles From Natural Gas Soot. Chemistry of Materials, 2009. 21(13): p. 2803-2809.

Tumolva, L., et al., *Morphological and Elemental Classification of Freshly Emitted Soot Particles and Atmospheric Ultrafine Particles using the TEM/EDS.* Aerosol Science and Technology, 2010. **44**(3): p. 202-215.

Turpin, B.J. and H.-J. Lim, *Species contributions to PM2. 5 mass concentrations: Revisiting common assumptions for estimating organic mass.* Aerosol Science & Technology, 2001. **35**(1): p. 602-610.

van Meerloo, J., G.J.L. Kaspers, and J. Cloos, *Cell Sensitivity Assays: The MTT Assay*, in *Cancer Cell Culture: Methods and Protocols*, I.A. Cree, Editor. 2011, Humana Press: Totowa, NJ. p. 237-245.

van Poppel, L.H., et al., *Electron tomography of nanoparticle clusters: Implications for atmospheric lifetimes and radiative forcing of soot.* Geophysical Research Letters, 2005. **32**(24).

Venkataraman, B. and G.K. Fraenkel, Proton Hyperfine Interactions in Paramagnetic Resonance of Semiquinones1. Journal of the American Chemical Society, 1955. 77(10): p. 2707-2713.

Vikneswaran, R., S. Ramesh, and R. Yahya, Green synthesized carbon nanodots as a fluorescent probe for selective and sensitive detection of iron(III) ions. Materials Letters, 2014. 136: p. 179-182.

Virbasius, J.V. and M.P. Czech, *Map4k4 Signaling Nodes in Metabolic and Cardiovascular Diseases.* Trends in Endocrinology & Metabolism, 2016. **27**(7): p. 484-492.

Wagner, S., R. Jaffé, and A. Stubbins, *Dissolved black carbon in aquatic ecosystems.* Limnology and Oceanography Letters, 2018. **3**(3): p. 168-185.

Wang, D., et al., *Facile and Scalable Preparation of Fluorescent Carbon Dots for Multifunctional Applications.* Engineering, 2017. **3**(3): p. 402-408.

Wang, F., et al., Down-and up-conversion luminescent carbon dot fluid: inkjet printing and gel glass fabrication. Nanoscale, 2014. 6(7): p. 3818-3823.

Wang, F., et al., Fluorescence quenchometric method for determination of ferric ion using boron-doped carbon dots. Microchimica Acta, 2016. 183(1): p. 273-279.

Wang, F., et al., Graphene quantum dots as a fluorescent sensing platform for highly efficient detection of copper(II) ions. Sensors and Actuators B: Chemical, 2014. 190: p. 516-522.

Wang, F., et al., *One-Step Synthesis of Highly Luminescent Carbon Dots in Noncoordinating Solvents.* Chemistry of Materials, 2010. **22**(16): p. 4528-4530.

Wang, L., et al., *Carbon dots based turn-on fluorescent probes for the sensitive determination of glyphosate in environmental water samples.* RSC Advances, 2016. **6**(89): p. 85820-85828.

Wang, Q., et al., *Microwave–hydrothermal synthesis of fluorescent carbon dots from graphite oxide.* Carbon, 2011. **49**(9): p. 3134-3140.

Wang, W., et al., *Water-soluble and phosphorus-containing carbon dots with strong green fluorescence for cell labeling.* Journal of Materials Chemistry B, 2014. **2**(1): p. 46-48.

Wang, Y. and N. Herron, *Nanometer-sized semiconductor clusters: materials synthesis, quantum size effects, and photophysical properties.* The Journal of Physical Chemistry, 1991. **95**(2): p. 525-532.

Warner, J.H., et al., *Water-Soluble Photoluminescent Silicon Quantum Dots.* Angewandte Chemie International Edition, 2005. **44**(29): p. 4550-4554.

Waters, R.S., et al., EDTA chelation effects on urinary losses of cadmium, calcium, chromium, cobalt, copper, lead, magnesium, and zinc. Biological Trace Element Research, 2001. 83(3): p. 207-221.

Weller, H., *Quantum size colloids: From size-dependent properties of discrete particles to self-organized superstructures.* Current Opinion in Colloid & Interface Science, 1998. **3**(2): p. 194-199.

Wolfbeis, O.S., *An overview of nanoparticles commonly used in fluorescent bioimaging.* Chemical Society reviews, 2015. **44**(14): p. 4743-4768.

Womiloju, T.O., et al., Methods to determine the biological composition of particulate matter collected from outdoor air. Atmospheric Environment, 2003. 37(31): p. 4335-4344.

Xu, X., et al., *Electrophoretic Analysis and Purification of Fluorescent Single-Walled Carbon Nanotube Fragments.* Journal of the American Chemical Society, 2004. **126**(40): p. 12736-12737.

Yan, F., et al., Fluorescent carbon dots for ratiometric detection of curcumin and ferric ion based on inner filter effect, cell imaging and PVDF membrane fouling research of iron flocculants in wastewater treatment. Sensors and Actuators B: Chemical, 2019. 287: p. 231-240.

Yang, H. and J.Z. Yu, Uncertainties in Charring Correction in the Analysis of Elemental and Organic Carbon in Atmospheric Particles by Thermal/Optical Methods. Environmental Science & Technology, 2002. 36(23): p. 5199-5204.

Yang, Y., et al., *Bottom-up fabrication of photoluminescent carbon dots with uniform morphology via a soft–hard template approach.* Chemical Communications, 2013. **49**(43): p. 4920-4922.

Yang, Z.-C., et al., Intrinsically fluorescent carbon dots with tunable emission derived from hydrothermal treatment of glucose in the presence of monopotassium phosphate. Chemical communications, 2011. 47(42): p. 11615-11617.

Yao, S., Y. Hu, and G. Li, *A one-step sonoelectrochemical preparation method of pure blue fluorescent carbon nanoparticles under a high intensity electric field.* Carbon, 2014. **66**: p. 77-83.

Ye, Q., et al., Formation of N, S-codoped fluorescent carbon dots from biomass and their application for the selective detection of mercury and iron ion. Spectrochimica Acta Part A: Molecular and Biomolecular Spectroscopy, 2017. 173: p. 854-862.

Yu, C., et al., *Carbon-dot-based ratiometric fluorescent sensor for detecting hydrogen sulfide in aqueous media and inside live cells.* Chemical Communications, 2013. **49**(4): p. 403-405.

Yuen, A.K., et al., The interplay of catechol ligands with nanoparticulate iron oxides. Dalton Transactions, 2012. 41(9): p. 2545-2559.

Zhai, X., et al., *Highly luminescent carbon nanodots by microwave-assisted pyrolysis.* Chemical Communications, 2012. **48**(64): p. 7955-7957.

Zhang, B., C.-y. Liu, and Y. Liu, *A Novel One-Step Approach to Synthesize Fluorescent Carbon Nanoparticles.* European Journal of Inorganic Chemistry, 2010. **2010**(28): p. 4411-4414.

Zhang, H., et al., *Solid-Phase Synthesis of Highly Fluorescent Nitrogen-Doped Carbon Dots for Sensitive and Selective Probing Ferric Ions in Living Cells.* Analytical Chemistry, 2014. **86**(19): p. 9846-9852.

Zhang, J., et al., *Creating new fluorescent probes for cell biology.* Nature Reviews Molecular Cell Biology, 2002. **3**(12): p. 906-918.

Zhang, R. and W. Chen, *Nitrogen-doped carbon quantum dots: Facile synthesis and application as a "turn-off" fluorescent probe for detection of Hg2+ ions.* Biosensors and Bioelectronics, 2014. **55**: p. 83-90.

Zhao, W., et al., Intercalation of Few-Layer Graphite Flakes with FeCl3: Raman Determination of Fermi Level, Layer by Layer Decoupling, and Stability. Journal of the American Chemical Society, 2011. 133(15): p. 5941-5946.

Zheng, M., et al., On–Off–On Fluorescent Carbon Dot Nanosensor for Recognition of Chromium(VI) and Ascorbic Acid Based on the Inner Filter Effect. ACS Applied Materials & Interfaces, 2013. 5(24): p. 13242-13247.

Zheng, M., et al., *Self-targeting fluorescent carbon dots for diagnosis of brain cancer cells.* ACS nano, 2015. **9**(11): p. 11455-11461.

Zhou, J., et al., *An Electrochemical Avenue to Blue Luminescent Nanocrystals from Multiwalled Carbon Nanotubes (MWCNTs).* Journal of the American Chemical Society, 2007. **129**(4): p. 744-745.

Zhou, J., et al., *Facile synthesis of fluorescent carbon dots using watermelon peel as a carbon source.* Materials Letters, 2012. **66**(1): p. 222-224.

Zhou, J., et al., *Time-series analysis of mortality effects of fine particulate matter components in Detroit and Seattle.* Environ Health Perspect, 2011. **119**(4): p. 461-6.

Zhu, H., et al., *Microwave synthesis of fluorescent carbon nanoparticles with electrochemiluminescence properties.* Chemical Communications, 2009(34): p. 5118-5120.

Zhu, S., et al., *Surface Chemistry Routes to Modulate the Photoluminescence of Graphene Quantum Dots: From Fluorescence Mechanism to Up-Conversion Bioimaging Applications.* Advanced Functional Materials, 2012. **22**(22): p. 4732-4740.

Zhu, Y., et al., Graphene and Graphene Oxide: Synthesis, Properties, and Applications. Advanced Materials, 2010. 22(35): p. 3906-3924.

Zhuo, Y., et al., *One-step synthesis of high quantum-yield and excitation-independent emission carbon dots for cell imaging.* Materials Letters, 2015. **139**: p. 197-200.

Zipfel, W.R., et al., *Live tissue intrinsic emission microscopy using multiphoton-excited native fluorescence and second harmonic generation.* Proc Natl Acad Sci U S A, 2003. **100**(12): p. 7075-80.

Zong, J., et al., *Synthesis of photoluminescent carbogenic dots using mesoporous silica spheres as nanoreactors.* Chemical Communications, 2011. **47**(2): p. 764-766.

Zu, F., et al., *The quenching of the fluorescence of carbon dots: A review on mechanisms and applications.* Microchimica Acta, 2017. **184**(7): p. 1899-1914.

Zuo, P., et al., *Single-step preparation of fluorescent carbon nanoparticles, and their application as a fluorometric probe for quercetin.* Microchimica Acta, 2014. **181**(11): p. 1309-1316.

VITA

Christopher Lee Sumner, Jr. was born in Americus, Georgia, to Mr. Christopher Sumner and Mrs. Sheila Sumner. He graduated from Early County High School in Blakely, GA, in 2008. He attended Shorter University in Rome, GA, from which he received a Bachelor of Science in Chemistry with Biology and Spanish minors in 2012. After graduating from Shorter, Chris worked at Lewis Chemical Company in Rome, GA, as a quality control chemist before being promoted to Lab Manager for 1 year. He then moved on to teach 10^{th}, 11^{th}, and 12^{th} grade Chemistry and Physics at Unity Christian School in Rome, GA, for 2 years. In 2015, Chris moved to Baton Rouge to pursue his Ph.D. in Chemistry at Louisiana State University. He joined the research group of Prof. Robin McCarley in January 2016, and he graduated during the summer commencement in August 2020.